Jül-4282

Jülich Center for Hadron Physics (JCHP)
Institut für Kernphysik (IKP)
COSY

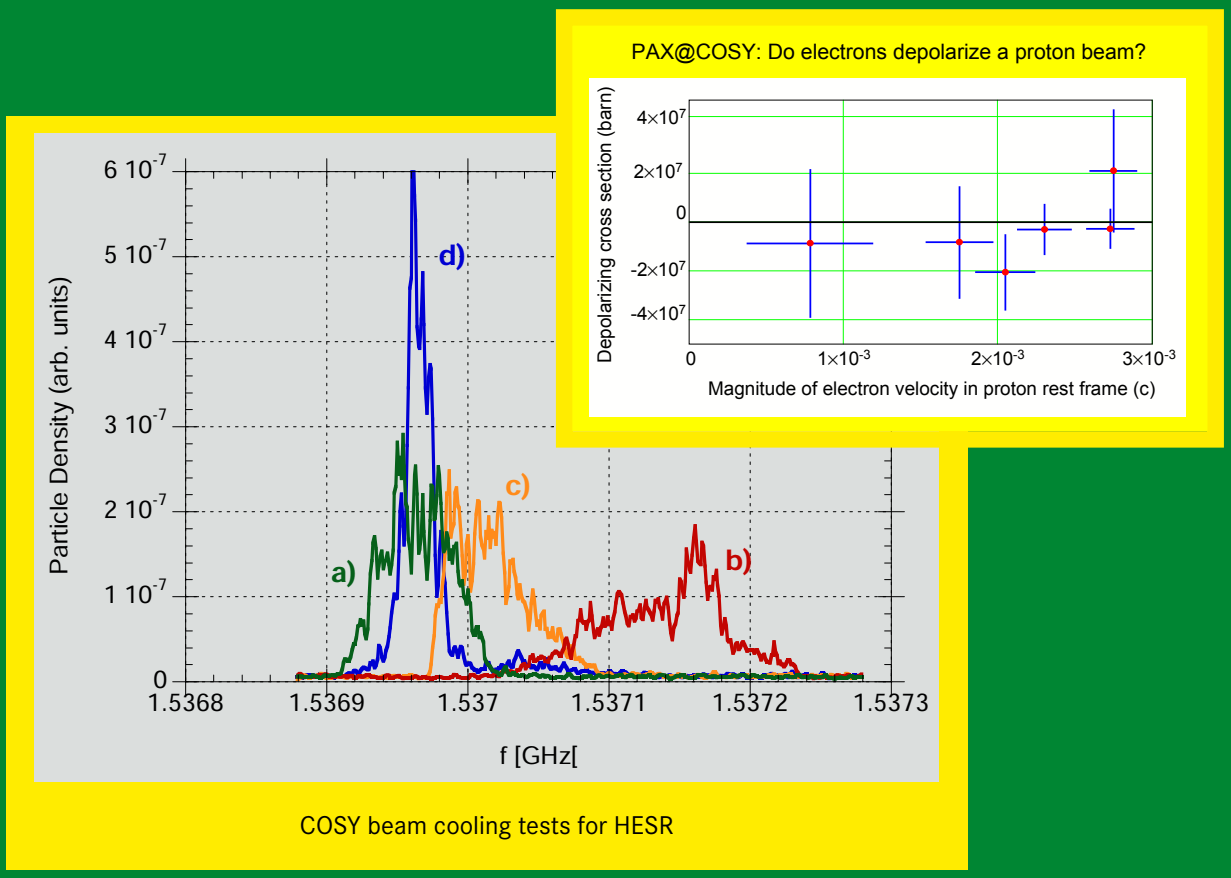

ANNUAL REPORT 2008

JÜLICH
FORSCHUNGSZENTRUM

Annual Report 2008

Institut für Kernphysik / COSY

Cover picture:

Lower figure: COSY has been used to develop methods to compensate the mean energy loss and energy spread of the stored antiproton beam at HESR during internal target experiments. The Schottky spectra of the COSY proton beam has been measured using the WASA frozen-pellet target, a prototype barrier bucket HF cavity for the HESR and COSY's stochastic cooling system: a) starting distribution, b) final distribution after 160 s only pellet-target, c) final distribution with longitudinal stochastic cooling and d) final distribution with cooling and barrier bucket.
Upper figure: The measurement of the depolarizing $\vec{p}e$ cross section settled a long-standing controversy about the role of electrons to the polarization buildup of a stored beam by spin-flipping. Electrons in the COSY e-cooler have been used to study their depolarizing effect on a 49.3 MeV polarized proton beam. The depolarizing cross section is plotted as a function of the electron velocity in the proton rest frame, indicating an upper limit of a few 10^7 b.

Preface

On July 1, the board of directors of the Forschungszentrum Jülich (FZJ) founded the **Jülich Center for Hadron Physics (JCHP).** The main goal of the JCHP is to coordinate the hadron physics activities at the FZJ for the FAIR project. This includes activities at the Institute for Advanced Simulations (IAS), the Institut für Kernphysik (IKP), the Zentralinstitut für Elektronik (ZEL) and the Zentralabteilung Technologie (ZAT). Within the Helmholtz Association (HGF) research field *Structure of Matter*, the FZJ operates the COSY facility and has achieved an excellent international reputation due to the close cooperation between accelerator physicists, experimentalists and theoreticians. In cooperation with ZEL and ZAT, the IKP is in charge of the construction and operation of the High Energy Storage Ring HESR and makes a strong contribution to the PANDA detector and its physics. PAX is exploiting methods to effectively polarize (anti-)protons for a possible future upgrade at FAIR.

The FZJ operates the JUGENE/JSC supercomputer and hosts the John von Neumann institute which develops lattice gauge simulation calculations of quantum chromodynamics (QCD) and hadron structure. The JCHP coordinates these activities by establishing a direct connection between the lattice QCD simulation groups and hadron physicists. Moreover, the infrastructure provided by the IAS for mass storage, presently used for COSY data, may handle FAIR data and perform Monte Carlo simulations of HESR experiments.

External users are essential for the success of an accelerator complex, therefore, the JCHP facilitates the contact of external users with the FZJ and supports external activities in the field of hadron physics. Presently an initiative of the universities within North-Rhine Westfalia and the FZJ, called NRW-FAIR, is forming to coordinate their FAIR-related activities.

Starting December 1, 2008, the IKP-3 theorists also work in IAS-4, the strong interaction physics branch of the Institute for Advanced Simulations (IAS). The Virtual Institute *Spin and Strong QCD* has presented its first results on June 1 in Ferrara.

A Helmholtz-Russia Joint Research Group, the first one in Jülich, will receive funding from the Impuls- und Vernetzungsfond of the Helmholtz Association and from the Russian Foundation for Basic Research for the next three years. In a joint effort of the FZJ, the Budker Institute in Novosibirsk, TU Dortmund and JINR Dubna methods for electron cooling in the MeV region, relevant for FAIR, will be developed.

The IKP has initiated a cooperation with the 100-TW laser facility at the Heinrich-Heine University Düsseldorf. The potential of new particle acceleration technologies with limited-mass targets will be explored, exploiting the know-how on frozen-pellet targets gained at the IKP.

The year 2008 has seen important experimental and theoretical progress:

- The WASA-at-COSY facility began operation in 2007, and in 2008 the first results have been submitted for publication. Data on the $\eta \to 3\pi^0$ decay was used to determine the quadratic slope parameter $\alpha = -0.027 \pm 0.008(\text{stat}) \pm 0.005(\text{syst})$, consistent with previous measurements, and clearly indicating the importance of pion-pion final state interactions. WASA has also taken exclusive high statistics data on the $pn \to pn\pi^0\pi^0$ process to study the ABC effect, and a strong resonance-like structure has been observed in the excitation function.

- ANKE has published results on isolation of the $\Lambda(1405)$ hyperon in the $\Sigma^0\pi^0$ channel, diproton formation in the γ- and π final states, kaon pair production and kaon final state interaction, and neutron-proton charge-exchange amplitudes at 585 MeV. In addition, it has presented a paper about the Schottky method for luminosity determination in internal experiments.
- TOF has performed first experiments using the new straw tube tracker. This is an important technological progress directly relevant for the central detector of PANDA. Moreover, it is the first step to determine the spin dependence of the Λp scattering length.
- PAX has performed and analysed depolarization experiments with the COSY electron cooler, thereby showing that the cross section is much smaller than needed for effectively polarizing the beam.
- The theory institute has studied three-nucleon forces in chiral effective field theory including the Δ_{33} resonance as an explicit degree of freedom with subsequent applications to isospin violating effects in few-nucleon systems. Nuclear lattice simulations with three-body forces have been performed to obtain the neutron-deuteron S-wave phase shifts. The $Y(4660)$ resonance recently observed at Belle does not fit into the conventional quark model. An interpretation as a quasi-bound state consisting of the ψ' and the $f_0(980)$ mesons has been worked out and predictions for the $K\bar{K}$ decay have been made, which eventually will be tested at PANDA. Scaling laws in the Coulomb excitation of neutron halo nuclei have been proposed.
- IKP-4 has developed components for the HESR and new methods in parallel to the routine operation of COSY. This research and development benefits from the unique capabilities provided by COSY. First successful operations of the barrier-bucket cavity beam with pellet target and stochastic cooling have been performed. The HESR lattice has been completed with normal conducting magnets. The physical specifications for all components have been finished. New insights into the loss mechanisms while operating the electron cooling show potential for an intensity increase. A new technique to overcome spin-deploarizing resonances based on Kondratenko crossing has been tested.

In October 2008, Prof. U.-G. Meißner has been elected as Dean of the Faculty of Mathematics and Natural Sciences of the University of Bonn. We congratulate both M. Wolke and C. Hanhart for having received offers from Uppsala University. Prof. J. Ritman and PD C. Hanhart have been elected as members of the scientific-technical council (WTR) and its executive committee (HK) in 2008, C. Hanhart has become vice chair of the WTR. Congratulations are given to Prof. H. Machner for receiving the Merentibus Medal of the University of Cracow.

Finally I would like to express my sincere gratitude to all our colleagues and co-workers, since without their help and support, we would not have been able to achieve our milestones. We also acknowledge the continuous support by the board of management of the FZJ and HGF.

Jülich, January 2009 James Ritman

Contents

1 Experimental Hadron Physics

1.1 ANKE

Energy dependence of the $pp \to K^+n\Sigma^+$ reaction

Yu. Valdau[1,2] for the ANKE collaboration

In contrast to the neuttral light hyperons, Λ and Σ^0, very little is known about Σ^+ production in pp collisions. The $pp \to K^+n\Sigma^+$ reaction can be measured by detecting K^+n in the final state and identifying the Σ^+ via a missing-mass spectrum. Using this method, values of the total cross section for this reaction were obtained for the first time at two close-to-threshold energies by the COSY-11 collaboration [1]. It was found, surprisingly, that the values thus obtained were extremely high. At the lowest energy where measurements were performed (13 MeV above the threshold) it is as high as the total cross section for the $pp \to K^+p\Lambda$ reaction. Furthermore, the ratio $\sigma(\Sigma^+)/\sigma(\Sigma^0)$ of the total cross sections for Σ^+ and Σ^0 production was found to be 230 ± 70 and 90 ± 40 at $\varepsilon = 13$ MeV (1.826 GeV) and $\varepsilon = 60$ MeV (1.958 GeV), respectively.

The COSY-11 publication triggered studies of Σ^+ production at ANKE. Our measurement of the total cross section at $\varepsilon = 129$ MeV [2] showed that at this energy the production in this channel is roughly equal to that for Σ^0. Following the acceptance of the ANKE proposal in 2007 [3], the cross section of the $pp \to K^+n\Sigma^+$ reaction has been studied at four energies between the Σ^+ threshold and 2.02 GeV. A measurement below the Σ^+ threshold was also performed to provide a cross-check. At ANKE we avoid neutron detection and its associated problems, relying instead on the excellent K^+ identification provided by our range telescopes. These detect K^+ decay products and allow us to identify unambiguously the kaons even if the background is 10^6 higher. K^+p correlation spectra were constructed by measuring the proton in the positive side detector as well as the forward detector.

At the energies where measurements have been performed, there are only three possible reactions channels that lead to K^+ production in pp collisions: $pp \to K^+p\Lambda$, $pp \to K^+p\Sigma^0$, and $pp \to K^+n\Sigma^+$. All the hyperons produced in these three reactions have a decay mode which has a proton in the final state. Signals from all the reactions can therefore be found, not only in the K^+ inclusive spectra, but also in the K^+p coincidence spectra. However, only the Σ^+ hyperon decays (BR $= 48.51\%$) with a π^+ in the final state. As a consequence, by detecting a K^+ in coincidence with π^+, one can identify the $pp \to K^+n\Sigma^+$ reaction unambiguously.

Studies of the $pp \to K^+n\Sigma^+$ reaction at ANKE are undertaken through the simultaneous analysis of K^+p and $K^+\pi^+$ correlations as well as inclusive K^+ production. In Fig. 1 the missing-mass spectra from K^+p correlations are presented at the five energies where measurements were undertaken at ANKE. The experimental data are compared with the phase-space simulations of K^+p correlations expected for all three contributing channels. The known total cross sections for Λ and Σ^0 production were used as weights in the simulations for two of the channels. For the third, it was assumed that $\sigma_{\Sigma^0} = \sigma_{\Sigma^+}$. Individual contributions to the K^+p missing mass spectra from the Σ^+ production, normalised to the number of Σ^0 events, are presented in the Fig. 1 by the dotted line. Since this represents the dominant contribution at large missing masses, these data are also quite sensitive to the value of the Σ^+ cross section.

A publication presenting a simultaneous analysis of all three experimental spectra is in the course of preparation.

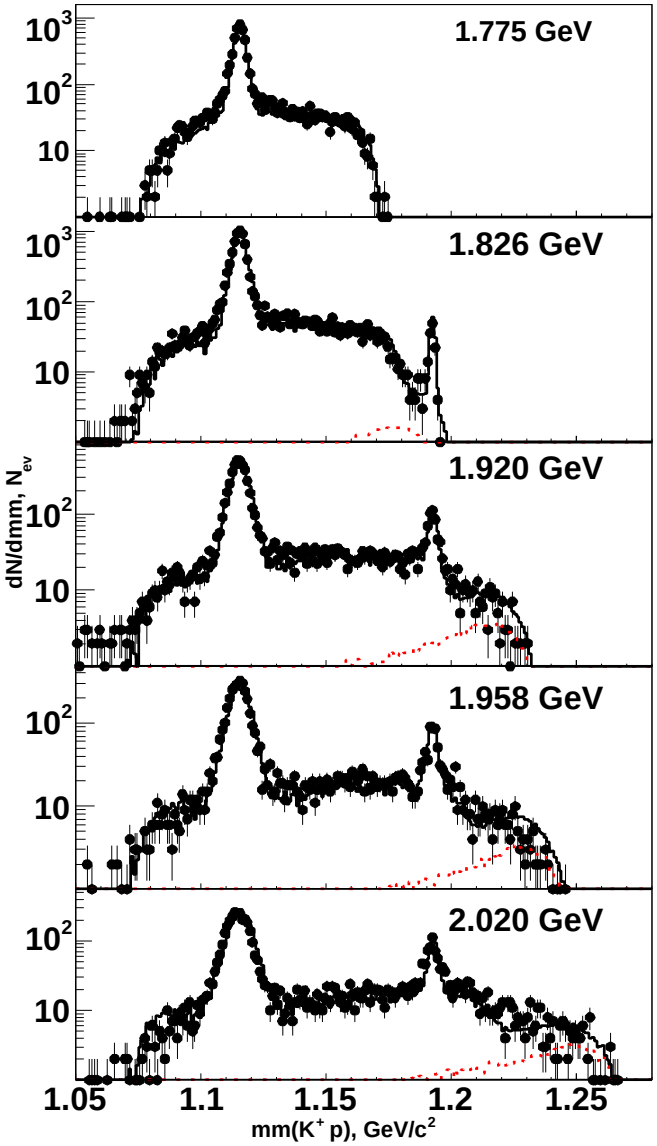

Fig. 1: K^+p missing-mass spectra measured at five different energies (circles with error bars). The solid line shows the sum of the simulations of the individual contributions from all the different possible channels. The individual contribution from the $pp \to K^+n\Sigma^+$ reaction is shown by the dotted line.

References:

[1] T. Rożek et al., Phys. Lett. B 643 (2006) 251.
[2] Yu. Valdau et al., Phys. Lett. B 652 (2007) 245.
[3] Yu. Valdau et al., COSY proposal #171, http://www.fz-juelich.de/ikp/anke/en/proposals.shtml

1 High Energy Physics Department, Petersburg Nuclear Physics Institute, 188350 Gatchina, Russia
2 Institut für Kernphysik, Forschungszentrum Jülich, 52425 Jülich, Germany

Final state interactions in $K\bar{K}$ pair production*

A. Dzyuba[a,b], M. Büscher[b], M. Hartmann[b], V. Koptev[a], Y. Maeda[c], and C. Wilkin[d] for the ANKE collaboration

Measurements of the $pp \to ppK^+K^-$ reaction at both COSY-11 and ANKE [1] have shown that the interaction of the K^- with the final protons is much stronger than that of the K^+ . Thus, if we define the ratio of the acceptance–corrected distributions in the Kp invariant masses $R_{Kp} = [d\sigma/dM(K^-p)]/[d\sigma/dM(K^+p)]$, then this shows a very strong preference for low values of $M(Kp)$ provided that the invariant mass of the K^+K^- is chosen to be away from the region of the ϕ peak. The three-particle invariant-mass distribution ratio R_{Kpp} shows same behaviour.

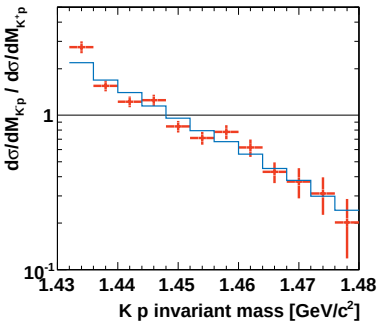

Fig. 1: Ratios of the differential cross sections for the $pp \to ppK^+K^-$ reaction at $Q_{K\bar{K}}$ = 51 MeV away from the $\phi(1020)$ region. Experimental data (red) are compared to a Monte Carlo simulation (blue).

The magnitude and mass dependence of both the R_{Kp} and R_{Kpp} ratios can be described quantitatively at all the COSY-11 and ANKE energies by assuming that there are overlapping final state interactions (*fsi*) between the pp and both K^-p pairs. Within the framework of this simple *ansatz*, the only free parameter is an effective K^-p scattering length of $|a_{\bar{K}p}| = 1.5$ fm.

Although the above *ansatz* describes the vast bulk of all the available data, there is evidence of $K\bar{K}$ *fsi* at very low K^+K^- invariant masses for all beam energies. This is shown clearly in Fig. 2 where, to increase the limited statistics, the average of the ratio of the experimental data to the simulation involving just the K^-p and pp *fsi* is compared to fits that include both K^+K^- plus a charge exchange contribution, where a $K^0\bar{K}^0$ pair is converted into K^+K^- through a *fsi* [2].

Detailed investigation of this coupled channel effect allows to extract ratio of the B_0 and B_1 — the $pp \to ppK\bar{K}$ amplitudes for producing s-wave $K\bar{K}$ pairs in isospin-0 and 1 states, respectively. These amplitudes, which already include the *fsi* in the K^-p and pp channels, are then distorted through a fsi corresponding to elastic scattering. The subsequent fitting of the data is best achieved with $|B_1/B_0|^2 = 0.38^{+0.24}_{-0.14}$.

Since the antikaon is so strongly attracted to the proton, it is interesting to investigate its interaction with nuclei. For the simplest of nuclei, this is possible by using the $pp \to dK^+\bar{K}^0$ reaction, which has been recently reanalysed [3]. Similar effects to those observed in the $pp \to ppK^+K^-$ case are also seen here, with the strong tendency for the $\bar{K}^0d$ invariant mass to be lower than that of the K^+d system, as illustrated in Fig. 3.

The analysis is complicated for this reaction by the spin-parity requirement that even near threshold one of the final particles must be in a P-wave. The data show that this is overwhelmingly the K^+, with the $\bar{K}^0d$ being in an S-wave. Such a difference would come about through a strong $\bar{K}d$ attraction. A combined fit to the two data sets with the inclusion of final-state interactions in both the $K^+\bar{K}^0$ and $\bar{K}^0d$ systems has been done. The data is well discribed by the wide $a_0^+(980)$-resonance and $\bar{K}^0d$ *fsi* with typical value of $a_{\bar{K}d} \approx (-1.0 + i1.2)$ fm.

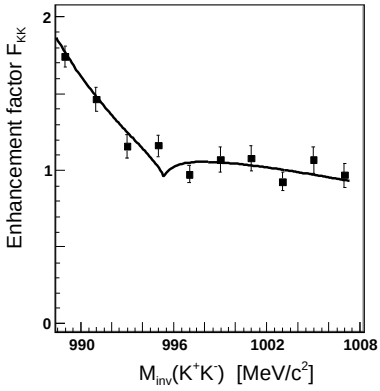

Fig. 2: Ratio of the K^+K^- invariant mass spectra from the $pp \to ppK^+K^-$ reaction to the simulation presented in Ref. [1]. The experimental points correspond to the weighted average of ANKE data taken at 2.65, 2.70, and 2.83 GeV. The solid curve includes both K^+K^- *fsi* and charge exchange $K^0\bar{K}^0 \to K^+K^-$ contributions.

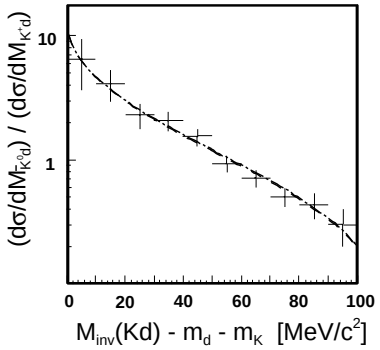

Fig. 3: Ratio of the differential cross section for the $pp \to dK^+\bar{K}^0$ reaction at an excess energy of 104.7 MeV in terms of the $\bar{K}^0d$ and K^+d invariant masses. The dashed curve represents the best fit to the data [3].

The natural continuation of the ANKE programme to study the antikaon-nucleon/nucleus interaction will be to measure the cross section for $pd \to {}^3\mathrm{He}K^+K^-$ to investigate the ${}^3\mathrm{He}K^-$ system.

References:

[1] Y. Maeda *et al.*, Phys. Rev. C **77** (2008) 015204.
[2] A. Dzyuba *et al.*, Phys. Lett. B **668** (2008) 315.
[3] A. Dzyuba *et al.*, Eur. Phys. J. A **38** (2008) 1.

[a] Petersburg Nuclear Physics Institute, Russia
[b] IKP and JCHP, FZJ, Germany
[c] Osaka University, Japan
[d] University College London, U.K.
* supported by COSY–FFE programm

Amplitude analysis of the reaction $pp \to d K^+ \bar{K}^0$ near threshold

V. Yu. Grishina [a], C. Hanhart, L.A. Kondratyuk[b] and M. Büscher

The $pp \to d K^+ \bar{K}^0$ reaction has recently been measured at ANKE-COSY [1, 2]. In the analysis of this reaction only the lowest allowed partial waves were included to describe the available data on the differential cross sections [1, 2, 3], which are Sp and Ps, where the first label denotes the orbital angular momentum between the $K^+\bar{K}^0$ pair and the second one that of the kaon-antikaon pair relative to the deuteron. In both cases the initial pp pair has spin one and is in the P or F partial wave. These properties of the $pp \to d K^+ \bar{K}^0$ reaction amplitude follow from angular momentum and parity conservation laws combined with the Pauli principle for the initial proton-proton state.

Each of the reaction amplitudes $M_{Sp}(\hat{\boldsymbol{p}}, \boldsymbol{S}; \boldsymbol{k}, \boldsymbol{\epsilon})$ or $M_{Ps}(\hat{\boldsymbol{p}}, \boldsymbol{S}; \boldsymbol{q}, \boldsymbol{\epsilon})$ can be presented as the superposition of four spin structures

$$
\begin{aligned}
&A_1\left(\boldsymbol{S}; \boldsymbol{\epsilon}\right) = \frac{\sqrt{2}}{\sqrt{3}} \left(\boldsymbol{S} \cdot \ \boldsymbol{\epsilon}^\dagger\right), \\
&A_2\left(\hat{\boldsymbol{p}}, \boldsymbol{S}; \boldsymbol{\kappa}, \boldsymbol{\epsilon}\right) = \left\{\left(\hat{\boldsymbol{p}} \cdot \boldsymbol{S}\right)\left(\boldsymbol{\kappa} \cdot \ \boldsymbol{\epsilon}^\dagger\right) - \left(\boldsymbol{\kappa} \cdot \boldsymbol{S}\right)\left(\hat{\boldsymbol{p}} \cdot \ \boldsymbol{\epsilon}^\dagger\right)\right\}, \\
&A_3(\hat{\boldsymbol{p}}, \boldsymbol{S}; \boldsymbol{\epsilon}) = \sqrt{3}\left\{\left(\hat{\boldsymbol{p}} \cdot \boldsymbol{S}\right)\left(\hat{\boldsymbol{p}} \cdot \ \boldsymbol{\epsilon}^\dagger\right) - \frac{1}{3}\left(\boldsymbol{S} \cdot \ \boldsymbol{\epsilon}^\dagger\right)\right\}, \\
&A_4\left(\hat{\boldsymbol{p}}, \boldsymbol{S}; \boldsymbol{\kappa}, \boldsymbol{\epsilon}\right) = \left\{\left(\hat{\boldsymbol{p}} \cdot \boldsymbol{S}\right)\left(\boldsymbol{\kappa} \cdot \ \boldsymbol{\epsilon}^\dagger\right) + \right. \\
&\left. + \left(\boldsymbol{\kappa} \cdot \boldsymbol{S}\right)\left(\hat{\boldsymbol{p}} \cdot \ \boldsymbol{\epsilon}^\dagger\right) - 2\left(\hat{\boldsymbol{p}} \cdot \boldsymbol{S}\right)\left(\hat{\boldsymbol{p}} \cdot \ \boldsymbol{\epsilon}^\dagger\right)\left(\hat{\boldsymbol{p}} \cdot \boldsymbol{\kappa}\right)\right\}, \qquad (1)
\end{aligned}
$$

where $A_2\left(\hat{\boldsymbol{p}}, \boldsymbol{S}; \boldsymbol{\kappa}, \boldsymbol{\epsilon}\right)$ and $A_4\left(\hat{\boldsymbol{p}}, \boldsymbol{S}; \boldsymbol{\kappa}, \boldsymbol{\epsilon}\right)$ should be taken at the corresponding value of the momentum $\boldsymbol{\kappa} = \boldsymbol{k}$ or $\boldsymbol{q}$. Here $\boldsymbol{q}$ is the relative momentum between the two kaons, $\boldsymbol{k}$ the deuteron cms momentum, and $\hat{\boldsymbol{p}}$ is the unit vector parallel to the beam direction. The polarisation vectors of the intial pp pair and the final deuteron are denoted by $\boldsymbol{S}$ and $\boldsymbol{\epsilon}$, respectively. The contributions to the matrix element from the Sp and Ps final states are

$$
\begin{aligned}
&M_{Sp} = a^1_{Sp}\ \left(\hat{\boldsymbol{p}} \cdot \boldsymbol{k}\right) A_1\left(\boldsymbol{S}; \boldsymbol{\epsilon}\right) + a^2_{Sp}\, A_2\left(\hat{\boldsymbol{p}}, \boldsymbol{S}; \boldsymbol{k}, \boldsymbol{\epsilon}\right) + \\
&a^3_{Sp}\ \left(\hat{\boldsymbol{p}} \cdot \boldsymbol{k}\right) A_3\left(\boldsymbol{S}; \boldsymbol{\epsilon}\right) + a^4_{Sp}\, A_4\left(\hat{\boldsymbol{p}}, \boldsymbol{S}; \boldsymbol{k}, \boldsymbol{\epsilon}\right); \qquad (2) \\
&M_{Ps} = a^1_{Ps}\ \left(\hat{\boldsymbol{p}} \cdot \boldsymbol{q}\right) A_1\left(\boldsymbol{S}; \boldsymbol{\epsilon}\right) + a^2_{Sp}\, A_2\left(\hat{\boldsymbol{p}}, \boldsymbol{S}; \boldsymbol{q}, \boldsymbol{\epsilon}\right) + \\
&a^3_{Sp}\ \left(\hat{\boldsymbol{p}} \cdot \boldsymbol{q}\right) A_3\left(\boldsymbol{S}; \boldsymbol{\epsilon}\right) + a^4_{Sp}\, A_4\left(\hat{\boldsymbol{p}}, \boldsymbol{S}; \boldsymbol{q}, \boldsymbol{\epsilon}\right). \qquad (3)
\end{aligned}
$$

Here the two sets of coefficients a^i_{Sp} and a^j_{Ps} are independent complex amplitudes which in general depend upon the scalar kinematic quantities q^2, k^2, and $\boldsymbol{k} \cdot \boldsymbol{q}$. The structures $A_1(\hat{\boldsymbol{p}}, \boldsymbol{S}; \boldsymbol{\epsilon})$ and $A_3(\hat{\boldsymbol{p}}, \boldsymbol{S}; \boldsymbol{\epsilon})$ in Eq. (2) or Eq. (3) are multiplied by the corresponding kinematic factor $(\hat{\boldsymbol{p}} \cdot \boldsymbol{k})$ or $(\hat{\boldsymbol{p}} \cdot \boldsymbol{q})$.

The basic structures introduced in Eqs. (1) satisfy the condition of orthogonality, i.e. for non-diagonal interference terms arising in the matrix element squared after the procedure of averaging over the initial spins of the protons and summation over the spin states of the final deuteron we have

$$
\overline{A^\dagger_i\, A_j} = 0 \quad \text{for} \quad i \neq j\,. \qquad (4)
$$

Furthermore, $\overline{A^\dagger_2\left(\hat{\boldsymbol{p}}, \boldsymbol{S}; \boldsymbol{\kappa}, \boldsymbol{\epsilon}\right) A_4(\hat{\boldsymbol{p}}, \boldsymbol{S}; \boldsymbol{\kappa'}, \boldsymbol{\epsilon})} = 0$ also at $\boldsymbol{\kappa'} \neq \boldsymbol{\kappa}$. The non-zero diagonal terms are

$$
\begin{aligned}
&\overline{A^\dagger_1\left(\boldsymbol{S}; \boldsymbol{\epsilon}\right) A_1(\boldsymbol{S}; \boldsymbol{\epsilon})} = \overline{A^\dagger_3\left(\hat{\boldsymbol{p}}, \boldsymbol{S}; \boldsymbol{\epsilon}\right) A_3(\hat{\boldsymbol{p}}, \boldsymbol{S}; \boldsymbol{\epsilon})} = 1, \\
&\overline{A^\dagger_2\left(\hat{\boldsymbol{p}}, \boldsymbol{S}; \boldsymbol{\kappa}, \boldsymbol{\epsilon}\right) A_2(\hat{\boldsymbol{p}}, \boldsymbol{S}; \boldsymbol{\kappa'}, \boldsymbol{\epsilon})} = \\
&\overline{A^\dagger_4\left(\hat{\boldsymbol{p}}, \boldsymbol{S}; \boldsymbol{\kappa}, \boldsymbol{\epsilon}\right) A_4(\hat{\boldsymbol{p}}, \boldsymbol{S}; \boldsymbol{\kappa'}, \boldsymbol{\epsilon})} = \\
&= \left[\left(\boldsymbol{\kappa} \cdot \boldsymbol{\kappa'}\right) - \left(\hat{\boldsymbol{p}} \cdot \boldsymbol{\kappa}\right)\left(\hat{\boldsymbol{p}} \cdot \boldsymbol{\kappa'}\right)\right].
\end{aligned}
$$

The basic amplitudes from Eqs (2–3) are related to the parameters a^i_{Sp} or a^i_{Ps} as the result of the linear transformation applied to the set of spin structures $(\boldsymbol{S} \cdot \boldsymbol{\epsilon}^\dagger)\,(\hat{\boldsymbol{p}} \cdot \boldsymbol{\kappa})$, $(\hat{\boldsymbol{p}} \cdot \boldsymbol{S})(\boldsymbol{\kappa} \cdot \ \boldsymbol{\epsilon}^\dagger)$, $(\boldsymbol{\kappa} \cdot \boldsymbol{S})(\hat{\boldsymbol{p}} \cdot \ \boldsymbol{\epsilon}^\dagger)$ and $(\hat{\boldsymbol{p}} \cdot \boldsymbol{S})(\hat{\boldsymbol{p}} \cdot \ \boldsymbol{\epsilon}^\dagger)(\hat{\boldsymbol{p}} \cdot \boldsymbol{\kappa})$ taken at $\boldsymbol{\kappa} = \boldsymbol{k}$ or $\boldsymbol{q}$ and previously used for the amplitudes M_{Sp} and M_{Ps} in Ref. [3]. For the analysis of unpolarized measurements of the $pp \to d K^+ \bar{K}^0$ reaction performed close to its threshold the square of the matrix element with the lowest allowed parial waves taken into account should be averaged over the initial and summed over the final spins. This leads to the following expression

$$
\begin{aligned}
&\overline{|M(\boldsymbol{k}, \boldsymbol{q})|^2} = \overline{|M_{Sp}(\boldsymbol{k}) + M_{Ps}(\boldsymbol{q})|^2} \\
&C^k\ \left(\hat{\boldsymbol{p}} \cdot \boldsymbol{k}\right)^2 + S^k\ \left[k^2 - \left(\hat{\boldsymbol{p}} \cdot \boldsymbol{k}\right)^2\right] + \\
&+ C^q\ \left(\hat{\boldsymbol{p}} \cdot \boldsymbol{q}\right)^2 + S^q\ \left[q^2 - \left(\hat{\boldsymbol{p}} \cdot \boldsymbol{q}\right)^2\right] + \\
&+ C^{kq}\ \left(\hat{\boldsymbol{p}} \cdot \boldsymbol{k}\right)\ \left(\hat{\boldsymbol{p}} \cdot \boldsymbol{q}\right) + S^{kq}\ \left[\left(\boldsymbol{k} \cdot \boldsymbol{q}\right) - \left(\hat{\boldsymbol{p}} \cdot \boldsymbol{k}\right)\ \left(\hat{\boldsymbol{p}} \cdot \boldsymbol{q}\right)\right]. \qquad (5)
\end{aligned}
$$

The C- and S-coefficients are bilinear combinations of the amplitudes a^i_{Sp} and a^j_{Ps} of Eqs. (2) and (3):

$$
\begin{aligned}
&C^k = \left|a^1_{Sp}\right|^2 + \left|a^3_{Sp}\right|^2, \quad S^k = \left|a^2_{Sp}\right|^2 + \left|a^4_{Sp}\right|^2, \\
&C^q = \left|a^1_{Ps}\right|^2 + \left|a^3_{Ps}\right|^2, \quad S^q = \left|a^2_{Ps}\right|^2 + \left|a^4_{Ps}\right|^2, \\
&C^{kq} = 2\,\mathrm{Re}\left(a^{1\,*}_{Sp}\, a^1_{Ps}\right) + 2\,\mathrm{Re}\left(a^{3\,*}_{Sp}\, a^3_{Ps}\right), \\
&S^{kq} = 2\,\mathrm{Re}\left(a^{2\,*}_{Sp}\, a^2_{Ps}\right) + 2\,\mathrm{Re}\left(a^{4\,*}_{Sp}\, a^4_{Ps}\right). \qquad (6)
\end{aligned}
$$

It is seen that there is no dependence on the relative phases between the a^i and a^j amplitudes at $i \neq j$ in the square of the matrix element $\overline{|M(\boldsymbol{k}, \boldsymbol{q})|^2}$ (5) summed over the spin states of the final deuteron and averaged over the spins of the initial protons. The above mentioned relative phases can be determined only from the polarization observables. Hence, the general form used for the contributions from the lowest allowed partial waves M_{Sp} (2) and M_{Ps} (3) to the $pp \to d K^+ \bar{K}^0$ reaction amplitude near the threshold gives minimum number of the interference terms in the matrix element squared summed over the final and averaged over the initial spins. Moreover, *the parameters that could not be measured in unpolarized experiment are eliminated*.

This work was supported by the grant DFG 436 RUS 113/940/0 and the Russian Federal Agency of Atomic Energy.

References:

[1] V. Kleber *et al.*, Phys. Rev. Lett. **91** (2003) 172304.
[2] A. Dzyuba *et al.*, Eur. Phys. J. A **29** (2006) 245.
[3] A. Dzyuba *et al.*, Eur. Phys. J. A **38** (2008) 1.

[a]Institute for Nuclear Research, 60th October Anniversary Prospect 7A, 117312 Moscow, Russia
[b]Institute for Theoretical and Experimental Physics, B. Cheremushkinskaya 25, 117218 Moscow, Russia

Cross section determination for the dd → αK⁺K⁻ reaction with ANKE*

X. Yuan[1,2] for the ANKE collaboration

An attempt to measure the $dd \to \alpha f_0 \to \alpha K^+K^-$ process at maximum COSY beam momentum of $p_d = 3.7$ GeV/c has been carried out using the magnetic ANKE spectrometer. The K^+ mesons have been selected in the ANKE side detector (SD) [1] mainly by a time-of-flight criterion. The coincident fast α particles were identified in the forward counters (FD) [2] via their detection time and energy losses. Using the reconstructed α and K^+ momenta, the non-observed K^- mesons have been selected via a missing-mass criterion.

As the first step of the analysis, the K^+ selection has been tuned with dK^+ pairs that are produced at a much higher rate than the αK^+ events of interest. Figure 1 shows that after selection of deuterons in the FD (upper), dK^+ correlations can be separated from $d\pi^+$ background events (lower).

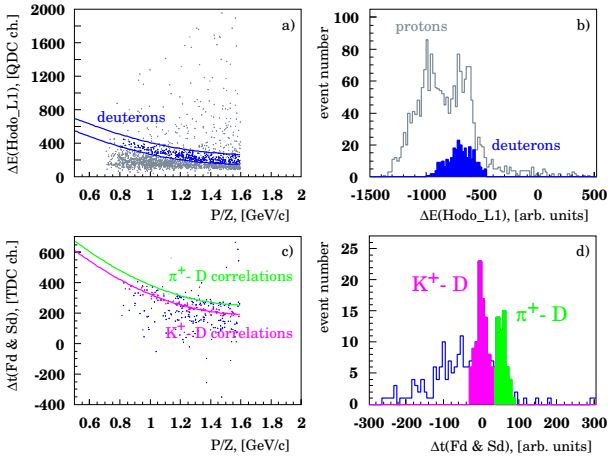

Fig. 1: a), b): d identification by energy losses in the FD. The filled histogram in b) depicts the remaining d candidates within the cut shown in Fig. a). c), d): Deuterons correlated with K^+ & π^+ can be identified.

In the next step, the FD information of fast particles — detected in coincidence with π^+ mesons from the SD — has been investigated, see Fig. 2a) and b). Since $m_\alpha \approx 2m_d$ and $Z_\alpha = 2Z_d$, $\alpha\pi^+(K^+)$ events are hidden under the time-of-flight band of $d\pi^+(K^+)$ pairs. The necessary d-α discrimination can be achieved from energy losses in three scintillator layers of the FD. Figure 2d) (blue histogram) shows the energy loss in one of these layers for the d and α events from solid blue histogram in b). Most of the background deuterons can be removed by the cut indicated in c), leaving the events marked in green. After applying corresponding cuts in the remaining two layers, about 100 $\pi^+\alpha$ events survive (red).

After applying the selection criteria for K^+ (Fig. 1) and for α (Fig. 2), 15 αK^+K^- candidates with a missing mass in the K^- region remain, see Fig. 3a). These events also fulfill the selection criteria shown in Figs. 3b)–f).

With the integrated luminosity $L_{\rm int} = 35\,{\rm pb}^{-1}$ [3], a (preliminary) total production cross section of $\sigma_{\rm tot} = (9 \pm 3_{\rm sta} \pm 4_{\rm SysLumi} \pm 1_{\rm SysAcc})$ pb is obtained.

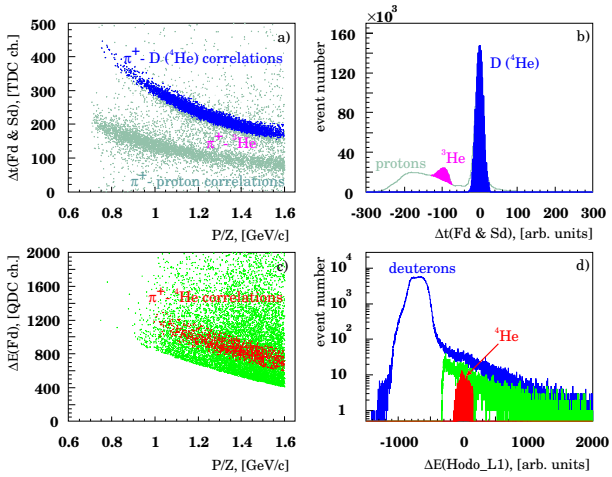

Fig. 2: a), b): Δt(FD–SD) *vs.* rigidity plot of FD particles correlated with π^+ mesons. c), d): The α band in a ΔE(FD) *vs.* rigidity plot can be determined from the energy losses in three FD scintillator layers.

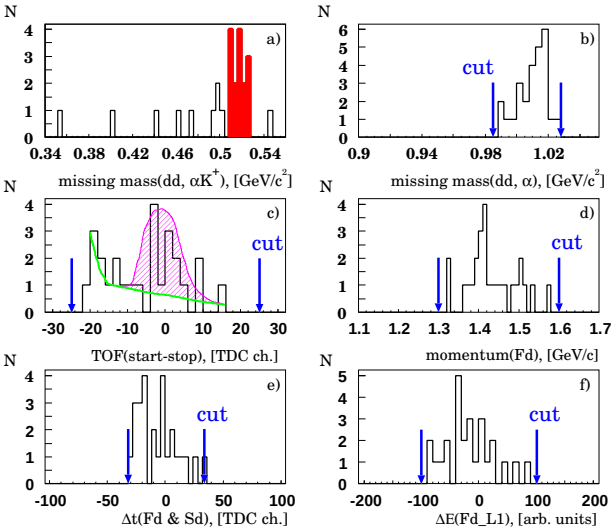

Fig. 3: a) Missing mass spectrum of $dd \to \alpha K^+X$ events; b) missing $dd \to \alpha X$ mass spectrum; c) time of flight in the SD, the expected K^+ signal is indicated; d) FD momentum distribution; e) time difference between FD and SD; f) energy loss in FD scintillators.

References:

[1] M. Büscher et al., *Nucl. Instrum. Methods Phys. Res. A* **481**, 378 (2002).
[2] S. Dymov et al., *Phys. Lett. B* **635**, 270 (2006).
[3] Xiao-Hua Yuan et al., *Chin. Phys. C* **20**, 33 (2009).

[1] Institute of Mordern Physics, CAS, Lanzhou, P.R. China
[2] IKP, FZ Jülich

* Supported by CSC, DAAD, DFG, HGF

Subthreshold and near-threshold charged kaons production in proton-nucleus collisions*

E. Paryev[1], M. Hartmann, Yu. Kiselev[2], A. Polyanskiy

The study of kaon and antikaon production in proton-nucleus collisions at incident energies near or below the free nucleon-nucleon thresholds has received considerable interest in recent years (see, for example, [1–13]). This interest has been particularly motivated by the hope to extract from this study information about both the intrinsic properties of target nuclei (such as high-momentum components of the nuclear wave function) and the in-medium kaon and antikaon properties at the density of ordinary nuclei (mean-field nuclear potentials, their momentum dependences). Evidently, to draw firm conclusions on these properties from proton-induced reactions it is of principal importance to disentangle reliably the underlying reaction mechanisms, since if they are clearly identified the above quantities can be fixed by comparison with the data. Therefore, we focus on the different elementary processes that lead to the kaon and antikaon production at beam energies close to their production thresholds in free NN collisions (1.58 GeV for K^+ creation and 2.5 GeV for K^- creation in these collisions).

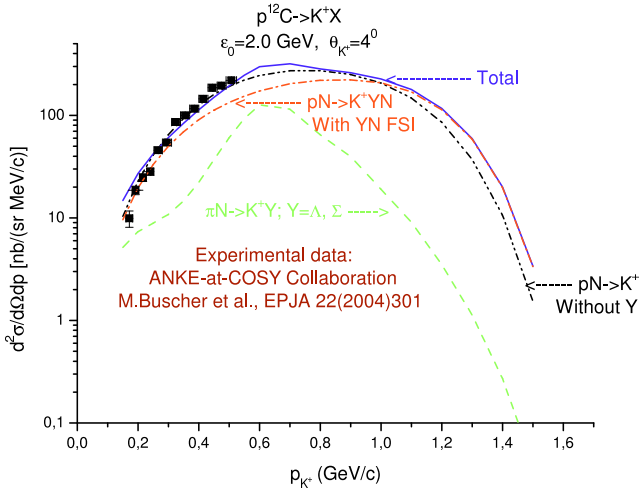

Fig. 1: Double differential cross sections for the production of K^+ mesons at an angle of 4° in the interaction of 2.0 GeV protons with the ^{12}C nuclei as functions of kaon momentum. The experimental data (full squares) are from [8]. The curves are our calculation. The dashed lines with one and two dots are calculations for the primary production processes $pN \to K^+YN$; $Y = \Lambda, \Sigma$ with and without including the FSI effects among the outgoing hyperons and nucleons. The dashed line is calculation for the secondary production processes $\pi N \to K^+Y$ with an intermediate pion. The solid line is the sum of the dashed and dash-dotted lines.

The inclusive K^+ meson production in proton-nucleus reactions in the near-threshold and subthreshold energy regimes is analyzed (see Fig. 1) with respect to the commonly used main one–step ($pN \to K^+YN$, $Y = \Lambda, \Sigma$) and two–step ($pN \to \pi X$, $\pi N \to K^+Y$) incoherent production processes on the basis of an appropriate folding model [5, 10], which takes into account only the struck target nucleon momentum distribution, extracted from the K^+ production experiment [5], and free elementary cross sections.

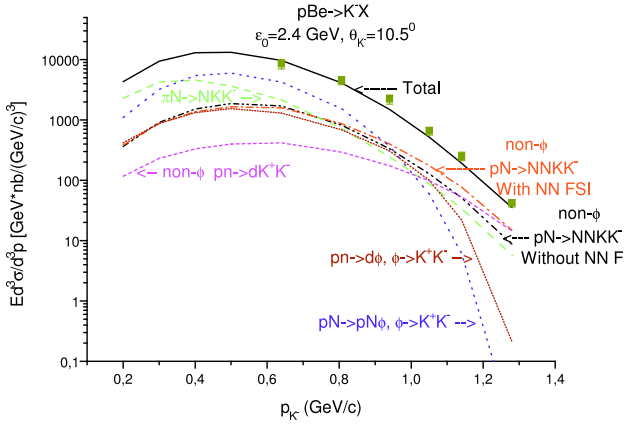

Fig. 2: Invariant cross sections for the production of K^- mesons at an angle of 10.5° in the interaction of 2.4 GeV protons with the ^{9}Be nuclei as functions of antikaon momentum. The experimental data (full squares) are obtained at the ITEP accelerator. The curves show our calculation. The dashed lines with one and two dots show the calculation for the primary production process $pN \to NNKK^-$ with and without including the FSI effects among the outgoing nucleons. The dashed and short-dashed lines represent the calculation, respectively, for the secondary production process $\pi N \to NKK^-$ and direct non-ϕ $pn \to dK^+K^-$ channel. The dotted and short-dotted lines show the calculation for the secondary creation processes $pN \to pN\phi$, $\phi \to K^+K^-$ and $pn \to d\phi$, $\phi \to K^+K^-$. The solid line is the sum of the dash-dotted, dashed, short-dashed, dotted and short-dotted lines.

The inclusive K^- meson creation in such reactions is investigated (see Fig. 2) within the same model not only with respect to the conventional direct ($pN \to NNKK^-$) and two–step ($pN \to \pi X$, $\pi N \to NKK^-$) antikaon production processes, but also using the new elementary reaction channels: $pN \to pN\phi$, $pn \to d\phi$, $\phi \to K^+K^-$; non-ϕ $pn \to dK^+K^-$. The total cross sections of the elementary reactions $pp \to pp\phi$, $pn \to d\phi$, non-ϕ $pn \to dK^+K^-$, needed for our calculations, have been recently measured in the threshold region by the ANKE-at-COSY Collaboration [14–16]. Figures 1 and 2 demonstrate that the agreement between our model calculations and the experimental data is quite good and, therefore, there is only little room left, for instance, for the subthreshold K^- production in pA reactions via other mechanisms, employed in [11]. Such good agreement with the experimental data is achieved, as may be seen from the figures 1 and 2, in particular, if we account for (in line with the corresponding Watson-Migdal theory) the final-state interaction (FSI) effects between, on the one hand, the hyperons and nucleons and, on the other hand, the nucleons originating, respectively, from the primary K^+ and K^- creation processes $pN \to K^+YN$ and $pN \to NNKK^-$. To reproduce the high-momentum part of the antikaon spectrum it was also important to take into consideration the contribution from the new K^- production channel non-ϕ $pn \to dK^+K^-$.

The results, obtained in our study, may be useful in the analysis of the future experimental data on near-threshold non-resonant and resonant (via ϕ decay) antikaon production in *pA* interactions from the ANKE-at-COSY detector system [17].

References:

[1] V. P. Koptev *et al.*, Sov. Phys. JETP **67**, 2177 (1988).
[2] S. Schnetzer *et al.*, Phys. Rev. C **40**, 640 (1989).
[3] M. Debowski *et al.*, Z. Phys. A **356**, 313 (1996).
[4] A. Badala *et al.*, Phys. Rev. Lett. **80**, 4863 (1998).
[5] A. V. Akindinov *et al.*, JETP Lett. **72**, 100 (2000).
[6] V. Koptev *et al.*, Phys. Rev. Lett. **87**, 022301 (2001).
[7] M. Nekipelov *et al.*, Phys. Lett. B **540**, 207 (2002).
[8] M. Büscher *et al.*, Eur. Phys. J. A **22**, 301 (2004).
[9] E. Ya. Paryev, Eur. Phys. J. A **5**, 307 (1999).
[10] A. V. Akindinov *et al.*, JETP Lett. **85**, 142 (2007).
[11] W. Scheinast *et al.*, Phys. Rev. Lett. **96**, 072301 (2006).
[12] A. Sibirtsev *et al.*, Z. Phys. A **351**, 333 (1995).
[13] E. Ya. Paryev, Eur. Phys. J. A **9**, 521 (2000).
[14] Y. Maeda *et al.*, Phys. Rev. C **77**, 015204 (2008).
[15] Y. Maeda *et al.*, Phys. Rev. Lett. **97**, 142301 (2006).
[16] Y. Maeda *et al.*, Phys. Rev. C, *in print*; arXiv:nucl–ex/0811.4303.
[17] M. Hartmann, Yu. Kiselev *et al.*, ANKE-COSY proposal #147 (2005).

[1] Institute for Nuclear Research, Russian Academy of Sciences, Moscow 117312, Russia
[2] Institute for Theoretical and Experimental Physics, Moscow 117218, Russia

* Supported by DFG

Bound kaonic nuclear states with ANKE@COSY

I.Zychor[a] for the ANKE Collaboration

Study of deeply bound kaonic nuclear states deals with one of the most important, yet unsolved, problems in hadron physics: how the hadron masses and hadron interactions change in the nuclear medium and what is the structure of cold dense hadronic matter. The hypothesis of deeply bound kaonic nuclear states (also indicated as kaonic nuclear clusters) is six years old, in the structured form of a phenomenological model [1]. A successful example of deeply bound pionic atomic states did already exist, after their observation at GSI in 1996 [2, 3]. Some experimental indications of kaonic nuclear clusters have been recently obtained at E471, E549, E548@KEK-PS [4], FINUDA@DAFNE [5], FOPI@GSI [6], OBELIX [7] and E930@BNL-AGS [8].

In the FINUDA experiment, the evidence of the kaon-bound state K^-pp through its decay into a Λ and a proton has been observed. The invariant-mass distribution of the Λp pair shows a significant mass decrease with respect to the mass of the system expected in case of a simple K^-pp absorption. The mass of the K^-pp system is equal to 2370 MeV/c^2. The state K^-pp has a binding energy of $115^{+6}_{-5}(stat)^{+3}_{-4}(syst)$ MeV and a decay width of $67^{+14}_{-11}(stat)^{+2}_{-3}(syst)$ MeV.

In the re-analysis of the DISTO data obtained in the $pp \to pK^+\Lambda$ reaction measured at a proton beam energy of 2.85 GeV a large broad peak has been observed [9]. It is then concluded that the structure with a mass of 2265 MeV/c^2 and a width of 118 MeV/c^2 is most likely due to a K^-pp bound state formed in the $pp \to K^+X^+$ reaction followed by the $X^+ \to p\Lambda$ decay. The signal has been observed only with a selection of large–angle proton emission in the restricted phase space. The maximum of the observed peak coincides with the $\pi\Sigma N$ threshold. In the chiral framework such a broad state in the deep subthreshold region would be interpreted in terms of $\pi\Sigma N$ dynamics [10].

The $pp \to K^+X^+$ reaction has been investigated with ANKE@COSY at a beam energy of 2.83 GeV, see Ref. [11] for more experimental details. Assuming a decay of the X^+ into $p\Lambda$, followed by the $\Lambda \to p\pi^-$ decay, the final state comprising of K^+, two protons and π^- could be observed: $pp \to K^+X^+ \to K^+p\Lambda \to K^+pp\pi^-$. Positively charged kaons were measured in telescopes. The protons from the X^+ decay were identified in the forward counters and protons from the Λ decay in telescopes and side-wall scintillators.

In Fig. 1 the missing-mass $MM(K^+)$ distribution measured with ANKE@COSY is shown (blue points). In addition, there is indicated a mass of the ppK^- system together with a binding energy and a width measured by the FINUDA collaboration. No events have been found for $MM(K^+)$ <2365 MeV/c^2. Since ANKE can identify both positively charge kaons and negatively charged pions in a limited momentum range, *i.e.* K^+ with momenta lower than 700 MeV/c^2 in the telescope counters and π^- with momenta higher than 200 MeV/c^2, we conclude that a restricted acceptance of the ANKE spectrometer is responsible for a non-

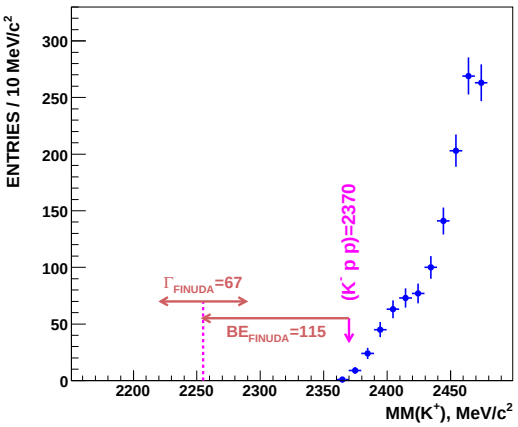

Fig. 1: The experimental missing-mass $MM(K^+)$ distribution measured in the reaction $pp \to K^+X^+$ (blue points). There is indicated a mass of the ppK^- system together with a binding energy and a width measured by the FINUDA collaboration. All values are in MeV/c^2.

observation of the X^+ with a mass of 2255 MeV/c^2 and a width of 67 MeV/c^2, if it exists.

In Fig. 2 the $MM(K^+)$ vs K^+ momentum distribution calculated for the $pp \to K^+X^+$ reaction is shown (black points). The horizontal box shows a $MM(K^+)$ mass range expected for the X^+ with a mass of 2255 MeV/c^2 and a width of 67 MeV/c^2. As it is seen, the mass ~2255 MeV/c^2 could be connected with kaons produced at higher momenta up to ~1.5 GeV/c. So, it is possible to identify the $pp \to K^+X^+$ reaction by measuring kaons in the side–wall counters together with protons from the X^+ decay in telescopes and protons from the Λ decay in forward part of the ANKE detector system. Such simulated spectrum is shown in Fig. 3. The analysis of data under the above specified conditions could be considered.

References:

[1] Y. Akaishi and T. Yamazaki, Phys. Rev. C **65**, 044005 (2002).
[2] T. Yamazaki *et al.*, Z. Phys. A **355**, 219 (1996).
[3] T. Yamazaki *et al.*, Phys. Lett. B **418**, 246 (1998).
[4] T. Suzuki *et al.*, Phys. Lett. B **597**, 263 (2004), T. Suzuki *et al.*, Nucl. Phys. A **754**, 375c (2005), M. Iwasaki *et al.*, Nucl. Phys. A **804**, 186 (2008), M. Sato *et al.*, Phys. Lett. B **659**, 107 (2008).
[5] M. Agnello *et al.*, Phys. Rev. Lett. **94**, 212303 (2005).
[6] P. Kienle, Nucl. Phys. A **804**, 286 (2008).
[7] P. Montagna *et al.*, Few Body Syst. (2008), in print.

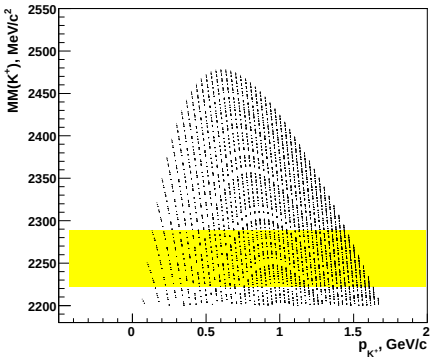

Fig. 2: The missing-mass $MM(K^+)$ vs K^+ momentum distribution calculated for the $pp \to K^+X^+$ reaction is shown as black points. The horizontal box shows a $MM(K^+)$ mass range expected for the X^+ with a mass of 2255 MeV/c^2 and a width of 67 MeV/c^2.

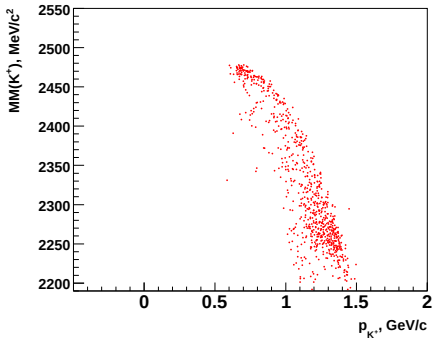

Fig. 3: The simulated missing-mass $MM(K^+)$ vs K^+ momentum distribution with kaons identified in side-wall scintillators, protons from the X^+ decay identified in telescopes and protons from the Λ decay in forward part of the ANKE detector system.

[8] T. Kishimoto *et al.*, Nucl. Phys. A **754**, 383c (2005).
[9] T. Yamazaki *et al.*, arXiv:0810.5182.
[10] A. Doté, T. Hyodo and W. Weise, arXiv:0811.0869.
[11] I. Zychor *et al.*, Phys. Lett. B **660**,167 (2008).

[a] The Andrzej Sołtan Institute for Nuclear Studies,Świerk,Poland

Deuteron breakup $p + d \to \{pp\}_s + n$ at GeV energies with forward emission of the $\{pp\}_s$ diproton

V. Komarov[1], T. Azaryan[1], S. Dymov[1,2], A. Kulikov[1], V. Kurbatov[1],
G. Macharashvili[1], S. Merzliakov[1,2], D. Tsyrkov[1,2], Yu. Uzikov[1], B. Zalikhanov[1] for the ANKE collaboration.

Study of the deuteron breakup $pd \to \{pp\}_s n$ with forward emission of a fast proton pair $\{pp\}_s$ with small excitation energy $E_{pp} < 3$ MeV has been performed in the T_p=0.5–1.97 GeV beam energy range using the ANKE spectrometer. In kinematically complete experiment with higher than in [1] statistics the E_{pp} spectra, the θ_k angular distribution of the proton momentum in the pair c.m.s., and the distribution of the neutron emission angle in the range $\theta_n = 168 - 180°$ were measured. The E_{pp} spectra essentially differ from the phase space distributions but, as expected, are well described (Fig. 1) within the Migdal-Watson approach of the $^1S_0$ final state interaction of the protons in a pair (except for 1.97 GeV where both descriptions fail). The proton angle θ_k is distributed isotropically, also consistent with the $^1S_0$ state of the pair. The θ_n distribution is non-isotropic and T_p energy dependent (Fig. 2); this might be a reflection of the fact that contributions of different mechanisms crucially change with energy as predicted by the ONE+SS+Δ model [2]. The differential cross section $d\sigma/d\Omega$ at $\theta_n = 180°$ follows an exponential drop with T_p energy in the range 0.5–1.4 GeV but significantly deviates from this dependence at 1.97 GeV (Fig. 3). Such a change of the regime is similar to that observed for the $pd \to dp$ backward elastic scattering [3] where flattening of the energy dependence is observed at 2.0–2.5 GeV.

The one-pion exchange (OPE) mechanism together with the one-nucleon exchange (ONE) contribution were used recently [4] for description of the energy dependence of the differential cross section averaged over the 8° angular interval around 180° obtained in our earlier measurements [1]. The model qualitatively describes also the entire set of the data.

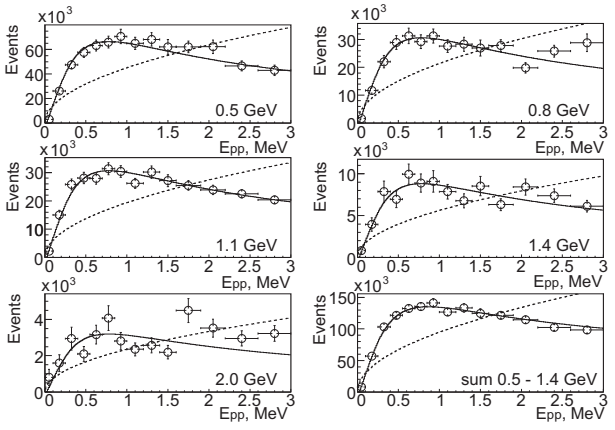

Fig. 1: Spectra of the kinetic energy E_{pp} in c.m.s. of the proton pair. Solid line corresponds to the Migdal-Watson approach, dotted line is the phase space distribution.

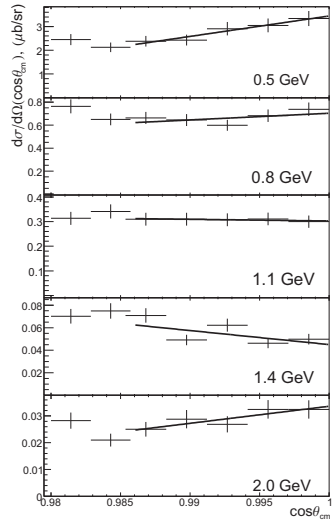

Fig. 2: Dependence of the differential cross section on the neutron emission angle in c.m.s. of the reaction.

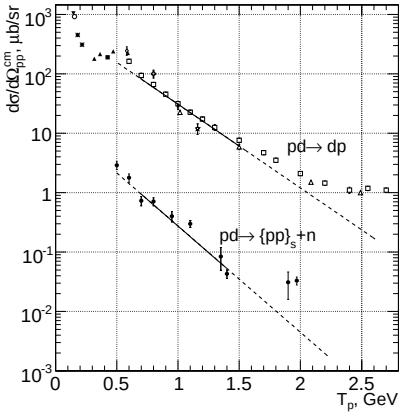

Fig. 3: Energy dependence of the differential cross sections of the $pd \to \{pp\}_s n$ and $pd \to dp$ processes at θ_n=180°. Full circles: present experiment; the $pd \to dp$ data: from [3] and refs. therein.

References:

[1] V.Komarov et al., Phys.Lett. B553 (2003) 179.

[2] O.Imambekov and Yu.N.Uzikov, Sov.J.Nucl.Phys. 52 (1990) 862.

[3] P.Berthet et al., J.Phys.G: Nucl.Phys. 8 (1982) L111.

[4] Yu.Uzikov, J.Haidenbauer, C.Wilkin, Phys.Rev. C75 (2007) 014008.

[1] LNP, JINR, 141980 Dubna, Russia
[2] IKP Forschungszentrum Jülich

A measurement of deuteron breakup at 49 MeV using Silicon Tracking Telescope.

S. Bertelli[1], M.Contalbrigo[1], P.Lenisa[1], M.Tabidze[2], G.Macharasvili[2], P. Thörngren Engblom[3].

Using a proton beam with kinetic energy of 49.3 MeV impinging on a deuterium target only two channels are accessible: $pd \rightarrow pd$ elastic scattering and $pd \rightarrow ppn$ deuteron breakup. The pd elastic scattering was the test channel for the depolarization measurement at COSY February 2008. For this measurement the breakup channel was the background. As described in [1], the Silicon Tracking Telescope (STT) system, with left-right geometry, is optimized to detect charged particles and in particular the pd elastic channel.
A comparative analysis between Monte Carlo and data shows that the STT is also able to identify the deuteron breakup reaction in a so far unexplored kinematical region [4]. Since the neutron is invisible to the STT, in order to identify deuteron breakup it is necessary to detect two stopped protons in the final state. For stopped protons the kinetic energies can be deduced and the missing mass can be calculated using the four-momentum conservation formula (in proton deuteron breakup reactions this should peak at the neutron mass). The information of the process is thus kinematically complete.
Monte Carlo events have been generated, according to February 2008 STT setup, using PLUTO and GEANT code [2]. They are separated into 10^6 elastic events and 10^6 deuteron breakup events. Moreover deuteron breakup simulated events are divided in $5 \cdot 10^5$ neutron spectator, $pd \rightarrow (pp)n$, and $5 \cdot 10^5$ proton spectator, $pd \rightarrow (pn)p$. The condition to detect two protons inside the STT acceptance suppresses the neutron spectator channel, so the analysis is restricted to proton spectator channel, in which the neutron is scattered in the forward direction.

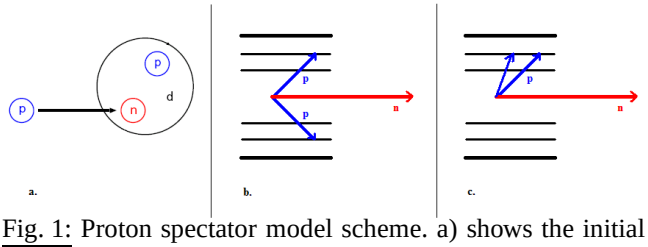

Fig. 1: Proton spectator model scheme. a) shows the initial state in which the proton beam impinges on the neutron of the deuteron target. b) shows the final state in which the neutron is forward emitted and the two protons are scattered at large angles and detected by the STT. In c) is shown a particular final state where the two protons are emitted in the same direction at low relative momentum.

The analyzed data have been taken from three test runs (136, 260, 262) of February 2008 data taking [3]. In the real data, it is necessary to disentangle particles coming from elastic scattering and the ones coming from deuteron breakup using all kinematical information. Since at this energy two final states are possible, by the exclusion of overconstrained elastic events, only breakup events remain. With this aim a double track selection, based on correlations between polar and azimuthal angles has been applied [4]. This coplanarity cut rejects the main concentration of elastic events. But as the deuteron breakup reaction involves three bodies in the final state, the phase space covered is flat and overlaps the elastic phase space and some good events are also inevitably rejected by this cut. A single track cut based on the deposited energy in the detector, discussed in [3], has been applied to reject events with deuteron signal. These two cuts isolate the main concentration of breakup events. Stopped protons are identified by the analysis of STT plots with $\Delta E/E$ method.

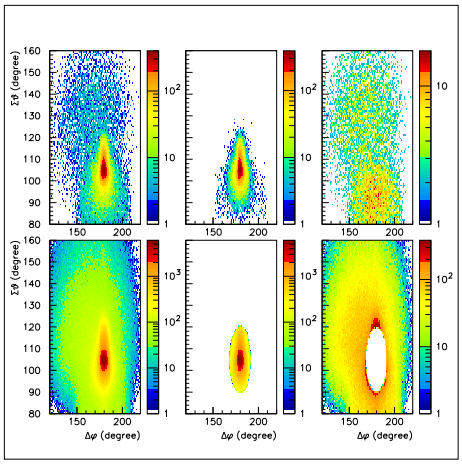

Fig. 2: Non-planarity cut. In the upper panel Monte Carlo data are displayed. Starting from the left: elastic and breakup together, in the middle pure elastic events and on right pure breakup events. In the lower panel the data are shown. From the left: all events without cuts, in the middle the ellipse which contains the majority of elastic events, the right panel shows the application of the non-planarity cut which isolates the main concentration of breakup events.

The reconstruction of breakup events with two stopped tracks has been carried out for four samples, named $2-1$, (see fig:3), $2-2$, $3-1$, $3-2$. The definitions of these samples are based on the number of hits that make up each track. For the case of February 2008 STT setup, a track can be reconstructed using at most three hits. So three types of tracks exist: short track S (one hit per track so the proton reaches the 1^{st} layer of STT), medium track M (two hits which means proton enters the 2^{nd} layer of STT), long track L (three hits, case with a proton stopped in the 3^{rd} layer of STT). The trajectory followed inside the detector by the proton (supposed to be linear) is traced from the hits of the first two layers and, for L track, connected to the third layer hit. In all these cases protons are stopped so the energy is known.

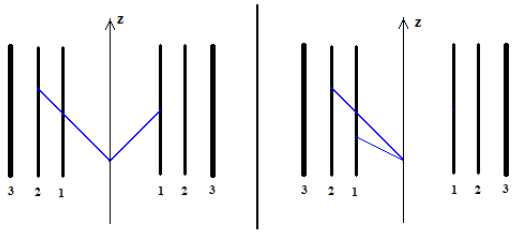

Fig. 3: Sample 2-1 configuration. The two tracks traced by particles can intercept the two opposite side of the detector or intercept the same side of the detector. This can happen also for all other samples.

For a proton stopped in the 1^{st} layer of STT, the track reconstruction procedure is different since only one silicon hit

is available. An S track must be considered together with a track composed at least by two hits. This M or L track can be extended until the point of intersection with the incident beam to have the vertex coordinates; after that, the S track is traced connecting the vertex point to the single hit of the particle supposed to be stopped in the 1^{st} layer. To be sure that this particle is really stopped in the 1^{st} layer of STT, its track is forward extended to check if there is an hit at the point in which it intercepts the STT 2^{nd} layer acceptance. If there is an hit on the 2^{nd} layer it means that the particle did not stop in the 1^{st} layer. All the breakup samples listed above are combination of these kind of tracks.
The Missing Mass method could not be applied as a selection criterion in this particular kinematical and energetic range because the background of incorrectly reconstructed events is also distributed around the neutron mass.

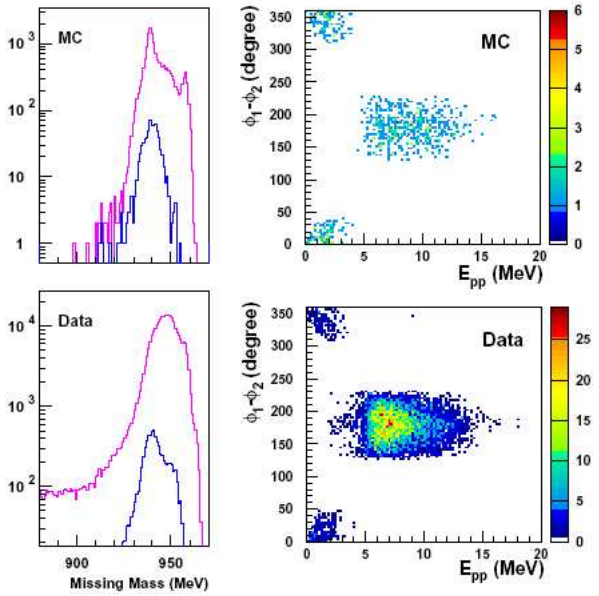

Fig. 4: Missing Mass and azimuthal angles dependence on energy excitation of the di-proton for 2-1 sample. In the upper panel Monte Carlo data and in the lower panel real data are reported. From the left: the magenta line shows the Missing Mass distribution for 2-1 sample for not stopped events, the blue line is the Missing Mass for 2-1 stopped events. The magenta spectrum is broader probably due to the overlap of the deposited energies of the proton and the deuteron. In the right panel two concentrations of events at low E_{pp} are shown. This happens when the two tracks are emitted in the same direction; the one at large E_{pp} realizes when protons hit the two opposite side of the STT. The Monte Carlo events are distributed according pure phase space.

The Missing Mass has been applied only as a control criterion. In general the application of stopped events to the Missing Mass formula generates a more narrow spectra of this function, (see fig:4), and this means that stopped events cuts are quite efficient. The study described in [4] has been developed for a restricted phase space region in which the energy excitation of the pp, di-proton system, E_{pp} is lower then 3 MeV. This corresponds to the cases 3-1 and 2-1 of deuteron breakup reaction with tracks emitted in the same direction, (see fig:4). These events can be analyzed as quasi-elastic scatterings and the di-proton polarization observable A_y^{pp} can be calculated using elastic channel complementary informations.

$$\frac{\sigma^{el}}{\sigma_o^{el}} = 1 + A_y^d \cdot P_B \cdot \cos(\phi^d), \tag{1}$$

where σ^{el} (σ_o^{el}) is the polarized (unpolarized) elastic cross section, P_B the beam polarization and ϕ^d is the deuteron azimuthal angle. A_y^d enters in the definition of the asymmetry parameter ε [3]:

$$\varepsilon^d = P_B \cdot \langle \cos(\phi)^d \rangle A_y^d(\theta), \tag{2}$$

Once ε and A_y are known, the beam polarization can be calcuted. The same procedure can be extended to the quasi-elastic channel, replacing the deuteron with the di-proton system:

$$\varepsilon^{pp} = P_B \cdot \langle \cos(\phi)^{pp} \rangle A_y^{pp}(\theta). \tag{3}$$

since the two channels are measured simultaneously, the beam polarization value in eq.2 and eq.3 is the same and A_y^{pp} can be extracted as:

$$A_y^{pp} = \frac{\varepsilon^{pp}}{\varepsilon^d} \frac{\langle \cos(\phi)^d \rangle}{\langle \cos(\phi)^{pp} \rangle} \cdot A_y^d. \tag{4}$$

The number of identified deuteron breakup events with Energy excitation, $E_{pp} < 3\ MeV$ in three test run are about 800. The statistics of elastic events sufficient for a polarization measurement is of the order of 10^5. The time required for a data taking to obtain 10^5 breakup events for samples 2-1 and 3-1 with $E_{pp} < 3\ MeV$ can be estimated in around 5 days.

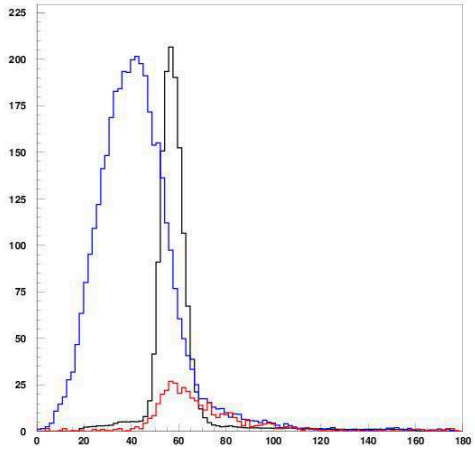

Fig. 5: Black line shows the deuteron polar angle, blue line shows the polar angle of the di-proton system for the 2-1 and 3-1 samples together, red line shows the di-proton polar angle for 2-1 and 3-1 samples with $E_{pp} < 3\ MeV$. The red curve (quasi-elastic channel) overlaps the region occupied by the elastic channel and in this range the calculation of A_y^{pp} can be applied.

References:

[1] A.Mussgiller, Ph.D. thesis, University of Cologne.
[2] M.Tabidze et al., Simulation Results for Depolarization Experiment at 45 MeV.
[3] G.Macharasvili, $p_{\uparrow}d \rightarrow pd$ analysis (EXP_181) Pax Feb-2008 beam time.
[4] S.Bertelli, Diploma thesis, University of Ferrara.

1 INFN, Ferrara, Italy.
2 Tbilisi State University, Tbilisi, Georgia.
3 Dep.of Physics, Stockholm University, Stockholm, Sweden.

Neutron–proton charge–exchange amplitude studies*

D. Chiladze[a,b], A. Kacharava[b], and C. Wilkin[c] for the ANKE collaboration

An understanding of the NN interaction is fundamental to the whole of nuclear and hadronic physics. The database on proton–proton elastic scattering is enormous and the wealth of spin–dependent quantities measured by EDDA collaboration has allowed the extraction of NN phase shifts in the isospin $I = 1$ channel up to a beam energy of at least 2 GeV. The situation is far less advanced for the isoscalar channel where the much poorer neutron–proton data only permit the $I = 0$ phase shifts to be evaluated up to at most 1.3 GeV but with significant ambiguity above about 800 MeV.

The ANKE collaboration has been embarked on a systematic programme to measure the differential cross section and analysing powers of the $dp \to \{pp\}n$ reaction up to the maximum energy at COSY of 1.15 GeV per nucleon, with the aim of deducing information on the np amplitudes. Higher energies per nucleon will be achieved through the use of a proton beam and deuterium target. Spin correlations will also be studied with a polarised beam and target. However, for these to be valid objectives, the methodology has to be checked in a region where the np amplitudes are reasonably well known.

The charge–exchange amplitude of the elementary $np \to pn$ scattering may be written in terms of five scalar amplitudes in the cm system as

$$\begin{aligned} f_{np} &= \alpha(q) + i\gamma(q)(\vec{\sigma}_1 + \vec{\sigma}_2)\cdot\vec{n} + \beta(q)(\vec{\sigma}_1\cdot\mathbf{n})(\vec{\sigma}_2\cdot\vec{n}) \\ &\quad + \delta(q)(\vec{\sigma}_1\cdot\vec{m})(\vec{\sigma}_2\cdot\vec{m}) + \varepsilon(q)(\vec{\sigma}_1\cdot\vec{l})(\vec{\sigma}_2\cdot\vec{l}), \end{aligned}$$

where α is the spin–independent amplitude between the initial neutron and final proton, γ is a spin–orbit contribution, and β, δ, and ε are the spin–spin terms. The one–pion–exchange pole is contained purely in the δ amplitude and this gives rise to its very rapid variation with momentum transfer, which influences very strongly the deuteron charge–exchange observables.

Impulse approximation applied to $dp \to \{pp\}_{^1S_0}n$ then leads to the following predictions for the differential cross section and deuteron spherical analysing powers:

$$\begin{aligned} \frac{\mathrm{d}^4\sigma}{\mathrm{d}t\,\mathrm{d}^3k} &= I\left[S^-(k,\tfrac{1}{2}q)\right]^2\Big/3, \\ I\,it_{11} &= 0\,, \\ I\sqrt{2}t_{20} &= \left[|\beta(q)|^2 + |\delta(q)|^2|\mathcal{R}|^2 - 2|\varepsilon(q)|^2 + |\gamma(q)|^2\right], \\ I\,t_{22} &= \sqrt{3}\left[|\beta(q)|^2 - |\delta(q)|^2|\mathcal{R}|^2 + |\gamma(q)|^2\right]/2\,. \end{aligned}$$

In this $^1S_0$ limit, a measurement of the differential cross section, t_{20}, and t_{22} would allow one to extract values of $|\beta(q)|^2 + |\gamma(q)|^2$, $|\delta(q)|^2$, and $|\varepsilon(q)|^2$ for small values of the momentum transfer $\vec{q}$ between the initial proton and final neutron. However, even if a sharp cut of 1 MeV is placed upon E_{pp}, there still remain small contributions from proton–proton P–waves that dilute the analysing power signal. Such effects must be included in any analysis aimed at providing quantitative information on the neutron–proton amplitudes.

The variation of the cross section with momentum transfer can be found in Fig. 1 for $E_{pp} < 3$ MeV [1]. The impulse approximation describes well the dependence on this variable out to $q = 140$ MeV/c. It should be noted that no adjustment has been made to the model or the experimental data; the luminosity was evaluated independently using the quasi-free $np \to d\pi^0$ reaction.

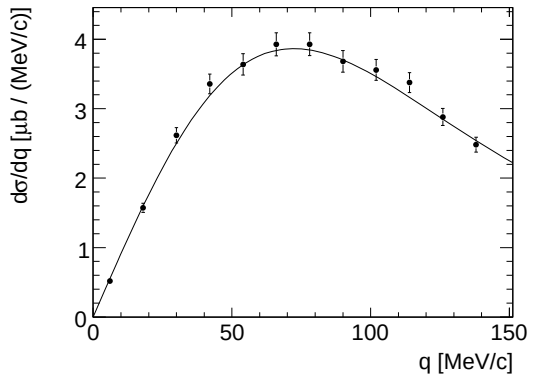

Fig. 1: Unpolarised differential cross section at $T_d = 1.17$ GeV for the $dp \to \{pp\}n$ reaction of $E_{pp} < 3$ MeV compared with the impulse approximation.

Our experimental values of the two tensor analysing powers are shown in Fig. 2 as a function of the momentum transfer.

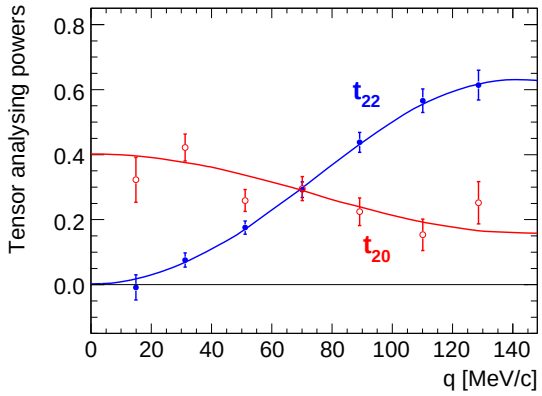

Fig. 2: Spherical tensor analysing powers t_{20} (open symbols) and t_{22} (closed) for the $\vec{d}p \to \{pp\}n$ reaction at $T_d/2 = 585$ MeV for $E_{pp} < 1$ MeV. The solid curves are the impulse approximation predictions.

The rapid rise of t_{22} with q is mainly a result of the fall in the $\delta(q)$ amplitude which, in a simple absorbed one–pion–exchange model, should vanish for $q \approx m_\pi c$. The much smoother variation of t_{20} is also expected, with a gentle decline from the forward value, once again being mainly driven by the fall in the $\delta(q)$ amplitude. All these features are well reproduced by the impulse approximation model using reliable np amplitudes.

Although all the experimental data agree with the impulse approximation model one could, invert the question. How well one could determine the amplitudes if there were no information available from the np phase shifts? Although the data reported here were obtained over short run, these are already sufficient to determine quite well the ratio of the $|\varepsilon(0)|/|\beta(0)|$ in the forward direction. Since little dilution of the t_{20} signal is expected at $q = 0$, all the data for $E_{pp} < 3$ MeV were fitted to a quadratic in q^2 for $q \le 100$ MeV/c.

The value obtained at the origin gives $t_{20} = 0.37 \pm 0.02$, where the error is purely statistical. The uncertainty introduced by the beam polarisation would, however, contribute less than ± 0.01 to this. Since there is little or no dilution of the analysing power by the P-waves at $q = 0$, this result translates into an amplitude ratio of

$$|\varepsilon(0)|/|\beta(0)| = 0.61 \pm 0.03\,.$$

The proof–of–principle achieved here for the method suggests that measurements at higher energies will provide useful information in regions where the existing np database is far less reliable.

References:

[1] D. Chiladze et al., nucl-ex/0811.3288.

[a] IKP FZJ, Germany
[b] IHEPI Tbilisi State University, Georgia
[c] University College London, U.K.
* supported by COSY–FFE

Di-proton identification with positive detector of ANKE*

S. Dymov[a,b], A. Kacharava[c], and H. Shtröher[c] for the ANKE collaboration

Processes involving the deuteron, the simplest nucleus, has been studied intensively both experimentally and theoretically. This attracts special interest to processes in which in the final state a diproton (a proton pair with low excitation energy) is produced instead of a deuteron. This quasi-particle will be almost exclusively in the $^1S_0$ state and the reaction kinematics will be similar to processes with the deuteron.

First experiments with diproton detection at ANKE were performed with the forward detector (Fd) [1]. The emerging proton pairs were identified by evaluating the difference $\Delta_{\rm tof}$ between the times of flight measured with the hodoscope and those calculated from the particle momenta, assuming the particles to be protons [2].

The same method can be applied to the pairs recorded in the ANKE Positive detector (Pd). The Pd can identify each of the particles by the TOF between its Start and Stop scintillation counters. Use of $\Delta_{\rm tof}$ is complementary to this possibility. To measure the Start-Stop TOF the two protons must hit different Start and Stop counters, while the $\Delta_{\rm tof}$ criterion can be used as long as the two particles hit different counters in at least one of the counter groups.

To construct an absolute TOF difference one has to know the delays between the counter hits (we assume here that the channel size is known). The delays can be found using events with the particle type tentatively identified by the Start-Stop TOF. Such identification is possible on the basis of spectra of the raw meantimer difference since pion and proton peaks are clearly separated in such spectra built for each Start-Stop counter combination. The delays of every counter can be defined relative to one of them. Then, the delay between the i-th Start and j-th Stop counter is $\Delta_{ij} = \Delta_i^{Sa} - \Delta_j^{So}$, where the latter two delays are defined relative to the selected reference counter, and the total number of parameters is number of Start and Stop counters minus 1. The delays can be found then by minimizing the expression:

$$\chi^2 = \sum_{Sa,So} \frac{\left(T_i - T_j + \Delta_i^{Sa} - \Delta_j^{So} - \tau_{ij}(l,p,m)\right)^2}{\sigma^2},$$

where T_i, T_j are the times measured in i-th Start and j-th Stop counter and $\tau_{ij}(l,p,m)$ is the Start-Stop TOF calculated from the track length between the counters, the reconstructed particle momentum and the particle mass. The sum is constructed over all the Start-Stop counter combinations in the Pd acceptance. Since the χ^2 form is linear over its parameters, the minimization is equivalent to solving a system of linear equations.

In Fig. 1 the TOF difference $\Delta_{\rm tof}$ measured in Pd is compared with the corresponding difference $\Delta\tau(p_1,p_2)$ calculated under assumption of two protons detected. The proton pairs are located on the main diagonal and are clearly distinguishable from the other pairs of particles. The resolution

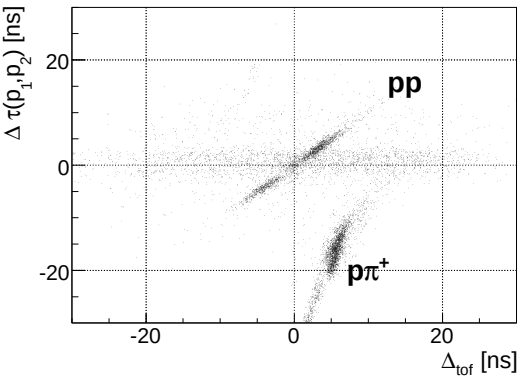

Fig. 1: Measured difference of times of flight of two particles $\Delta_{\rm tof}$ vs. calculated difference $\Delta\tau(p_1,p_2)$

of $\frac{1}{\sqrt{2}}\left(\Delta_{\rm tof} - \Delta\tau(p_1,p_2)\right)$ at 350 MeV proton beam energy is 0.45 ns. The M_X^2 distribution in the process $pp \to \{pp\}_s X$ is shown in Fig. 2 for the events with the diprotons identified by the $\Delta_{\rm tof}$ criterion. One can see two peak, one for single pion production located at $M_X^2 = m_{\pi^0}^2$ and a peak at $M_X^2 = 0$ formed by events from the $pp \to \{pp\}_s\gamma$ process.

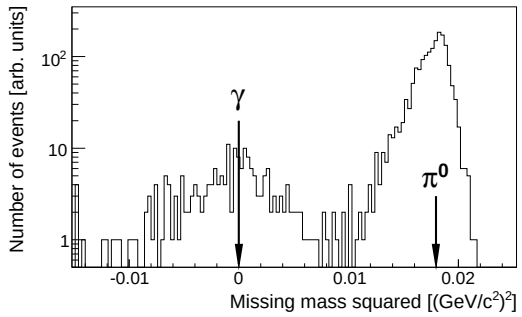

Fig. 2: Missing mass squared distribution in the $pp \to \{pp\}_s X$ process for selected proton pairs.

From such spectra it will be able to obtain the cross section for $pp \to \{pp\}_s X$ reaction over a large angular range.

References:

[1] V. Kurbatov et al., Phys. Lett. B **661**, 22 (2008)
[2] S. Dymov et al., Particles and Nuclei, Letters **2**, 40 (2004)

[a] Erlangen University, Erlangen, Germany
[b] JINR Dubna, Russia
[c] IKP FZ-Jülich, Germany
* supported by COSY–FFE

Energy dependence of the cross section for $pp \to \{pp\}_s\gamma$ at intermediate energies at ANKE*

D. Tsirkov[1,2], T. Azaryan[1], S. Dymov[1,2], V. Komarov[1], A. Kulikov[1], V. Kurbatov[1], G. Macharashvili[1,3], Yu. Uzikov[1] for the ANKE collaboration.

The deuteron photodisintegration $\gamma d \to pn$ is a testing ground of the existing models of NN interaction, see refs. in [1]. Much less is known on the similar reaction of diproton photodisintegration $\gamma\{pp\}_s \to pp$, where $\{pp\}_s$ is a proton pair in $^1S_0$ state. This reaction is more sensitive to the short range NN interaction because the $M1$ transition, which dominates $\gamma d \to pn$ via the $\Delta(1232)$ isobar excitation, is forbidden. Since two protons cannot form a nucleus, the diproton photodisintegration has only been observed with a diproton bound in ^{3}He and heavier nuclei, having large contamination from many-nucleon absorbtion.

The reaction $pp \to \{pp\}_s\gamma$ has been observed with the ANKE spectrometer at COSY-Jülich. It can be considered as inverse photodisintegration of a free $^1S_0$ diproton for photon energies $E_\gamma \approx T_p/2$. A cut on $E_{pp} < 3$ MeV was made to ensure that proton pairs are mainly in the $^1S_0$ state. Missing mass squared distributions show a clear peak at zero mass for proton beam energies of $T_p =$ 0.353, 0.500 and 0.550 GeV [1]. Beam energies of 0.318, 0.625 and 0.800 GeV suggest much less confidence in the existence of the photon peak, but knowing the fact that $\{pp\}_s\gamma$ production actually takes place, these data were analyzed to get energy dependence of the cross section. The integral cross section of the reaction was determined in the range of c. m. angles $0° < \theta_{pp} < 20°$ according to the setup acceptance (see fig. 1).

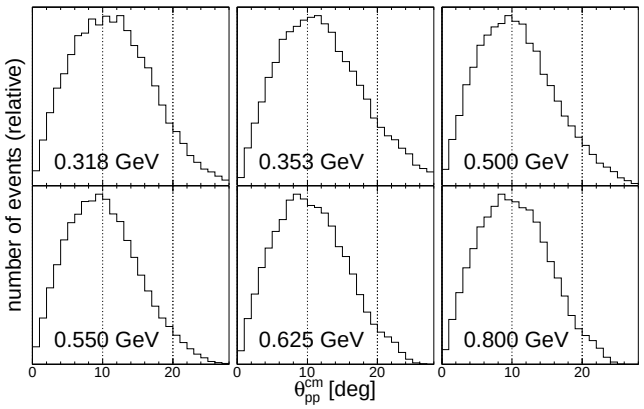

Fig. 1: Simulated setup acceptances for $pp \to \{pp\}_s\gamma$ for 0.318, 0.353, 0.500, 0.550, 0.625 and 0.800 GeV as a function of the diproton c. m. s. angle.

The number of $pp \to \{pp\}_s\gamma$ events was obtained by analyzing the missing mass spectra of the diproton. The procedure of obtaining these spectra is similar to that described in [1,2]. At the beam energy of 0.318 GeV very low statistics is available, allowing us to obtain only the upper limit of the cross section. Extraction of the photon peak for 0.625 and 0.800 GeV is much more complicated compared to [1], since the π^0 peak, which gives the main background, becomes wider, due to kinematical reasons, with increase of the energy. Pion and photon peak shapes were obtained by the Monte-Carlo simulation using program package GEANT3. An example for the procedure of extraction is shown in fig. 2. It is seen, that at 0.625 GeV introducing a photon peak significanly improves χ^2/ndf of the fit in the region around the zero mass: from 62/27 to 24/26. There is no such clear improvement for 0.800 GeV, therefore only the upper limit of the cross section can be estimated for this energy.

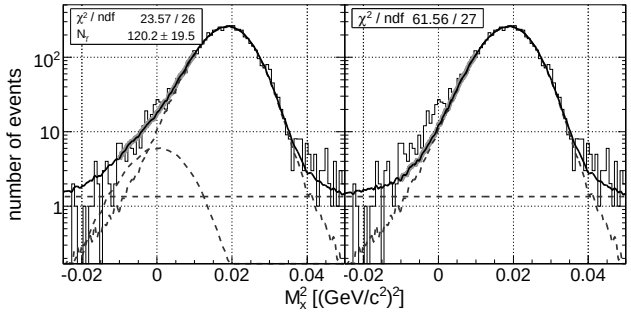

Fig. 2: Example of fitting the missing mass squared distribution for 0.625 GeV (left). Fit without the photon peak (right) is shown for comparison.

Energy dependence of the cross section integrated in the $0° \le \theta_{pp}^{cm} < 20°$ angular range is shown in fig. 3. Luminosities needed for the cross section calculation were taken from [2]. Data for $T_p = 0.353$, 0.500 and 0.550 GeV originated from [1].

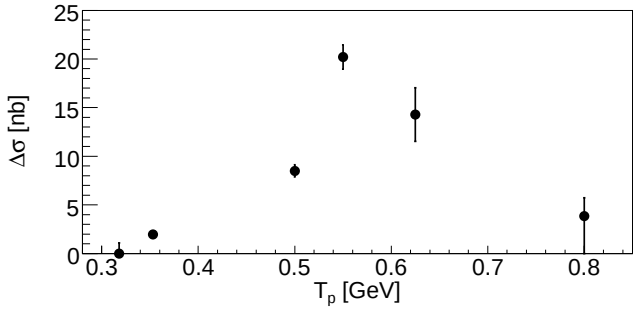

Fig. 3: Energy dependence of the integral cross section in the $0° \le \theta_{pp}^{cm} < 20°$ angular range.

The spectrum obtained shows a clear bump around $T_p = 0.5$–0.6 GeV, which may reflect the influence of the $\Delta(1232)$ excitation, even though this channel is suppressed compared to the similar $np \to \gamma d$ reaction. The Δ-peak would mean that the expected short-range effect is weak.

References:

[1] V. Komarov et al., Phys. Rev. Lett. **101** 102501 (2008).
[2] V. Kurbatov et al., Phys. Lett. B **661** 22 (2008).

[1] LNP JINR, 141980 Dubna, Russia
[2] IKP FZJ, 52425 Jülich, Germany
[3] HEPI TSU, 0186 Tbilisi, Georgia
* supported by COSY-FFE

The cross section of the reaction $pp \to \{pp\}_s\gamma$ in the Δ-isobar region

Yu. N. Uzikov[a]

Quasi-binary reactions $AB \to \{pp\}_sC$ with formation of a proton pair at small excitation energy $E_{pp} = 0 - 3$ MeV, i.e. the $^1S_0$ diproton $\{pp\}_s$, are of great interest at high transferred momenta since transition amplitudes of these reactions require high momentum components of the pp-wave function. In comparison to very similar (in kinematics) reactions $AB \to dC$ with the final deuteron d, the reactions with the diproton are expected to give more definite information on short-range NN-dynamics. The reason is that the contribution of non-short range mechanisms related to excitation of the Δ-isobars in intermediate states is expected to be strongly suppressed for the $AB \to \{pp\}_sC$ reactions as compared to the $AB \to dC$ due to isospin symmetry and conservation of angular momentum and parity. So, in the reaction $pd \to \{pp\}_sn$ this suppression is given by the factor $\frac{2}{9}$. Furthermore, the intermediate S-wave ΔN state is completely forbidden in the reaction $pp \to \{pp\}_s\pi^0$. Similarly, in the reaction $pp \to \{pp\}_s\gamma$ direct excitation of the $\Delta-$isobar, dominating the $\gamma d \to pn$ reaction via $M1$ transition is also forbidden [1].

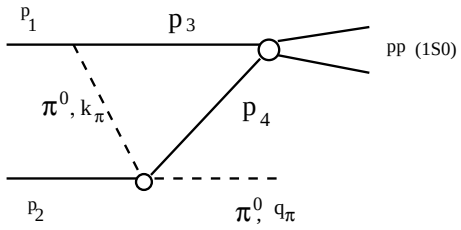

Fig. 1: The one–pion–exchange (OPE) mechanisms considered for

Contrary to those expectations, the reactions $pp \to \{pp\}_s\pi^0$ [2] and $pp \to \{pp\}_s\gamma$ [3] recently measured in forward direction for beam energies $0.5 - 2.0$ GeV and $0.35 - 0.55$ GeV, respectively, demonstrate prominent peaks in the $\Delta(1232)$-isobar region. In the deuteron breakup reaction $pd \to \{pp\}_sn$ the $\Delta(1232)$ peak is nonvisible in the energy dependence of the cross section for the backward scattered neutron [4], however, theoretical analyses [5] suggest, that the Δ contribution dominates in this reaction at $0.5 - 1.3$ GeV.

Observation of the Δ peaks in the data on the reactions $pp \to \{pp\}_s\pi^0$ [2] and $pp \to \{pp\}_s\gamma$ [3] would mean that the high momentum component of the NN-wave function, which might be hidden by the Δ- contribution in the corresponding reactions with the deuteron, is actually rather week. In other words, new data [2, 3], most likely, confirm the result of the previous analysis of the reaction $pd \to \{pp\}_sn$ [5], which suggests softness of the NN-interaction potential at short distances. To some extent this conjecture is supported by the one-pion exchange (OPE) model calculation [6], which allows to explain the observed shape of the cross section of the reaction $pp \to \{pp\}_s\pi^0$ by means of the $\Delta(1232)$-isobar excitation in the subprocess $\pi^0 p \to \pi^0 p$ (see Fig.1).

Here we consider the reaction $pp \to \gamma\{pp\}_s$ within the OPE model. The relevant OPE diagram is similar to those in Fig. 1, but with the subprocess $\pi^0 p \to p\gamma$ in the down vertex. Although there is no direct contribution of the intermediate S-wave ΔN states in the reaction $pp \to \gamma\{pp\}_s$, the non-direct excitation of the $^5S_2$ ΔN state is possible in the E2 transition. The OPE model of the reaction $pp \to \{pp\}_s\gamma$ allows to account for the Δ contributions via the subprocess $\pi^0 p \to p\gamma$. The result of the OPE calculations are shown in Fig.2. One can see that this model explains the observed in Ref. [3] rise of the cross section almost quantitatively. The second bump at 1.6 GeV is caused by the energy dependence of the $\pi^0 p \to p\gamma$ cross section [8] and related to excitation of more heavy nucleon isobars.

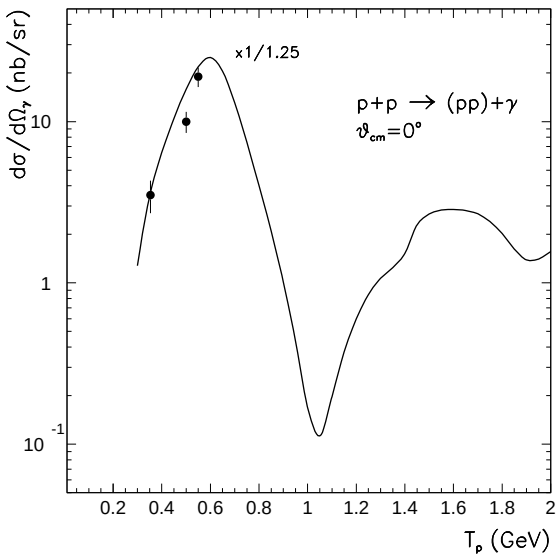

Fig. 2: The forward differential cross section of the reaction $pp \to \{pp\}_s\gamma$ versus the beam energy. The curve (multiplied by 0.8) is the OPE model calculation. Data (•) are taken from Ref. [3].

[a] Joint Institute for Nuclear Research, Dubna, Russia

References:

[1] P. Wilhelm, J.A. Niskanen, H. Arenhövel, Nucl. Phys. **A 597**, 613 (1996).
[2] V. Kurbatov et al., Phys. Lett. **B 661**, 22 (2008).
[3] V. Komarov et al., Phys. Rev. Lett. **101** (2008) 102501.
[4] V. Komarov et al., Phys. Lett. **553** (2003) 179.
[5] J. Haidenbauer, Yu.N. Uzikov, Phys. Lett. **B 562**, 227 (2003).
[6] Yu.N. Uzikov, arXiv:0803.2342 [nucl-th].
[7] Yu.N. Uzikov, In: Baldin ISHEPP XIX (Dubna, Russia, 29 September 29 - October 4, 2008, Dubna)
[8] R.A. Arndt et al., Phys. Rev. C **48** (1993) 1926; http://gwdac.phys.gwu.edu.

Two pion production study at ANKE

S. Dymov[a,b], A. Kacharava[a], V. Komarov[b], A. Kulikov[b], V. Kurbatov[b], G. Macharashvili[b,c], F. Rathmann[a], H. Ströher[a], Yu. Uzikov[b], C. Wilkin[d] *for the* **ANKE** *Collaboration*

The ABC effect, which is a enhancement of the two-pion invariant mass spectrum near its threshold, has presented a puzzle for hadron physicists for almost fifty years. It was first observed in a $pd \to {}^3\mathrm{He}X$ missing-mass experiment [1] and further confirmed in other reactions.

The aim of the experiment carried out with the ANKE setup was the study of the $pp \to \{pp\}_s X$ reaction under the condition that the excitation energy in the final diproton system is low, $E_{pp} < 3$ MeV. The experiment has been set up to investigate the reaction at four proton beam energies $T_p = 0.8$, 1.1, 1.4, and 2 GeV.

The proton beam was directed onto a hydrogen cluster jet target with an areal density of $2 \cdot 10^{14} atoms/cm^2$. Positively charged particles were registered in the forward detectors of ANKE setup. Particle momenta were reconstructed by the back-tracing Runge-Kutta method through the analysing magnetic field. The momentum reconstruction uncertainty is equal to 1% on average [2]. Proton-pairs were identified by the time-of-flight difference Δt measured by the hodoscope and the same difference calculated using the reconstructed particle momenta assuming proton masses. The remaining background does not exceed 0.1%.

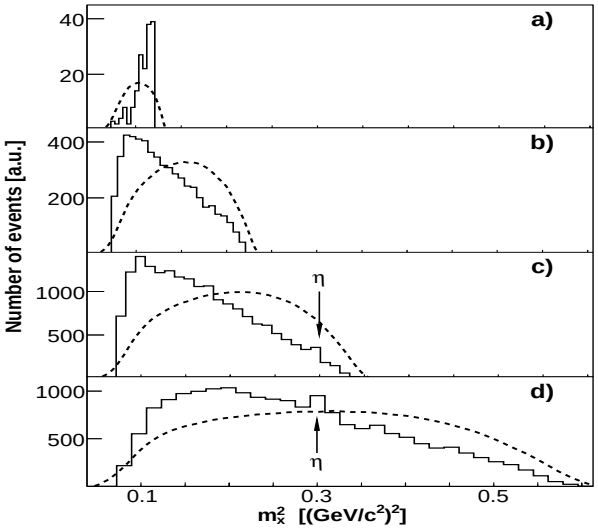

Fig. 1: Distribution in missing-mass squared for the $pp \to \{pp\}_s X$ reaction for $E_{pp} < 3$ MeV and $\cos\vartheta_{pp} > 0.95$ at a) 0.8, b) 1.1, c) 1.4, and d) 2.0 GeV. The η signal is seen at the expected position for the two higher energies. The lines represent normalized simulations within a phase-space model.

Fig.1 shows the pp-system missing-mass squared distribution for the multipion region at different beam energies. Two protons in the relative ${}^1S_o$ state were selected by applying the cut on the excitation energy $E_{pp} < 3 MeV$. The selected proton pairs weighted by the detection efficiency are distributed isotropically in the pair rest system which reveals that they actually are in the ${}^1S_o$ state. Event distribution over the two proton excitation energy E_{pp} also clearly shows the *final state interaction* enhancement corresponding to the ${}^1S_o$ state. The events in the forward cone with $cos\vartheta_{pp} > 0.95$ were selected for the further analysis.

Only at the highest energy $2 GeV$ there might be any significant contribution of three-pion production while at the lower energies it is negligible. Therefore, the model description should be based upon the assumption that two-pion production dominates.

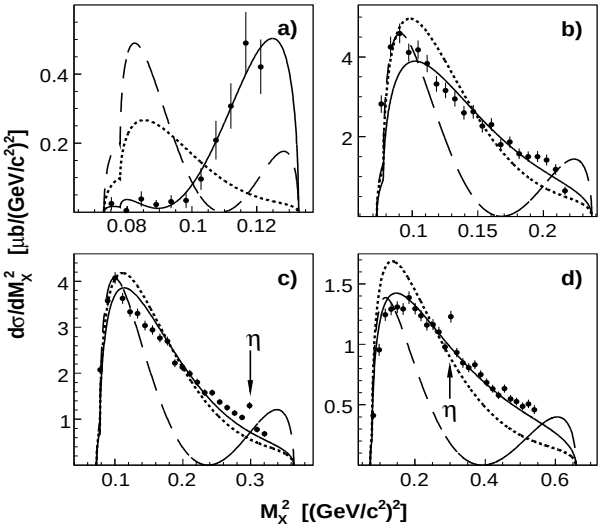

Fig. 2: The $pp \to ppX$ differential cross section with statistical errors as a function of the square of the missing mass at a) 0.8, b) 1.1, c) 1.4, and d) 2.0 GeV for $E_{pp} < 3$ MeV and $\cos\vartheta_{pp} > 0.95$. The η peaks are indicated. Events were simulated using Eq. (1) with $A_D = 0$ (long dashes), with $A_S = 0$ (short-dashed), and with the best fit of A_S/A_D ratio (solid line).

Fig.2 shows the measured differential cross sections and the results of implementing a simple double–Δ model. The matrix element squared (averaged over the pion angles) for this model can be written in the form

$$\langle|\mathcal{M}|^2\rangle = |A_S(\alpha^2 k^2 - \beta^2 q^2) + \tfrac{1}{2} A_D \alpha^2 (3k_z^2 - k^2)|^2 + \tfrac{1}{5}|A_D|^2 \beta^4 q^4 \,. \quad (1)$$

where α and β are the kinematical factors, q is the ππ pair momentum in c.m.s, and k pion momenta in the ππ system. The S and D–wave amplitudes A_S and A_D are scalar functions that may depend upon T_p.

We have measured the differential cross section for the $pp \to \{pp\}_s(\pi\pi)^o$ reaction at four beam energies from 0.8 to 2.0 GeV under conditions mentioned above. Strong structure is observed in the missing-mass variable, with a peak in M_x whose position varies with beam energy. Gross structure of the distributions is well described within the ΔΔ model. Exclusive measurements of $pp \to \{pp\}_s(\pi\pi)^0$ over a wider range of angles would provide more stringent tests of the phenomenological description.

References:

[1] A. Abashian *et al.*, Phys.Rev.Lett. **5**, 258 (1960).
[2] S. Dymov *et al.*, Part. Nucl. Lett. **2** (119), 40 (2004).

[a] IKP, FZ-Juelich, Germany
[b] JINR, Dubna, Russia
[c] Tbilisi State University, Tbilisi, Georgia
[d] University College, London, UK

Measurement of the $pn \to d\omega$ reaction at ANKE

S. Barsov[1], R. Schleichert[2], D. Chiladze[3], S. Dymov[3], A. Dzyuba[1], D. Oellers[2], S. Merzlyakov[2], S. Mikirtychyants[1,2], M.Nekipelov[2], S. Trusov[2], P. Wüstner[4], C. Weidemann[2] for the ANKE collaboration.

As it was discussed in [1], the study of ω-production in the *pn* isospin channel is important to clarify the production mechanism and to test the OZI-rule in ϕ/ω cross section ratio. The only published data on the $pn \to d\omega$ total cross section [2] are too poor for this purpose. Moreover, neither in the *pp* nor in the *pn* channels differential cross sections are so far measured below an excess energy of Q=90 MeV. Now, as a result of the experiment successfully carried out at ANKE in the end of July 2008, high-statistics data for the determination of total and differential cross sections of the $pn \to d\omega$ reaction in 10 MeV to 90 MeV Q-range will be obtained.

The measurements were done at two proton beam energies of 2.124 GeV and 2.219 GeV. Two Silicon Tracking Telescopes were installed at 3cm distance to the left (STT1) and the right (STT2) from the ANKE deuterium cluster target to detect low energetic particles in coincidence with fast particles going into the ANKE Forward detector (Fd). Besides the acceptance increase to about 2 *sr*, the use of 2 STT allows to cover the full c.m. angular range up to Q=70MeV. Each of the STT, consisting of 3 double-side segmented detectors (70μm / 300μm / 5mm), provides a clean identification (Fig. 1) and momentum determination for particles stopped in either the 2nd or the 3rd detector. Detected in STT1, deuterons from the pd elastic scattering will be finally used for the normalization.

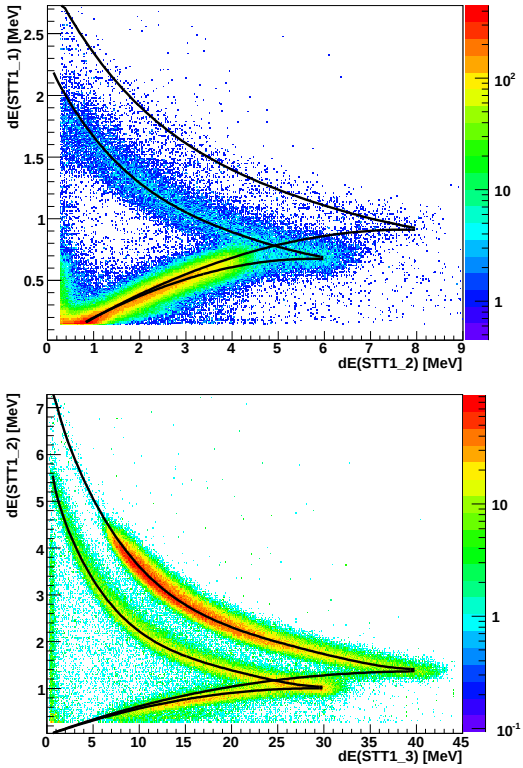

Fig. 1: dE-E plots for the STT1. The upper panel shows the energy loss correlation for the 1st and the 2nd detectors, the lower panel - the same for the 2nd and the 3rd ones. Expected dE-E dependences for protons and deuterons are shown by solid lines. Low energetic deuterons are suppressed because corresponding protons are beyond the Fd angular acceptance.

Since at ANKE the $pn \to d\omega$ reaction can be identified by the missing mass technique only, one has to pay a special attention to the missing mass reconstruction. This can be verified using the pd and the quasi-free NN elastic scattering reactions which are very sensitive to the actual detector positions. The alignment of the silicon detectors as well as of the Fd multiwire chambers was investigated using pd elastic scattering. The relative displacement of detectors was found to be very small - 0.2mm for both the STT and about 0.6mm for the Fd chambers. Having these corrections fixed, missing mass distributions for the $pd \to ppX$ reaction were obtained (see Fig. 2). One of protons in final state was selected using the dE-E dependence to be stopped in the 2nd detector of either STT1 or STT2. Any particle detected in coincidence by the Fd was considered as the second proton because the admixture of pions and deuterons is known to be less than 5%. Peaks corresponding mainly to the quasi-free NN elastic scattering are well positioned at the neutron mass with only a small background.

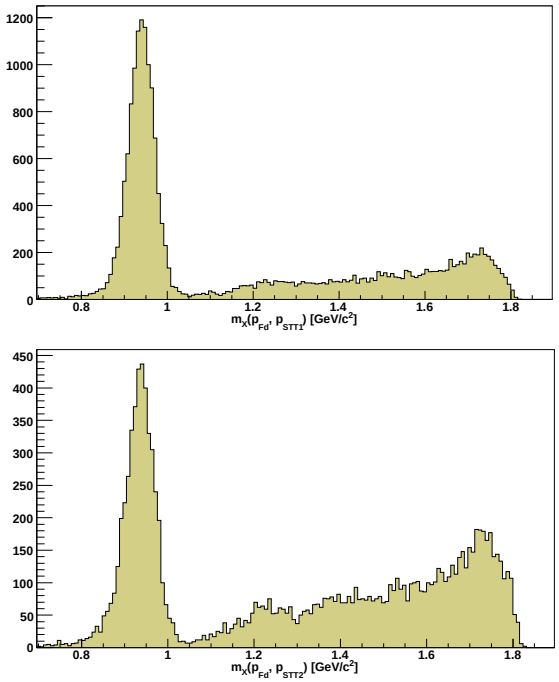

Fig. 2: Missing mass of two protons. One proton is detected in the Fd and other either in the STT1(upper panel) or in the STT2(lower panel).

The further data analysis is in progress. Taking into account the knowledge from our previous measurement [2], the total statistics collected in this experiment can be roughly estimated from the inelastic continuum (Fig. 2) to be, at least, 100 times higher than it has been before.

References:

[1] Proposal COSY-175 (2007)
[2] S.Barsov et al., EPJ A 21, 521 (2004)

1 PNPI, 188350 Gatchina, Russia
2 IKP, FZ Jülich, 52425 Jülich, Germany
3 JINR, 141980 Dubna, Russia
4 ZEL, FZ Jülich, 52425 Jülich, Germany

COSY Beam Calibration within the η Mass Measurement at COSY-ANKE

P. Goslawski*, M. Mielke*, M. Papenbrock*, T. Rausmann*, A. Täschner* and A. Khoukaz*
for the ANKE-Collaboration and the COSY-Crew+

Recent measurements on the η-meson mass performed at different experimental facilities (i.e. CERN-NA48, COSY-GEM, CESR-CLEO, DAΦNE-KLOE, MAMI-Crystall Ball) resulted in very precise data but differ partly by up to more than eight standard deviations, i.e. $0,5\,\mathrm{MeV/c^2}$ [1]. In order to clarify this situation a new high precision measurement using the ANKE spectrometer at the COoler SYnchrotron has been realised in March 2008.

Using the two-body reaction $d\,p \rightarrow {}^3\mathrm{He}\,\eta$ at low excess energies the η-mass can be determined only from pure kinematics by the determination of the production threshold. Therefore, twelve data points at fixed excess energies in the range of $1 - 10\,\mathrm{MeV}$ were investigated. The final momentum p_f of the ^{3}He-particles

$$p_f\,(s) = \frac{\sqrt{\left[s - (m_{^3He} + m_\eta)^2\right] \cdot \left[s - (m_{^3He} - m_\eta)^2\right]}}{2 \cdot \sqrt{s}}\ ,$$

measured with high precision using the ANKE spectrometer, is very sensitive on the value of the η-mass and the total energy $\sqrt{s}$ which is completely defined by the masses of the initial particles and the momentum of the deuteron beam. For a precise determination of the production threshold two quantities, the final momentum of the ^{3}He-particles and the beam momentum have to be measured with high accuracy.

To obtain a total precision of $\Delta m_\eta < 50\,\mathrm{keV/c^2}$ on the η-mass, which is comparable to other experiments, the beam momentum has to be determined with an accuracy of $\Delta p/p < 10^{-4}$, reached only in one test measurement at COSY [2]. This can be achieved by using an artificial spin resonance, induced by a horizontal rf-magnetic field from a solenoid to depolarize a vector polarized accelerator beam [3]. The frequency of the depolarizing resonance f_r depends on the kinematical γ-factor (i.e. the beam momentum $p = m\sqrt{\gamma^2 - 1}$) and the beam revolution frequency f_0 via the resonance condition:

$$f_r = (k + \gamma G)\, f_0\ ,$$

where k is an integer and G the gyromagnetic anomaly of the beam particle (for deuterons: $G_d = -0.142987272$).

To obtain the exact beam momentum for each energy the revolution frequency f_0 and the spin resonance frequency f_r have to be measured with high accuracy.

By studying the Schottky spectra, stored within four days, the revolution frequency for each energy was determined with an accuracy of $\Delta f_0/f_0 \approx 4 \cdot 10^{-6}$, with an uncertainty dominated by the systematic uncertainty of the Schottky measuring system.

The position of the resonance can be determined accurately by operating the rf-solenoid with fixed amplitude at several frequencies around the induced depolarizing resonance for a certain time and measuring the remaining polarisation with the EDDA-detector afterwards. For each energy the spin resonance spectrum was measured twice at a four days interval to investigate possible resonance frequency shifts over time. Between the two measurements the resonance frequency may vary up to 20 Hz, which is caused by a shift of the orbit length up to 3 mm. As an important by-product the spin resonance method enables for the determination of the orbit length for COSY (183.44 m) with an accuracy of less than 0.3 mm [4]. Figure 1 presents the spin resonance measurements for all twelve energies, normalized with respect to the polarisation as function of the solenoid frequency. The shapes of the resonance curves, especially

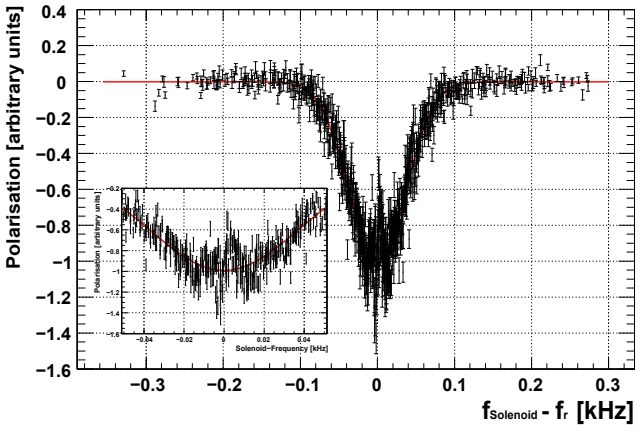

Fig. 1: Normalized spin resonance spectrum. The inlay shows the structure in the resonance maximum.

the structures in the resonance maximum are argued to be dominiated by synchrotron oscillations of the beam particles induced by the barrier bucket cavity. Despite this structure the achievable precision in beam momentum by analysing the spin resonance spectra is better than $\Delta p/p < 8 \cdot 10^{-5}$, i.e. the beam momentum in the threshold range of $3100 - 3200\,\mathrm{MeV/c}$ was estimated with an accuracy of less than $250\,\mathrm{keV/c}$ [4]. The uncertainty is dominated by the systematic shift in orbit length during the measurement. In comparsion to the usual momentum determination from the nominal orbit length and the revolution frequency the spin resonance method allwos for an improvement of $\Delta p/p$ of more than one order of magnitude.

Supported by COSY-FFE

References:

[1] C. Amsler et al., Phys. Lett. B **667**, 1 (2008)
[2] H. Stockhorst et al., IKP An. Rep. 2007, **33** (2007)
[3] V.S. Morozov et al., Phys. Rev. Spec. Top. Accelerators and Beams **8**, 061001 (2005)
[4] P. Goslawski, Diploma thesis, Westfälische Wilhelms Universität Münster (2008)

* Institut für Kernphysik, Westfälische Wilhelms Universität Münster, 48149 Münster, Germany
+ Institut für Kernphysik, Forschungszentrum Jülich, Germany

1.2 COSY-TOF

Λ production in the reaction $pn \rightarrow pK^0\Lambda$ using a deuterium target

M. Krapp*, W. Eyrich*, C. Pizzolotto* and W. Schroeder* for the COSY-TOF collaboration

An essential part of the program at COSY-TOF aims at the production of Λ-, Σ^0- and Σ^+-hyperons in proton-proton collisions and in a further stage also in proton-neutron reactions (including Σ^--hyperons) by use of a deuterium target. Up to now predominantly Λ-production was investigated in detail. One of the main results is a strong influence of various N^*-resonances and significant contribution of the p-Λ final state interaction. These results where especially obtained from the Dalitz plots. The study of isospin relations between different final states allows extended access to the dynamics of the reaction especially including the role of N^*-resonances in the different reaction channels (see e.g. [1]). Clearly this requires additional measurements with a deuterium target in order to investigate hyperon production with the pn entrance channel. The TOF detector is well suited to investigate the following reactions: $pn \rightarrow pK^0\Lambda$, $pn \rightarrow nK^+\Lambda$, and $pn \rightarrow nK^0\Sigma^+$. In particular the reaction $pn \rightarrow pK^0\Lambda$ with two delayed decay vertices (K_s and Λ) has a unique signature allowing a complete reconstruction of the events. It provides a clean trigger condition. First exploratory measurements with a deuterium target using a beam momentum of $3.06 GeV/c$ were performed in order to see whether a future investigation of hyperon production in pn induced reactions is feasible. Due to its low energy, the spectator proton in the deuterium target can not be detected. Nevertheless the Fermi motion of the neutron within the deuterium can be measured because of the kinematically complete reconstruction of the events.

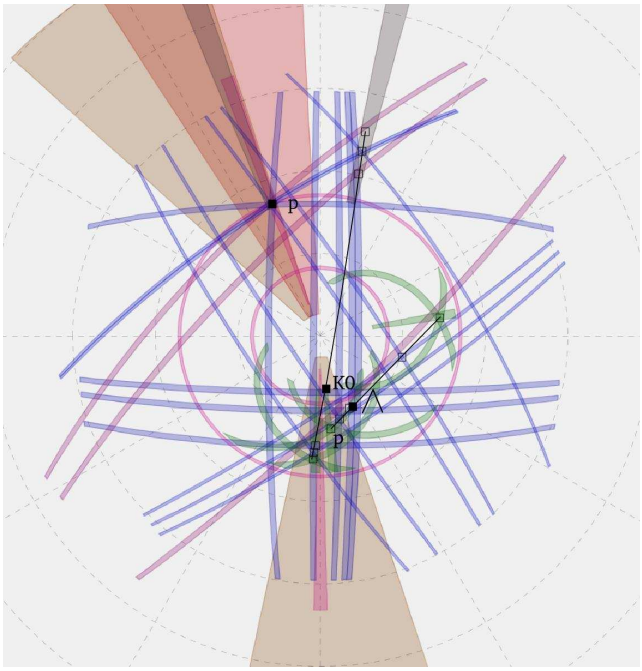

Fig. 1: Reconstructed Monte Carlo event in $\phi - \theta$−projection with the reconstructed tracks of two decays (K^0 and Λ) and the primary track of the proton. The determined missing mass of the Λ particle as well as the reaction topology are consistent with the simulation.

The extention of the analysis program for data gathered from deuterium measurements for the reaction $pn \rightarrow pK^0\Lambda$ was already successfully done. The trigger condition used for this

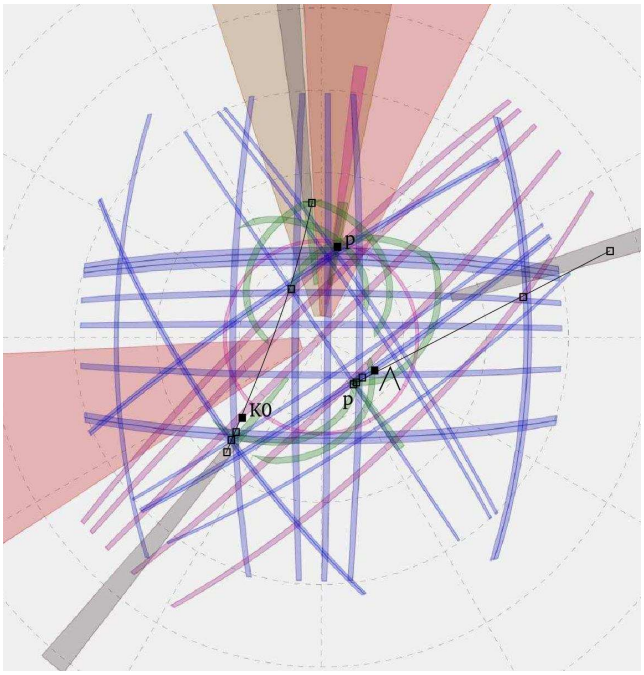

Fig. 2: Typical event candidate of the reaction $pn \rightarrow pK^0\Lambda$ from the data taken at beam momentum $3.06 GeV/c$. The reconstructed tracks are indicated. The missing mass $1.14 GeV/c^2$ determined by the analysis program is in good agreement with the the Λ mass.

analysis allows one or two coincident hits in the starttorte and claims at least four hits in the stop detector. This condition takes into account that there are two secondary vertices which lead to four tracks. The K^0 vertex has to be distinguished from the Λ vertex which requires a mass reconstruction algorithm that is able to select the vertices with the best solution. For the optimization, which is still in progress, Monte Carlo simulations are used. A typical reconstructed event found in Monte Carlo data is shown in fig. 1 which shows the detector elements fired by the reaction products. The track of the primary proton is seen in the common intersection point of detector elements at different distances from the target, whereas the hits of the chargered particles from the delayed decays of Λ and K_s correspond to approximately straight lines connecting the hits in the differend subdetectors in the correct order.

Also first tests with measured data have been performed. The preliminary results are in agreement with the expectation regarding the event topology and the precision of the reconstruction of the kinematic variables including the missing mass of the Λ hyperon. A typical event candidate is shown in fig. 2. The analysis of this event gives a value of $1.14 GeV/c^2$ for the Λ mass.

After finishing the optimization of the analysis program the available event sample will be completeley analysed including differential observables.

References:

[1] K. Tsushima, A. Sibirtsev, A.W. Thomas, Phys. Rev. **C 59** (1999) 369.

Status of the Straw Tube Tracker at COSY-TOF

M. Roeder, V. Kozlov, S. Orfanitski, J.Ritman, P. Voigtlaender, P.Wintz, for the COSY-TOF Collaboration

Introduction The Straw Tube Tracker (STT) at COSY-TOF is an essential upgrade of the existing apparatus which is mandatory for the *Strangeness Physics at COSY-TOF* program. It accounts for excellent tracking and vertex reconstruction of the primary and delayed decay tracks of the $pp \to pK^+\Lambda$ reaction. This will allow for instance the measurement of the Λ-Nucleon scattering length to an accuracy better than 0.3 fm.
The STT consists of 3120 straws with 10 mm inner diameter and 1050 mm length, close packed in 30 layers at 3 different azimuthal alignments. These are operated at 1.25 bar Ar/CO_2 (10% CO_2) absolute pressure in the TOF vacuum so that they are self supporting despite their mylar wrapping being only 30 μm thick. As a result the total radiation length of all 30 layers amounts to only $\approx$1 %.

Installation The installation of the STT was completed in July 2008. This included mounting at the inner side of the TOF front-endcap, delivery of HV and gas supplies and setup of the complete readout electronics.
A pressure controlled gas system for the purpose of driftgas mixing, analysing and logging was set up. The control rack is located outside the TOF beam area and is connected to the STT via 40 m long stainless steel pipes, what allows for permanent user access.
For the readout system delivered by ZEL, electronic components for eight crates of ASD-8 discriminators and GPX TDCs were tested and installed next to the TOF detector. In total 40.5 km signal cables were mounted and more than 5000 connectors were plugged. A dedicated flange at the TOF front cap, developed by ZAT, provides the connection of the 3120 signal lines. Since it also carries the 75 high voltage channels and 30 gas lines the total number of vacuum feed-throughs adds up to $\approx$8000.
As for the operation with HV it turned out that a TOF vacuum of $< 7 \times 10^{-3}$ mbar is required for stable conditions. For the STT this demands that the gas leakage is at the permeation level. Although tested for that during several month beforehand, the leak rates of some straw layers increased during operation in vacuum. To ensure stable conditions for HV, we had to evacuate 6 pairs of layers sharing one gas support each. The remaining 18 layers on the other hand retained the same leak tightness during 6 months of operation in vacuum. The cause is yet unclear and will be investigated in 2009 even though the number of working layers isr sufficient for the physics program.

Commissioning During the three day commissioning beam time with 3 GeV protons in August and December 2008 the detector and the readout electronics were set up and tested under experiment conditions. There was sufficient data collected to determine the efficiency and resolution, as well to calibrate the STT[1].
In Figure 1, the number of hits per straw in the first two layers are shown. The straws are numbered 0-103 for the first layer and 104-207 for the second, respectively. Since this numbering is related to the position in the detector one can clearly see the structure of reaction particles in each layer with the beam axis around 50 and 160. It is remarkable how smooth the shape is. This proves that the discriminator thresholds, shared by groups of 16 straws, are well set and promises good results on the efficiency. Also note that the number of "dead" channels is negligible.

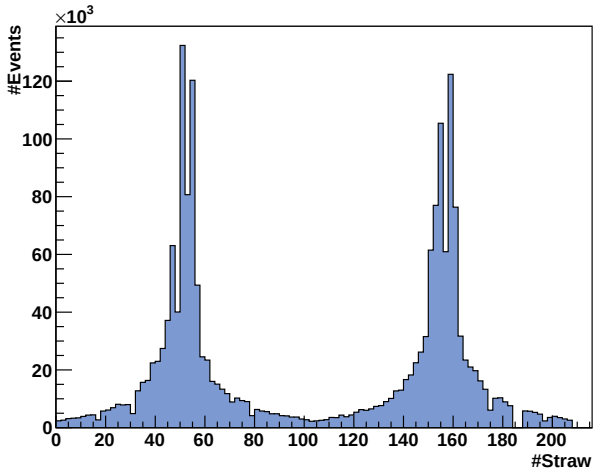

Fig. 1: Number of hits per straw in the first two layers. The straws are numbered 0-103 for the first layer and 104-207 for the second, respectively.

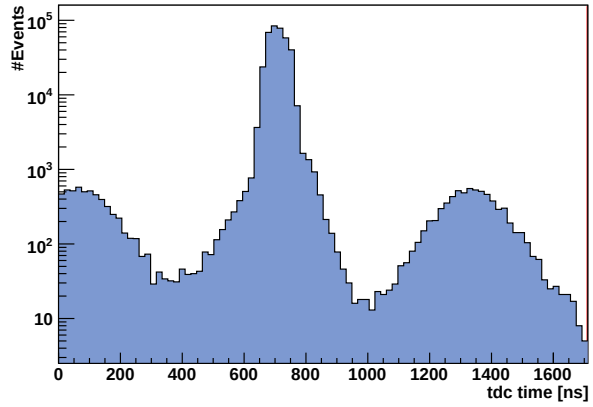

Fig. 2: TDC spectrum for 16 straws. Events from triggered reactions lie between 650 and 750 ns. Background events are below the 1% level.

In Figure 2, the spectrum from 16 TDC channels is shown. The events from triggered reactions are found between 650 and 750 ns. See [1] and [2] for a detailed view. They lie on top of background events, correlated to the beam circulation time in COSY showing bumps every $\approx$650 ns. The background events are more than two orders of magnitude suppressed compared to signal events. A measure for noise is given by the number of entries between the bumps which is about another two orders of magnitude lower. Thus we can conclude that the detector and the readout work well and deliver high quality data with a background below the 1 % level.

References:

[1] First calibration results of the STT for COSY-TOF, IKP Annual reports (this volume).
[2] Commissioning of the COSY-TOF Straw Tracker, IKP Annual reports highlights (2008), p. 10.

First Calibration Results of the Straw-Tube-Tracker for COSY-TOF

P. Voigtländer, V. Kozlov, S. Orfanitski, J. Ritman, M. Röder and P. Wintz
For the COSY-TOF collaboration

In summer 2008 the new COSY-TOF Straw-Tube-Tracker (STT) was installed and afterwards a few days of beam time were used for commissioning of the detector. Data from the reactions $pp \rightarrow pp$ and $pp \rightarrow d\pi^+$ are employed for the calibration of the STT.

The calibration of the STT is realised in several steps, beginning with the classification of the data and the comparison with the simulation to understand all effects.

The shape of the straw drifttime distribution was studied using the Garfield package with the experimental gas parameters and high voltage as input and tested for the necessary number of primary electrons to exceed the discriminator threshold. A comparison between the TDC data and the simulated drifttime spectrum, based on a homogeneous illumination of the straw tube and offset-added and scaled to the TDC spectrum, is shown in Fig. 1. As can be seen there is a good agreement within 5ns using a sensitivity to 9 primary electrons in the simulation. With 2-3 electrons per cluster this corresponds to an average 3 to 4 clusters. For the chosen gas mixture ($Ar/CO_2 = 90\%/10\%$) the simulation of a 1 GeV proton track through the center of a straw tube delivers a mean number of about 100 primary electrons per cm. From this we get the information to consider for the later calibration a minimum isochrone radius of $450\mu m$.

The comparison of the TDC time distributions for different straws shows that they agree within 5 ns (Fig. 2). This gives a hint that the calibration of one straw could be applied to the whole STT as a good approximation.

To confirm that for all straws the difference (t_{diff}) between minimal and maximal TDC time (t_{tdcmin} and t_{tdcmax}) of the events in the TDC spectrum, that is the event spectrum, are compared for the straws with at least 2000 entries to guarantee sufficient statistics. To get t_{tdcmin} and t_{tdcmax} the rising and falling edges of the event spectrum are fitted by a convolution of a Heaviside function describing the idealised spectrum, and a Gauss function describing clustering effects (especially near to the wire), diffusion (especially for high drifttimes) and electronic noise. To detect the beginning of the event spectrum the value of the jump discontinuity of the Heaviside function minus σ of the Gauss function was taken, resulting in $t_{\mathrm{tdcmin}} \approx 655$ns. Similarly the upper end

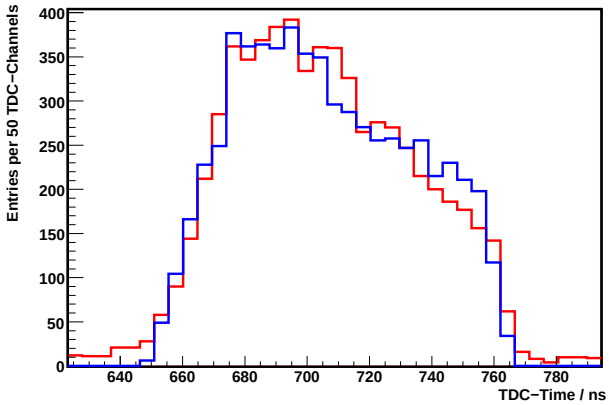

Fig. 1: Comparison between data (red) and simulation (blue)

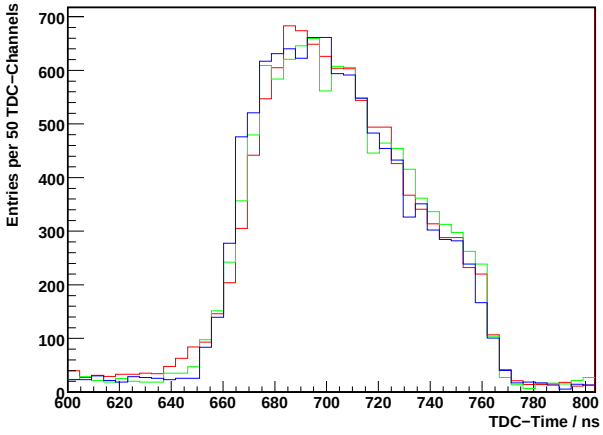

Fig. 2: TDC-Time spectra of three different straws in different layers (normalized to the same integral)

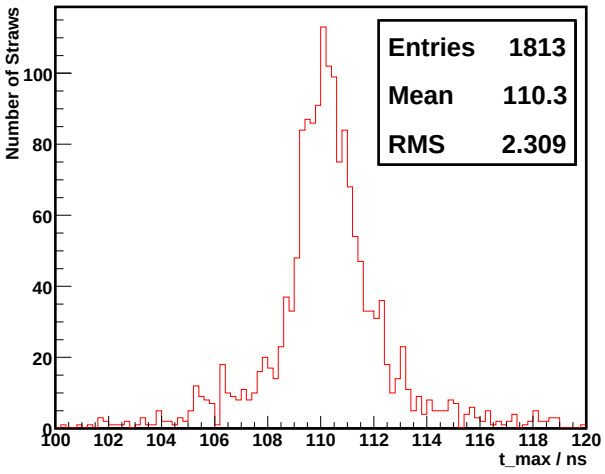

Fig. 3: Distribution of the determined times t_{max} of run 8122

of the event spectrum is obtained by adding σ to the value of the jump discontinuity of the falling edge. This results in $t_{\mathrm{tdcmax}} \approx 765$ns. Finally, $t_{\mathrm{diff}} \approx 110$ns is set equal to the maximum drifttime t_{max}. The results from the whole STT for one run is shown in Fig. 3. One sees a mean t_{max} of 110.3 ns with a RMS of 2.3 ns.

To conclude, it is possible to simulate the data with the Garfield package with the hint of the sensitivity to 9 electrons. Also a comparision between different straws shows that their TDC spectra are very similar to each other. So the calibration of one straw can be used for all straws.

The next step will be to get the isochrone-drifttime-relation from the drifttime spectrum. Assuming a homogeneous illumination a direct relation between the number of entries within a drifttime spectrum interval and the isochrone radius can be established.

References:

[1] P. Wintz et al., ”Resolution and Efficiency of the Straw Tracker for COSY-TOF”, IKP Annual Reports 2004.

Including the Straw Detector into the software analysis package of the COSY-TOF detector

E. Roderburg
for the COSY-TOF Collaboration

1.) Monte Carlo Simulation

In order to determine the acceptance, resolution and efficiency of the COSY-TOF spectrometer it is described with a GEANT 3.21 Monte Carlo program. Each detector - as e.g. quirl, ring, barrel - is represented with its geometrical and physical parameters as a GEANT volume. The straw detector is described as a set of 15 volumes, each corresponding to a double layer of 208 straw tubes, which themselves are composed of wire- gas- and foil-volumes with the geometrical form of tubes. The parameters of these volumes are given in Table 1.

	gas volume	foil	wire
length [mm]		1050	
		517.5 for short tubes	
inner diameter [mm]	0.02	10.07	0.00
outer diameter [mm]	10.07	11.00	0.02
material	Ar(80%) CO_2(20%)	Mylar ($C_{10}H_4O_6$)	Tungsten
radiation length [cm]	9540	28.7	0.35
density [g/cm^3]	0.002	1.39	19.3

The position of the tubes in the reference system of a double layer is shown in Fig. 1 together with the position of two adjacent double layers.

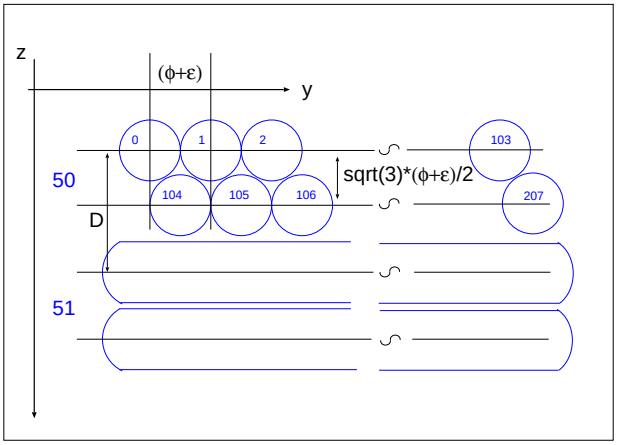

Fig. 1: Geometry parameters of the tube volumes in the double layer volume. Two adjacent double layers are shown. The numbers 50, 51 indicate the numbering of the double layers and the numbers from 0 to 207 indicate the numbering of the tubes inside a double layer. The parameters defined in the drawing are ε=1 mm, ϕ= 10 mm and D = $(\sqrt{3}+2)\cdot(\phi+\varepsilon)/2$, z is the beam direction.

The φ-orientation of the double layers varies in steps of 60°, starting with the first double layer with $\varphi = 30°$. The z position of the first layer in the simulation is 30 cm.
The position of a simulated track passing a straw tube is stored as the shortest track distance to the anode wire r_{min}. In order to simulate the limited resolution of the straw tube, which is dependent on the track-wire distance itself, r_{min} is multiplied by a random number, generated with the weight of a Gaussian distribution with a root mean square rms. This rms is calculated from r_{min} as $rms = 0.15643 - 0.04379 \cdot r_{min} + 0.00442 \cdot r_{min}2$ (rms and r_{min} in [mm]). This function is a fit to measured resolution values of the straw detector [1]. In order to get - as in the case of real measured data - integer TDC values, the result is multiplied with 1000 and stored as straw TDC value. In the analysis program the transformation from TDC values to the value r_{min} has to be replaced for these Monte Carlo data by r_{min}[mm] = TDC / 1000.

2.) Analysis Program tof++

The geometry of a straw double layer is described with the class "strawlayer". The parameters to describe the position of the layer in space and its φ orientation and the positions of the single tubes inside the double layer as shown in Fig. 1 are fixed during the class construction. For each straw double layer a class called "hitsOfDetector" is implemented, this class contains the geometrical information of the "strawlayer" class and in addition the rules for calibration and limits for histogramming of the straw TDC values. The implementation of this class in tof++ are named "StrawDetDL0 .. StrawDetDL14".
The standard procedure of track finding in the tof++ program is to assume straight lines between the target center and each stop detector pixel, which has fired. Each of theses lines is a track candidate. For each detector element, which has a hit, the intersection points of these lines with the mid-plane of the detector element is calculated. If this intersection point is inside the detector, the intersection point is added to a track candidate. A straight line fit is performed to the collected points - the weigths proportional to the detector geometry at the intersection point. Depending on the number of attached detector elements and on the $\chi 2$ of the fit, the track candidate is assumed to be a particle track [2].
Up to now the straw tubes are handled in this scheme without regarding the measured time i.e. they are treated as proportional counters. As an intermediate solution the tracking of the straw detector is done independently from the other detectors by a software package which is described in [3]. The tracks found by this program are now handled as track candidates and detector elements are added to these candidates as described before. In the final fit the weight of the straw detector is set - according to the better resolution - to a factor of 200 higher compared to the other detector components. This procedure allows to use the existing geometrical fitting routines for one and two vertices and the calculation of the track velocity as needed for the $pK\Lambda$ reaction [2].

3.) Results

In order to calculate the track resolution of the COSY-TOF detector, the elastic scattering reaction is simulated (at a beam momentum of 3.059 GeV/c) and the reconstructed tracks are compared to the Monte Carlo start values. The resolution of the scattering angle with the straw detector and with five scintillating fiber layers is shown in Fig. 2. The improvement of resolution for this quantity with the straw

detector is more than a factor of three.

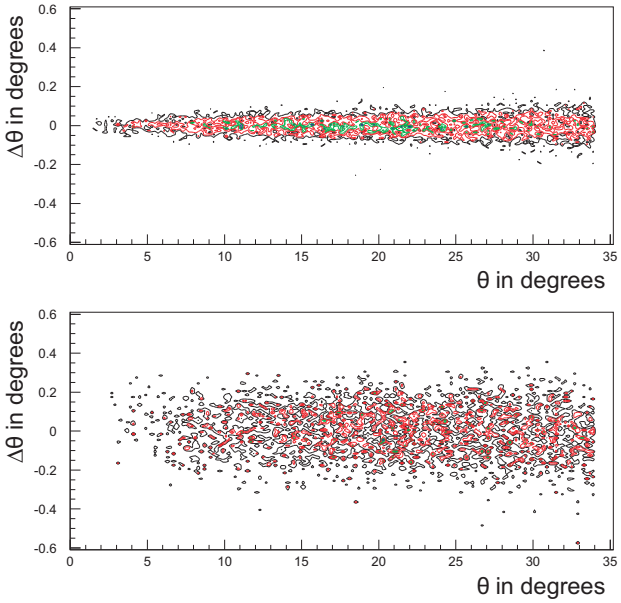

Fig. 2: The difference of the reconstructed scattering angle to the start value of the Monte Carlo program is plotted against the scattering angle of the first track of the elastic proton proton reaction. In the upper figure the tracks are reconstructed including the straw detector, in the lower figure the tracks are reconstructed with the former COSY-TOF setup.

The vertex - and the invariant p-Λ mass resolution of the reaction $pp \rightarrow pK\Lambda$ has been studied. The first condition of identifying a pKΛ event is to measure 4 tracks and two vertices. A vertex is defined by two tracks with a distance of closest approach of less than 10 mm. The z component of the primary vertex (proton, kaon) has to be closer than ± 20 mm to the target center. The z component of the secondary vertex (Λ decay point) has to lie downstream from the target center. The four tracks are submitted to a "four-track and two-vertices fit", which has the constraint, that the line between both vertices (i.e. the Λ track) is located in the plane spanned by the tracks of the secondary vertex. The result is submitted to a kinematic fit, which has the constraints of the particle masses and the beam momentum. The final decision to accept the event as a pKΛ event is done by a cut in the χ2 distribution of the fit. In the following table the results of the pKΛ reconstruction with the simulated straw detector are compared to the former COSY-TOF setup , where five planes of fiber hodoscopes were installed.

	COSY-TOF with straw detector	COSY-TOF with 5 planes of fibers
Δθ of prim. proton	0.13°	0.32°
Δx,y of sec. vertex	0.9 [mm]	3.2 [mm]
Δz of sec. vertex	3.5 [mm]	9.4 [mm]
FWHM pΛ invariant mass	3.5[MeV]	10.2[MeV]
reconstruction efficiency	35.0%	16.2%

The setup with the straw detector allows to reconstruct events with the Λ decay near to the target up to 40 cm downstream (Fig. 3). In case of the setup with five scintillating fiber layers the Λ decay point has to be between the target and 20 cm, this is the position of the last two fiber planes. In addition there is a gap in the reconstruction efficiency at the position of the first three fiber layers around 10 cm (Fig. 4).

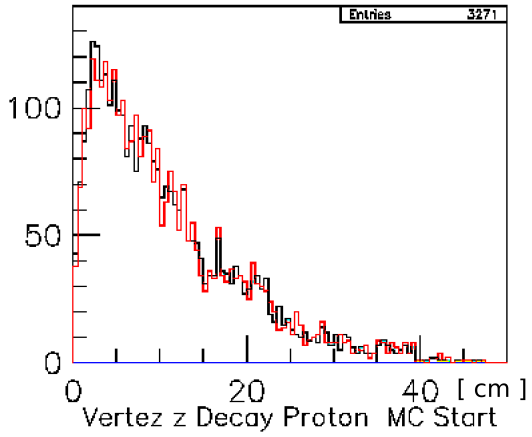

Fig. 3: COSY-TOF with the straw detector: The z component of the secondary vertex of reconstructed $pK\Lambda$ events (black line: Monte Carlo start values) (red line: reconstructed values).

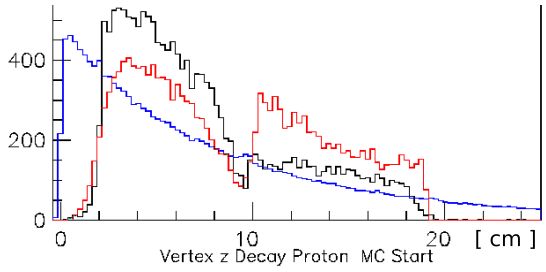

Fig. 4: COSY-TOF with five fiber hodoscope planes: The z component of the secondary vertex of reconstructed $pK\Lambda$ events (blue line: all Monte Carlo start values (not to scale), black line: mc start values of reconstructed events, red line: reconstructed values).

The given values of the resolution obtained with the straw detector represent upper limits, as the kinematic fit and the vertex fit parameters can still further be optimized for the tracks measured with the straw detector.

References:

[1] P. Wintz, private communications

[2] A. Filippi, R. Geyer, D. Hesselbarth, COSY-TOF Internal Note 2001 http://www.fz-juelich.de/ikp/COSY-TOF/manuals/tracking.pdf

[3] R. Castelijns COSY-TOF Internal Note 2006 http://www.fz-juelich.de/ikp/COSY-TOF/manuals/Manuals/straws/index.html

The Silicon Microstrip Quirl Telescope SQT

W. Gast, T. Batsch, D. Wolski
for the COSY-TOF collaboration

Introduction

The Silicon Microstrip Quirl Telescope SQT of the COSY TOF spectrometer has been setup for the first in-beam test. The main aim of this experiment was to test, whether the sensitivity of the SQT and the connected signal processing electronics is sufficient to discriminate minimum ionizing charged particles against the background, whether its segmentation into Archimedian spirals is able to provide the desired first precise tracking information close behind the target, and whether all technical challenges regarding vacuum, light tightness, cabeling, signal processing and triggering could be solved. The reconstructed tracks obtained from a preliminary analysis of the first experimental data demonstrate that the expected performance could be achieved (Fig. 1).

Mechanical setup

Two detector assemblies, i.e. two segmented silicon wafers of 300μ thickness each and their supporting ceramic rings with the Capton cables were mounted in the radial center of their corresponding circular mounting frames, the diameters of which are adapted to the COSY-TOF entry region. The two mounting frames, which consist of large aluminum rings and ring shaped printed circuit boards acting as part of the vacuum system and vacuum feedthroughs for the 512 signal lines, and as support for the 16 preamplifier boxes, were stacked together and mounted to the flange of the first hodoscope. The two detector assemblies were also stacked together and fixed to one detector holder axially positioned on the plane defining the interface between the start detector and the first mounting frame of the whole SQT assembly in beam direction. In this way a small distance of 6mm between the two Silicon microstrip detectors, and a small distance of 40mm between target and the first Silicon microstrip detector could be achieved. The mounting frames together with the preamplifier boxes and the motherboards were produced and assembled by the Andrzej Soltan Institute for Nuclear Studies in Otwok-Swierk, Poland.

Electronics and trigger

The electronic setup employed a conventional signal processing chain with charge sensitive preamplifier (PA), main shaping amplifier (SH), and peak sensing analog to digital converter (ADC). For the PA a sensitivity of 55mV/MeV(Ge) at a linear working range of $\pm$4 V, and for the semi-gaussian main shaper (SH) a symmetric shaping time of 1 μs at a gain of 200 was chosen. A slow coincidence signal of 2 μs width was derived from the main trigger signal of the COSY-TOF trigger and fed to the common gate inputs of the ADC's. The low dissipation, small size preamplifiers and the remote programmable shaping amplifiers were custom designed and produced by the Hungarian Academy of Science, Foundation for Information Technology (KFKI-MSZKI). A schematic layout of the electronics is given in Fig. 2.

Analysis and results

During the test experiment only coincidence events, correlated to the COSY-TOF main trigger, were recorded. The events were offline sorted into individual histograms for each detector segment. A software threshold was applied to the resulting 512 spectra using an automatic fitting routine. The example spectra given in Fig. 3 show the result of this procedure and confirm the good signal to noise performance of the SQT. A new approach was developed to extract the correct pixels out of the approx. n^2 combinatorial possibilities for a number of n coincident hits, and to determine their exact geometrical positions, which is a basic requirement to allow a precise tracking. The new approach uses the actual measured experimental data and the fact that they provide redundant information. From the target position and the positions and hit patterns of the other TOF detectors a charged particle track and its path trough the two detectors of the SQT placed at a hypothetically assumed geometrical position can be estimated. A statistical analysis of the correlation between these pathes and the measured SQT hit patterns for the different geometrical parameters defining the hypothetical positions of the SQT detectors yields a correlation function which peaks at the correct combinatorial choice and the actual value of the corresponding geometrical parameter. Fig. 4 shows as an example the result of such a correlation analysis for the determination of the correct combinatoric of the hit pattern as a function of the resulting φ angle of all possible pixels. In this plot the difference between the hypothetically assumed and the actual value of the geometrical parameter φ, corresponding to the rotation of the SQT detectors around the beam axis, has been already corrected for (peak at 0 degree).

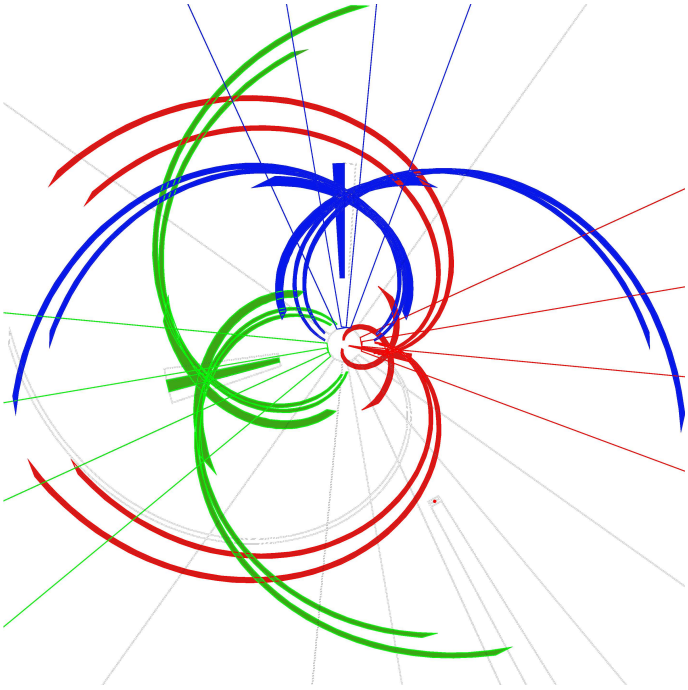

Fig. 1: Eventplot of reconstructed charged particle tracks. The crossing points of the large spirals of identical color represent the positions where a charged particle passed the Silicon Microstrip Quirl Telescope SQT.

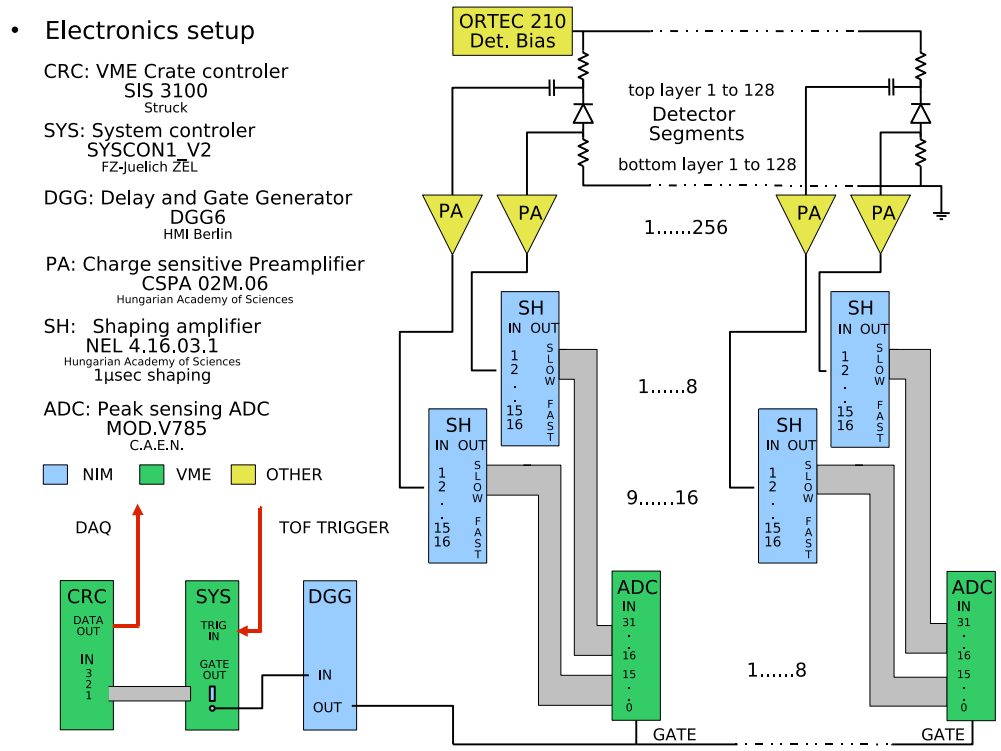

Fig. 2: Schematic layout of the electronics for the Silicon Microstrip Quirl Telescope SQT.

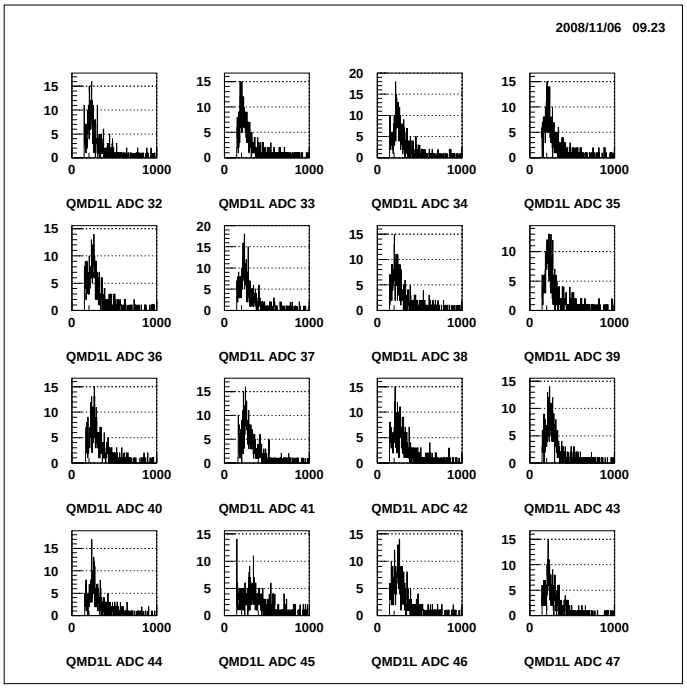

Fig. 3: Amplitude distribution of coincident signals vs. ADC channel number of some segments of the SQT. The small amplitude noise is cut by an automatic routine applying an individual software threshold to the spectral response of each segment.

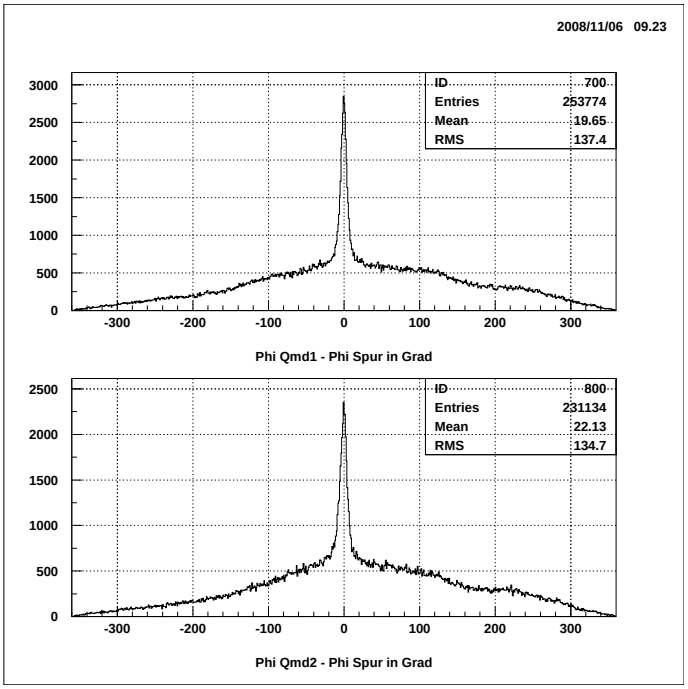

Fig. 4: Correlation analysis of the SQT hit patterns to calibrate the geometrical parameters of the SQT detectors (see text).

Online Control Package for the COSY-TOF experiment

E. Borodina
for the COSY-TOF Collaboration

1.) Motivation

The new Straw Tube Tracker (STT) and Quirl Microstrip Detectors have been installed at the COSY-TOF experiment. These new detectors increase the number of channels of the COSY-TOF detector by a factor of about 3 from 1500 to 5000. Therefore, a new control package to adjust the electronic parameters and to control the proper functionality of all channels is nessesary. The development of this package is decribed in the following. The online controlling based on real time visualization of the key parameters of the detector system plays an important role.

2.) Description

The program package (Fig. 1) consists of the conversion software, which transforms a binary data stream from the data acquisition system (DAQ) to a detector oriented event format, methods of Inter-Process Communications (IPC), and the graphical user interface (GUI). To achieve data transfer through the network and real time data performance the IPC tools - sockets and shared memory - are used.

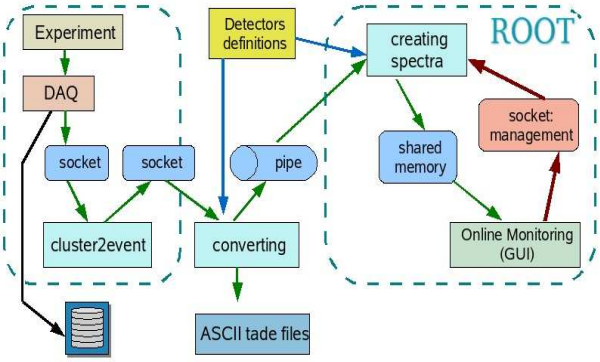

Fig. 1: Scheme of the online control package

Data processing at the COSY-TOF experiment starts from retrieving data by the DAQ, which provides data digitalization, transport and management, first processing and storing. Parallel to the data storage the cluster2event code recombines subevent data blocks from different electronic modules, to full events. The converting code receives these event data from the DAQ socket, deciphers them from different hardware defined binary formats to the more user friendly TADE format (TDC-ADC-Detector-Element) based on physical data interpretation (Fig.1). The converting code is used for online data decoding and for offline analysis. In this case the data are written on disk as ASCII files.

Another part of the program package creates different types of spectra for all detectors and their elements and continuously updates them in the shared memory.

User friendly data visualisation is performed by a special GUI, TOF-ONLINE, which is based on ROOT classes. It provides a convenient choice of plots of data from selected detectors, real time visualisation of different types of spectra, as well as additional services such as saving figures, printing data etc (Fig. 2).

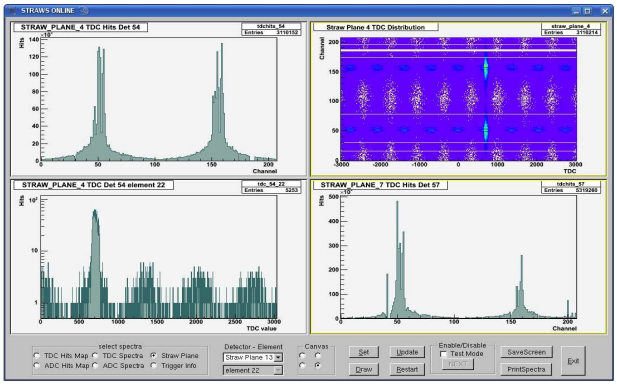

Fig. 2: Example of the GUI TOF-Online with straw spectra

3.) Results

Simple visualisation helps to spot the dead or noisy channels, wrong pedestal values etc.The program package in addition has the option to check and set new pedestal values automatically and to check the corresponding definition files.

Fig. 3 shows how the visualisations of different straw spectra allow to spot wrong allocated channel numbers. The hit map pattern of Fig. 3, showing the Straw Detector hit map, should look like the spectra in the upper left panel of Fig. 2.

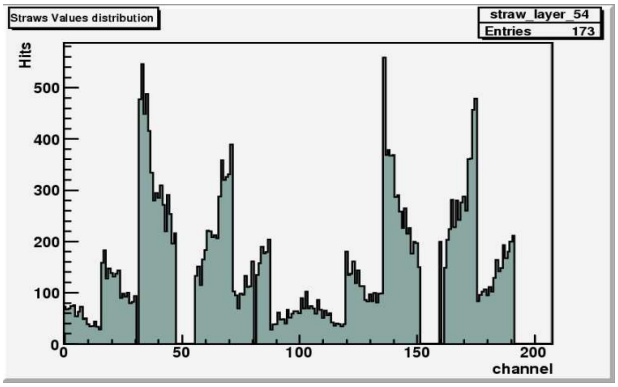

Fig. 3: First examples of STT Hit Map for one double layer

The converting routines for the new GPX TDC's and CAEN ADC's were tested during the STT commissioning beam time in August 2008. In addition this package is being used in an offline mode to convert the collected data for analysis software and to adjust the parameters of the new detectors.

1.3 WASA-at-COSY

Charge Symmetry Breaking in dd Collisions with WASA-at-COSY

V. Hejny, A. Magiera[1], P. Podkopał[1,*], T. Smolinski[1,2,*], W. Węglorz[2,3,*], A. Wrońska[1]

One of the primary objectives of the experimental programme with the WASA-at-COSY detector is the determination of *p*-wave contributions to the charge symmetry breaking amplitude in the reaction $dd \to {}^4He\pi^0$ at 1.2 GeV/c beam momentum [1].

Charge symmetry is a special case of isospin symmetry, and thus a fundamental symmetry of QCD [2]. Isospin symmetry is broken by the different masses of the up and down quarks. In addition, quarks are distinguished by the electromagnetic interaction. Nowadays those contributions can be treated theoretically within the framework of Chiral Perturbation Theory (ChPT). Thus, a detailed study of isospin violation in low energy hadron physics is a unique window to the quark masses and thus to fundamental parameters of the Standard Model. To get access to the quark mass difference it is advised to look at Charge Symmetry Breaking (CSB) observables. Here the relative π-mass difference, which is of electromagnetic origin, does not contribute. As the reaction $dd \to {}^4He\pi^0$ violates charge symmetry, the cross section is directly proportional to the square of the CSB amplitude.

Triggered by first high-precision experiments on CSB performed at TRIUMF and IUCF [3, 4] an international collaboration has been formed aiming at a consistent description of CSB within ChPT. In the course of the ongoing analysis [5, 6, 7], a set of essential observables has been identified, which are now being addressed by the experimental programme of WASA-at-COSY. The (unknown) total cross section at a beam momentum of 1.2 GeV/c has been estimated to about 100 pb. This requires high average luminosities of close to $1 \cdot 10^{32}\,\mathrm{cm}^{-2}\mathrm{s}^{-1}$ and good control over the detector conditions.

As a first step towards the measurement of CSB in $dd \to {}^4He\pi^0$ pion production in $dd \to {}^3AN\pi$ was studied in December 2007. The aim of this experiment was two-fold:

i) Data on *s*- and *p*-wave single pion production in dd-interactions at a these excess energies, which are currently not available. Besides serving as a testing ground for the theoretical framework, the reaction provides essential information on dd initial-state interaction with the same partial waves involved as in $dd \to {}^4He\pi^0$.

ii) Studying the experimental conditions with a deuteron beam at this low beam momentum in combination with a high density deuterium target and a 4π detector setup. Beam quality and beam lifetime had to be checked as well as detector response, detector rates and trigger capabilities.

In this run about 200.000 events on $dd \to {}^3Hen\pi^0$ have been collected, which will be used to extract a high statistics Dalitz plot. Due to smaller acceptance and a pre-scaled trigger the available statistics on $dd \to {}^3Hep\pi^-$ will be in the order of 20.000 events, still sufficient for differential cross sections and a Dalitz plot.

The first, preliminary results show that the experimental boundary conditions for $dd \to {}^4He\pi^0$ are quite favourable. Trigger conditions and the performance of the data acquisition allow to run at the required high luminosities. Furthermore, the discrimination of charge 1 particles in the forward detector in combination with two neutral hits in the central detector is sufficient to get a clean pion peak.

Consequently, a dedicated high luminosity run on $dd \to {}^4He\pi^0$ was accepted by the COSY-PAC in spring 2008 and carried out in June 2008. A reliable pellet target operation at 5000 deuteron pellets/s and maximum beam intensities of up to $5 \cdot 10^{10}$ stored deuterons allowed us to run at the desired luminosities. In spring 2008 the new Forward Trigger Hodoscope had been installed and the improved detector performance could be utilised. First estimates from the data show, that during the two week period a total of about $5 \cdot 10^6$ He-π^0 coincidences with low background had been written to disk. Provided the cross section estimates are correct this implies an expected number of roughly 500 ${}^4He\pi^0$ events.

The data analysis is currently in progress. As the most crucial task is the discrimination of ${}^3He$ and ${}^4He$ by means of energy loss in the Forward Window Counter and the Forward Trigger Hodoscope, a precise energy calibration is mandatory. Here, the large number of $dd \to {}^3Hen\pi^0$ events allows a dedicated He calibration from data not limited by statistics. The particle identification will be supplemented by kinematic cuts in order to distinguish between $dd \to {}^4He\pi^0$ (two body final state) and $dd \to {}^3Hen\pi^0$ (three body final state). The absolute normalisation at this beam momentum will be done by means of pp and pd quasi-elastic scattering.

The next step will be defined by the results of this analysis and will comprise a run with polarised beam. Polarisation is a necessary tool, because the dd inital state is symmetric and, therefore, in any unpolarised run *sp* interferences (as all unsymmetric terms) are not allowed, which would normally be used to discriminate *p* and *d* waves. *p* waves and angular symmetric *sd* interferences have the same signature. The only method to unambiguously identify *p* wave contributions are polarisation observables.

Provided the ongoing analysis shows that the reaction can be identified and that the cross section is not significantly smaller, our goal is to submit a proposal in September 2009 on $\vec{d}\vec{d} \to {}^4He\pi^0$. The actual total cross section is crucial, because polarised beam implies a reduced beam intensity and, thus, a longer run.

References:

[1] H.H. Adam *et al.* [WASA-at-COSY Collaboration], arXiv:nucl-ex/0411038.
[2] G.A. Miller *et al.* Phys. Rept. **194** (1990) 1.
[3] A.K. Opper *et al.* Phys Rev. Lett. **91**, 212302 (2003).
[4] E.J. Stephenson *et al.*, Phys. Rev. Lett. **91**, 142302 (2003).
[5] U. van Kolck *et al.*, Phys. Lett. B**493**, 65 (2000)
[6] A. Gårdestig *et al.*, Phys. Rev. C**69**, 044606 (2004)
[7] A. Nogga *et al.*, Phys. Lett. B**639**, 465 (2006)

[1]Institut für Kernphysik and Jülich Center for Hadron Physics, Foschungszentrum Jülich, Jülich, Germany
[2]Institute of Physics, Jagiellonian University, Cracow, Poland
[3]Institute of Physics, University of Silesia, Katowice, Poland
*Supported by COSY-FFE

Search for the scalar mesons $a_0/f_0(980)$ in pd $\rightarrow {}^3$HeX data from WASA-at-COSY*

M.Büscher, P.Fedorets[a,b], C.Zheng[c]

Data on inclusive $pd \rightarrow {}^3\mathrm{He}X$ production have been recorded during a test beam-time in November 2007 at a beam momentum of $p_p = 2.935\,\mathrm{GeV/c}$. This was the first step towards a study of the nature of the light scalar mesons $a_0/f_0(980)$ via detection of their radiative decays into vector mesons ($a_0/f_0(980) \rightarrow \gamma V$, $V = \rho,\ \omega$) [1]. Major goal was to observe the strong decay channels of the $a_0/f_0(980)$, which will provide important information for the preparation of the subsequent measurements: First, the production cross section for the a_0/f_0 resonances in $pd \rightarrow {}^3\mathrm{He}X$ reactions is yet unknown. Based on the measured cross sections into the $\pi\eta$ and $\pi\pi$ decay channels and predicted [2, 3] branching ratios for the radiative decays, one can estimate the total beam time needed to achieve the physics goals outlined in the proposal [1]. Second, the strength of the non-resonant $\pi\pi$ and $\pi\eta$ background under the a_0/f_0 mass distributions is unknown and has to be determined experimentally.

During one week (~ 68.5 hours) of data taking 274 Runs have been collected with an inclusive ^{3}He trigger in the forward detector (FD). The average effective luminosity, determined from *pd* elastic scattering, was $L = 3.2 \cdot 10^{30}\,\mathrm{s^{-1}cm^{-2}}$. This value agrees with the one obtained from data on *pp* quasielastic scattering and with an estimate based on the beam intensity and target thickness [4].

The energy-loss spectra in the forward range hodoscope (FRH) (Fig. 1) show clear bands from the ^{3}He ($\sim$1200000 candidates). The overall missing-mass $m.m._{\mathrm{tot}}^2$ spectrum (Fig. 2) shows a clear and strong peak around zero for the ^{3}He4γ final state. For selection of a particular decay channel in the central detector (CD) a multiplicity criterion on charged and neutral tracks as well as a $\pm 0.1\,\mathrm{GeV}^2$ window in the $m.m._{\mathrm{tot}}^2$ spectrum have been applied. CD tracks have been defined as valid or noise based on the time difference between FD and CD. The number of neutral tracks had to be equal or larger than four.

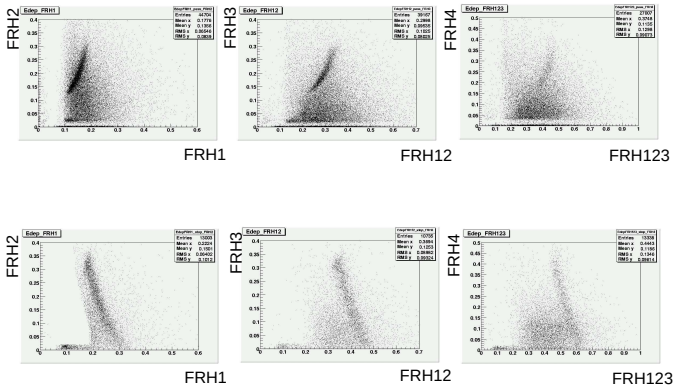

Fig. 1: 2D spectra of deposited energy (y axis) in individual layers of the FRH for particles stopped in that particular plane (lower) and for particles passing through (upper) *vs.* the total deposited energy in the preceeding planes (x axis).

The invariant-mass spectrum of any possible 2γ combination in 4γ events reveals a distinct peak at the π^0 mass. After selection of one 2γ pair with a mass around the π^0, the invariant-mass spectrum of the second pair unveils two peaks, one at the π^0 and a second at the η mass (Fig. 2). That proves the existence of the $\pi^0\eta$ and $2\pi^0$ channels.

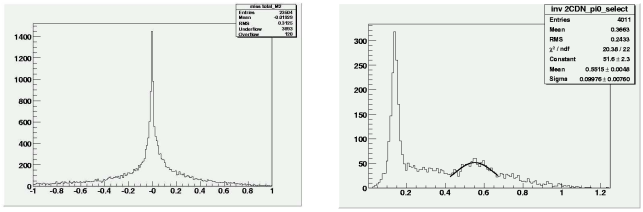

Fig. 2: Overall missing mass $m.m._{\mathrm{tot}}^2$ for ^{3}He4γ events (left). Invariant-mass distribution for ^{3}He4γ events of the remaining 2γ pair after selecting an invariant mass of the first pair around the π^0 (right).

Figure 3 shows the $m.m.(^3\mathrm{He})$ spectra for both channels after a kinematic fit with $probability > 0.1$. For the $\pi^0\eta \rightarrow 4\gamma$ channel, there is an indicaton of an a_0^0 signal around 1.0 GeV, while for $2\pi^0 \rightarrow 4\gamma$ no obvious structure is visible.

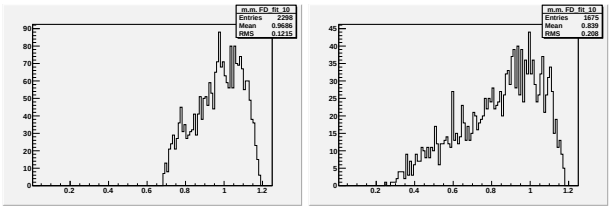

Fig. 3: $m.m.(^3\mathrm{He})$ missing-mass spectra for the $^3\mathrm{He}\,\pi^0\eta$(left) and $^3\mathrm{He}\,2\pi^0$(right) final states.

For the next step of the data analysis, the FRH calibration will be fine tuned, in order to remove discrepancies between the measured and Monte-Carlo energy-loss spectra. Only after that final conclusions about the feasibility of a_0/f_0 studies with WASA-at-COSY can be drawn. At the moment one can conclude, that both investigated channels $pd \rightarrow {}^3\mathrm{He}\,\pi^0\eta \rightarrow {}^3\mathrm{He}\,4\gamma$ and $pd \rightarrow {}^3\mathrm{He}\,2\pi^0 \rightarrow {}^3\mathrm{He}\,4\gamma$ are seen in the data and that non-resonant production is dominant here.

References:

[1] M.Büscher et al., Proposal "First Measurent of Radiative Decays of Scalar Mesons $a_0/f_0(980) \rightarrow \gamma V$ with WASA"

[2] Yu. Kalashnikova et al., *Phys. Rev. C* **73** 045203 (2006) [arXiv:nucl-th/0512028].

[3] D. Black et al., *Phys. Rev. Lett.* 88, 181603 (2002).

[4] C. Zheng, *Investigation of pd Elastic Scattering for Luminosity Determination with WASA-at-COSY*, contribution to this Annual Report.

[a]ITEP, Moscow, Russia
[b]IKP & JCHP, Forschungszentrum Jülich
[c]IMP, Lanzhou, China

*Supported by COSY-FFE, CSC, DFG, HGF, RFFI.

Charged decays of the η-meson measured with WASA-at-COSY

C. F. Redmer[1], M. Berłowski[2], H. Bhatt[3], L. Yurev[1,4,*]

The charged decay channels of the η-meson allow to study aspects related to the investigation of chiral symmetry breaking, the anomalies of QCD, the eta transition form factor and possibly, a flavor conserving CP violation. The studies form an important part of the physics program of WASA-at-COSY. The Central Detector of the WASA-at-COSY detection setup [1], with its Plastic Scintillator Barrel (PSB) and the Mini Drift Chamber (MDC) situated in the magnetic field of a superconducting solenoid, is well equipped for the investigation of the charged decay modes of the η-meson.
During the first production run of WASA-at-COSY in April 2007, dedicated to neutral decay channels of the η meson, especially $\eta \to \pi^0\pi^0\pi^0$, first data on charged decays were parasitically taken.

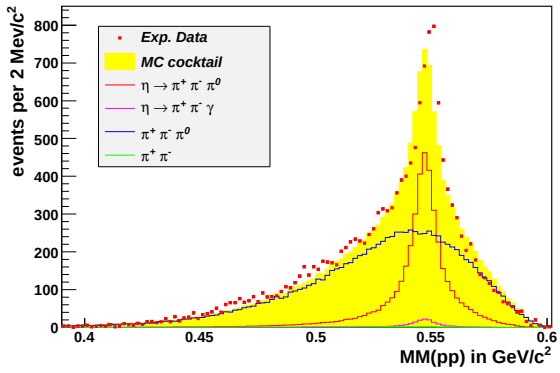

Fig. 1: Missing Mass spectrum of two protons, fitted with Monte-Carlo

For the most abundant of the charged decay channels, $\eta \to \pi^+\pi^-\pi^0$, the analysis is still on the exploratory level [2]. Fits with Monte-Carlo distributions show that the signals are understood (Fig. 1).Thus, this analysis was used to develop triggers for charged η decays. It is now possible to take up to $3-4$ $\eta \to \pi^+\pi^-\pi^0$ events per second at a luminosity of $5 \times 10^{31} s^{-1} cm^{-2}$ without prescaling. The trigger efficiency is on the level of 60%.

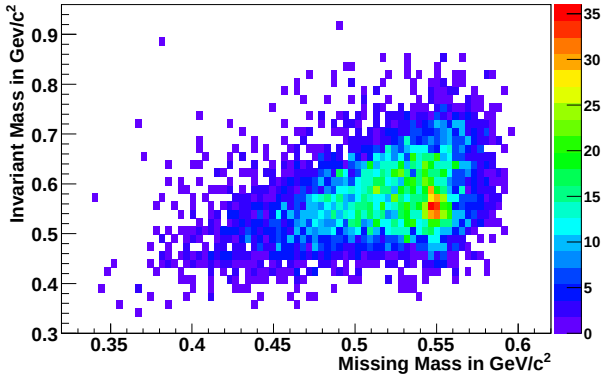

Fig. 2: Invariant Mass of $\pi^+\pi^-\gamma$ as a function of the Missing Mass of two protons.

The analysis of $\eta \to \pi^+\pi^-\gamma$ is trying to make use of the full available information.

The total missing mass, the missing mass of subsystems as well as spatial correlations, e.g. opening angles between neutral and charged tracks, are used to suppress the background from multi pion production.
Fig. 2 shows the preliminary result after all cuts. Despite all efforts, the spectra are still strongly dominated by the signals of $\pi^+\pi^-$-production, so that finally a statistical background subtraction based on Monte-Carlo simulations will have to be done.
Two analyses are dealing with the Dalitz decay $\eta \to e^+e^-\gamma$ of the η-meson. While the first is aiming at the determination of the transition form factor, the second is part of background studies for the very rare decay $\eta \to e^+e^-$. Fig. 3 shows the

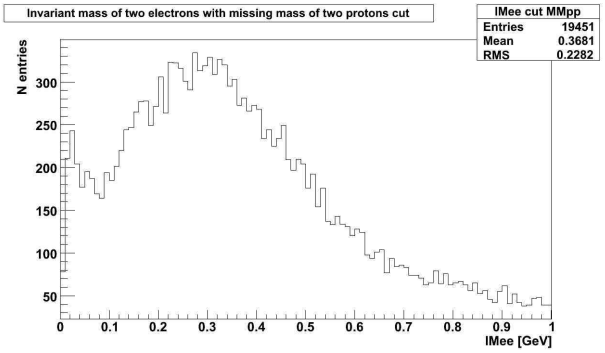

Fig. 3: Invariant Mass spectrum of two lepton pair candidates. The peak at lowest masses is characteristic for leptons.

invariant mass spectrum for lepton pair candidates selected by simple conditions, as e.g. a cut on the ratio of momentum and deposited energy. The enhancement of the distribution at low masses is a characteristic of dileptons, arising from the kinematics of lepton pairs. Thus Fig. 3 provides clear evidence for the feasibility of studies of decay channels containing electron positron pairs.

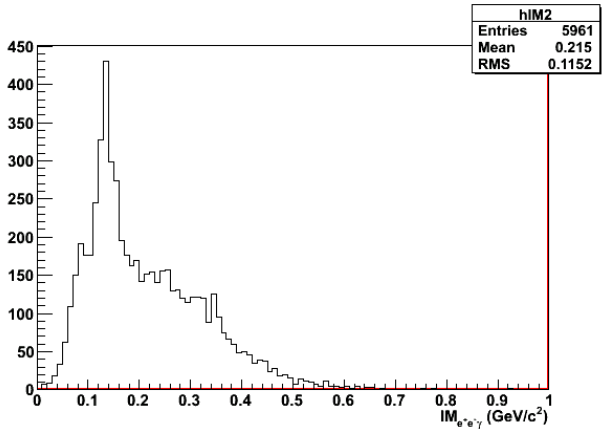

Fig. 4: Invariant Mass spectrum of two leptons and a photon, dominated by the decay of π^0.

In Fig. 4 the invariant mass spectrum of reconstructed $e^+e^-\gamma$ final states is shown. At this preliminary stage the distribution is still dominated by the Dalitz decay of the π^0. More

details on this analysis can be found in the contribution of H. Bhatt.

One of the most challenging channels from the point of view of analysis techniques is the decay $\eta \to \pi^+\pi^- e^+e^-$. A good particle identification is indispensable.

The configuration of the CD allows for the identification via the measurement of the specific energy loss of all particles. The momentum information measured in the MDC combined with the deposited energy in the PSB permits the separation of electrons and pions up to a momentum of 125 MeV/c. For higher momenta the energy deposited in the calorimeter has to be used.

Further details about the application can be found in [3]. Efficiency and purity of these methods are currently under evaluation.

The search for the double Dalitz decay $\eta \to e^+e^-e^+e^-$ focusses on the kinematics of dileptons, i.e their opening angles. The events selected in this way give hope for a few event candidates, especially, when studied with the single event display, as shown by Fig. 5.

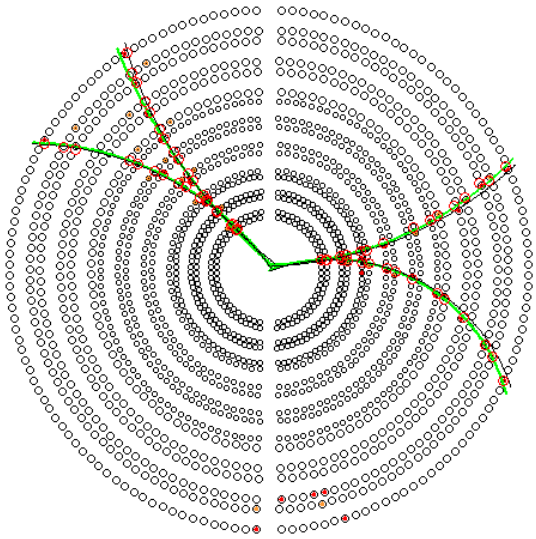

Fig. 5: An event candidate for $\eta \to e^+e^-e^+e^-$ in the Single Event Display

In October 2008 another production run has been carried out, producing the η-mesons in the reaction pd $\to^3$ Heη. The production cross section for η is 25 times lower compared to proton proton collisions, but there are advantages.

On the one hand, contributions from multi pion production are significantly smaller. A cross section lower by two orders of magnitude, yields a signal to background ratio of approximately one to one. On the other hand, the center of mass velocity is lower, causing a larger acceptance. This makes the η-production in proton deutron collision very appealing for Dalitz plot studies of the decay $\eta \to \pi^+\pi^-\pi^0$. In addition, particle identification becomes easier, since more decay products are emitted into those parts the CD, which have a higher resolution and efficiency.

Another advantage of the meson production in proton deutron collisions, is the possibility of the detection setup to identify ^{3}He on the trigger level. This reduces event rates significantly and makes the trigger independent of the decay signature. In this way $10^7\eta$ have been recorded on disk.

The analysis of these data is currently ongoing and first results are very promising. For 2009 another eight weeks of η production run are scheduled in pd.

The high statistics, needed to extract physics results beyond upper limits on branching ratios from the very rare decay channels $\eta \to \pi^+\pi^- e^+e^-$ and $\eta \to e^+e^-e^+e^-$, can only be obtained when the η-mesons are produced in proton-proton-collisions.

References:

[1] H.-H. Adam et al, Proposal for the Wide Angle Shower Apparatus (WASA) at COSY-Jülich, COSY Proposal (2004), e-Print arXiv: nucl-ex/0411038

[2] C. F. Redmer, First signals of charged η decays at WASA-at-COSY, COSY/IKP Annual Report (2007)

[3] M. Janusz, Identification of pions and electrons using WASA facility, COSY/IKP Annual Report (2007)

[1] IKP & JCHP, Forschungszentrum Jülich, Germany
[2] INS Warsaw, Poland
[3] IIT Bombay, India
[4] JINR Dubna, Russia

* Supported by COSY-FFE

Analysis of $\eta \to e^+e^-\gamma$ with WASA-at-COSY

H.Bhatt*

We would like to measure the transition form factor of the η meson by analyzing the Dalitz decay $\eta \to \gamma\gamma^* \to e^+e^-\gamma$. The time like virtual photon converts into a lepton pair. The invariant mass of lepton pairs is equal to the four momentum transferred squared ($q^2 = m^2_{l^+l^-}$), allowing us to obtain the form factor as a function of momentum transfer square. It is possible to determine experimentally the transition form factor $|F(q^2)|^2$ in the time-like region of momentum transfer by using,

$$\frac{d\Gamma_{\gamma e^+e^-}}{dq^2} = |\frac{d\Gamma_{\gamma e^+e^-}}{dq^2}|_{QED}|F(q^2)|^2$$

A production run of $pp \to pp\eta$ taken in April-May 2007 at the beam energy 1.4 GeV has produced in a total of 10^7 η mesons. To analyze the decay channel $\eta \to e^+e^-\gamma$ (branching ratio (BR) = 4.9 $\times 10^{-3}$), charged particle identification is necessary. In the analysis, events with two oppositely charged tracks and one neutral track in the central detector (CD) and two charged tracks in forward detector (FD) are selected (See Figure 1 in the contribution by C. Zheng). Reactions like $\eta \to \pi^+\pi^-\gamma(BR = 4.68\%)$, $\eta \to \pi^+\pi^-\pi^0(BR = 22.6\%)$ satisfy the same conditions with larger branching ratio making it necessary to distinguish leptons from pions. The reaction $\eta \to \gamma\gamma(BR = 39\%)$ contributes as a major background, where one photon converts into a lepton pair in the beam pipe.

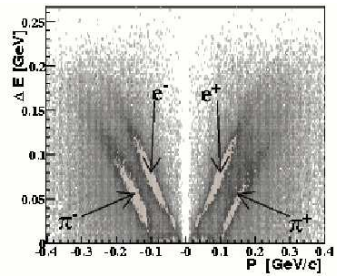

Fig. 1: E_{dep} in scintillating electromagnetic calorimeter (SEC) vs q*P in MDC for a reaction $\eta \to \pi^+\pi^-e^+e^-$(from simulation)

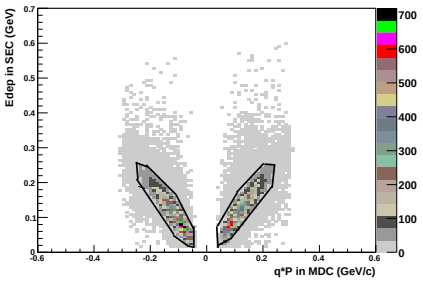

Fig. 2: Cut on E_{dep} in SEC vs q*P in MDC from simulation for $\eta \to e^+e^-\gamma$, selecting leptons.

In simulation studies, we have used the $\Delta E - P$ method for the identification of charged particles which do not stop in the mini drift chamber (MDC). It is evident that electrons and pions fall in a different region (Fig 1). Selecting events lying on the electron bands (Fig 2) we reconstruct the invariant mass of the η (Fig 3) and missing mass of two scattered protons (Fig 4). We have put the following additional constraints :

1. Energy of reconstructed protons in FD $>$ 100 MeV.
2. E_{dep} (deposited energy)for charged track in CD $>$ 20 MeV and E_{dep} for neutral track in CD $>$ 180 MeV.
3. Missing energy of the system should be in the range of -0.20 GeV to 0.20 GeV.
4. The Invariant Mass distribution of η ($e^+e^-\gamma$) with cut on the missing mass (530 - 570 MeV).
5. The Missing Mass distribution of two scattered protons with cut on the invariant mass (500 - 600 MeV).

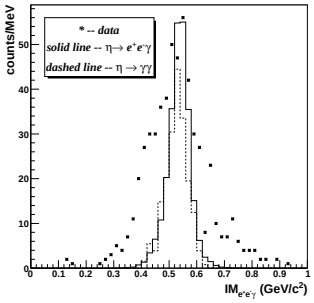

Fig. 3: Invariant mass of η in the Central Detector compared with simulations

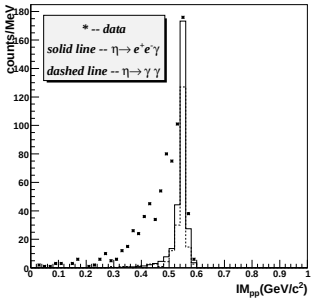

Fig. 4: Missing Mass of two scattered protons in Forward Detector compared with simulations

After applying all cuts as shown in Fig. 3 & 4, we find that the $\eta \to \gamma\gamma$ reaction still contributes significantly and moreover, the simulation does not match with the data. We are investigating other possible background reactions and are investigating ways to suppress the $\eta \to \gamma\gamma$ reaction. The efficiency of the condition on E_{dep} vs charge*momentum (Fig. 2)has also to be examined.

* Indian Institute of Technology Bombay, India

Dielectron Production in the $\eta \to \gamma e^+e^-$ Decay with WASA-at-COSY.

M.Hodana[a b] and P.Moskal[a b]

The physics issues concerning the $\eta \to \gamma^*\gamma$ transision form factor is the main motivation of the ongoing analysis. One can study decays involving two photons from which at least one is virtual. Virtual photons convert into a lepton-antilepton pair. The square of the invariant mass of a created lepton-antilepton pair is equal to the square of the four-momentum of the virtual photon. Deviations from the QED expectation are due to the inner structure of the meson and can be characterized with the transition form factor

In October 2008 investigations of the η decays have been conducted using the WASA-at-COSY detector. The η meson has been produced in proton-deuteron collisions with a proton beam energy of 1.69 GeV. Based on the online analysis we expect that about 10^7 η mesons were produced. Currently, the detector calibration is carried out.

Here we report on the studies of the $\eta \to \gamma e^+e^-$ decay. Events of interest will be reconstructed using missing and invariant mass techniques. The identification of photons in the WASA calorimeter [1] is possible with $\frac{\sigma_E}{E} = \frac{5\%}{\sqrt{E}}$ resolution. In Fig. 1 one can see the polar angle distribution and Fig. 2 shows the kinetic energy for photons in the calorimeter. The picture comes from simulations of the $\eta \to \gamma e^+e^-$ decay and shows that 90% of the photons can be detected. The reconstruction of electrons and positrons is less efficient and optimization of existing algorithms has to be done in order to improve the number of identified particles. At present in order to estimate the number of expected $\eta \to \gamma e^+e^-$ decays, we assume that the acceptance and selection cuts will be the same as used in the analysis of the WASA/CELSIUS data [2]. Under this assumption the expected number of fully reconstructed $pd \to {}^3He\,\eta$ events with $\eta \to \gamma e^+e^-$ amounts to about 15000.

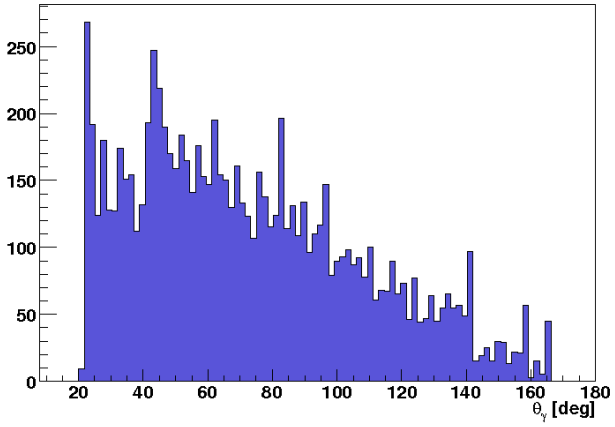

Fig. 1: Polar angle distribution of photons from the $pd \to {}^3He\,\eta \to {}^3He\gamma e^+e^-$ reaction. 90% out of 10^4 gammas produced, have been detected. Picture presents results of simulation without selection cuts.

For the discrimination between electrons and positrons, the dependence of the energy depositions in the Plastic Barrel detector on the momentum will be used. After the selection of events with γe^+e^- in the final state, the number of events coming from $pd \to {}^3He\,\eta \to {}^3He\gamma e^+e^-$ will be calculated using the missing mass technique for the $pd \to {}^3HeX$ reaction. Here, the momentum of the ${}^3He$ ions will be reconstructed based on energy losses in subsequent layers of the forward scintillators.

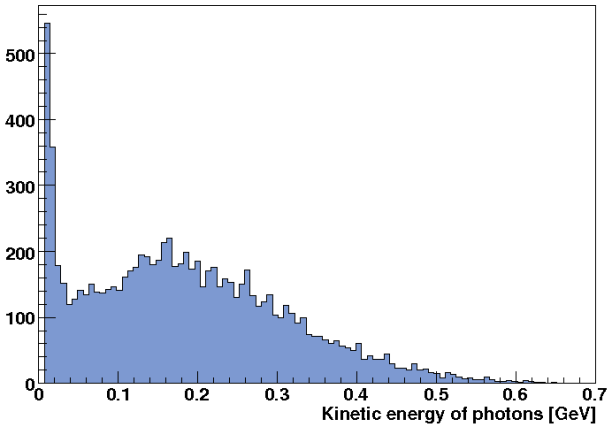

Fig. 2: Kinetic energy of photons from the $pd \to {}^3He\,\eta \to {}^3He\gamma e^+e^-$ reaction. Picture presents results of simulation without selection cuts.

The analysis of the data is in progress. The expected statistics should allow us to distinguish between expectations based on different models [3, 4].

References:

[1] see Fig. 1 in the contribution by C. Zheng.
[2] M. Berlowski et al., Phys. Rev. **D 77**, 032004 (2008).
[3] J. Stepaniak et al., Phys. Scr. **T99** 133-139, (2002).
[4] L. G. Landsberg, Physics Reports, **128** (6), p.301-376, Nov 1985.

[a] Institut für Kernphysik and Jülich Center for Hadron Physics, D-52425 Jülich, Germany
[b] Institute of Physics, Jagiellonian University, PL-30059 Cracow, Poland

Simulations for a Feasibility Study of the Reaction pd$\rightarrow$ ^{3}He $\eta \rightarrow$ ^{3}He $\pi^0\gamma\gamma$ with WASA-at-COSY

Kavita Chandwani*

The measurement of the branching ratio for $\eta \rightarrow \pi^0\gamma\gamma$ is a precision test of Chiral Perturbation Theory as the leading order and next to leading order do not contribute. The first sizable contribution to the branching ratio of this channel comes from O(p^6). There have been a number of experimental measurements of the branching ratio of this decay channel with contradictory results (Table 1) because of the significant background coming from other decay channels (direct $2\pi^0$ production and $\eta \rightarrow 3\pi^0$).

Table 1: Experimental Measurements

Experiments	BR ($\eta \rightarrow \pi^0\gamma\gamma$)
GAMS-2000	$(7.1 \pm 1.4) \times 10^{-4}$ [1]
Crystal Ball	$(3.5 \pm 0.7_{stat} \pm 0.6_{sys}) \times 10^{-4}$ [2]
KLOE	$(8.4 \pm 2.7_{stat} + 1.4_{sys}) \times 10^{-5}$[3]

The situation is equally uncertain on the theoretical front. This is primarily because there are 96 terms which contribute at order p^6. The calculation of these terms is not straightforward.

Here we present first simulation results concerning the feasibility for a proposed study with the WASA Detector, using the reaction pd$\rightarrow$ ^{3}He $\eta \rightarrow$ ^{3}He $\pi^0\gamma\gamma$ at 1 GeV. At this energy the cross section of double π^0 is 1.5 μb and the eta production cross section is 0.4 μb. Identification plot for ^{3}He in the Forward Detector is shown in Fig.1.

To optimize the cuts, we have analyzed Monte Carlo data (500k events), for the signal $\eta \rightarrow \pi^0\gamma\gamma$ and the background reactions $2\pi^0$ and $\eta \rightarrow 3\pi^0$ at a beam energy of 1 GeV.

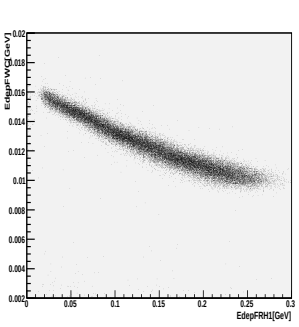

Fig. 1: Energy deposited in the first plane of the Forward Window Counter vs energy deposited in the first plane of the Forward Range Hodoscope [4].

To reduce the contribution of the $2\pi^0$ and $\eta \rightarrow 3\pi^0$ reactions, we use the following cuts

1. Energy deposited in the first plane of the Forward Range Hodoscope has to be in the range of 0 to 0.35 GeV.
2. Two σ cut on the invariant mass of π^0 and invariant mass of bachelor γ's $> 0.200\ GeV/c^2$, where σ is 8 MeV.
3. Missing energy of the system has to be in the range of -0.15 to 0.15 GeV.
4. One σ cut on the invariant mass of η ($\pi^0\gamma\gamma$).

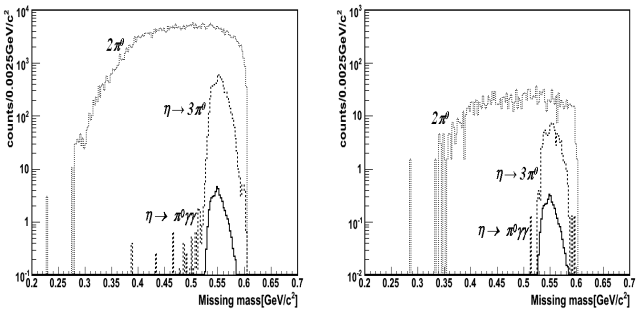

Fig. 2: Missing mass of ^{3}He in the Forward Detector (a) without cut (b) with cuts from 1 to 4. Dotted line: direct $2\pi^0$ production, Dashed line: $\eta \rightarrow 3\pi^0$ and Solid line: $\eta \rightarrow \pi^0\gamma\gamma$

The results are shown in Fig.2. Here the missing mass spectra from MC are scaled according to cross section. We are now investigating how to increase the signal to background ratio further.

References:

[1] D. Alde et al., Z Phys.C **25** 225 (1984).
[2] S. Prakhov et al., Phys. Rev.C **72** 025201 (2005).
[3] B. Di Mico et at., Acta Phys. Slov. **56** 403 (2006).
[4] C. Zheng, Matching Trigger Efficiency of the Forward Detector of WASA-at-COSY.

* Indian Institute of Technology, Bombay, India
Supported by DST-DAAD

Analysis of the decay $\eta \longrightarrow \pi^+\pi^-\gamma$ measured with WASA-at-COSY

Christoph Florian Redmer

The decay $\eta \rightarrow \pi^+\pi^-\gamma$ is driven by the box anomaly of the chiral Lagrangian, which describes a direct coupling of a photon and three pseudoscalar mesons. But since the η is not a massless Goldstone-Boson, the decay width predicted by the anomaly is significantly lower than the one experimentally determined. Therefore, extensions to Chiral Perturbation Theory have been developed. These involve intermediate vector mesons (VMD, [1]) or dynamically generated resonances (Chiral Unitary Approach, [2]).
Precise studies of the two pion system allow for tests of the Chiral Perturbation Theory and its unitarized extensions. Moreover, this decay channel also provides a test for C-violation in electromagnetic interactions of strongly interacting particles.
Therefore, the final goal of the analysis is to provide background free and acceptance corrected invariant mass distributions of the two pion system. At the same time, C-nonconserving decay parameters can be checked.
First data to investigate this decay channel were taken during the first production run of WASA-at-COSY in April 2007. Since it was dedicated to the measurement of $\eta \rightarrow 3\pi^0$, triggers picking up charged decay signatures had to be suppressed.
For the reconstruction of this decay channel only events are accepted, in which two tracks assigned to particles of opposite charge as well as one neutral track are found in the Central Detector (CD). The three tracks have to be correlated in time with two protons reconstructed in the Forward Detector (FD) which serve as a time reference signal for the event.
As proton candidates, tracks within a certain time limit accepted. The multi layer structure of the FD permits the use of the ΔE-E–method for particle identification. Protons can be separated from other particles, e.g. decay products that have been emitted into the acceptance of the FD, by their characteristic energy losses.
The resulting event sample still contains a large amount of missidentified events. Three or two pion final states can mimic the signature either by a photon, lost due to the limited acceptance of the CD, or by the charged particles causing additional signals in the calorimeter that are registered as neutral.
The cuts applied in the analysis aim for the suppression of fake neutral particles. They are expected to be low energetic and closely located to charged tracks. Hence, the energy of the reconstructed photons is required to be larger than 150 MeV and the opening angle between a charged and the neutral track is required to be larger than 30°. The latter criterion reduces the amount of $\eta \rightarrow \pi^+\pi^-\gamma$ events in the sample only by a few percent. The cut on the photon energy is a temporary solution, since it drastically cuts into the phase space of the signal channel.
To make sure that the selected events containing pions as charged particles, the missing mass distribution of the protons and the photon can be checked. It starts from 270 MeV, which is twice the pion rest mass.
Contributions from three pion final states can be identified in the missing mass distribution of the protons and the charged pions. They cause a peak at the pion mass. The distribution originating from the decay $\eta \longrightarrow \pi^+\pi^-\gamma$ is peaked at zero. Finally a cut on the total missing energy and the total missing

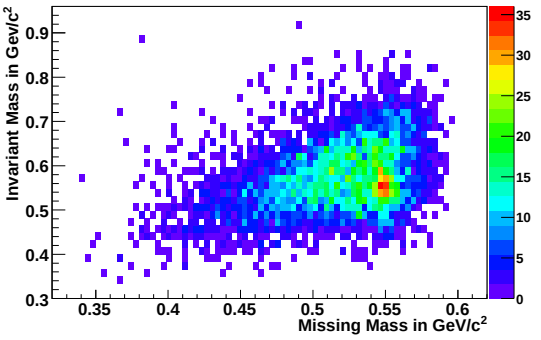

Fig. 1: Invariant Mass of $\pi^+\pi^-\gamma$ as a function of the Missing Mass of two protons after the cuts are applied

momentum puts further constraints to ensure the quality of event reconstruction. The resulting distributions are shown in Fig. 1. The major background contribution originates from direct $\pi^+\pi^-$-production. This is even more obvious when the energy threshold of the photons is lowered to a value of 50 MeV, as shown in Fig. 2. The reduction of this background channel remains the most challenging task.

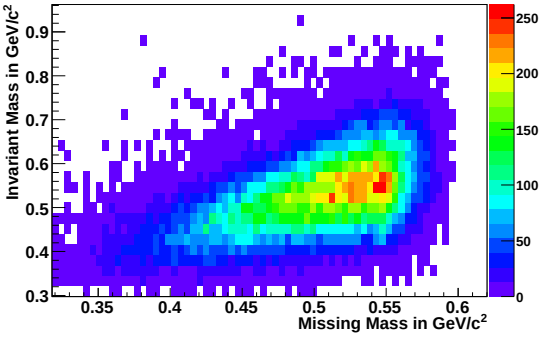

Fig. 2: Invariant Mass of $\pi^+\pi^-\gamma$ as a function of the Missing Mass of two protons, with a reduced threshold on the photon energy.

Very promising, especially with respect to the two pion background, is the analysis of the data taken in October 2008.
Here the η-mesons were produced in the reaction $pd \rightarrow {}^3He\eta$. The cross section for $\pi^+\pi^-$-production is two orders of magnitude lower than in proton-proton-collisions. The analysis of these data has already started. Results are expected in 2009.

References:

[1] B. R. Holstein, Allowed eta decay modes and chiral symmetry, Phys. Scripta T99:55-67, 2002
[2] B. Borasoy and R. Nissler, $\eta, \eta' \rightarrow \pi^+\pi^- l^+ l^-$ in a chiral unitary approach, Eur. Phys. J. A 33:95-106, 2007

Rare eta-meson decay $\eta \to \pi^0 + e^+ + e^-$ at WASA-at-COSY

A. Winnemöller*, A. Khoukaz*, F. Bergmann*, A. Passfeld*, and T. Rausmann*

The C-violating η decay $\eta \to \pi^0 + e^+ + e^-$ is studied using p + d $\to$ ^{3}He + η data and p + p $\to$ p + p + η data obtained at the WASA-at-COSY facility. The dominant C conserving contribution to the decay is via a $\pi^0 + \gamma^* + \gamma^*$ intermediate state with an expected branching ratio of approximately 10^{-8} [1]. An observation of a significantly higher branching ratio would, therefore, be an indication of a C violation. Aim of the presented study is a significant improvement of the current upper limit of the branching ratio of $4 \cdot 10^{-5}$ [2].

The first step in the analysis is to reduce the amount of background data drastically by a cut on the signature of the data. Thus only events with two respectively one charged tracks in the forward detector (according to two protons respectively one ^{3}He, depending on the production process) and two charged ($e^+ + e^-$) and two neutral tracks (two gammas from the π^0 decay) in the central detector are stored in the first preselection. This causes a data reduction of more than a factor of 100 from 1.5 TB before the preselection to 12 GB after the preselection.

There are several competitor reactions that have the same signature as the desired decay, for example the direct production of $\pi^0 + \pi^+ + \pi^-$. The amount of those reactions without an η-meson involved can be reduced by applying a cut around the η-mass in the missing mass distribution of the protons and the ^{3}He, respectively (Fig. 1).

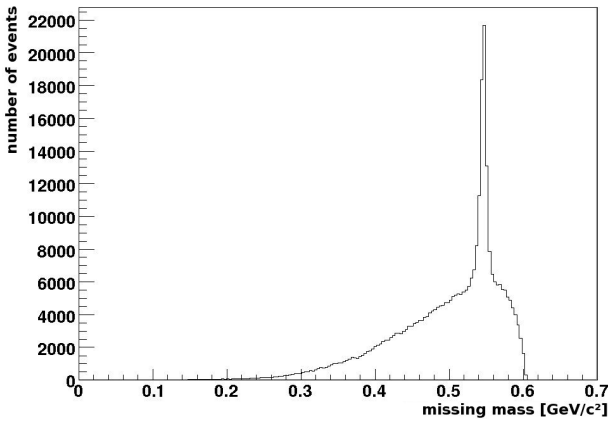

Fig. 1: Missing mass spectrum of the ^{3}He with η-peak

In the next step a cut on the invariant mass of the two gamma system is applied. Since they are expected to be produced in the decay of the π^0 the cut is applied around the according mass.

The worst background reaction that still remains in the data is the decay $\eta \to \pi^0 + \pi^+ + \pi^-$. Due to the high branching ratio of 22,7% and the signature that is very similar to the reaction of interest most of the remaining data originate from this decay. To dispose that decay an extremely accurate distinction between electrons and pions is of high importance and the main challange of this analysis. For that reason several cuts are neccessary. The main cut is shown in Fig. 2 for Monte Carlo simulations. Here the energy deposition in the central detector is plotted against the momentum multiplied with the sign of the charge of the particles. The cut indicated by the solid lines was prepared using Monte Carlo data. When applied to the data it reduces the amount of pions by a factor of approximately 1000 while reducing the amount of electrons only by a factor of 2. A sample for real data with clearly visible bands of electrons and pions is shown in Fig. 3.

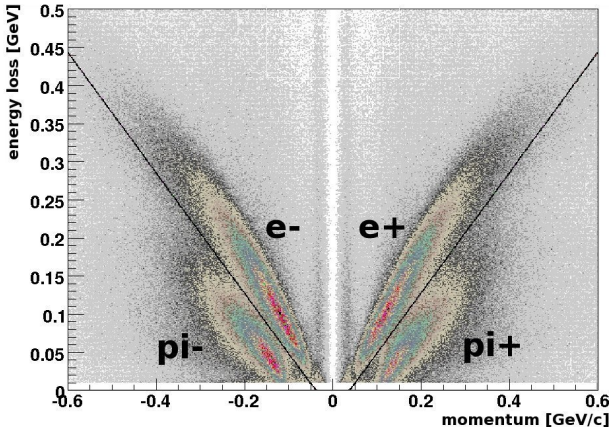

Fig. 2: Main cut for distinction between electrons and pions

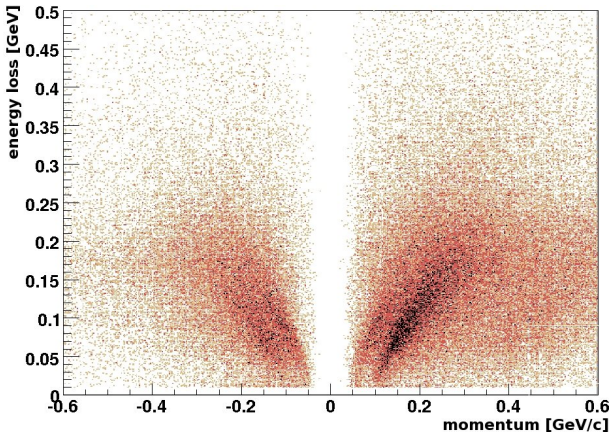

Fig. 3: Distribution of real data

In the next step the invariant mass of all four particles in the central detector is used. Assuming the electron mass for the charged particles a signal at the η-mass should appear for the invariant mass of the system $\gamma + \gamma + e^+ + e^-$. For misidentified pions the peak is shifted towards lower energies due to the fact that the wrong mass for the charged particles is assumed. Such a cut leaves the number of electrons nearly unchanged while reducing the amount of pions by a factor of 200.

After all cuts are applied there is a ratio of 1/150000 in the reduction facors between electrons and pions. Assuming sufficient statistics these cuts will allow for an improvement of the current upper limit by a factor of 15.

Supported by COSY-FFE

References:

[1] J. Smith, Phys. Rev. **166**, 1629 (1968)
[2] M.R. Jane et al., Phys. Lett. B **59**, 99 (1975)

* Institut für Kernphysik, Westfälische Wilhelms-Universität Münster, 48149 Münster, Germany

T. Tolba and C. Pauly

Double pion production, in proton-proton collisions provides information on the nucleon-nucleon (*NN*) interaction and on nucleon resonance properties.
Near threshold, the Roper resonance (N*(1440)P_{11}) is expected to dominate. The Roper resonance is expected to decay via two decay modes, the first one is the direct decay into a proton and two pions, (pp→pN*(1440)→pππ). The other is the decay to pion and Δ(1232) which then decays to proton and pion, (pp→pN*→πΔ→pπ). At higher excess energies double Δ(1232) or ρ^0(770) meson production are expected to dominate, (pp→Δ(pπ)Δ(pπ)), (pp→ppρ^0→$\pi^+\pi^-$), ref [1-3].
The aim of this work is to compare the contribution of the different decay models with the analyzed data in region of high excess energy.
Data on this final state were collected during April-May 2008 using a 1.4 GeV proton kinetic energy.
Selecting exactly 2 charged tracks in the FD and 4 neutral tracks in the CD was the first step in analyzing the data (for an overview of the WASA-at-COSY detector see Fig.1 in the contribution by C.Zheng). Proton identification in FD was accomplished by using the ΔE-E method, by comparing the deposited energy in the first layer of the forward range hodoscope to the deposited energy in all layers. A 2-dimensional cut on the proton band was used to select protons, (Fig. 1).

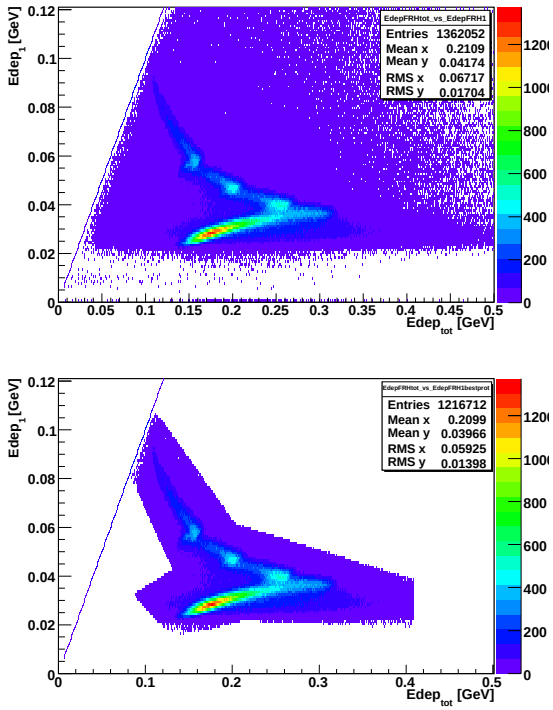

Fig. 1: Total Edep Vs. Edep in the first layer of the forward range hodoscope of FD. Before cut on proton band (upper figure), after cut on proton band (lower figure).

In order to determine the correct combinations of 2 pairs of 2 photons to reconstruct the π^0→γγ decay of both pions a χ^2 approach was used (formula 1).

$$\chi^2 = [\frac{IM_{\gamma_1\gamma_2} - 0.135}{\sigma_{IM_{2\gamma}}}]^2 + [\frac{IM_{\gamma_3\gamma_4} - 0.135}{\sigma_{IM_{2\gamma}}}]^2 (1)$$

$$\sigma_{IM_{2\gamma}} = 13.4 MeV$$

The missing mass of the 2 protons and invariant mass of the 4γs ($2\pi^0$) were reconstructed, (Fig. 2).
The lowest value populated in the missing mass and invariant mass spectra should be at least two times the π^0 mass (270 MeV/c^2) and the upper limit should have the excess energy of the system (330 MeV, i.e. end at 600 MeV). Instead we see tails in the high and low energy regions in both histograms. This can be due to the effect of background, wrong γγ (π^0) combination and/or finite resoultion.
Therefore, additional constraints were applied on the minimum χ^2 plot ($\chi^2 \leq 10$) and on the total missing mass squared in the system (-0.04≤TotMM^2≤0.04 GeV/c^2) in order to clean the data sample from background, (Fig.2 dashed line).
The next step is to use a full kinematical fit to suppress the background and to improve the data analysis.

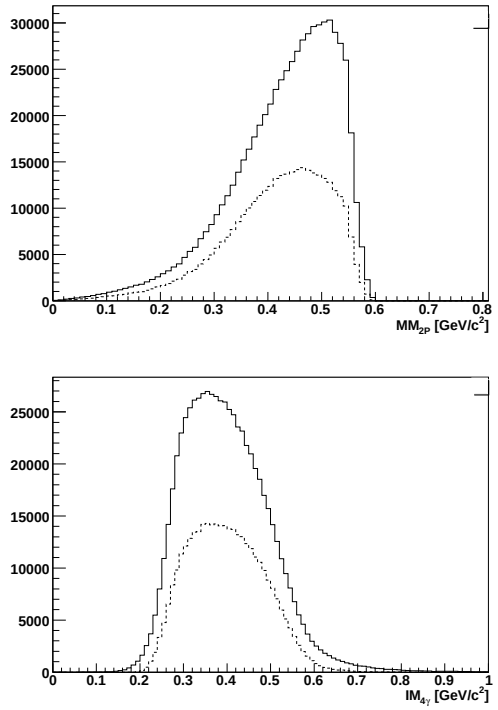

Fig. 2: Missing mass of the 2 protons (upper figure), Invariant mass of the 4 gammas (lower figure). Before cuts (solid line), after cuts (dashed line)

References:

[1] W. Brodowski et al., Phys. Rev. Lett. 88, 192301 (2002)
[2] F. Balestra et al. DISTO Collaboration. Phys. Rev. Lett. 89, 092001 (2002)
[3] H. Calèn et al., Phys. Scripta. Vol. T104, 15 (2003)

Search for eta Mesic Helium
using WASA-at-COSY

W. Krzemień [1,2] P. Moskal [1,2] J. Smyrski [2]

In June 2008 a measurement of the production of $p\pi^0X$, $p\pi^-X$ as well as of $Tp\pi^0$ and $^3Hep\pi^-$ in the dd collisions with WASA-at-COSY was performed. During the experimental run the momentum of the deuteron beam was varied continuously within each acceleration cycle from 2.185 GeV/c to 2.400 GeV/c, crossing the kinematical threshold for the η production in the $dd \rightarrow {}^4\mathrm{He}\,\eta$ reaction at 2.336 GeV/c. This range of beam momenta corresponds to the excess energy variation from -51.4 MeV to 22 MeV with respect to the $^4\mathrm{He}-\eta$ system. The experimental method is based on the measurement of the excitation function for chosen decay channels of the $\mathrm{He}-\eta$ system and a search for a resonance-like structure below the $\mathrm{He}-\eta$ threshold. The relative angle between the outgoing *nucleon* – *pion* pair which originates from the decay of the N*(1535) resonance created via absorption of the η meson on a nucleon in the He nucleus, is 180° in the N* reference frame and is smeared by about 30° in the center-of-mass frame (see Fig.1) due to the Fermi motion of the nucleons inside the He nucleus. The center-of-mass kinetic energies of the nucleon and pion originate from the mass difference $m_\eta - m_\pi$ and are around 50 MeV and 350 MeV, respectively.

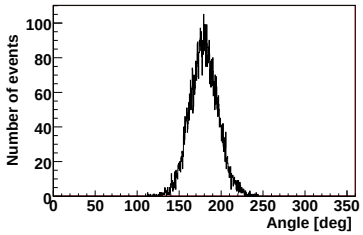

Fig. 1: Distribution of the relative $p-\pi$ angle seen in the reaction center-of-mass system as simulated for the processes leading to the creation of the eta-helium bound state: $dd \rightarrow ({}^4He\eta)_{bound} \rightarrow {}^3Hep\pi$.

At the time of the experiment the cooling of the solenoid was broken and the measurement was conducted without the magnetic field. That fact excluded the possibility of direct momentum determination in the Central Detector as well as use of the standard identification method for the charged particles registered in the Central Detector. However, for the momentum determination of the charged particles an information about directions of the particles in the Central Detector,as well as, the momentum of the He can be used. The He momentum was determined on the basis of energy losses in the Forward Detector. Knowing the beam momentum, He momentum, and directions of two other particles one can calculate the momenta from the Momentum Conservation Principle. Monte Carlo expectation for energy loss in the Plastic Scintillator combined with the energy deposited in the Electromagnetic Calorimeter was used to identify protons and pions.

At present we have established the excitation function only for the $dd \rightarrow {}^3He(two\ charged\ particles)$ reaction. The result may be treated as a very conservative estimation of the upper limit for the prompt $dd \rightarrow {}^3Hep\pi^-$ reaction. The excitation function is presented in Fig. 3.

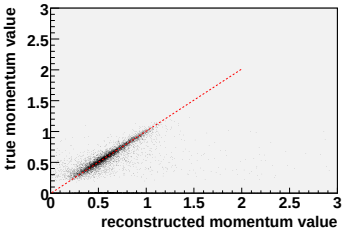

Fig. 2: Monte Carlo:Reconstructed momentum versus true momentum for two charged particles registered in the Central Detector with the condition that the He ion was detected in the Forward Part.

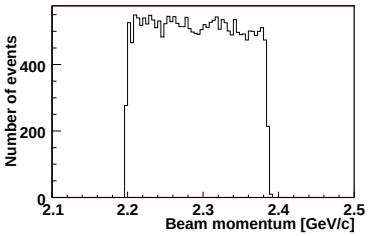

Fig. 3: Excitation functions for the $dd \rightarrow {}^3He$ *two charged* as a function of the relative angle betwen charged particles measured in the Central Detector determined for the angular range between 160 and 200 degrees.

Taking into account the obtained average luminosity of $2\cdot 10^{30}\mathrm{cm}^{-2}\mathrm{s}^{-1}$, the detection acceptance reconstruction efficiency of about 50%, and the measurement time we obtain that the observed yield corresponds to the cross section of 2 μb. However, regarding additionally that the spectrum includes not only $p\pi^-$ pairs but also pairs of $\pi^+\pi^-$, $p\pi^+$, $\pi^+\pi^+$, $\pi^-\pi^-$ we could roughly guess that the contribution from the reaction $dd \rightarrow {}^3Hep\pi^-$ alone, which can be identified in the next experiments with the presence of the magnetic field, amounts to about 0.4 μb.

In 2010 two-week measurements with WASA-at-COSY for $dd \rightarrow {}^3\mathrm{He}p\pi^-$ channel was recommended by the COSY Program Advisory Committee. The use of the solenoid will permit better proton-pion identification, as well as better momentum determination in the Central Detector. After two weeks of measurement with the assumed luminosity of $4*10^{30}cm^{-2}s^{-1}$, we expect a sensitivity of a few nb with a statitical significance of 1 σ. In the case of non-observation of signal this result would significantly lower the upper limit for the existence of the bound state.

[1] Institut für Kernphysik and Jülich Center for Hadron Physics, Forschungszentrum Jülich, Jülich, Germany

[2] Institute of Physics, Jagiellonian University, Cracow, Poland

Strangeness Production with WASA-at-COSY

A. Kowalczyk[a,b,*]

In the spectrum of strange particles, the excitation modes of hyperons are less known. In particular, the $\Lambda(1405)$ state has received increased attention, since its nature is under debate. Various theoretical investigations predict for this possibly dynamically generated state a two-pole structure [1, 2, 3].
This calls for a detailed investigation of the resonsnce line shape.
A feasibility study for measurements of the production and the decay of hyperon states has been started with WASA-at-COSY. Here, we report on the investigation of ground state Σ production in the reaction channel $pp \to p\Sigma^+(1189)K^0$, with the mostly neutral final state involving three pions:
$p\Sigma^+K^0 \to p(p\pi^0)(\pi^0\pi^0)$.
An experimental data set taken in April/May 2008, at 2.95 GeV/c beam momentum has been employed. Six photons coming from the decay of the three pions and two protons are the final state products of the reaction. Protons are detected in the forward part of the detection system, photons in the central part, see Figure 1 in the contribution by C.Zheng.
A first view into the experimental data is shown in Figures 1 and 2.

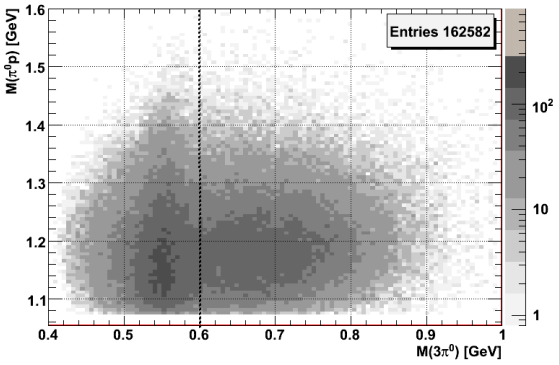

Fig. 1: Invariant mass M(π^0p) versus M($3\pi^0$). The M(π^0p) contain Σ^+ events. The vertical structure stems from the dominant $\eta \to 3\pi^0$ decay. The dashed line indicates the cut to suppress these events.

Reaction channel	Cross section
$pp \to p\Sigma^+K^0 \to pp\pi^0\pi^0\pi^0 \to pp6\gamma$	$0.75\mu b$ [4]
$pp \to pp\eta \to pp\pi^0\pi^0\pi^0 \to pp6\gamma$	$13\mu b$ [5]
$pp \to pp\pi^0\pi^0\pi^0 \to pp6\gamma$	$40\mu b$ [6]

Table 1: Cross section for the reaction channels with $2p6\gamma$ final state.

It is a challenge to find the strange particles, since in addition to the investigated reaction channel, there are two significant background channels:
(i) η production (already suppressed, as shown in Figure 1),
(ii) direct $3\pi^0$ production.
Cross sections for the reactions are compared in Table 1.

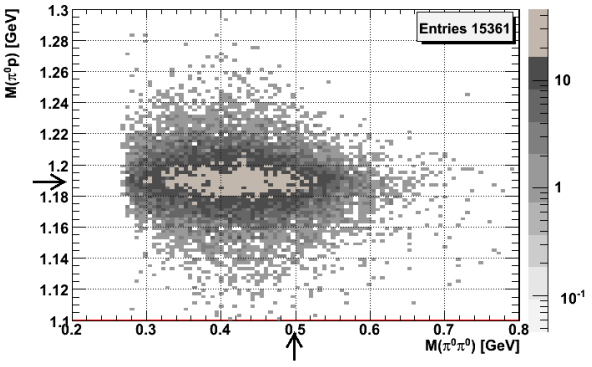

Fig. 2: Invariant mass M(π^0p) versus M($\pi^0\pi^0$) after the cut to suppress $\eta \to 3\pi^0$ events. Also, combinatorial background is suppressed by choosing the best π^0p combination, i.e. closest to the Σ^+ mass. The remaining two pions form a broad distribution, covering the location expected for a (K^0,Σ^+) correlation (0.497GeV,1.189GeV, indicated by arrows).

The further analysis should employ additional methods (i.e. full kinematic fit) to suppress the remaining, most dominant background channel as well as to improve particle identification.

References:

[1] V.K. Magas, E. Oset and A. Ramos, *Phys. Rev. Lett.* **95**, 052301 (2005).
[2] D. Jido, et al., *Nucl. Phys.* **A725**, 181 (2003).
[3] M. Kimura, et al., *Phys. Rev.* **C62**, 015206 (2000).
[4] A. Sibirtsev, et al., *Nucl. Phys.* **A646**, 427 (1999).
[5] P. Moskal, et al., *Phys. Rev.* **C69**, 025203 (2004).
[6] C. Pauly, et al., *Phys. Lett.* **B649**, 122 (2007).

[a] Institut für Kernphysik and Jülich Center for Hadron Physics, D-52425 Jülich, Germany

[b] Institute of Physics, Jagiellonian University, PL-30059 Cracow, Poland

* Supported by COSY-FFE

η Meson Production in pp Collisions and Luminosity with WASA-at-COSY

N.Shah[a]

We would like to study the role of the S_{11} (1535) resonance in the production of the η meson. To study this we look at the angular distribution and the invariant mass distributions of the proton-proton and proton-η systems. A production run for the η mesons was taken in April-May 2007. We have collected approximately 10^7 η mesons in the proton-proton reaction.
To select events we apply the following conditions on the data which have been obtained as a result of detailled simulations:

1. Two charged tracks in the Forward Detector (FD)(see Figure 1 in the contribution by C.Zheng)
2. Six neutral clusters in the Central Detector (CD)
3. Energy deposited in the FD and CD $>$ 0.025 GeV
4. -0.15 GeV$<$ Missing Energy of the total system $<$ 0.15 GeV

We apply a kinematic fit with :

1. constraints on energy-momentum conservation
2. constraints on π^0 mass

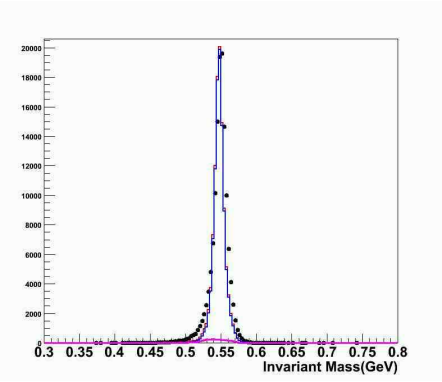

Fig. 1: Invariant mass of η (•-data points, Blue-$\eta \rightarrow 3\pi^0$, Pink-$pp \rightarrow pp3\pi^0$)

In figure 1, the invariant mass distribution of the η meson is plotted. We are working on the background subtraction and efficiency corrections.
For absolute cross sections, we need to determine the luminosity. We use proton proton elastic scattering. We clean up the data by ensuring the following physical constraints[1], for an elastic collision between two particles of equal mass:

$$|\phi_1 - \phi_2| = \pi \qquad (1)$$

$$tan\Theta_{1,lab} * tan\Theta_{2,lab} = \frac{1}{\gamma_{cm}{}^2} \qquad (2)$$

Equation (1) is the co-planarity condition and equation (2) is known as kinematical correlation. The Lorentz factor γ_{cm} describes the movement of the laboratory system with respect to the center of mass system and can be written as

$$\gamma_{cm} = \sqrt{1 + \frac{T_{lab}}{2m}} \qquad (3)$$

where T_{lab} is the kinetic energy of the incident beam and m is the rest mass of the beam particle.

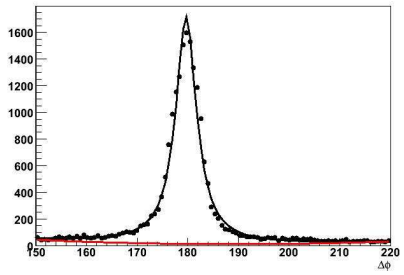

Fig. 2: The co-planarity condition.(•-data points, Black-fitted line, Red-background)

The pp elastic scattering events are selected with the condition that we have one charged track in the FD and one charged track in the CD. The co-planarity distribution is plotted for a single experimental run taken in April 2007 in Figure 2. The co-planarity distribution peaks at the value of 180° as expected.
The data points are fitted by assuming the signal to be Gaussian and background to be a 2^{nd} order polynomial. After subtracting the background, we get the average luminosity, $\mathbf{L} = 7.73 \times 10^{30} cm^{-2} s^{-1}$. The analysis for the complete data set is in progress.

References:

[1] Levent Demiroers, Investigating Interactions of Deutrons and Protons with the Hydrogen Pellet Target of the CELSIUS/WASA experiment, Dissertation thesis, University of Hamburg(2005).

[a] Indian Institute of Technology Bombay, Mumbai, India
* Supported by DST-DAAD

Energy Resolution of the WASA-at-COSY Electromagnetic Calorimeter

A. Kowalczyk[a,b,*]

The electromagnetic calorimeter, which is part of the Central Detector of the WASA-at-COSY system (see Figure 1 in the contribution by C.Zheng) allows for neutral particle detection, especially photons. The study of the calorimeter energy resolution is a crucial task for all neutral decay channels [1]. The currently quoted photon energy resolution is $5\%/\sqrt{E}$ [2] and has been achieved with an indirect method. It is the result of a comparative study of Monte Carlo and data, i.e. it reproduces the invariant mass widths of π^0 and η.

Here, we report on the investigation of the photon energy resolution in a quasi-direct way, where the $pd \rightarrow {}^3He(\eta \rightarrow \gamma\gamma)$ reaction is used as a photon source.

An experimental data set, taken in October/November 2008, at 1.69 GeV/c beam momentum has been used.

The two photons stemming from the eta decay are detected in the central part of the detection system, the ${}^3He$ particle in the forward part.

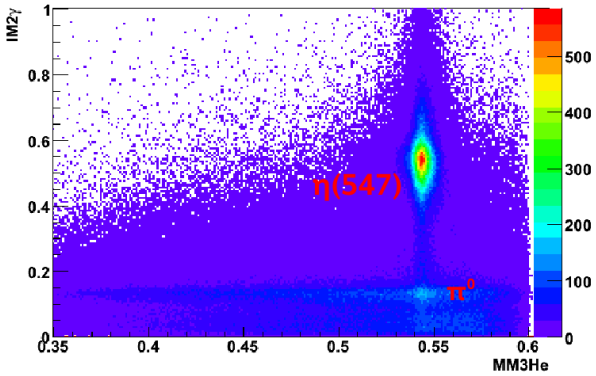

Fig. 1: Invariant mass IM(2γ) versus missing mass MM(^3He).

This is an almost background free reaction. Based on the dependance shown in Figure 1, η meson production can easily be selected.

For each of the final state particles three variables are measured: energy, azimuthal (Θ) and polar (Φ) angles. Taking into account four-momentum conservation, there are five independent variables. Due to the overconstraint, the energy of photons can be treated as unknown in a kinematic fit.

Balancing the four-momentum conservation using the kinematic fit , the energy of photons is calculated. The calorimeter resolution is defined as the difference between the measured and the fitted photon energy.

The relative resolution as a function of the photon energy known from the fit is shown in Figure 2.

The photon energy resolution is different for the different calorimeter rings: in the central part of the calorimeter (see upper panel of Figure 2) it is consistent with the $5\%/\sqrt{E}$, for rings in the forward and backward part of the calorimeter (see lower panel of the Figure 2) it does not agree.

Therefore, further detailed investigations (i.e. studies of the systematical effects based on Monte Carlo simulations) are needed to understand this behavior.

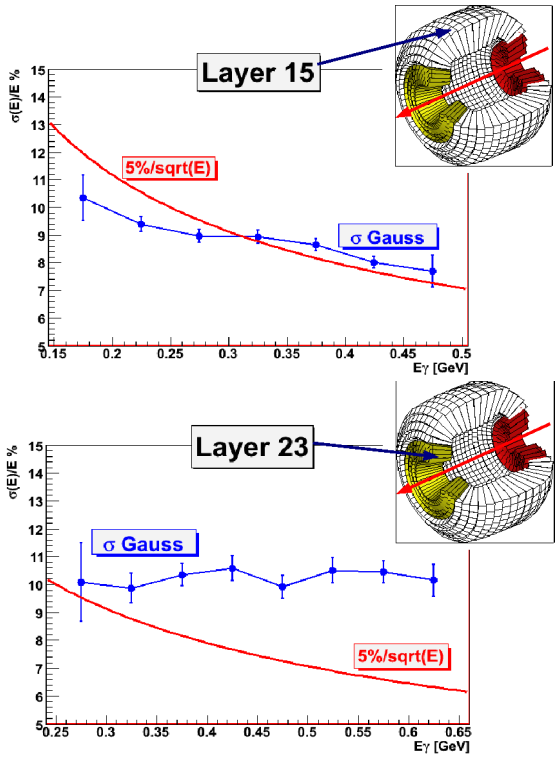

Fig. 2: The relative photon energy resolution for the selected calorimeter rings versus the fitted photon energy. Red curves correspond to the currently used value, blue data points to the quasi-direct method.

References:

[1] Proposal "WASA-at-COSY", `nucl-ex/0411038`.
[2] C. Bargholtz, et al., *Nucl.Instr.Meth.* **A594**, 339 (2008).

[a] Institut für Kernphysik and Jülich Center for Hadron Physics, D-52425 Jülich, Germany

[b] Institute of Physics, Jagiellonian University, PL-30059 Cracow, Poland

* Supported by COSY-FFE

Investigation of pd Elastic Scattering for Luminosity Determination with WASA-at-COSY*

C. Zheng[a,b], M. Büscher, P. Fedorets[a,c]

We describe the luminosity determination for a test beam-time on $a_0/f_0(980)$ production in $pd \to {}^3A\,X$ processes at a beam momentum of $p_p = 2.935$ GeV/c ($T_p = 2.143$ GeV) [1]. Three independent methods have been used which yield consistent numbers, thus justifying the assumptions that had to be made during data analysis:

i) Based on the beam intensity and target thickness the luminosity can be estimated as $L = j \cdot \rho_{\mathrm{eff}} \sim 5.4 \cdot 10^{30}\,\mathrm{s^{-1}cm^{-2}}$. Here, j is the beam current (protons/s), deduced from the number of particles in the flat top of the beam and from the revolution frequency. ρ_{eff} is the effective target density (atoms/cm^2) calculated from the parameters of the pellet flux assuming 100% beam-target overlap. A typical reduction factor of 6 for the lower effective pellet frequency, and beam losses during the cycle has been applied.

ii) From pp quasi-elastic scattering with the neutron being a spectator, the average effective luminosity can be figured out when assuming the same cross section as for pp elastic scattering. The total pp elastic cross section at $T_p = 2.1$ GeV is 17.0 ± 0.8 mb [3], which leads to $L \sim 3.1 \cdot 10^{30}\,\mathrm{s^{-1}cm^{-2}}$.

iii) pd elastic scattering events, with the proton detected in the Forward Detector (FD, see Figure 1 in the contribution by C. Zheng.) and the deuteron in the Central Detector (CD), could be identified on top of a huge background from the pp quasi-elastic scattering. The evaluation of these events, described in the following in more detail, yields $L = (3.2 \pm 0.2) \cdot 10^{30}\,\mathrm{s^{-1}cm^{-2}}$.

The pd data analysis starts with the selection of one charged track in the FD and CD, respectively. After a FD-CD time coincidence cut, the coplanarity of the two charged tracks is exploited. The corresponding azimuthal angle correlation is plotted in Fig. 1 (left). The background under the peak within the $\pm 3\sigma$ region can be further suppressed by about a factor two by requiring that the number of neutral tracks in the CD is less than two. For the remaining events the polar angle correlation of the charged FD and CD tracks is depicted in Fig. 1 (right). It is seen that most events are located around the pp elastic line (determined from a MC simulation) and thus stem from pp quasi-elastic scattering. Thus, further background suppression is required.

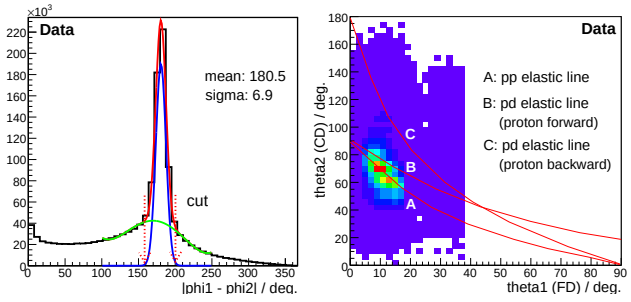

Fig. 1: The angular correlation of two charged tracks for the azimuthal (left) and polar angles (right).

For the charged tracks in the CD, the ΔE-*vs.*-momentum distribution is presented in Fig. 2 (left) together with the expected proton and deuteron lines obtained from a Monte-Carlo simulation. A cut is applied, which then allows one to extract the pd elastic-scattering events from the strongly reduced pp quasi-elastic background. For the deuteron candidates the agreement between the polar-angle value measured directly in the CD and the one calculated from the charged track in the FD is checked on an event-by-event basis. Figure 2 (right) shows that a clear peak of forward pd elastic scattering appears around zero angular difference.

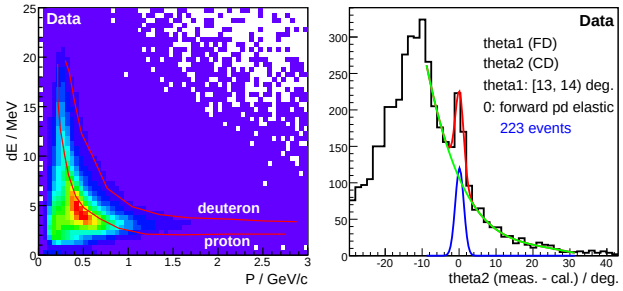

Fig. 2: Left: Energy deposited in the plastic scintillator of the CD *vs.* momentum reconstructed from the track curvature in the solenoid field with the straw chamber. Right: Difference of the measured polar angle (theta2) of the charged track in the CD and the one reconstructed from the measured FD polar angle (theta1) assuming forward pd elastic kinematics. theta1 has been restricted to angles between 13°and 14°.

To compute the original number of scattering events, efficiency corrections were considered, such as geometric acceptance, detector efficiency, track-reconstruction efficiency and cut efficiency, which is obtained from Monte-Carlo simulation. The efficiency of the momentum reconstruction is $\sim 65.9\%$ and has been determined from the data. In addition, the trigger pre-scaling factor and the DAQ dead time factor were included. When calculating the effective beam time, the ratio of beam-on to beam-off in one cycle was taken into account.

The average effective luminosity of $L = (3.2 \pm 0.2) \cdot 10^{30}\,\mathrm{s^{-1}cm^{-2}}$ is finally calculated from the differential cross section of forward pd elastic scattering at an incident proton kinetic energy of 2.0 GeV [2]. After the conversion from c.m. to the Lab frame, the number is (314.6 ± 10.2) μb/sr for protons emitted at 13.7°.

References:

[1] M. Büscher et al., "Search for the scalar mesons $a_0/f_0(980)$ in $pd \to {}^3$HeX data from WASA-at-COSY"; contribution to this Annual Report.
[2] E. Coleman et al., Phys. Rev. **164**(1967):1655-1661.
[3] T. Fujii et al., Phys. Rev. **128**(1962):1836-1841.

[a] Institut für Kernphysik and Jülich Center for Hadron Physics, Forschungszentrum Jülich, D-52425 Jülich, Germany
[b] Institute of Modern Physics, Chinese Academy of Sciences, 509 Nanchang Rd., 730000 Lanzhou, China
[c] Institute for Theoretical and Experimental Physics, B. Cheremushkinskaya 25, 117218 Moscow, Russia
* Supported by COSY-FFE, CSC and HGF

Matching Trigger Efficiency of Forward Detector of WASA-at-COSY*

C. Zheng[a,b]

This report describes the results of trigger study of the forward detector of WASA-at-COSY. In the forward detector most of the planes of plastic scintillators can be used as trigger modules, such as FWC, FTH, FRH and FVH. [1] (see Fig.1)

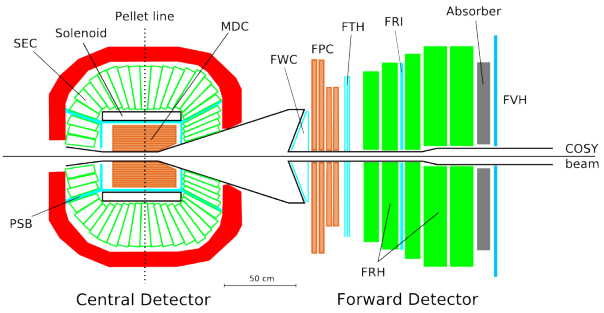

Fig. 1: Side view of the WASA at COSY.

A trigger, called matching trigger, involves four planes, the double planes of FWC (fwca and fwcb), the straight plane of FTH (fhds) and the first plane of FRH (frha). There are 48 elements in fhds and 24 elements in each plane of fwca, fwcb and frha. The elements in each plane are "pizza-piece" shaped with a sector coincidence, as indicated by the shaded pieces in Fig. 2.

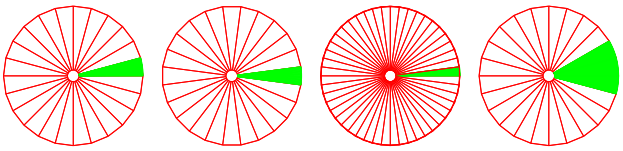

Fig. 2: A sketch of a sector coincidence of the forward planes. From left to right: fwca, fwcb, fhds, frha.

If a charged particle hits the forward detector, then it has passed through FWC and FTH before it is stopped in FRH, or arrives at FVH. On its track, the charged particle leaves energy deposited in one or two neighboring elements of each plane, called clusters. The matching trigger is designed to select tracks with sector coincident clusters in the above planes of fwc(a or b), fhds and frha. Using the multiplicity of charged particles, the matching trigger can be set to "fhdwr1", which means one or more sector coincident clusters, or as "fhdwr2", which means two or more sector coincident clusters. Furthermore, the planes of FWC have two level discriminator thresholds which can be adjusted separately. The matching trigger with the high level threshold is marked as "fHedwr1". Though the plane of frha has only one-level threshold, it could be tuned to a high level to work together with the high level threshold of fwca and fwcb, which is marked as "fHedwrH1". The "fhdwr1" and "fhdwr2" are suited to select proton, deuteron, or triton in the forward detector. However, the "fHedwr1" and "fHedwrH1" are more effective to select ^{3}He or ^{4}He, which deposits more energy in the forward planes.

To examine the efficiency of the matching trigger we chose a lower bias trigger which involved only one or two planes. From the lower bias trigger events, we concentrated on finding events with clusters fulfilling the sector coincidence in the forward planes, called "matching track found" events. We counted the number of events with matching track found as A, and the number of events with both matching track found and matching trigger fired as B. Then the efficiency of matching trigger was calculated as $(B \div A) \times 100\%$.

The results are summarized in Table 1. The matching trigger efficiency was also computed for each sector along the 48 elements of FTH, which were recombined to 24 sectors. (see Fig. 3)

Table 1: Main results of the matching trigger efficiency.

matching trigger	lower bias trigger	efficiency (%)
fhdwr1	frha1	98.7±0.6
fhdwr2	frha2	86.3±0.7
fHedwrH1	fwHeb1|frhaH1	85.2±0.5
fHedwr1	fwHea1	79.2±0.5

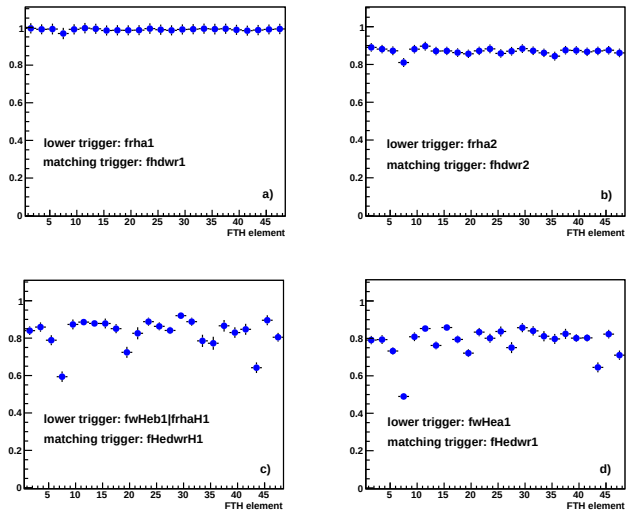

Fig. 3: The matching trigger efficiency for each sector along the 48 elements of FTH.

It is expected that the matching trigger efficiency is independent of lower bias trigger selection. The efficiency of fHedwrH1 was checked with three more lower bias triggers, which were frhaH1 with $(84.2\pm2.6)\%$, fwHea1 with $(79.0\pm2.8)\%$ and fwHeb1 with $(83.3\pm2.4)\%$.

In addition, the purity of matching trigger, the ratio of matching track found events to the total events pre-selected by matching trigger, was obtained as $(99.3\pm1.4)\%$ for fhdwr1, $(98.4\pm1.2)\%$ for fhdwr2, $(96.6\pm0.3)\%$ for fHedwrH1 and $(97.7\pm0.3)\%$ for fHedwr1.

References:

[1] Proposal "WASA at COSY", nucl-ex/0411038.

[a] Institut für Kernphysik and Jülich Center for Hadron Physics, Forschungszentrum Jülich, D-52425 Jülich, Germany
[b] Institute of Modern Physics, Chinese Academy of Sciences, 509 Nanchang Rd., 730000 Lanzhou, China
* Supported by COSY-FFE, CSC and HGF

B.R. Jany[a,b,*]

The Forward Range Hodoscope **FRH**, which is a part of the Forward Detector of the WASA-at-COSY detector system, see Fig. 1 in the contribution by C. Zheng, consist of five layers of plastic scintillators with a stopping power for protons of $\sim$ 300MeV [1].

The reconstruction of the kinetic energy of particles in the FD by the dE-E method is performed in the "standard" way, using a parametrisation of deposited energy (E_{dep}) versus true kinetic energy (E_{true}) relations depending on the particle type. A method using the full multidimensional information from the FRH, taking into account all correlations simultanously - not iteratively - of the particle loosing energy in the five layers, is presented below.

Knowing the energy deposit of the particle in the five layers of the FRH one wants to find the estimator of the kinetic energy of the particle $E_{rec} = T(E_{true})$. The Maximum Likelihood Estimation (**MLE**) provides asymptotically optimal estimators: independent of the distribution of the measurements, the estimators are asymptotically unbiased and asymptotically most efficient [2]. The method is general with optimal performance of the estimators. The estimator of the kinetic energy of the particle $T(E_{true})$ maximizes the Likelihood function L (corresponding to minimisation of $l = -\log(L)$) depending on the deposited energies in five layers of the FRH detector and the true kinetic energy as a parameter. The Likelihood function was derived using a Monte-Carlo GEANT3 simulation generating single tracks in the FRH. The reconstruction of the proton kinetic energy is the priority due to the interest of studying the η' meson decays [4, 5]. Therefore, the reconstruction properties are studied in detail for highly energetic protons.

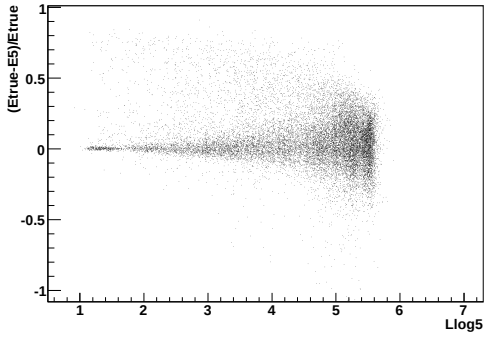

Fig. 1: Relative resolution for the reconstructed kinetic energy versus the minimised Likelihood function l for the Monte-Carlo single proton tracks.

The kinetic energy was reconstructed for single Monte-Carlo proton tracks within an energy range up to 2GeV. In Fig. 1 the relative resolution for the reconstructed kinetic energy $(E_{true} - E_{rec})/E_{true}$ as a function of the minimised Likelihood $l = -\log(L)$ is presented. When the Likelihood l is getting larger (the degree of belief is getting smaller) the relative resolution becomes worse. Cutting on the Likelihood value rejects events with bad resolution i.e. events of low degree of belief.

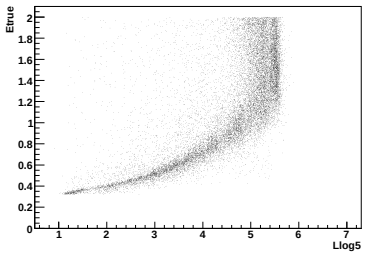

Fig. 2: True kinetic energy E_{true} versus the Likelihood l for the Monte-Carlo single proton tracks.

The true kinetic energy and the Likelihood L are directly correlated as seen in Fig. 2. Performing a cut on the Likelihood l, one can select a certain range of the true kinetic energy of the particle.

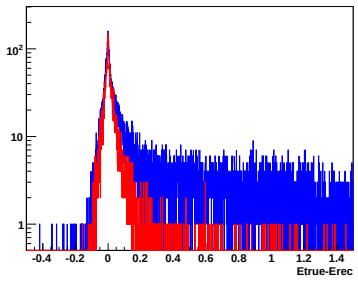

Fig. 3: Energy resolution $E_{true} - E_{rec}$ for the reconstructed kinetic energy based on the Monte-Carlo single proton tracks using "standard" (blue) and Likelihood based (red) kinetic energy reconstruction.

The benefits of the Likelihood method are seen in Fig. 3: the wrongly reconstructed particles are cut out without loosing efficiency.

References:

[1] H. H. Adam, et al. (2004), `nucl-ex/0411038`.

[2] A.W. van der Vaart, *Asymptotic Statistics - Cambridge Series in Statistical and Probabilistic Mathematics*, (1998), `ISBN-13:9780521784504`.

[3] G. D'Agostini, *Bayesian reasoning in data analysis - A critical introduction*, (2003), `ISBN-13:9789812383563`.

[4] B.R. Jany, *AIP Conf. Proc.* **950**, 209–212 (2007), `nucl-ex/07092834`.

[5] D. Duniec and B.R. Jany, *AIP Conf. Proc.* **950**, 213–215 (2007).

[a] Institut für Kernphysik and Jülich Center for Hadron Physics, D-52425 Jülich, Germany

[b] Institute of Physics, Jagiellonian University, PL-30059 Cracow, Poland

* Supported by COSY-FFE

The WASA-at-COSY missing mass resolution for η' tagging

M. J. Zieliński[a,b], A. Kupść[c] and P. Moskal[a,b]

The studies of the η' meson decays are one of the main goals of the WASA-at-COSY experiment [1]. Due to cross section considerations the most appropriate way for the production of the η' meson would be the $pp \to pp\eta'$ reaction where mesons can be tagged by means of the missing mass technique. In this report we discuss analytical parametrisations of the missing mass resolution.

The resolution of the missing mass determination can be described e.g. by one of two functions: exponential

$$f_e(\mu) = A\exp(B|\mu| + C\mu), \tag{1}$$

or asymmetric Gauss:

$$f_g(\mu) = A\exp\left(-\frac{\mu(\mu-|\mu|)}{4\alpha^2} - \frac{\mu(|\mu|+\mu)}{4\beta^2}\right) \tag{2}$$

where $\mu = mm - m_{\eta'}$, with mm denoting the value of the reconstructed mass. For a given shape of the peak $f(\mu)$ one can find the optimal value of the $\Delta\mu$ region as a value corresponding to the minimum of [2]:

$$\frac{\sqrt{\Delta\mu}}{\int_{-\Delta\mu_-}^{\Delta\mu_+} f(\mu)d\mu}, \tag{3}$$

which is expected to be around $\Delta\mu = FWHM$.

In Fig. 1 the distribution of the difference between the reconstructed and real mass of the η' meson is shown. The superimposed lines were fitted using formulas (1) and (2). The figure indicates that due to the relatively large tails the exponential function describes the shape of the spectrum better than the Gaussian. Further on Fig. 2 shows a dependence of

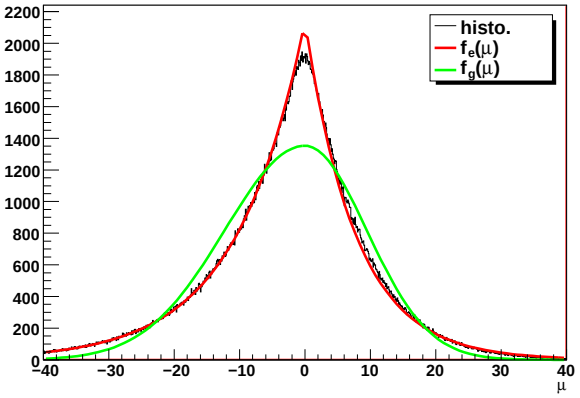

Fig. 1: Figure shows results of the Monte-Carlo simulations of the μ ditribution for excess energy Q = 40 MeV. Simulations were conducted for the $pp \to pp\eta'$ reaction using ROOT event generator whitout beam spread and including only energy resolution for registration of protons. Superimposed lines denote the fit with: exponential function $f_e(\mu)$ - red line; and asymmetric Gauss function $f_g(\mu)$ - green line.

a missing mass resolution simulated for Q = 40 MeV, as a function of the energy resolution. The values of FWHM represented by triangles were obtained applying the formula:

$$\Delta\mu = FWHM = ln(2)\left(-\frac{1}{B+C} + \frac{1}{C-B}\right), \tag{4}$$

with parameters B and C determined by fitting expression 1 to the simulated spectra of μ. Moreover, as shown by the solid

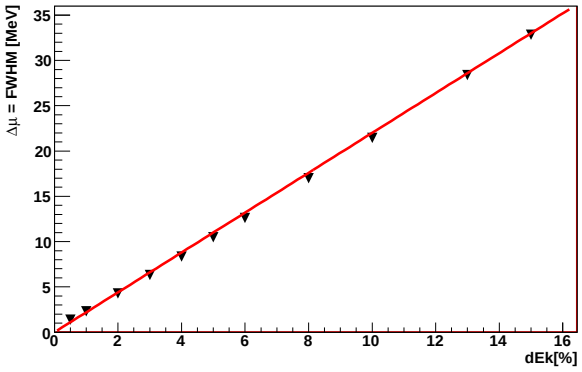

Fig. 2: The FWHM of the missing mass spectra as a function of energy resolution of protons simulated at Q = 40 MeV for the $pp \to pp\eta'$ reaction. The black triangles denote the FWHM calculated fromexpression (4), and the superimposed red line indicates parametrisation according to formula (5).

line, the observed dependence may be parametrized by:

$$\Delta\mu = 11\frac{\Delta E}{E}\sqrt{Q}. \tag{5}$$

where ΔE denotes the the energy resolution of protons. The systematic and statistical errors in the evaluations of studied decay channels will depend on the precision of the missing mass reconstruction. Using the $f_e(\mu)$ function one can describe the resolution function of the missing mass in a analitical way which facilitate determining of the optimal value of the $\Delta\mu$ region.

References:

[1] H. H. Adam et al., arXiv:nucl-ex/0411038 (2004)

[2] M. J. Zieliński, Dip. Thesis, Jagiellonian University, arXiv:0807.0576 [hep-ex] (2008)

[a] Institut für Kernphysik and Jülich Center for Hadron Physics, D-52425 Jülich, Germany

[b] Institute of Physics, Jagiellonian University, PL-30059 Cracow, Poland

[c] Department of Physics and Astronomy, Uppsala University, 75121 Uppsala, Sweden

Predictions for cusp Effect in the $\eta \to 3\pi^0$ Decay observed with WASA-at-COSY

C.-O. Gullstrom

In the three body hadronic decay $K \to 3\pi$ a cusp was observed. The cusp arises from the re-scattering of two pions in the final state when the energy of the two virtual charged pions are enough to be real. The behavior of the re-scattering function J_i at threshold results in a cusp in the decay rate. From this cusp effect pion scattering lengths were determined with high precision[1]. In hadronic η decays a similar cusp should exist for the final state with $3\pi^0$. The cusp is not yet experimentally confirmed and is predicted to be weaker than for K mesons. A theory for first and second order non-relativistic effective field theory has recently been put forward by M.Bisseger, A.Fuhrer, J.Gasser, B.Kubis and A.Rusetsky [2]. In non-relativistic effective field theory the total matrix element is a sum of matrix elements for each order of perturbation

$$M_0^\eta = M_{tree}^\eta + M_{1-loop}^\eta + M_{2-loop}^\eta \cdots \tag{1}$$

The tree level contributions is

$$M_0^{\eta\,tree} = K_0 + K_1\left(X_1^2 + X_2^2 + X_3^2\right) \tag{2}$$

where K_i are effective Lagrangian couplings and $X_i = p_i^0 - M_{\pi^0}$. At tree level M is by theory constant but experimentally parameters are found to be $K_0 = 1.062$, $K_1 = -0.916$ from Crystal Ball[4].
For the 1-loop perturbation the matrix element is

$$M_{1-loop}^\eta = \sum_i B_0^1(s_i)\,J_0(s_i) + B_0^2(s_i)\,J_0(s_i) \tag{3}$$

where s_i is the invariant mass of pion $j/neqi$ and $k/neqi/neqj$ in the final state, J_i is the loop function for pion re-scattering and the couplings are

$$B_0^1(s_1) = (2A_0 + D_0 Y_{10})\left\{K_0 + K_1\left[X_1^2 + 2Z_1^2 + \frac{Q_1^2}{6s_1}Y_{10}\right]\right\} \tag{4}$$

$$B_0^2(s_1) = 2\,(2A_\pm + D_\pm Y_{1\pm})\left\{L_0 + L_1 X_1 + L_2 X_1^2 + L_3\frac{Q_1^2}{3s_1}Y_{1\pm}\right\} \tag{5}$$

with $Z_i = \frac{Q_i^0}{2} - m_{\pi^0}$, $Q_1^0 = p_2^0 + p_3^0$ (cyclic permutation), $Q_i^2 = \frac{\lambda(m_\eta^2, m_i^2, s_i)}{4m_\eta^2}$, $Y_{ig} = s_{i-4m_{\pi g}^2}$,$\lambda\left(m_\eta^2, m_i^2, s_i\right)$ the full triangular function $\lambda(x,y,z) = x^2 + z^2 + y^2 - 2xz - 2xy - 2yz$ and L_i are the effective lagrangian couplings in the charged channel. The A_i's and D_i's are in standard pion scattering length

$$3A_0 = 32\pi(a_0 + 2a_2)\,,\; 3A_\pm = 32\pi(a_0 - a_2)\,, \tag{6}$$

$$3D_0 = 32\pi(l_0 + 2l_2)\,,\; 3D_\pm = 32\pi(l_0 - l_2) \tag{7}$$

with $l_i = \frac{r_i}{4} + \frac{a_i^3}{4m_\pi^2}$. The pion scattering lengths are experimentally $a_2 = 0.220 \pm 0.005$ and $a_0 = 0.0444 \pm 0.001$ [2]. For the D_i's the parameters are $r_0 = \frac{0.276}{m_\pi^2}$ and $r_2 = \frac{0.0803}{m_\pi^2}$ [3].
As a first approach use C_i , K_0 and L_0 and set the rest of the parameters to zero. The coefficient ratio between charged and neutral channel is for statistical reasons there are three possible re-scattering channels for $\eta \to 3\pi^0 \to 3\pi^0$ but only one for $\eta \to \pi^+\pi^-\pi^0 \to 3\pi^0$. The ratio is then $L_0/K_0 = \frac{1}{3}$. As a second approach we use the experimental lagrangian couplings $L_0 = 1.46$, $L_1 = -8.36$, $L_2 = -43.7$, $L_3 = 4.8$ from KLOE [5]. In fig.1 the result from a Monte Carlo Simulation clearly shows that the pion scattering length do not suffice as experimental parameters. Also experimental couplings L_i's from $\eta \to \pi^+\pi^-\pi^0$ can be used.

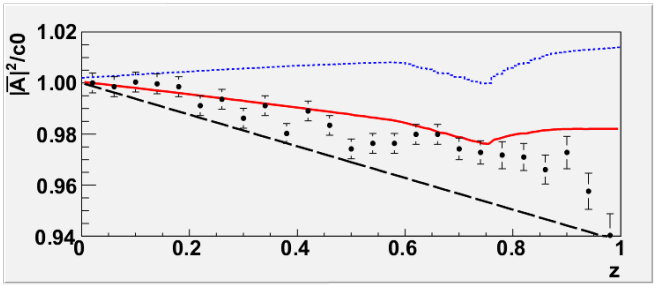

Fig. 1: $|A|^2$ normalized to 1 at z=0 for the decay $\eta \to 3\pi^0$: solid line theoretical second approach, dotted theoretical first approach, dashed line experimental tree amplitude from Crystal ball , points measurement from the KLOE detector [6]. Z is the Dalitz plot variable $z = \frac{2}{3}\sum_i \left(\frac{3p_i^0 - m_\eta}{m_\eta - 3m_{\pi^0}}\right)^2$.

The radiative correction of final state pionium and second order corrections are possibly needed to explain the behavior at large z. The decay $\eta \to 3\pi^0$ was succefully measured using the WASA-at-COSY detector and an improvement method for simulation will guide future mesurements.

References:

[1] J.R. Batley et al. [NA48/2 Collaboration], Phys. Lett. B 633 (2006) 173 [arXiv:hep-ph/0604084]
[2] M.Bisseger, A.Fuhrer, J.Gasser, B.Kubis, A.Rusetsky, Phys. Lett. B 659 (2008)
[3] G.Colangelo, J.Gasser, H.Leutwyler, Nuc. Phys. B 603 (2001) 125-179
[4] W.B Tippens,et al., Phys. Rev. Lett. 87, 192001(2001)
[5] F.Ambrosino, et al., (2007), arXiv:0707.2355 [hep-ex]
[6] F.Ambrosino, et al., (2007), arXiv:0707.4137 [hep-ex]

*Uppsala University, Sweden

Simulations for the $\pi^0 \rightarrow e^+ e^-$ Experiment with WASA-at-COSY

G. Wouda[a]

The decay $\pi^0 \rightarrow e^+ e^-$ is very rare, the theoretical branching ratio from the Standard Model is $(6.23 \pm 0.09) \times 10^{-8}$ [1]. A proposal to observe this decay was submitted to the COSY PAC. As a diploma project, simulations of the background, the beam energy- and trigger choices were performed and are presented in this report.

The reaction chosen for producing π^0's is $pp \rightarrow pp\,\pi^0$ with a beam energy below the $2\pi^0$ threshold (T_p = 580 MeV). As a first choice of trigger two charged particles in the Forward Detector (FD) are required.

T_p^{lab} MeV	400	500	550	600
$pp \rightarrow pp$	22	24	25	25
$pp \rightarrow pp\,\pi^0$	0.09	0.52	1.3	2.1
$pp \rightarrow d\,\pi^+$	0.85	2.0	2.8	3.0
$pp \rightarrow pn\,\pi^+$	0.30	3.2	5.2	8.0

Table 1: Cross sections in mb for reactions with two charged particles in the final state in pp-collisions at different proton beam energies. [2]

In a short $pp \rightarrow pp\,\pi^0$ run at 400 MeV during spring 2007, the trigger selected two charged particles in FD resulting in a count rate of about $140\pi^0$ s^{-1}. At higher beam energies, where the yield for $pp \rightarrow pp\,\pi^0$ is higher, another trigger might be more suitable. First stage simulations were performed using pure phase space for all reactions as in Table 1. Three possible trigger regions were investigated in this simulation. Table 2 shows the geometrical acceptance of the $pp \rightarrow pp\,\pi^0$ reaction and the signal/total event rates.

T_p^{lab} MeV	400	500	550	600
A	34 (17)	20 (20)	17 (26)	15 (30)
B	35 (6)	35 (12)	33 (18)	31 (22)
C	17 (29)	26 (25)	26 (34)	26 (37)

Table 2: Geometrical acceptance and (Signal/Total) in % for the different triggers at different beam energies. A is two charged particles in FD, B is one in FD and one in PSF, C is two in PSF.

As can be seen, changing the trigger to e.g. B at 550 MeV will increase the π^0 count rate with a factor ~ 14 compared to the spring 2007 run. However, the triggers need to be further investigated for the final experiment and a third condition such as energy deposit is needed to reduce the random coincidence count rate.

The background simulations consist of the single Dalitz decay, $\pi^0 \rightarrow \gamma\, e^+ e^-$ and γ -conversion in the detector by photons from the decay $\pi^0 \rightarrow \gamma\,\gamma$. The background from the Dalitz decay is produced by simulating the process $\pi^0 \rightarrow \gamma\,\gamma^*$ according to phase space using the ROOT framework. In the Monte Carlo generator, the mass of the γ^* was randomly chosen from:

$$\frac{d\Gamma}{dq} = \frac{1}{q}\sqrt{1-\frac{4m_e^2}{q^2}}\left(1+\frac{2m_e^2}{q^2}\right)\left(1-\frac{q^2}{M_{\pi^0}^2}\right)^3,$$

which is the invariant mass distribution for the $e^+ e^-$ pair from Dalitz decays [3]. The invariant mass was drawn from the interval 0.1 - 0.135 GeV/c^2. The result of the simulation is shown in Figure 1:

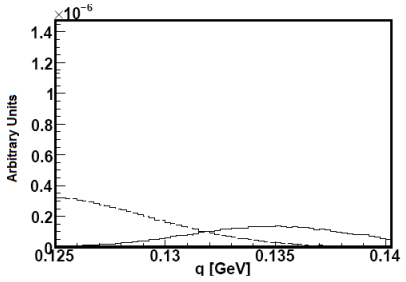

Figure 1: Background from single Dalitz decay of the $\pi^0$for 4% resolution. The peak with maximum located at 0.135 GeV is the $\pi^0 \rightarrow \gamma\, e^+ e^-$ signal.

The background from γ-conversion was simulated by implementing a weight based script which uses formulas for pair production and Compton scattering differential cross sections, angular- and energy distributions [4, 5]. An assumption made was that γ-conversion only takes place in the Be-beam tube and that only $e^+ e^-$ pairs from different γ's will contribute to the background (the rest can be excluded by vertex reconstruction). The Vertex reconstruction in the *rz*-plane was implemented and proper cuts, such as opening angles of the $e^+ e^-$ pair in lab-frame, were imposed.

The result of this simulation for 2% momentum resolution is that in the signal region 120-150 MeV/c^2 there is 5:1 background:signal ratio. However, the signal will be a peak centered at 135 MeV/c^2 and the background is a decreasing distribution. Thus, a reasonable estimate is that the ratio is 1:1 in the signal peak area. Finally, cuts in the *xy*-plane will reduce this background even further.

a) Uppsala University

[1] A. Dorokhov & M. Ivanov, Phys. Rev. **D**75, 114007 (2007)

[2] J. Stepaniak, TSL-ISV report 3, 1987

[3] Simulation of some η- and η' -decay modes, C. Gullström, Diploma Thesis, Uppsala, 2008

[4] H.A Bethe & L.C Maximon, Phys. Rev. vol 93, Number 4, 1945

[5] Introduction to Radiological Physics and Radiation Dosimetry, F.H Attix, Wiley, 1986, p. 124-152

Trigger Development for WASA-at-COSY

Pawel Marciniewski[1], Pawel Plucinski[1], Kjell Fransson[1], Andrzej Kupsc[1]

Motivation

The total rate of events generated in the WASA experiment approaches 10^7/s, which would be far beyond the speed and capacity of the data acquisition system. Only a fraction of events can and needs to be stored, necessitating a fast and efficient trigger system. The current coincidence-based trigger system is not sufficiently selective in order to achieve all of the goals of the WASA physics program. The system uses common signal amplitude discrimination levels while lacking the possibility of energy reconstruction. The efficiency of the trigger system can be improved by the use of digitized information of particle energy depositions in the detector.

The new trigger system

The new trigger system will take advantage of the newly developed continuous-sampling front-end QDC modules. The QDCs are equipped with 12-bit ADC converters running at 160 Msamples/s. The modules contain programmable logic (FPGA) used to extract arrival times and charge integrals of the detector signals. The trigger uses a rough extraction algorithm which runs in parallel to the regular data acquisition branch. The data for the trigger are transmitted by high speed serial optical links from the QDC to the trigger unit, which in turn evaluate complex physical quantities like invariant and missing masses, using the QDC information from the detector.

The prototype

The first prototype of such a system was installed in October 2008 and is shown in figure 1. The main component of the system, a Xilinx evaluation board ML555, features 2 optical links and a number of electrical input/output connectors. The prototype board receives signals from the 24 sectors of the Forward Range Hodoscope (FRH) and forms an analog sum of the signals from the detectors situated along the sectors. Additionally, the board will receive angular "theta" information for each sector, evaluated from the Forward Trigger Hodoscope (FTH).

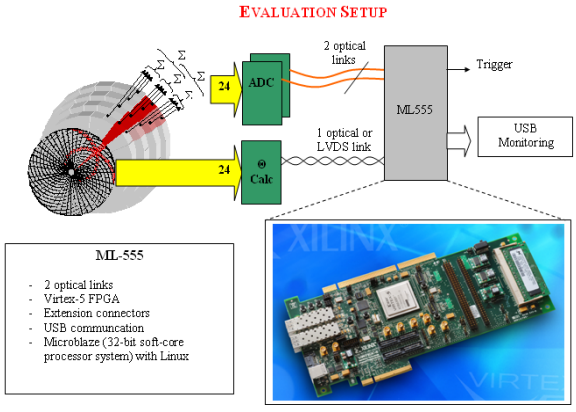

Fig. 1: The new trigger system – evaluation setup. (See figure 1 in C.Zheng's contribution for details of the WASA detector.)

The project status

The following project goals have already been achieved:

- The trigger unit (ML555) was installed and tested with two optical links (2 ADC units) and a high-speed differential connection to the "theta" board.
- The trigger data communication was successfully tested.
- Time matching of trigger signals was adjusted.
- An embedded microprocessor system supporting a USB communication was implemented on the ML555 board. It allows for data monitoring and feeding of trigger parameters.
- A user interface was implemented (data quality monitoring, loading the setup data, the trigger diagnostic and control).
- The event builder (data matching) is implemented; a test will soon be performed.

The plan is to use the prototype of the new trigger system to check and demonstrate trigger configurations and selection criteria. It is planned to use the prototype setup to evaluate the missing mass of an event and use it for event selection. The efficiency of such a system has not yet been estimated. The system suffers from limitations coming from analog summing of detector signals, making the estimation of the missing mass difficult and not inaccurate. Nevertheless, the new system should significantly improve the efficiency of selecting specific classes of events.

Further development

To overcome the limitations of the prototype design, it is necessary to increase the number of optical as well as electrical connections from the readout boards to the main trigger board, to obtain data from detectors in subsequent layers of the FRH and later information from the other forward detectors, like FTH, FWH, FVH, and central detectors PS, SEC (in groups), and MDC.

The work plan

- Development and testing of the data transceivers for the serial optical links between the QDCs and a trigger unit;
- Software development for the evaluation board to decide on the final system;
- Test FD trigger part at WASA runs;
- Purchase of the final trigger unit and evaluation tools, develop methods for the efficient programming of the device;
- Development of the final multiple channel scalable trigger system;
- Trigger optimization and efficiency studies.

Summary

The prototype trigger was installed at WASA experiment. The data communication was successfully tested and timings of trigger signals were adjusted. A user interface was implemented. The project is ready for test at WASA runs.

[1] Uppsala University

The WASA-at-COSY pellet target*

F. Bergmann[1], G. D'Orsaneo[2], G. D'Orsaneo[3], A. Khoukaz[1], A. Passfeld[1], P. Pistel[3], T. Rausmann[1] D. Spölgen[2], A. Täschner[1], and A. Winnemöller[1]

One focus of the WASA-at-COSY experiment are precision measurements on rare decays which require high luminosities. Therefore, a reliable and stable high performance pellet target is important. The pellet rate is one indicator for the performance of the target and measured with a pellet counter. Due to modifications at the pellet target it had to be readjusted during the maintanance last summer. In order to further improve the performance and stability of the WASA-at-COSY pellet target several changes have been made during the previous year. One important part of the pellet target that has been modified to improve the reliabilty is the gas supply system.

After a maintenance of the original gas purifier from Uppsala in Münster, it has been reinstalled into the gas system of the WASA-at-COSY pellet target. Additionally, the gas purifier from the ANKE experiment is used, which is installed in the gas line between the deuterium generator and the WASA gas purifier. Furthermore, a new gas pipe has been installed from the ANKE gas purifier to the WASA gas purifier at the pellet target. Instead of several smaller pipe parts it now consists of only one long gas pipe. By this possible leakage problems will be reduced. The new gas pipe will be connected in summer 2009.

Due to modifications of the gas system the uptime of the pellet target has been improved significantly. When using hydrogen for the target, the pellet target was running without breaks during the beam times last year, corresponding to three weeks of stable operation. While this was already the case in the past, the situation was improved significantly with deuterium as target. Figure 1 shows the performance of the pellet target during the last beam time in September / October 2008 for deuterium as target material.

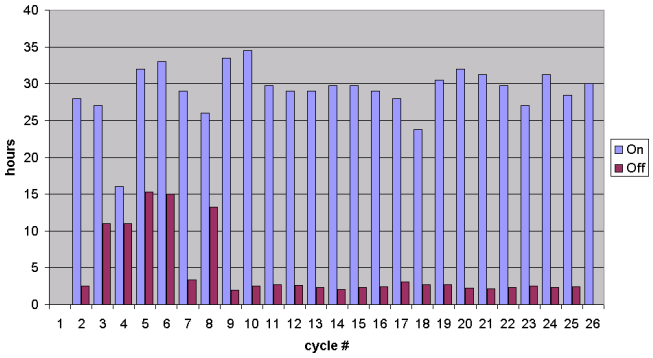

Fig. 1: Durations of the on - off cycles of the WASA-at-COSY pellet target when using D_2

In the past the pellet target needed to be warmed up to room temperature every 40 hours on average. Since cycle 8 in the September / October 2008 beam time the target only needs to be warmed up to about 150 K every 30 hours. This reduces the breaks from about 10 hours to 2 - 3 hours and increases the total uptime to above 90% for the September / October 2008 beam time.

Another reason for these improvements beside the changes of the gas system are the nozzles produced by the facility at the ZAT of the FZ Jülich, which has been established in 2007. Because of the high quality of the nozzles an exchange was only requried once in 2008 instead of several times like in the first half of 2007. The current nozzle diameter is 13.2 μm. One important part of the nozzles are the high quality sinter filters which are produced by MOTT since 2007 [1].

In order to further improve the performance of the pellet target the skimmer cap has been removed, resulting in a 1 mm skimmer diameter instead of 0.7 mm. While the pressure in the reaction chamber did not increase, the pellet rate and effective density have been improved significantly. During the deuterium beam time in September / October stable pellet rates of 20000 pellets per second have been achieved. Another advantage of the bigger skimmer diameter is that the pellet target needs less readjusting during beam times.

With all these changes a higher luminosity is possible. For the September - November beam time a luminosity of $L = 4 \cdot 10^{31}$ - $1 \cdot 10^{32}$ $cm^{-2}s^{-1}$ has been achieved.

Table 1 shows standard parameters for the pellet target operation at WASA-at-COSY.

pellet rate (H_2)	8000 pellets/s
pellet rate (D_2)	20000 pellets/s
pellet diameter	20 - 25 μm
target thickness (H_2)	$4 \cdot 10^{15}$ atoms cm^{-2}
target thickness (D_2)	$8 \cdot 10^{15}$ atoms cm^{-2}
pellet velocity	80 m/s
pellet distance	5 mm
target diameter at interaction point	
with 0.7 mm skimmer diameter	2.5 mm
with 1 mm skimmer diameter	3.5 mm
skimmer diameter	0.7 mm / 1 mm
nozzle diameter	13.2 μm
nozzle temperature (H_2)	17 K
nozzle temperature (D_2)	20 K
pressure in droplet chamber (H_2)	20 mbar
pressure in droplet chamber (D_2)	60 mbar
pressure in skimmer chamber	10^{-3} mbar
pressure after skimmer	10^{-5} mbar
pressure in beam dump	1 - 2 $\cdot 10^{-4}$ mbar
hydrogen consumption	250 l_n/day
deuterium consumption	250 l_n/day
helium consumption (H_2)	250 l_n/day
helium consumption (D_2)	1000 l_n/day

References:

[1] A. Winnemöller, G. D'Orsaneo, G. D'Orsaneo, A. Khoukaz, N. Milke, P. Pistel, T. Rausmann, D. Spölgen, and A. Täschner, Annual Reports 2007, **The WASA-at-COSY pellet target**, (2007)

* Supported by FZ Jülich FFE

[1] Institut für Kernphysik, Westfälische Wilhelms-Universität Münster, 48149 Münster, Germany
[2] IKP, Forschungszentrum Jülich
[3] ZAT, Forschungszentrum Jülich

A Pellet Tracking System for WASA-at-COSY

T. Tolba and J. Ritman

A Pellet Tracking System for WASA at COSY is being planned in order to determine the interaction point for each event between the COSY beam and the target pellets. The knowledge of the interaction vertex helps to reconstruct the paths of the different decay products and thus to improve the momentum resolution of the events. Furthermore, the system measures the position distribution of the pellets below their place of production and below the interaction point, allowing the geometrical alignment of the system to be improved.
The idea concept is to measure the x and z position of each pellet above and below the interaction point. That can be done by using a laser beam to illuminate the pellet and photographing it (using the scattered laser light from the pellet) by pairs of fast CCD line scan cameras. The pellet trajectories can be tracked from the position information of each plane and the relative timing, for more details see [ref. 1].
Setup optimization of a one-dimensional prototype of the pellet tracking system was done and the results are presented in [ref. 2].

PTS at the Moscow-Jülich Pellet Target

The Moscow-Jülich pellet target is the prototype of the PANDA pellet target, and since the PTS is thought to play an important role in determining the reaction vertex which is essential for the reconstruction of many physics channels (specially for the study of the Ψ(3770) decay into D-measons) planned to study at the PANDA detector [ref. 3], a one-dimensional prototype of the PTS was mounted and tested for the first time in the Pellet Target station of this system, (Fig. 1).

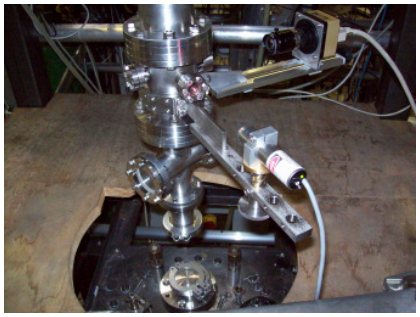

Fig. 1: The one-dimensional prototype of PTS mounted to the Moscow-Jülich pellet target.

The Moscow-Jülich pellet target was chosen because of many advantages:
- easy access to mount our equipment to the target station.
- easy handling with the system durinzg the operation time.
- vibration-free cooling, which lead to decrease the dispersion of the pellet beam.
- ability to produce pellets target from various gases with different sizes.

A special vacuum chamber, laser beam-camera alignment tool, camera holder with ability for free horizontal movement in order to adjust the focus between the target and the camera-lens, and laser beam holder capable of free vertical movement in order to adjust the plane between the camera and the laser beam for the brightest photo(Fig. 2).

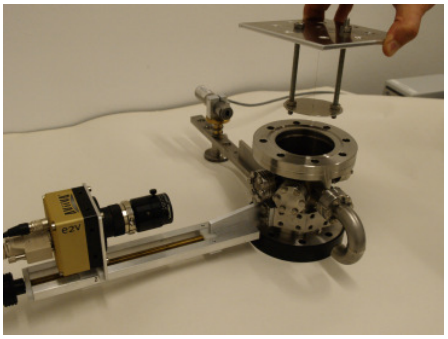

Fig. 2: Vacuum chamber, alignment tool, camera holder and laser beamer holder.

First results from PTS @ Moscow-Jülich Pellet Target

Due to the instability of the pellet production at the time of the experiment, only a few pictures of the pellet stream could be taken. Therefore, the analysis of those photos was not helpful in order to determine precisely the pellet stream distribution or the time difference between the pellets or the pellets size. Nevertheless, the photos taken by the setup and the data analyzed by the self-written online and off line codes show promising results. A few photos of the pellet beam, the distribution and the pellets size coming out from the online analysis are shown in Fig. 3, Fig. 4 and Fig. 5.

Fig. 3: Some online photos of individual pellet.

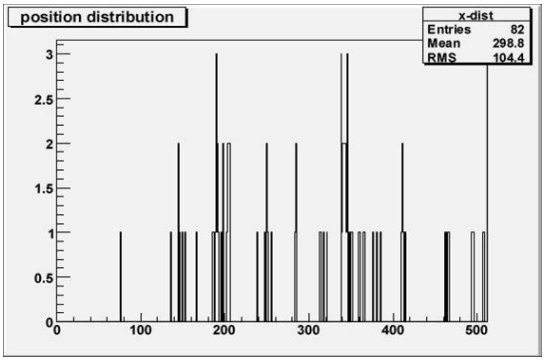

Fig. 4: spatial distribution of the pellets recorded in one second.

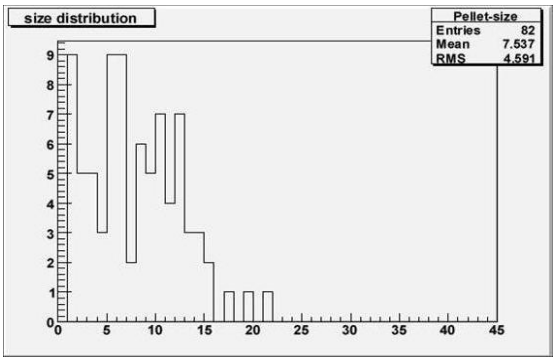

Fig. 5: Pellet-size distribution.

PTS at the WASA-at-COSY Pellet Target

The one-dimensional prototype of the PTS was mounted to the WASA pellet target at approximately 1.4 m from the nozzle and was tested in September.
Due to the difficult access to the pellet beam tube, at the position below the nozzle, a special flange was built in the IKP workshop, the camera and laser beam holders were mounted to this flange and tested for the sharpest and brightest photo in a special setup outside the beam tube. The whole system, after the adjustment, was transferred and mounted to the pellet beam tube, (Fig. 6).

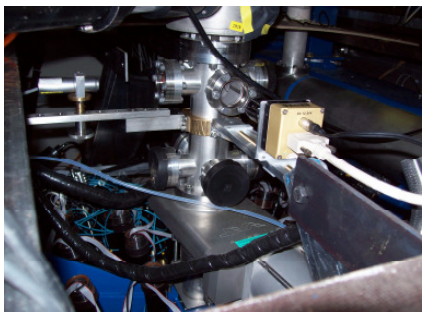

Fig. 6: The one-dimensional prototype of PTS mounted to the WASA-at-COSY pellet target.

Due to the difficulties we faced in accessing to the pellet tube and the time limitation before the WASA beam time, we could not reach a perfect alignment between the mounted system and the pellet beam tube. Nevertheless, we succeeded to photograph some pellets and analyze them online and also some other photos analyzed off line.
Some online photos for a individual pellets are presented in (Fig. 7), with some histograms of the analysis of those photos are presented in (Fig. 8 and 9).

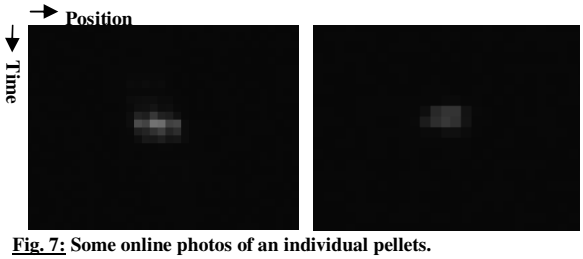

Fig. 7: Some online photos of an individual pellets.

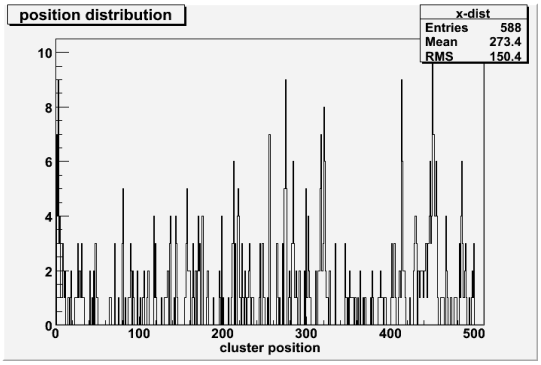

Fig. 8: Pellets spatial distribution.

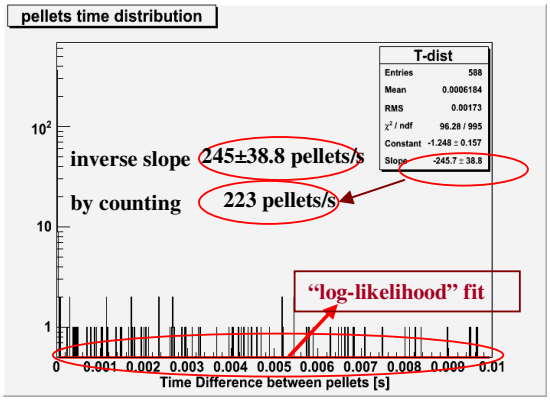

Fig. 9: Time difference between Pellets (as clusters).

Summary

- A one-dimensional prototype of the PTS was built and tested successfully.
- A first online and offline code was written and tested by analyzing photos of pellets taken by the PTS prototype.
- With optimal conditions of the setup, the pellets can be photographed and analyzed.
- Although some problems appeared during the tests and experiments, the system setup and the analysis codes appear to be promising.
- Some developments for the system and the analysis programs are needed in future to improve the data output from the photos.
- Some problems and difficulties need to be solving in future for easier access to the system, stability of the pellet beam production and a reasonable testing time.

Outlook

- The development of the system and solving the problems encountered seems to be very important for the in future.
- Building the two dimensional setup of PTS is a big step in the way to build the full system of the pellet tracking system.

References

[1] "A Pellet Tracking System for WASA at COSY", T.Tolba, J.Ritman. COSY/IKP Annual report, 2006.
[2] "A Pellet Tracking System for WASA at COSY", T.Tolba, J.Ritman. COSY/IKP Annual report, 2007.
[3] Ö. Nordhage et al., Nucl. Instr. and Meth. A 568 (2006) 561.

Performance of the New Plastic Scintillator Barrel Detector for WASA-at-COSY

P. Podkopał [a,*]

The Plastic Barrel (PSB) is an 8 mm thick layer of fast plastic scintillators, enclosing the MDC (see Figure 1 in the contribution by C.Zheng). It consists of a cylindrical central part, formed by 48 scintillator bars, and two endcaps (each has 48 trapezoidal elements) allowing a close to 4π acceptance. The main purpose of the PSB is the reliable separation of neutral and charged tracks especially on the trigger level, and in the data analysis. The deposited energy in the Plastic Barrel is used for particle identification via the ΔE – E method in conjunction with the total energy information from the calorimeter, or via the ΔE – p method using the momentum information from the MDC.

The results of study [1] and [2] had shown, that in the central part of the detector the light attenuation length was close to 50 cm whereas normally for this type of scintillator it should be 200 cm. The consequence was, that for some elements minimum ionizing particles were close to noise level, although the voltage applied to the photomultiplier was set to the maximum. This necessitated to lower the threshold, and yielded in less clean trigger conditions. Taking into account all mentioned effects we decided to exchange the central part of the PSB detector.

The new Plastic Scintillator Barrel has been installed during the COSY shutdown period in April 2008 and has been used in the experimental runs. We kept the same geometrical design of scintillators while the length of the lightguides was increased to optimize the connection with the photomultipliers. Prior to installation all elements had been tested [3] with a radioactive ^{207}Bi source.

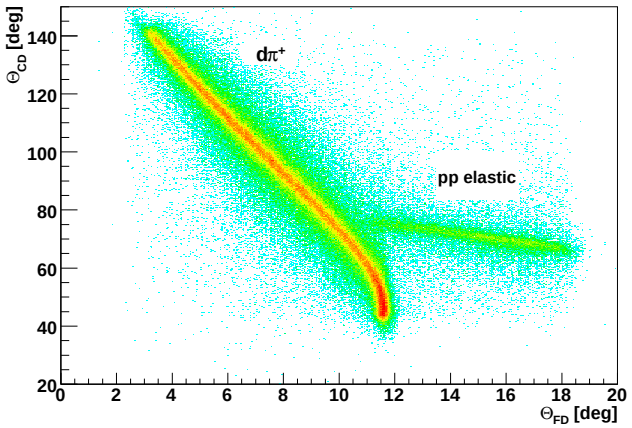

Fig. 1: Correlation between reconstructed polar angles of particles going to the forward and central detector, after applying cuts on the deuteron band in FD and the coplanarity condition.

In order to investigate the behaviour of the detector during experimental runs, a special sample of pp → dπ$^+$ events was collected. The advantage of this reaction is the strong correlation between the energy and scattering angle, thus it can be used for calibration as well as for detemination of the light attenuation. Applying proper cuts to the data shown in Fig. 1 we can select π$^+$ which are traversing through the central part of the PSB and check what is the energy dependence as a function of the polar angle. All elements reveal a uniform behavior and the yield of light is comparable.

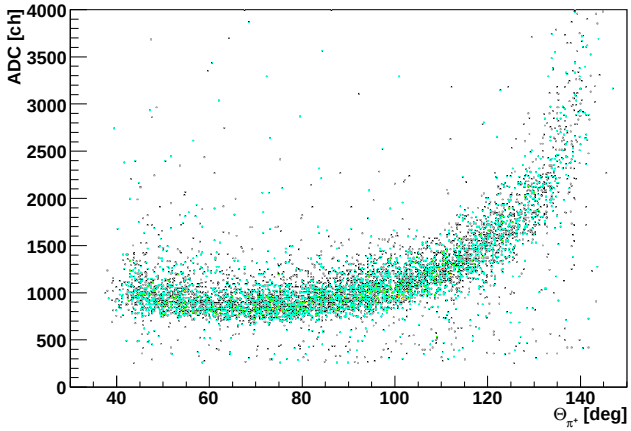

Fig. 2: Pulse height as a function of polar angle for one element of the PSB.

The typical light output as a function of scattering angle is presented in Fig. 2. Since we have rectangulary shaped elements we expect that particles which hit the scintillator close to the PMT will produce higher light output than particles which are emitted at small polar angles (larger distance to the PMT). Indeed, we observe this effect. In addition the installation of the new Plastic Scintillator Barrel significantly improves the trigger performance where this detector is involved and makes the particle identification easier, since background is discriminated more efficiently.

References:

[1] I.Keshelashvili, M. Mittag, Test of the WASA Plastic Scintillator Barrel, Annual Report 2006 .

[2] P.Podkopał, Energy calibration of the WASA Plastic Scintillator Barrel, Annual Report 2006 .

[3] P.Podkopał, T.Smoliński, The renewal of the WASA Plastic Scintillator Barrel, Annual Report 2007.

[a] Institute of Physics, Jagiellonian University, PL-30059 Cracow, Poland

* Supported by COSY-FEE

A DIRC Prototype for WASA-at-COSY: From Studies to Latest Results

C. Adolph*, A. Schmidt*, A. Teufel*, C. Vogel*, W. Eyrich*

The WASA-at-COSY experiment allows the study of production and decay of η and η' mesons in proton proton reactions with an almost full 4π covering detector including a forward spectrometer section. Particle identification for the decay products and to separate the huge background, one has to cope with, is substantial for this kind of investigation. Actually the so called Forward Range Hodoscope (FRH) in the forward angle spectrometer region determines the identity of the particles by measuring the energy loss ΔE-E. Simulations concerning the estimated background have shown, that an additional ring imaging Cherenkov detector in front of the FRH would significantly improve the particle identification and the energy resolution as well. Due to the very limited space, available at the intended detector position, the development of a DIRC (Detection of Internally Reflected Cherenkov light) detection system is under discussion: Cherenkov light is produced in a radiator bar by particles with velocity larger than the speed of light in this medium and then guided by total internally reflection at the inner surface of the bar to photon sensors located at the far end. In order to reduce the optical detection surface, additional optical focusing elements are used.

In the end of 2008 several PMMA(plexiglas)/fused silica radiator bars with various treated surfaces and two different DIRC prototypes, consisting of a radiator bar and a focusing optic, were tested using the external COSY beam behind the TOF experiment.

Radiators

Multianode photomultipliers (MAPMTs) were attached on both ends of the radiator bars. The proton beam hits the bars in different horizontal (x) positions and under different angles as shown in Fig. 1. The results show that no readout end is prefered at perpendicular incident of the protons at different x-positions. Fig. 2 shows that changing the incident angle causes strong asymmetrie as expected for Cherenkov light from the reflection conditions.

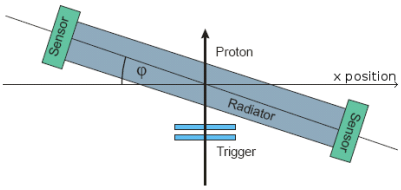

Fig. 1: measurement setup for asymmetry tests and number of photon counts

Prototypes

One prototype consists of a PMMA radiator bar glued to a focusing PMMA parabol coated with mylar foil. The other prototype uses a polynomial surface based on internal reflection for the focusing optic (see Fig. 3). A MAPMT was used as photosensor in both cases. According to the simulations a quasi vertical line at the end of the focusing optic is expected for the focused light. By varying the incident angle these lines have to move. The used proton energy of E_{kin} = 550Mev results in an Cherenkov cone with an angle of

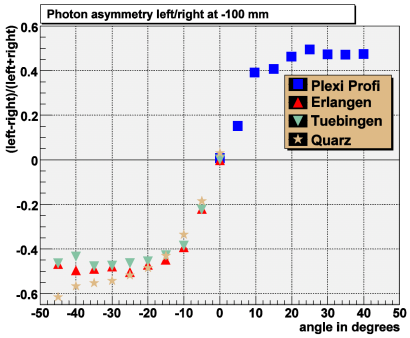

Fig. 2: photon asymmetry at different angles between proton beam and detector at 3.05 GeV/c protons

30.19°. The minimum angle for total reflection in PMMA is 42°. Both optics show similar results. In Fig. 4 the hit pattern on a 64-channel Hamamatsu H8500C MAPMT of a typical single Cherenkov event is shown where the prototype based on internal reflection is used at an incident angle of 25°.

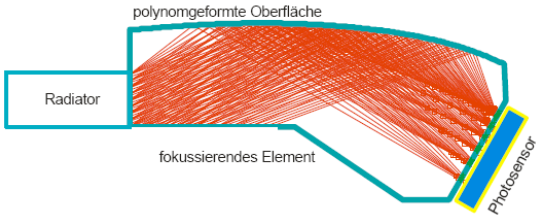

Fig. 3: focusing element based on internal reflection

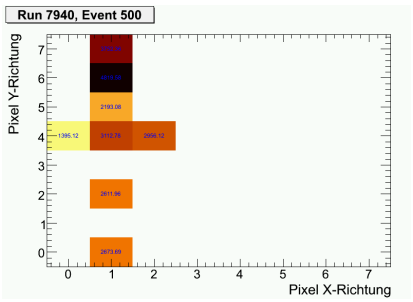

Fig. 4: eventpattern of a single event using the focusing optic based on internal reflection at 25 degrees after common mode correction

Outlook

On the basis of the obtained results, the next step will be building and testing a prototype consisting of several radiator bars and a common optic in 2009. This prototype will be one quater of the final DIRC.

*Physikalisches Institut, Universität Erlangen-Nürnberg, Germany

1.4 COSY-11

Study of the low energy dynamics in the ppK^+K^- system using the COSY-11 detection setup

M. Silarski[a], P. Moskal[a,b], D. Gil[a], J. Smyrski[a] for the COSY-11 collaboration

The near threshold production of K^+K^- pairs in proton-proton collisions has been investigated at ANKE and COSY-11 below and above the threshold for the ϕ meson production [1, 2, 3, 4, 5]. The excitation function determined for the $pp \to ppK^+K^-$ reaction cannot be described by a phase-space distribution including proton-proton final state interaction. The discrepancy may be assigned to the influence of K^+K^- or pK^- interaction. Indeed, as shown by the authors of reference [4, 5] the inclusion of the pK^-–FSI reproduces the experimental data for the excess energies down to the point at Q = 28 MeV. However, the inclusion of pp and pK^- final state interaction is still not sufficient to describe the data very close to threshold. This discrepancy may be due to the influence of the K^+K^- interaction, which was neglected in the calculations.

The authors of reference [4] pointed out that the enhancement of the total cross section near threshold may, at least partially, be due to the neglect of the pK^-–FSI in the calculations of the COSY-11 acceptance. As a consequence the obtained total cross sections might decrease, if the interaction would have been taken into account during the analysis of the experimental data. This suggestion encouraged us to check quantitatively the influence of the interaction in the pK^- subsystem on the acceptance of the detection setup. To this end we derived the distributions of the differential cross section for data at excess energies of Q = 10 MeV and Q = 28 MeV for two different assumptions. First we assumed that the acceptance depends only on the pp–FSI, then we included in addition the pK^-–FSI and derived analogous distributions. The resulting differential cross sections, which can be found in reference [6], show that the acceptance of the COSY-11 detection setup is only very weakly sensitive to the interaction between K^- and protons.

The derived distributions of the absolute values for the differential cross section constitute an additional information to the total cross sections published previously in reference [3]. In the article [3] the values of the cross sections were determined using the total number of events identified as the $pp \to ppK^+K^-$ reaction and the total acceptance of COSY-11. Now after the determination of the absolute values for the differential distributions one can calculate the total cross sections in the less model dependent manner, regardless of the assumption of the pp–FSI. The cross sections calculated for both excess energies resulting from the following integral:

$$\sigma_{tot} = \int \frac{d\sigma}{dM_{pp}} dM_{pp} ,$$

amount to $\sigma_{tot} = (0.95 \pm 0.17)$ nb for measurement at $Q = 10$ MeV and $\sigma_{tot} = (6.5 \pm 1.1)$ nb for $Q = 28$ MeV. These results are even larger than the previously obtained total cross sections by about 20 % for the lower excess energy and 50 % for Q = 28 MeV, which strengthen the confidence to the observed enhancement close to threshold. However, the total cross sections obtained in these two different analyses are statistically consistent.

The determination of the absolute values for the differential cross sections permitted us to establish the absolute values

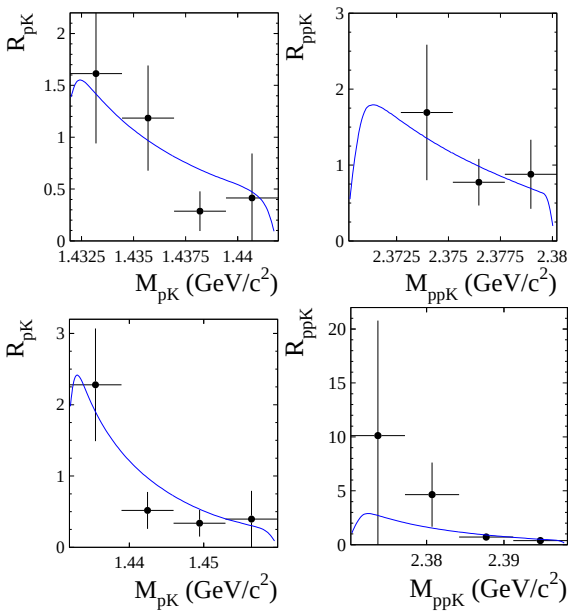

Fig. 1: The distributions of the ratios R_{pK} and R_{ppK} for data at Q = 10 MeV (upper panel) and Q = 28 MeV (lower panel). Solid curves represent calculations taking into account pp and pK^- final state interaction.

for the following ratios at the close to threshold region:

$$R_{pK} = \frac{d\sigma/dM_{pK^-}}{d\sigma/dM_{pK^+}} , \qquad R_{ppK} = \frac{d\sigma/dM_{ppK^-}}{d\sigma/dM_{ppK^+}} .$$

In the presence of the pp–FSI only, the distribution of R_{pK} as well as R_{ppK} should be flat and equal to unity. But as one can see in Fig. 1, and as presented already in the previous publication, by COSY-11 [3] and ANKE [4] R_{pK} for both excess energies is far from constant and increases towards the lower M_{pK} invariant masses. This effect might be connected with the influence of the pK^- final state interaction. Similarly the distributions of R_{ppK} differs from expectations assuming only interaction in the pp system. It is important to note that the determined absolute ratios of cross sections are satisfactory well described using the parametrisation introduced in article [4] and the values of the a_{K^-p} extracted from the ANKE data at higher excess energies [4].

References:

[1] M. Wolke, PhD thesis, IKP Jul-3532 (1997).
[2] C. Quentmeier, et al., Phys. Lett. B **515**, 276-282 (2001).
[3] P. Winter, et al., Phys. Lett. B **635**, 23-29 (2006).
[4] Y. Maeda, et al., Phys. Rev. C **77**, 015204 (2008).
[5] C. Wilkin, AIP Conf. Proc. **950**, 23 (2007).
[6] M. Silarski, P.Moskal, D. Gil, J. Smyrski, Acta. Phys. Pol. B Proc. Supp. 2009, in press.

[a] M. Smoluchowski Institute of Physics, Jagellonian University, 30-059 Cracow, Poland
[b] IKP, Forschungszentrum Jülich, D-52425 Jülich, Germany

Study of the spin triplet proton-lambda interaction with the COSY-11 detector

D. Grzonka for the COSY-11 collaboration

The YN interaction is not very well known compared to the *NN* system and even for the best studied Λp hyperon nucleon system the scattering length has large uncertainties. Elastic Λp scattering data are available for relative momenta above about 120 MeV/c which requires an extrapolation to zero energy with large experimental uncertainies to determine the scattering length. Data from production reactions with multiparticle final states including a Λp subsystem allow the selection of event samples with relative momenta down to zero. However, in this case the theoretical treatment for the extraction of the scattering length where effective range expansions are applied determine the error which is not under control.
Improvements in the theoretical consideration of these processes by the Jülich group [1, 2] with a well controlled error in the derivation of the scattering length from exprimental observables of below 0.3 fm will allow to extract more precise results from reactions like $pp \rightarrow pK^+\Lambda$.
For a detailed analysis a separation of spin singlet and spin triplet scattering lengths is required and measurements with polarised beam and target are necessary. The spin triplet scattering length only is measurable by studying the cross section combined with the analysing power if kaon emission around 90 $^\circ_{cm}$ is selected which needs only a polarised beam.
At the COSY-11 detection system Λ hyperon production via $\vec{p}\,p \rightarrow pK^+\Lambda$ has been measured at an excess energy of 40 MeV with a transverse polarised proton beam in order to extract the spin triplet Λp scattering length. With the asymmetric detection setup only one side can be measured and therefore the spin has to be flipped to get the analysing power. The COSY operation procedure was injection, acceleration to 2.457 GeV/c and measurement with stochastic cooling for 10 minutes with a fixed polarisation direction. Every second cycle the polarisation direction was flipped. The luminosity was monitored by additional detector components detecting elastic pp scattering in polarisation direction which is insensitive to the orientation of the polarisation. The polarisation of the beam is determined by a comparison of the measured asymmetry of elastic pp scattering in the plane perpendicular to the beam polarisation direction to the known asymmetry from EDDA data [3]. Elastic scattering events were selected by requesting one charged particle track with an additional entry in the Si-pad detector from the second proton and can be well identified around the kinematical ellipse expected for elastic pp scattering in the distribution of transverse versus logitudinal proton momentum. The mean polarisation during the measurement was around 50%.
The $pK^+\Lambda$ -events were separated by selecting events with one proton and one kaon both identified by the invariant masses of the two measured particles, and a Λ in the missing mass spectrum. In fig. 1 the missing mass distribution is shown where a clear Λ peak is seen. The angular distribution of the kaons resulting from $pK^+\Lambda$ -events covers the full range including the 90 $^\circ_{cm}$ region which is required for the extraction of the spin triplet scattering length. But unfortunately the preliminary analysis indicates a very small analysing power for kaon emission around 90 $^\circ_{cm}$ and therefore the observable which includes only spin triplet contributions ($A_y \cdot \sigma$) will be also very small with large error bars. The data are checked carefully and will be analysed once more with improved calibrations before the final results will be extracted.

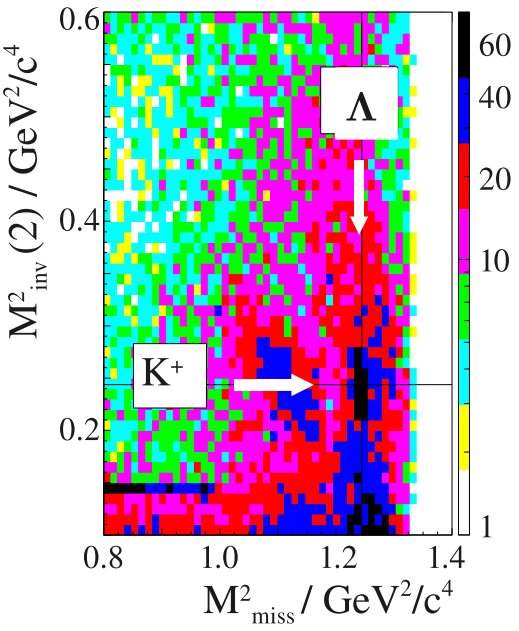

Fig. 1: Invariant mass squared of the second detected particle versus missing mass squared for events with an identified proton.

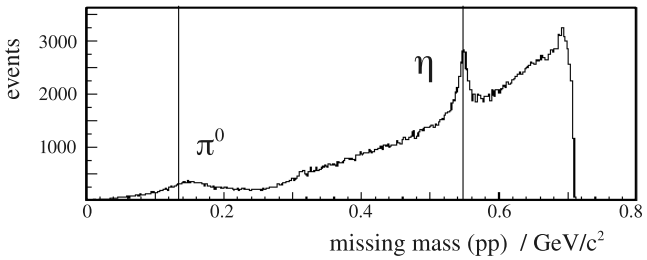

Fig. 2: Missing mass distribution for two proton events.

Besides the $pK^+\Lambda$ reaction also other reaction channels like $pp \rightarrow pn\pi^+$ and $pp \rightarrow pp\pi^0/\eta$ are included in the data. Fig. 2 shows the missing mass distribution with 2 identified protons where a clear η signal shows up. The analyses of the data will also include the study of the η production which will result in cross section and analysing power data for an excess energy of 164 MeV.

References:

[1] A. Gasparyan et al., *Phys. Rev.* **C69**, 034006 (2004).
[2] A. Gasparyan et al., *Phys. Rev.* **C72**, 034006 (2005).
[3] M. Altmeier et al., *Phys. Rev. Lett.* **85**, 1819 (2000).

Study of the efficiency of the COSY-11 neutral particle detector using GEANT-3 and FLUKA-2008 simulation packages.

J. Zdebik[a] and P. Moskal[a,b] on behalf of the COSY-11 collaboration.

The efficiency of the COSY–11 neutral particle detector – which is an important factor for determining the absolute values of cross sections – was determined using two indepenend simulation programs. In one program, a procedure based on the GEANT-3 (**GE**ometry **AN**d **T**racking) code [1] was used for simulation of the hadronic cascades induced in matter by neutrons. The same procedure was repeated using the FLUKA[1] (**FLU**ktuierende **KA**skade) [2, 3] simulation program.

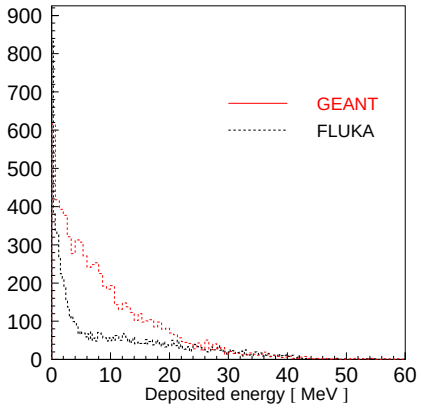

Fig. 1: The total energy deposited in the neutral particles detector for neutrons impinging on the detector with kinetic energy equal to 300 MeV as simulated using FLUKA-2008 (dashed line) and GEANT-3 (dotted line) packages.

The comparison of the simulated distributions of the total deposited energy in the neutron detector using FLUKA-2008 and the GEANT-3 packages is presented in Fig. 1. The simulation was performed for neutrons with a kinetic energy equal to 300 MeV. As can be seen, the range of deposited energy is the same for both cases, however GEANT simulations yield on the average higher energy response.

The efficiency of the neutron detector is given by the ratio of the number of generated neutrons to the number of events, for which an energy deposited in the scintillator material was larger than the threshold value in at least one of 24 detection units. The value of the calculated efficiency as a function of the kinetic energy of neutrons is shown in Fig. 2 (up). In this figure open squares denote result obtained using the GEANT-3 package and the outcome of simulations using FLUKA-2008 is presented as black circles.

The kinetic energy of neutrons from the $pn \to pn\eta'$ reaction varies from 300 MeV up to 700 MeV for the 3.35 GeV/c beam momentum, and as can be inspected from Fig. 2 the efficiency is fairly constant in this range.

It is worth to stress that two independent simulation tools lead to fairly good ($\pm 3\%$) agreement for the values of efficiency in the range of energy relevant for the studies of the $pn \to pn\eta'$ reaction.

We have also conducted studies of the variation of the efficiency depending on the threshold value.

[1]The simulations were performed with the new 2008 version.

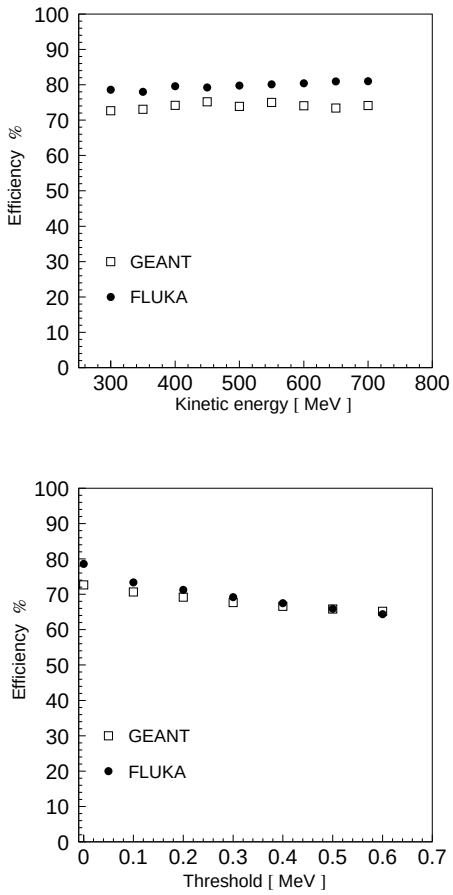

Fig. 2: **Top**: The efficiency distribution as a function of the kinetic energy of neutrons determined assuming that the threshold is equal to 0 MeV. **Bottom**: The relation between the threshold value and the efficiency for neutrons with energy of 300 MeV.

In the experiment the threshold was set to about 0.1 MeV and therefore we scanned the values from 0 up to 0.6 MeV. The result is presented in Fig. 2 (lower part). For both the GEANT and FLUKA-2008 simulations the values of efficiency change by about 10% over the 0.6 MeV range of the threshold.

References:

[1] http://wwwasdoc.web.cern.ch/wwwasdoc/geant_html3/geantall.html
[2] http://www.fluka.org
[3] J. Zdebik, Diploma Thesis, Jagiellonian Uni. (2008), arXiv:0811.1377.

[a] Institute of Physics, Jagiellonian University, Pl-30-059 Cracow, Poland
[b] IKP & ZEL, Forschungszentrum Jülich, D-52425 Jülich, Germany

Status of the analysis of the $pn \to pn\eta'$ reaction

J. Klaja and P. Moskal for the COSY-11 collaboration

In August 2004 –for the first time– using the COSY–11 [1] facility we have conducted a measurement of the η' meson production in proton-neutron collisions [2]. The aim of the experiment is a determination of the total cross section of the $pn \to pn\eta'$ reaction near the kinematical threshold. The comparison of the $pp \to pp\eta'$ and $pn \to pn\eta'$ total cross sections will help to understand production of the η' meson in different isospin channels and to investigate aspects of the gluonium component of this meson.

The experiment has been realized using a proton beam and a deuteron cluster target, since pure neutron targets do not exist. For the data analysis the proton from the deuteron is considered as a spectator which does not interact with the bombarding proton, but escapes undisturbed and hits the detector carrying the Fermi momentum possessed exactly at the time of the reaction. The Fermi motion of the target nucleons affects the centre-of-mass energy of the system, resulting from the 4-momentum of the beam proton and target neutron, on an event-by-event basis. Thus, the centre-of-mass energy of the final state can be reconstructed for each event provided that enough information is available. Therefore, the experiment is based on the registration of all outgoing nucleons from the $pd \to p_{sp}pnX$ reaction. Fast protons are measured in two drift chambers and scintillator detectors, neutrons are registered in the neutral particle detector, and slow spectator protons moving upstream compared to the beam are measured by a dedicated two-layer silicon-pad detector.

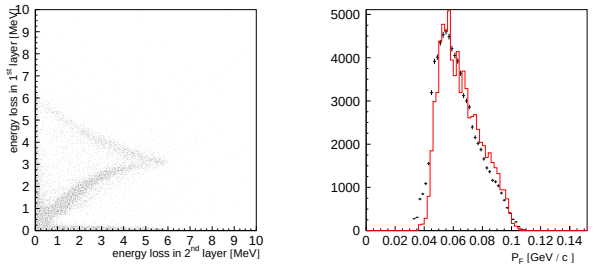

Fig. 1: **Left**: Energy losses in the first layer versus the second layer of the spectator detector as measured at COSY–11 with a deuteron target and a proton beam with momentu of 3.35 GeV/c. **Right**: Momentum distribution of the proton spectator as reconstructed in the experiment (points) in comparison with simulation taking into account Fermi momentum distribution of nucleons inside the deuteron (solid histogram).

Fig. 1 (left) shows energy losses in the 1^{st} layer of the spectator detector versus the 2^{nd} layer. Slow spectator protons are stopped in the first or second layer of the detector whereas fast particles cross both detection layers. Having the deposited energy and the emission angle we calculate the kinetic energy of the spectator proton and its momentum. Fig. 1 (right) shows the momentum distribution of protons considered as a spectator, as determined at COSY–11 with a deuteron target and a proton beam with a momentum of 3.35 GeV/c (points) compared to simulations taking into account a Fermi motion of nucleons inside the deuteron (solid line). The application of the missing mass technique allows to identify events with the creation of the meson under investigation. The total energy available for the quasi-free proton-neutron reaction is calculated for each event from the momentum vector of the spectator and beam protons. The absolute momentum of neutrons is determined from the time-of-flight between the target and the neutron detector. Fig. 2 (left) presents the time-of-flight distribution – for neutral particles – measured between the target and the neutral particle detector. A clear signal originating from gamma rays is seen over a broad enhancement from neutrons. This histogram shows that discrimination between signals originating from neutrons and gamma quanta can be done by a cut on the time of flight. From Monte Carlo simulations of the $pn \to pn\eta'$ reaction the largest expected momentum value of the neutron is eqaul to 1.4 GeV/c which corresponds to a time-of-flight value of 28.5 ns as it is indicated by the arrow in fig. 2 (left). Due to the smaller efficiency and lower resolution for the registration of the quasi-free $pn \to pn$ *meson* reaction in comparison to the measurements of the proton-proton reactions, the data collected have low statistics. Therefore, the excess energy range for $Q \geq 0$ has been divided only into four intervals of 8 MeV width each. For each interval we have calculated the missing mass. Next, from events with negative Q value the corresponding background missing mass spectrum was constructed, shifted to the kinematical limit and normalized to the experimental distribution at the very low mass values where no events from the η' production are expected.

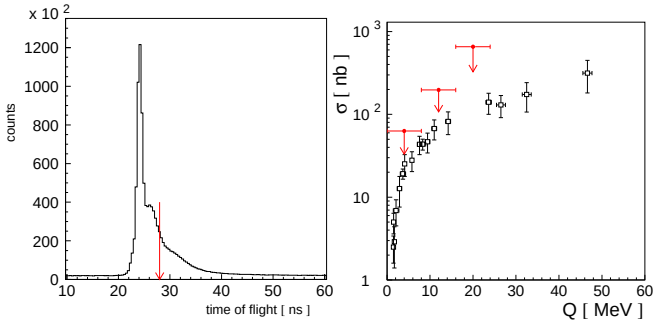

Fig. 2: **Left**: Distribution of the time–of–flight between the target and the neutron detector. **Right**: Total cross sections for the $pp \to pp\eta'$ reaction as a function of the excess energy (open symbols). Upper limit for the total cross section for the $pn \to pn\eta'$ reaction as a function of the excess energy (closed symbols).

After subtracting missing mass distributions for negative values of Q from spectra for Q values larger than 0 – due to the very low signal–to–background ratio – at the present stage of the data analysis, the signal from the η' meson was found to be statistically insignificant. Nevertheless, having the luminosity – established from the number of the quasi-free proton-proton elastic scattering events [3] – and the detection efficiency of the COSY-11 system we have estimated the upper limit of the total cross section for the quasi-free $pn \to pn\eta'$ reaction. The prelimnary results are shown in Fig. 2(right).

References:

[1] S. Brauksiepe et al., NIM **A 376** 396 (1996).
[2] P. Moskal et al., COSY Proposal **No. 133** (2003).
[3] P. Moskal, R. Czyżykiewicz, *AIP Conf. Proc.* **950**, 118 (2007).

Comparative studies of the low energy $pp\eta$ and $pp\eta'$ systems with the COSY-11 detector.

P. Klaja[a] and P. Moskal[a] for the COSY-11 collaboration

A qualitative phenomenological analysis of the determined differential squared invariant proton-proton and proton-η mass distributions for the $pp \to pp\eta$ reaction measured by the COSY-11 collaboration at an excess energy of 15.5 MeV [1] revealed an enhancement of the population density at the kinematical region corresponding to a small proton-η momentum. The observed enhacement could be explained by the significant role of the proton-η interaction [2, 3] in the final state, or by an admixture of the higher waves during the η production at the excess energy of 15.5 MeV [4], or by a possibile energy dependence of the production amplitude [5]. Those possibilities motivated the high statistics $pp \to pp\eta'$ reaction measurement in order to determine the distribution of events over the phase space at the same excess energy, equal to 15.5 MeV. The comparison of differential distributions of proton-proton and proton-meson invariant masses for the η and η′ production could help to judge between postulated explanations of observed effect and allow for a quantitative estimation between the proton-η and the proton-η′ interaction.

The $pp \to pp\eta'$ reaction has been measured using the COSY-11 detector setup [6]. The experiment was based on the measurement of two protons in the exit channel and the unobserved meson was identified using the missing mass technique. The analysis of the data was described in several referenceces [7, 8, 9], and here we would like the present the final distributions of the square of the proton-proton (s_{pp}) and proton-meson (s_{pmeson}) invariant masses as a result of that analysis.

We compared the distributions of the square of the proton-proton (s_{pp}) and proton-meson (s_{pmeson}) invariant masses determined for the $pp \to pp\eta$ and $pp \to pp\eta'$ reactions in figure 1. In both panels of the figure, it is seen that the experimental points of the $pp \to pp\eta$ measurement are in agreement with those from the $pp \to pp\eta'$ reaction within the statistical errors.

Unexpectedly, the shapes do not differ, showing the enhancement at the same values of the square of the proton-proton (s_{pp}) invariant mass.

If indeed the η′-proton interaction is much smaller than the η-proton as inferred from the excitation function, then the spectra being presented in this report rather exclude the hypothesis that the enhancement is due to the proton-meson interaction.

The final interpretation of the results is in progress.

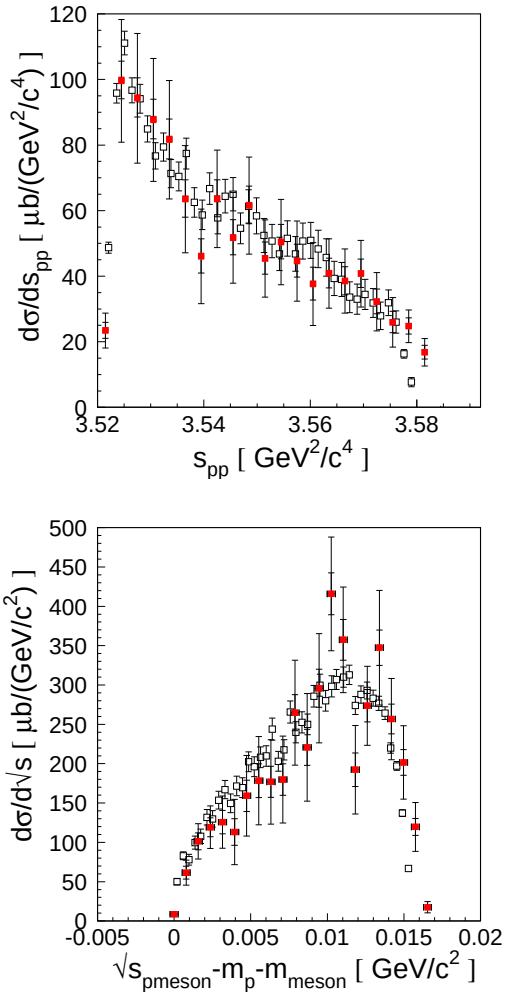

Fig. 1: The comparison of the distributions of the square of the proton-proton (s_{pp}) and proton-meson (s_{pmeson}) invariant masses determined experimentaly for the $pp \to pp\eta$ (full red squares) and $pp \to pp\eta'$ (open squares) reactions. The distributions of the η′ data were normalized to these of the η.

References:

[1] P. Moskal et al., Phys. Rev. **C 69** (2004) 025203.
[2] A. Fix, H. Arenhövel, *Phys. Rev.* **C 69** (2004) 014001.
[3] A. Fix, H. Arenhövel, *Nucl. Phys.* **A 697** (2002) 277.
[4] K. Nakayama et al., *Phys. Rev.* **C 68** (2003) 045201.
[5] A. Deloff, *Phys. Rev.* **C 69** (2004) 035206.
[6] S.Brauksiepe et al., *Nucl. Inst. and Meth.* **A 376** (1996) 397.
[7] P. Klaja, Proceedings MENU 2007, Jülich, Germany, 10-14 Sep 2007, pp 251.
[8] P. Klaja, et al., AIP Conf. Proc. **950** (2007) 103.
[9] P. Klaja, PhD thesis, in preparation.

[a] M. Smoluchowski Institute of Physics, Jagellonian University, 30-059 Cracow, Poland

Study of the $dp \to ppp\pi^-$ reaction near the η production threshold with COSY-11

J. Smyrski [1], W. Krzemień[1,2], P. Moskal [1,2] on behalf of the COSY-11 collaboration.

The excitation function as well as differential distributions for the $dp \to ppp\pi^-$ reaction have been measured near the η production threshold in a search for a signal from decays of ^{3}He$-\eta$ bound state. The measurements were done at the Cooler Synchrotron COSY-Juelich with the COSY-11 detection system [1]. Fig. 1 shows the c.m. distribution of the transversal vs. the longitudinal momentum components of the registered protons from the $dp \to ppp\pi^-$ reaction. This distribution is dominated by events of quasi-free π^- production in the process $np \to pp\pi^-$ where the neutron projectiles originate from the deuteron beam. The corresponding spectator protons from the deuteron (visible as a group of counts on the right hand side) were rejected in the further analysis by setting an upper limit for the longitudinal proton momenta equal to 0.18 GeV/c in the c.m. system, represented by the dashed line. The counting rate of all identified

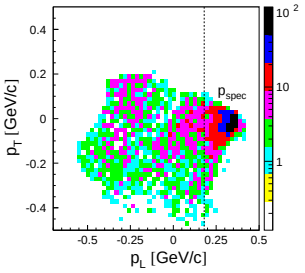

Fig. 1: Transversal vs. longitudinal momentum distribution of protons in the center of mass system.

$dp \to ppp\pi^-$ events including the quasi-free π^- production remains constant in the scanned range of the beam momentum. However, after rejection of the quasi-free events, the number of $dp \to ppp\pi^-$ counts in a beam momentum interval above the η threshold is higher than the number of counts in the beam momentum interval of equal width below the threshold.This difference is equal to $23-9=14$ and its statistical significance is of 2.5σ. The observation of this effect we reported already in Ref. [3]. As a possible reaction mechanism –explaining the observed enhancement– we suggested the production of "on-shell" η mesons in the reaction $dp \to {}^3\mathrm{He}\,\eta$ which subsequently convert to pions in the interaction with one of nucleons in the ^{3}He nucleus via excitation of the N(1535) resonance. In order to estimate the counting rate of the $dp \to ppp\pi^-$ events originating from the η absorption we assumed that the absorption cross section σ_{abs} is equal to the cross section for the $dp \to {}^3\mathrm{He}\,\eta$ reaction. This assumption we justify by the observation that the real and imaginary part of the ^{3}He$-\eta$ scattering length [2] have comparable values. The number ΔN of the $dp \to ppp\pi^-$ events corresponding to the momentum interval Δp of the ramped beam was calculated using the following formula:

$$\Delta N = \frac{\delta L}{\delta p} A \frac{1}{3}\frac{2}{3}\sigma_{abs}\Delta p, \qquad (1)$$

where $\frac{\delta L}{\delta p}$ is the integrated luminosity per beam momentum unit which was equal to about 1.0 nb^{-1}/MeV/c. A is the acceptance of the COSY-11 detection system for the $dp \to ppp\pi^-$ channel equal to 0.0005. It was calculated in computer simulations assuming that the two spectator protons have c.m. momenta described by the Fermi momentum distribution of protons in the ^{3}He nucleus taken from Ref. [4]. For the proton-pion pair associated with the two spectator protons, an isotropic angular distribution in the c.m. system of this pair was assumed. The factor $\frac{1}{3}$ in the above formula represents the probability of absorption on the neutron being one of three nucleons in the ^{3}He nucleus and the factor $\frac{2}{3}$ is the Clebsch-Gordan coefficient associated with the isospin coupling in the process $\eta n \to \pi^- p$.

The result of our estimation underestimates the experimental counts roughly by an order of magnitude and thus it does not corroborate the η absorption hypothesis.

In the momentum distribution for the spectator protons the experiment and the simulations of the direct production give much higher momenta than the η absorption. This indicates, that the dominant process in the observed $dp \to ppp\pi^-$ reaction is not associated with the η absorption. This is also confirmed by the distribution of the c.m. angles between the pion momentum vector and the momentum vector of the leading proton which, in the case of simulations of the η absorption, are close to 180° and for the experiment lie around 160°. Contrary to the discussed momentum spectra, the experimental angular distribution does not agree with the results of simulations for the direct production. One can expect, that due to very similar kinematical conditions, absorption of η mesons bound in the ^{3}He nucleus is characterized by differential distributions which are very close to the ones predicted in our simulations for the absorption of "on-shell" η mesons. In particular one can expect that the $\pi^- - p$ pairs originating from a decay of the η-mesic ^{3}He are emitted at c.m. angles concentrated predominately in the range $150^\circ - 180^\circ$ as it is the case for the η absorption. In this angular range, there are only two experimental counts. Assuming, that these two counts originate from decay of the ^{3}He$-\eta$ bound state, we estimated the cross section for the production of such a state in the $d-p$ collisions close to the η production threshold. The calculation was done using σ_{abs} derived from formula 1. The resulting cross section of 0.27 ± 0.19 μb should be considered as an upper limit for the production cross section of the ^{3}He$-\eta$ bound state since the observed two events might originate from other processes than the bound state decay. It is worthwhile to note that this limit is comparable with the near-threshold cross section for the $dp \to {}^3\mathrm{He}\,\eta$ reaction equal to about 0.4 μb.

References:

[1] S. Brauksiepe *et al.*, *Nucl. Instr. Meth. A* **376**, 397 (1996).
[2] J. Smyrski *et al.*, *Phys. Lett. B* **649**, 258 (2007).
[3] W. Krzemień *et al.*, e-Print: arXiv:0810.2330.
[4] S. K. Abdulin *et al.*, *JETP Lett.* **49, No 8**, 471 (1989).

[1] Institute of Physics, Jagiellonian University, PL-30059 Cracow, Poland

[2] IKP and JCHP, Forschungszentrum Jülich, D-52425 Jülich, Germany

Study of the total width of the η' meson - status of the data analysis

E. Czerwiński*,†, P. Moskal*,† and D. Grzonka* for the COSY–11 collaboration

The analysis of the $pp \to pp\eta'$ data from the COSY–11 measurement is essentially completed. During 2008 detailed studies of the position of the drift chambers, consituting the crucial factor in determining momenta of the outgoing protons, were performed. Under the assumption that the reconstructed trajectory of a particle through both drift chambers (DCs) should be a straight line the relative position of the DCs was corrected. The left plot in Fig. 1 shows the $\chi^2/nfree$ dependence (from a fit of a straight line to the reconstructed distance of the particle to the wires) on the relative position of DC2 with respect to DC1. As a next step the absolute position of the DCs was corrected using the shape of the kinematical ellipse of the elastically scattered protons (see [1] for details). Finally the position of DC2 was corrected by +0.42, -0.27 and +0.05 cm in X, Y and Z directions respectively and DC1 in X direction by +0.28 cm.

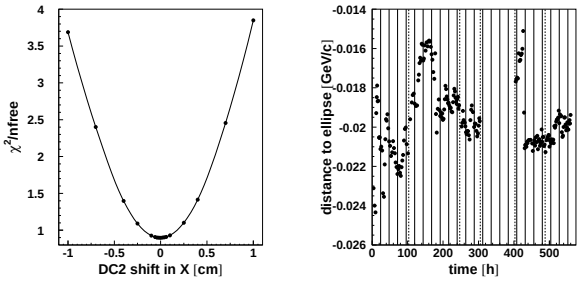

Fig. 1: **Left:** $\chi^2/nfree$ reulting from the fit of a straight line to the signals from both drift chambers as a function of the position of the second chamber with respect to the first one.
Right: Deviations of the position of the kinematical ellipse for elastically scattered protons from the expected position. Straight lines denote 24 h intervals and dashed lines separate different beam momenta (3218, 3211, 3214, 3213 and 3224 MeV/c respectively).

Having calibrated signals from all detectors one can focus on the check of stability of the reconstructed momenta of the outgoing protons, which depends on the stability of the beam momentum and position of the target (i.e. stability of the density of the target stream). These were monitored based on the momentum distribution of the elastically scattered protons. The fluctuations of the position of the kinematical ellipse of the elastically scattered protons are presented in the right plot in Fig. 1. In order to correct the mean deviation by adjusting the beam momentum one would need to apply changes ten times larger than the uncertainty of the beam momentum settings. Similarly, any variations of the target position in the X direction perpendicular to the proton beam would be in contradiction to the information from a diagnosis unit installed to determine the exact position of the target stream [2]. Therefore, the observed deviations can be plausibly explained only by variations of the density of the target stream along the Z direction (longitudinal to the proton beam). In

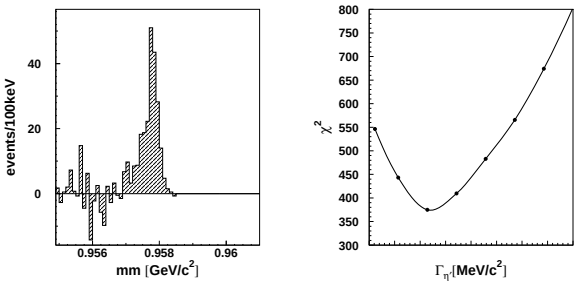

Fig. 2: **Left:** Example of a missing mass spectrum for the $pp \to ppX$ reaction for the energy closest to the threshold of the η' meson production ($Q = 0.9MeV$). Since the FWHM of the presented signal is $\approx 0.3MeV/c^2$ the achieved experimental missing mass resolution is comparable with the total width of the η' meson (≈ 0.2 MeV/c^2 [3]).
Right: χ^2 dependence for the fit of simulated distributions to experimental missing mass spectra for different total widths of the η' meson ($\Gamma_{\eta'}$) assumed in simulations. The only free parameters were the normalisation factors. The obtained statistical error ($\chi^2_{min} \pm 1$) amounts to about $\pm 0.01MeV/c^2$ (preliminary).

Z direction the target has a length of $\approx$ 1 cm, and in order to explain the discussed variations a shift of the center of the density distribution by $\approx$ 1 mm would be sufficient.
The corrections discussed above will be applied in the near future. The present preliminary results shown in Fig. 2 were obtained without taking into account the density variations inside the target. The left plot presents one out of five missing mass spectra obtained from data at a beam momentum of 3211 MeV/c. For each beam momentum a set of Monte Carlo histograms with different total width of the η' meson was prepared. Fitting simultaneously the spectra for all beam momenta by varying only the normalisation factors one can determine the total width of the η' meson from the form of the χ^2 plot (Fig. 2 right). Nevertheless, due to the still missing correction of fluctuation of the target position the evaluation of the total width of the η' meson is still in progress.

References:

[1] E. Czerwiński, Acta. Phys. Pol. **B** Proc. Supp. (2009), in print
[2] E. Czerwiński and P. Moskal, AIP. Conf. Proc. **950** 89 (2007)
[3] C. Amsler *et al.* (Particle Data Group), Phys. Lett. **B667**, 1 (2008)

* Institut für Kernphysik and Jülich Center for Hadron Physics, Forschungszentrum Jülich, Germany
† Institute of Physics, Jagiellonian University, Cracow, Poland

1.5 PISA

Double differential cross sections $d^2\sigma/d\Omega dE$ for production of light charged particles (H and He isotopes) and intermediate mass fragments (Li, Be, B, C ions) have been measured for p+Al reactions at three proton beam energies: 1.2, 1.9, and 2.5 GeV. In contrast to the energy dependence of the p+Au reactions studied earlier by the PISA collaboration [1, 2] (cf. Fig. 1), the present data for Al target almost do not change with increasing beam energy (cf. Fig. 2 and Table 1). Since this is the case for all studied ejectiles, it may be conjectured that the p+Al system in the present experiment

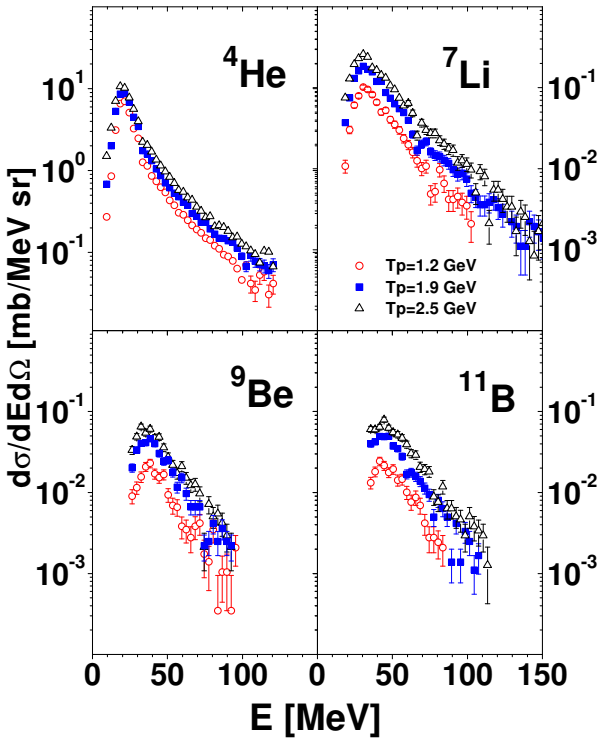

Fig. 1: Energy dependence of double differential cross sections measured for Au target at 35 degrees for particles: ^{4}He, ^{7}Li, ^{9}Be and ^{11}B

approaches the energy region where the limiting fragmentation occurs. It should be emphasized that both, total cross sections and energy spectra, vary only minimally in the energy range studied.

E_p/GeV	^{4}He	^{7}Li	^{7}Be	^{9}Be	^{11}B
1.2	660	21	8.0	3.0	5.0
1.9	650	23	9.5	3.4	6.2
2.5	640	24	10.1	3.7	6.9

Table 1: Total cross section (mb) for typical ejectiles emitted from p+Al reactions at three proton beam energies. The errors of the cross sections are about 10 %.

The different behavior of the double differential cross sections observed in the p+Al and p+Au systems indicates that approach to the limiting fragmentation region takes place at lower beam energies for p+Al than for p+Au system. This agrees well with the previously found energy dependence of total ^{7}Be production cross sections on various targets [3]. In Fig. 3 such a dependence is shown for Al and Au targets. It can be seen that the cross sections for the Al target are larger

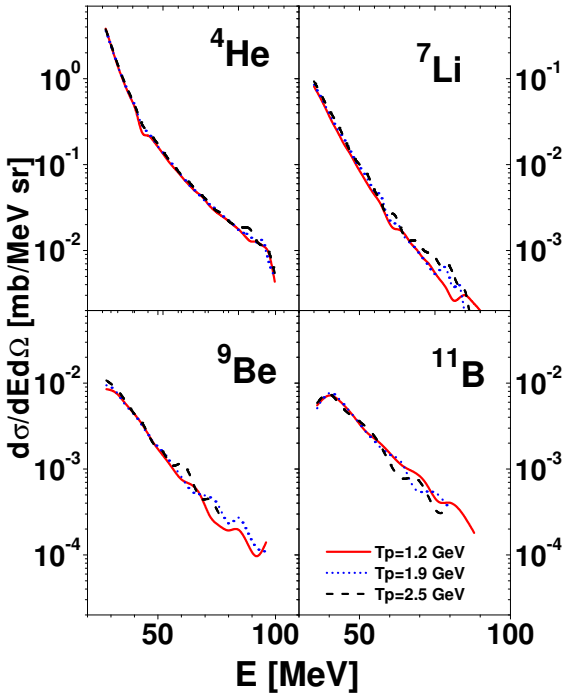

Fig. 2: Energy dependence of experimental double differential cross sections measured for Al target at 35 degrees for the same particles as in Fig. 1. Oscillation of lines are due to statistical errors.

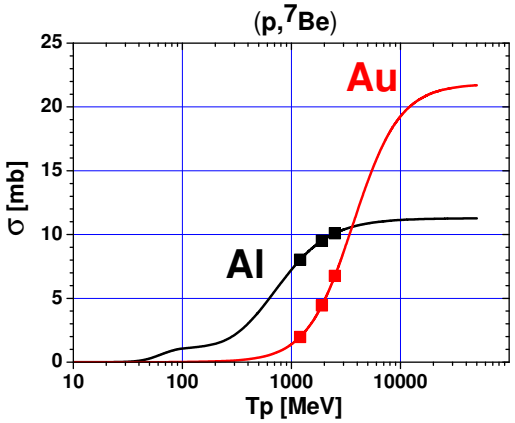

Fig. 3: Beam energy dependence of total ^{7}Be production cross section. The lines present parameterized experimental data as published in ref. [3]. The symbols depict the ^{7}Be cross sections at energies studied by the PISA.

than those for the Au target in the energy region studied. However, their variation with energy is much weaker.
It appears that in the proton energy range studied different reaction mechanisms dominate when using Al and Au targets.

References:

[1] A. Bubak et al., Phys. Rev. **C76**, 014618 (2007).
[2] A. Budzanowski et al., Phys. Rev. **C78**, 024603 (2008).
[3] A. Bubak et al., Nucl. Instr. and Meth. in Phys. Res. **B226**, 507 (2004).

Competition of fast breakup of the target with two-step mechanism for p+Ni reaction

B. Piskor-Ignatowicz for the PISA Collaboration

It was shown by the PISA Collaboration [1, 2] that a standard two step model (intranuclear cascade of nucleon-nucleon collisions coupled with a coalescence model [3], followed by evaporation of products) is not able to describe proton induced reactions on Au target at three proton beam energies: 1.2, 1.9, and 2.5 GeV. It was necessary to take into account a fast breakup of the target nucleus which lead to the additional emission of particles from three moving sources. The emission from the "fireball", i.e., fast and hot moving source, turned out to be dominating among them for light charged particles (LCPs). On the other hand, the "fireball" was not visible for intermediate mass fragments (IMFs) where another, slower and colder source participated. The full energy range spectra are well reproduced by model calculations thanks to the inclusion of these contributions.

To check the validity of the proposed mechanisms, an experiment has been performed with a Ni target using the same experimental setup and the same proton beam energies as for the Au target. It was found that the differential cross sections for Ni behave in a very similar manner like those for Au. The shape of the spectra is almost the same for all energies but the absolute value of the cross section increases with beam energy.

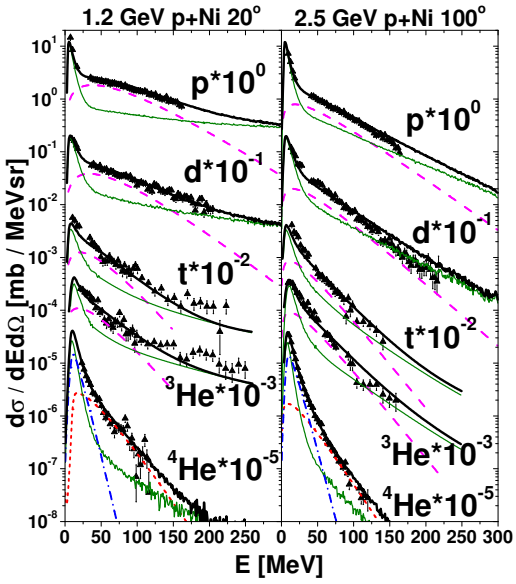

Fig. 1: Light Charged Particle (LCP) energy spectra for p+Ni collisions measured at two angles; 20^0 (for 1.2 GeV beam energy) and 100^0 (for 2.5 GeV). To separate the spectra they were multiplied by various factors depicted on the figure. The symbols represent experimental data whereas the lines show theoretical cross sections. The thick, solid (black) line represents the sum of all contributions. The thin, solid (green) line shows the prediction of a two-step reaction model (with inclusion of coalescence), and dashed (magenta) line presents the emission from "fireball". For ^{4}He the "fireball" does not contribute, but intermediate velocity (red, dotted line) and slow (blue, dash - dotted line) sources appear.

The quality of the data is illustrated by Fig. 1 (for LCPs) and Fig. 2 (for IMFs), where the energy spectra taken at three different angles and for three different energies are shown as symbols. It was found that the reaction mechanisms used for the description of the data for the Au target are also able to reproduce well all cross sections of the reactions induced by protons on the Ni target. An excellent quality of the data description may be concluded from the inspection of the figures where lines represent the model calculations.

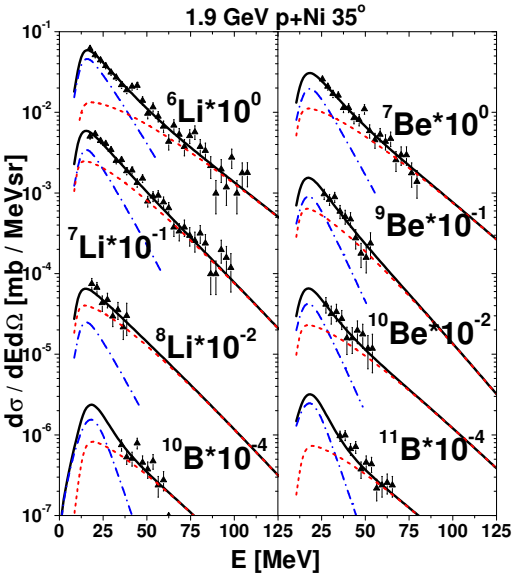

Fig. 2: Intermediate Mass Fragments (IMF) energy spectra for particles emitted at 35^0 in p+Ni reactions at beam energy of 1.9 GeV. Results for individual particles are multiplied by factors indicated in the figure to separate the spectra. Symbols correspond to experimental data, red (dotted) and blue (dash-dotted) lines represent contributions of intermediate velocity and slow moving sources, respectively.

Thus, it is evident that the proposed reaction mechanisms describe equally well not only the experimental data for the Au target [1, 2], but also those for the Ni target, which is almost 3 times lighter than the Au nucleus, has a much stronger binding energy and a completely different neutron to proton ratio. This suggests that the discussed mechanisms are present in proton induced reactions for all targets. Therefore it is desirable to verify this proposition by careful studies of proton induced reactions on few other targets. The PISA collaboration is presently analyzing the data for the Al target (cf. [4]) and for the Ag target.

References:

[1] A. Bubak et al., Phys.Rev. **C 76**, 014618 (2007)
[2] A. Budzanowski et al., Phys.Rev. **C 78**, 024603 (2008)
[3] A. Boudard et al., Nucl.Phys. **A 740**, 195 (2004)
[4] M. Fidelus for PISA collaboration, present report

BUU model description of neutrons produced in proton induced spallation process

A. Kowalczyk[a,b] *for the PISA Collaboration*

Spallation is one of the possible scenarios of proton - nucleus reactions. Its identification is based on experimental observations of one heavy nucleus (compared to the mass of the initial target), a small number of light fragments and numerous individual nucleons.

Spallation reactions induced by protons on atomic nuclei are especially important in accelerator technology, since a relatively large number of produced neutrons suggest using such reactions as neutron sources.

Several models have been developed in order to describe the reaction mechanism. It is considered as a two stage process involving projectile energy deposition inside the target nucleus, bringing it into an excited state (first stage) and subsequent deexcitation of the residual nucleus by evaporation of particles (second stage).

Here, we report on studies of the neutron production in proton - nucleus reactions with the Boltzmann-Uehling-Uhlenbeck (BUU) model [1, 2, 3, 4] for the first stage. For the second stage the statistical model (GEM) [5] was used.

Results of the calculations are presented in Figures 1 and 2.

The high energy part of the distributions are due to neutrons produced during the first stage, while the low energy part consists of neutrons produced during the second stage of the reaction.

Comparison of the calculations with experimental data shows, that independent of the value of the projectile energy, the calculated neutron spectra produced in proton induced reactions on light targets (e.g. Fe, see Figure 1) are in very good agreement with the experimental data [6].

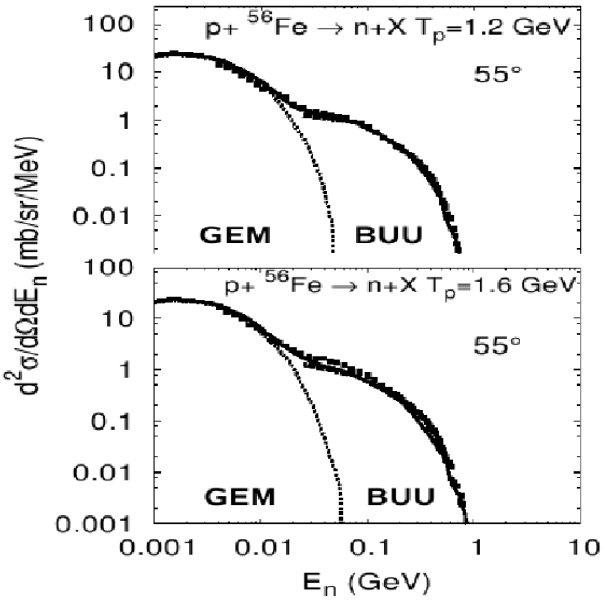

Fig. 1: Double differential inclusive cross section for neutron production in p+Fe reaction, at 1.2 and 1.6 GeV beam energy. Lines correspond to the model calculations, symbols to the experimental data [6].

In contrast, the calculations underestimate the experimental data in the central parts of the distributions for neutrons produced on heavy targets (e.g. Pb, see Figure 2).

The failure in the data description, in case of reactions on heavy targets indicates, that apart from the two stages assumed for the spallation reaction, there must be an additional intermediate stage, probably a preequilibrium stage.

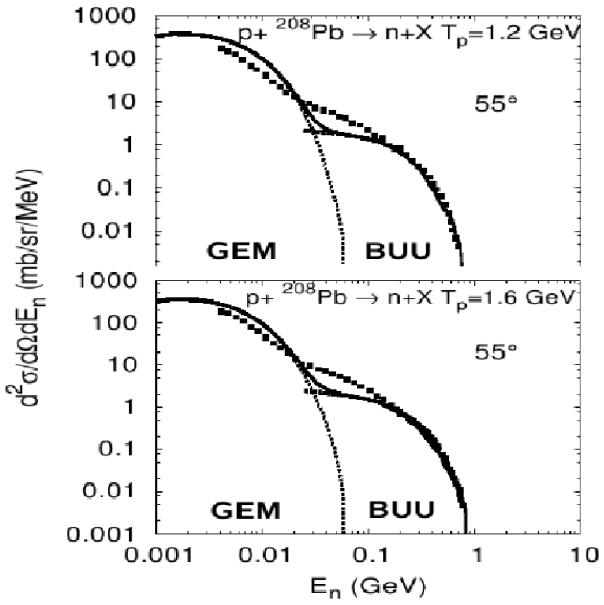

Fig. 2: Same as Figure 1, but for p+Pb reaction.

Based on a systematic study of angular distributions, the mass of the target nuclei and the projectile energy, we conclude that neutron production during this intermediate stage is dominant for reactions with heavy targets and negligible for reactions with light targets. Detailed studies of this effect are presented in [4].

References:

[1] K. Niita, W. Cassing and U. Mosel, *Nucl. Phys.* **A504**, 391 (1989).
[2] G.F. Bertsch and S. Das Gupta, *Phys. Rep.* **160**, 189 (1988).
[3] J. Geiss, W. Cassing, C. Greiner, *Nucl. Phys.* **A644**, 107 (1998).
[4] A. Kowalczyk, `nucl-th/0801.0700`.
[5] S. Furihata, *Nucl. Inst. Meth. in Phys. Res.* **B171**, 251 (2000).
[6] S. Leray et al., *Phys. Rev.* **C65**, 044621 (2002).

[a] Institut für Kernphysik and Jülich Center for Hadron Physics, D-52425 Jülich, Germany

[b] Institute of Physics, Jagiellonian University, PL-30059 Cracow, Poland

1.6 PAX

Status of the PIT for Spin-Filtering Studies at COSY and AD

A. Nass[a], G. Ciullo[b], K. Grigoriev[c], P. Lenisa[b], F. Rathmann[c], J. Sarkadi[c], M. Statera[b], E. Steffens[a], H. Ströher[c] and G. Tagliente[d]

The high physics potential of experiments with stored high-energy polarized antiprotons led to the PAX proposal [1] for the High Energy Storage Ring (HESR) of the FAIR facility (Facility for Antiproton and Ion Research) at GSI (Darmstadt/Germany). It is proposed to polarize a stored antiproton beam by spin filtering with a polarized hydrogen (deuterium) gas target. The feasibility of spin filtering has been demonstrated in the FILTEX experiment [2]. In the current theoretical interpretation [3] only the hadronic interaction is important. In order to test the spin filtering method and find the best operational energy, several experimental studies with protons (at COSY) as well as with antiprotons (at AD/CERN) have to be carried out. These investigations require the set-up of a polarized internal gas target (PIT) with a system of Silicon detectors implemented into a large acceptance section of the storage rings.

The former HERMES polarized atomic beam source (ABS) was set up in Jülich. The vacuum system with the microwave dissociator is operating well and intensities up to $6 \cdot 10^{16}$ atoms/s were reached. A new liquid-cooled microwave dissociator was tested on a test bench (Fig. 1) and will be implemented soon. It is supposed to increase the degree of dissociation at high nozzle throughputs and increase the atomic flow into the sextupole system of the ABS.

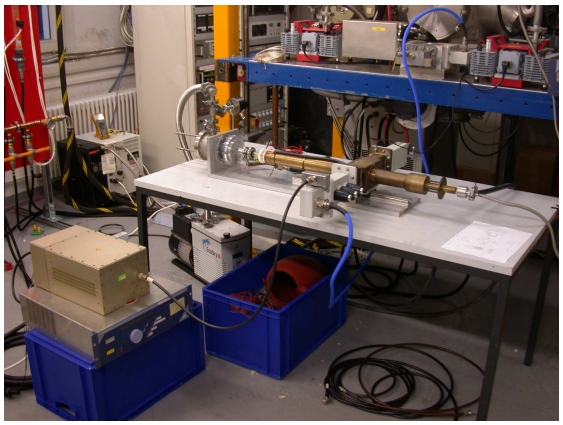

Fig. 1: The liquid-cooled microwave dissociator on the test bench.

The former HERMES Breit-Rabi polarimeter (BRP) [4] was set up in the LKW-Schleuse (Fig. 2). The sextupole magnet configuration was modified and a new strong-field "Dual Cavity" transition was designed and built in order to measure the polarization of hydrogen or deuterium without the usual replacement of the cavity. The cabling of the vacuum part was finished and the slow control system is running. As in the case of the ABS, also the BRP can be controlled and monitored via computer. The two quadrupole mass spectometers were tested and first mass scans were performed.

In order to reach the necessary areal densities for spin filtering, the use of a storage cell is mandatory. The present cell design consists of 5 μm Teflon walls supported by an aluminum frame. Teflon suppresses depolarization and recombination of the target gas inside the cell. The first prototype of the target cell has been built at INFN Ferrara. It will be tested with the use of the ABS and the BRP in Jülich in 2009, with an already modified analysis chamber of the ABS. Therefore, the ABS will be installed at the LKW-Schleuse in early 2009.

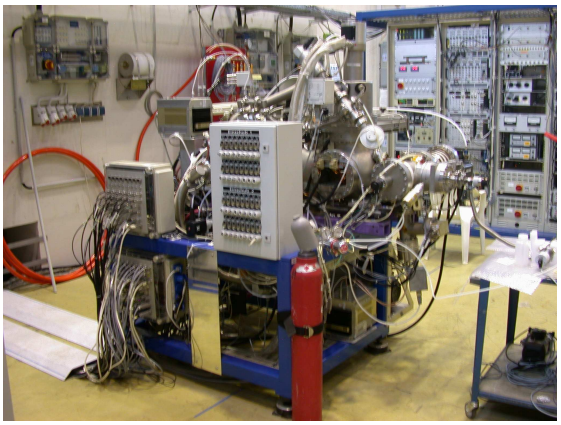

Fig. 2: The Breit-Rabi polarimeter.

The vacuum system of the target section comprises two turbo molecular pumps (TMP), backed with smaller TMPs, and a dry forevacuum pump. In addition, a large cryogenic pump will be used at the target chamber. This will ensure that most of the target gas exiting the storage cell is pumped within the target chamber. The adjacent sections will be pumped by a combination of ion getter pumps and TMPs. For the test setup only one TMP will be used.

In order to test the full setup in the LKW-Schleuse, large efforts of various COSY groups were necessary in 2008 to supply the area with water end electricity.

References:

[1] *Antiproton-Proton Scattering Experiments with Polarization*, Technical Proposal for the HESR at FAIR, Jülich (2006), Spokespersons: P. Lenisa and F. Rathmann, and references therein. Available from *www.fz-juelich.de/ikp/pax.*

[2] F. Rathmann et al., Phys. Rev. Lett. 72, 1379 (1993).

[3] A.I. Milstein and V.M. Strakhovenko, Phys. Rev. E 72, 066503 (2005).

[4] C. Baumgarten et al., Nucl. Instr. and Meth., A482 (2002) 606.

[a] Phys. Institut der Univerität Erlangen-Nürnberg, Germany
[b] Istituto Nationale di Fisica Nucleare, Ferrara, Italy
[c] Forschungszentrum Jülich, IKP, Jülich, Germany
[d] Istituto Nationale di Fisica Nucleare, Bari, Italy

1.7 Further experiments

Performance of the ATRAP Experiment at CERN in 2008

M.C. George, D. Grzonka, W. Oelert, T. Sefzick, and M. Zielinski for the ATRAP – Collaboration

The goal of the ATRAP experiment at the anti-proton decelerator AD of CERN is to study the physics of cold anti-hydrogen ($\bar{H}$) atoms. For this reason ground-state $\bar{H}$ atoms have to be confined in magnetic traps for e.g. a test of the CPT invariance by the comparison of hydrogen (H^0) to anti-hydrogen ($\bar{H}^0$) atom spectroscopy and a measurement of the gravitational force on antimatter atoms.
The investigations in 2008 concentrated on significant improvements of the second experimental set-up (called BTRAP) in the second generation facility of the ATRAP collaboration (ATRAP-II). The complete apparatus as being moved from the place of assembly to the super-conducting solenoid is shown in Fig. 1, with the photo of the pin-base underneath the $\bar{p}$ solenoid in Fig. 2.

Fig. 1: The BTRAP-experimental set-up showing (from top to bottom) the liquid He dewar, the xy-table, the Ioffe-trap, and the new $\bar{p}$ solenoid.

Fig. 2: Photo of the pin-base before the $\bar{p}$ solenoid is mounted.

The construction of the $\bar{p}$ solenoid, adding a magnetic field of up to 5 T to the main magnetic field when being operated at 89 A, provided a drastic increase in loading $\bar{p}$'s. Using for safety reasons only 54 A (additional 3 T to the main field of 1 T) a gain factor of up to five was observed depending on the electrical field profile of the electrodes. Thus with the new $\bar{p}$ solenoid the main magnetic field could be kept at a rather low value in favor of an effective deeper Ioffe-trap potential.

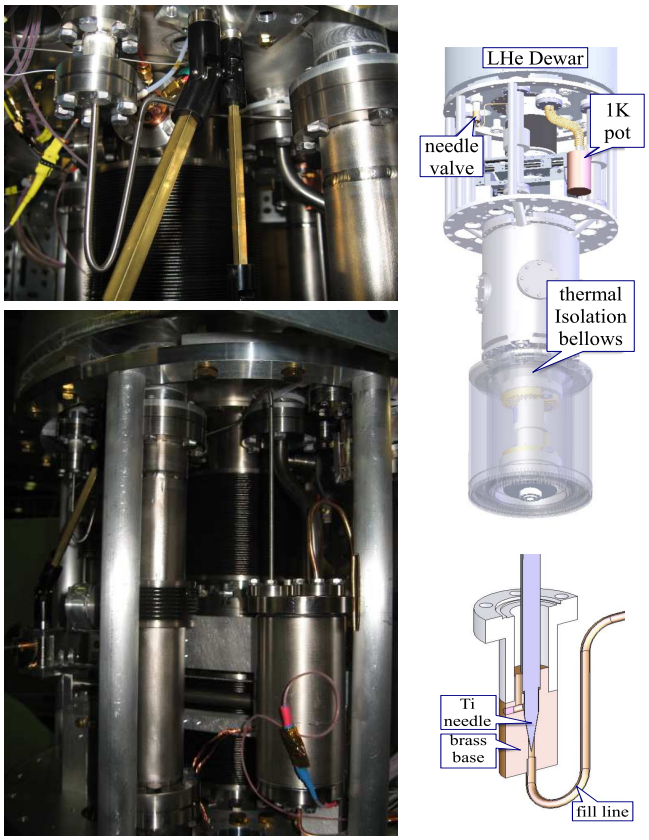

Fig. 3: Photo and technical drawing of the 1 K pot arrangement in BTRAP.

As demonstrated in Fig. 3 via photos and technical drawings a 1 K pot has been added to the BTRAP apparatus and has been successfully operated during the last year. Via pumping through a needle valve the 4K liquid He in the 250 cc pot is cooled to a temeperature of 1.1 ± 0.02 K. This improvement should provide lower temperature $\bar{p}$'s and subsequently lower temperature $\bar{H}$ atoms, necessary to keep them in the Ioffe-trap for times long enough for experiments.
Extensive plasma shape studies of e^- and e^+ clouds have been investigated taking advantage of the low temperature. As one example: using 20 eximer laser shots up to 40×10^6 e^+ were loaded during a continuous change of the electrical well in steps of 1 V/s up to a final value of 75 V. It has been observed that the plasma shape changes on the history of its loading. Different cloud shapes ranging from an axial ratio from $\alpha = 0.3$ (pancake structure) to $\alpha = 2.2$ (cigar shape) could be created, a very important step for achieving an optimal overlap between clouds of e^- and $\bar{p}$ to produce cold $\bar{H}$ atoms.

Confined-Particle Resonances and Exotic Atom Production Attempts

M.C. George, for the ATRAP – Collaboration

The ATRAP experiment at CERN has the goal to create, trap and study the bound states of an anti-proton ($\bar{p}$) and a positron (e^+) – the anti-hydrogen ($\bar{H}$) atom. Progress this year centered on gaining a better understanding of how the constituent particles behave in the ATRAP-II Penning-trap apparatus, and making use of this knowledge to further our ability to make more, and colder $\bar{H}$.

One of the new ways in which the IKP contributed to categorize the trapped particle behavior was by developing techniques and electronics to study the resonances of the particle-motions inside the Penning-trap. The three types of motion for charged particles in a harmonic well confined in a Penning-trap are cyclotron motion, magnetron motion, and axial motion, see Fig. 1.

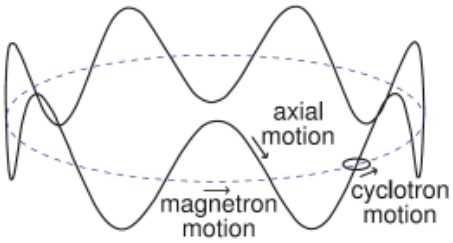

Fig. 1: Motions of a charged particle confined in a Penning-trap.

To study these motions, low noise, high-Q tuned resonant circuits, amplified by high gain FETs are placed on the experiment and cooled together with the ATRAP-II apparatus to 1K. The variation of the image charge on the Penning-trap electrodes from the confined particle-motions can be amplified by the cold amplifiers, and the response viewed on a spectrum analyzer. In order to have a good signal-to-noise ratio, the particle-motion needs to be in resonance with the amplifier tuned circuit. The IKP was involved in the careful and time consuming design and tuning of these particle-motion amplifiers.

The cyclotron motion of $\bar{p}$ was investigated first. To put energy into the cyclotron motion, an AC voltage drive is applied to a nearby electrode, and the frequency of the drive swept down through the expected cyclotron frequency over tens of seconds. During this sweep, if there are many $\bar{p}$'s confined in the Penning-trap then losses will be seen by the IKP system of fiber and paddle scintillating detectors when the AC voltage drive frequency exactly matches the $\bar{p}$ cyclotron resonance. Due to the distribution of relativistic speeds of the now highly excited $\bar{p}$'s, there is a spread for the observed cyclotron frequency. In addition to the expected frequency spread, we discovered a much larger frequency spread which was attributed to magnetic field inhomogeneities in this region. This happens also to be the region in the Penning-trap where $\bar{H}$ production occurs, so understanding these magnetic field gradients was very important. It was discovered that these gradients were due to hysteresis in the IKP Ioffe trap coils, which could be minimized or removed by ramping systematically the quadrupole coils of the Ioffe trap.

The techniques and electronics developed for viewing particle-motions were so successful that we had the ability to view the cyclotron motions of individual $\bar{p}$'s confined in the ATRAP-II Penning-trap. We were able to reduce the initially large number of $\bar{p}$'s in the trap, to just a few particles by lowering the voltage of the confining axial field. Once we had only a few confined $\bar{p}$'s, we were able to follow the de-energizing of individual $\bar{p}$'s (as their relativistic shifts became smaller, their cyclotron frequencies become larger). Figure 2 is a plot of the measured cyclotron frequency of an individual $\bar{p}$ as it gives up cyclotron energy. Theoretically, the $\bar{p}$ will de-excite to the zero energy point, the true modified cyclotron frequency of our trap. Knowing this value precisely

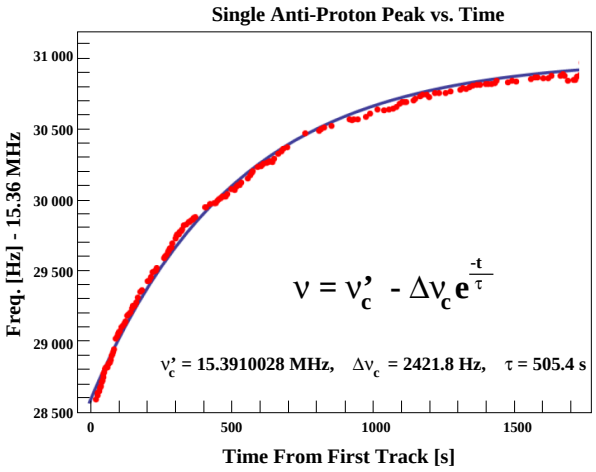

Fig. 2: Variation in observed cyclotron frequency for a single $\bar{p}$ over time. As the $\bar{p}$ cyclotron energy lowers, the frequency approaches the true cyclotron frequency.

allows us to determine very well various geometric constants of the Penning-trap apparatus.

In addition to studying the cyclotron motion of the $\bar{p}$'s, techniques were developed to determine the $\bar{p}$ magnetron frequency, and hence to calculate precisely the $\bar{p}$ axial frequency. This important information fully characterizes the $\bar{p}$ motion in the ATRAP-II apparatus.

Due to these exciting advances in monitoring in real-time the individual motion of $\bar{p}$'s, an experiment was devised to attempt to create and trap an $\bar{H}^+$ ion: an anti-proton bound with two positrons. The trapping of this exotic atom for long periods of study would be far easier than of the neutral $\bar{H}$, as a simple electrostatic trapping potential would suffice. There is a strong possibility of protons being trapped along with the created H^+ so the experience and understanding of monitoring $\bar{p}$ resonant motions in the apparatus was an essential prerequisite for this attempt. The early ending of the CERN-AD $\bar{p}$ beam run allowed for only preliminary experiments to produce $\bar{H}^+$.

Summarizing, the IKP was strongly involved in developing powerful techniques and apparatus to probe the behavior of the charged particles used during an $\bar{H}$ production experiment. This progress also led to better understanding of the ATRAP-II apparatus, attempts to create the easy-to-trap exotic atom of $\bar{H}^+$, and will lead to improved techniques for the production of cold, trapped $\bar{H}$ atoms.

Efficiency determination for the ATRAP detector system

M. George, D. Grzonka, W. Oelert, T. Sefzick, M. Zielinski for the ATRAP collaboration

The ATRAP experiment at the CERN Antiproton decelerator (AD) aiming for a precise CPT test by studying the antihydrogen atom includes a detection system for the antiproton annihilation products. Antihydrogen production studies require the knowledge of the produced antihydrogen atoms as well as absolute antiproton losses during the development.

In 2008 the ATRAP experiment has been modified by adding an additional solenoid to improve the $\bar{p}$ trapping and has been operated at a lower main field 1 T. Furthermore some photomultipliers have been exchanged and the PM voltages have been adjusted. Therefore the efficiency for the detection of an antiproton annihilation has been determined by using cosmic rays and Monte Carlo studies.

In order to get accurate values for the detection efficiency of a $\bar{p}$ annihilation one should trap a single antiproton, release it at a well defined time, observe the registered detector signals and do this procedure a sufficient number of times to reach a low statistical uncertainty. The trapping of single antiprotons within the ATRAP setup has been achieved in 2008 but it has to be further developed before this experimental efficiency determination is available.

Another possibility is the use of Monte Carlo studies which have been done by using the GEANT4 software package. As input for the simulation studies one needs a realistic geometry and the energy thresholds for the registration of a signal in the individual detector components.

As a first step the efficiency of the different detector components for the detection of a minimum ionized particle is determined by measuring cosmic particles. The detector system is sketched in fig. 1. It consists of four fiber rings sur-

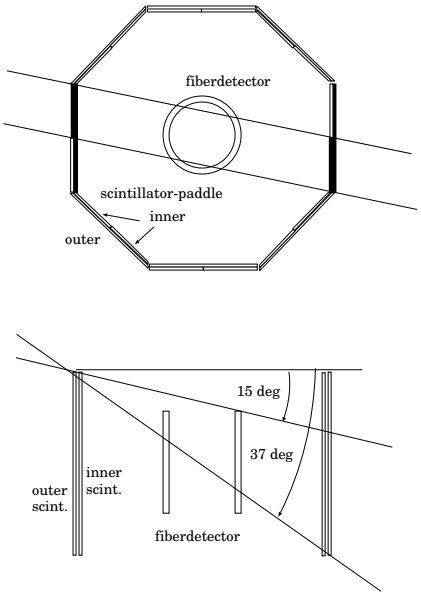

Fig. 1: Sketch of the detection system at ATRAP-II with the fiber detector and the outer scintillator paddles.

rounding the trap, two staggered straight fiber rings that a particle passing the double fiber ring must hit a scintillating fiber and two helical fiber rings where each fiber covers an angular range of about 155 °. At the outside of the magnet an arrangement of scintillator plates is installed, 8 large plates

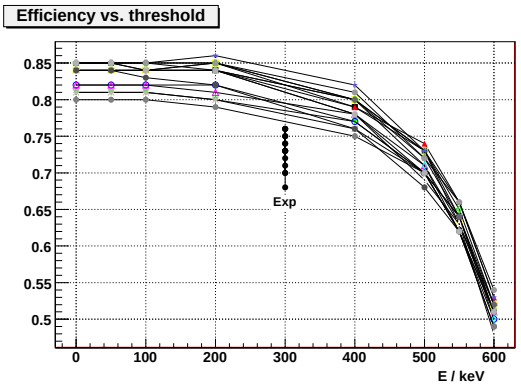

Fig. 2: Detection efficiency for the straight fiber layer from Monte Carlo data as a function of the energy threshold in keV compared to the experimental points.

(outer) and 16 smaller plates (inner) where every two inner are covering one outer. The lines in fig. 1 indicate straight tracks of cosmic particles.

The efficiency for the scintillator plates is determined by selecting cosmic events with a signal in two opposite large (small) scintillator plates and a signal in one corresponding small (large) scintillator plate. The detection efficiency is close to 100% which is consistent with the ADC distributions of these elements. For the detection efficiency of the straight fibers cosmic events are selected with signals in two opposite large and small scintillator plates. These cosmic particles have to pass also the fiber detector if the inclination angle is not too small. The distribution of hit straight fibers shows two bumps for the two regions of possible hit fibers which can be reproduced by Monte Carlo data. In fig. 2 the mean efficiency from Monte Carlo data as a function of the energy threshold E_{th} is shown. The comparison to the experimental points suggest a threshold of 470 keV which is compatible with the observed threshold in the ADC spectra. The mean efficiency determined by this method is 0.88 (the value has to be normalized to the value at zero threshold). Alternatively the fiber detection efficiency was determined by selecting cosmic events with the four outer scintillators and a straight (helical) fiber for the helical (straight) fiber efficiency from which values of 0.84 for the helical and 0.87 for the straight result.

The efficiency for the detection of a $\bar{p}$ annihilation is determined from Monte Carlo by including the extracted energy thresholds for the detetctor elements. It depends on the signals which are requested for the identification of a $\bar{p}$ annihilation. Depending on the fiber multiplicity (M_{fiber}) and the paddle multiplicity (M_{paddle}), whereby a paddle signal means here coincident signals in one large and one of the associated small scintillator plates, the signal to noise ratio can be improved but the optimal condition depends also on the total event number. For $M_{fiber} > 0$ and $M_{paddle} > 0$ the mean efficiency is 0.78, for $M_{fiber} > 1$ and $M_{paddle} > 0$ its 0.7, and for $M_{fiber} > 1$ and $M_{paddle} > 1$ it reduces to 0.4. For each condition used in the analysis the particular efficiency is determined and is used for the calculation of absolute numbers.

Precision Spectroscopy of Hydrogen with a Lamb-shift Polarimeter

R. Engels[a]., K. Grigoryev[a,c], M. Mikirtychyants[a,c], H. Paetz gen. Schieck[b],
G. Schug[a], A. Vasilyev[c], M. Westig[a,b], and H. Ströher[a]

For the Breit-Rabi diagram of the hydrogen states $2S_{1/2}, 2P_{1/2}$ and $2P_{3/2}$ (Fig. 1) experimental data of high precision exist only for weak magnetic fields about a few mG, which allow to check the results of advanced bound-state QED calculations. These experimental data stem from 2-photon laser-spectroscopy [1, 2] and the separated-oscillatory-field method [3]. At higher magnetic fields, the crossing of the β and the e states around 570 G were measured decades ago [4]. From the Breit-Rabi diagram the classical Lamb shift, the hyperfine splittings and, from the slope of the energy levels, the g-factors of those states can be determined. The calculation of these values by bound-state QED is on a very accurate level, so that the uncertainty now is dominated by effects like the charge distribution of the proton. With a very precise measured Breit-Rabi diagram a test of the bound-state QED seems possible, which is expected to contribute e.g. in the determination of the charge distribution in the proton.

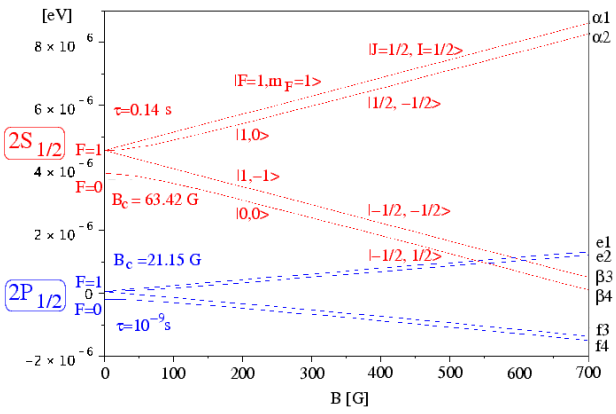

Fig. 1: The Breit-Rabi diagrams for the metastable $2S_{1/2}$ and the short-lived $2P_{1/2}$ hyperfine states.

A spinfilter, the most important component of a Lamb-shift Polarimeter [5], is able to produce a beam of metastable hydrogen (deuterium) atoms in only one hyperfine state ($\alpha 1$, $\alpha 2$ or $\beta 3$). From these states, $M1$ transitions into the other hyperfine states can be induced at different transverse magnetic fields and the population of these states can be measured with a second spinfilter. Based on the expected error of $\Delta f = 10$ kHz for a single measurement, 100 measurements between 0 and 100 G should lead to a relative error of 10^{-6} for the g-factors. Increasing of the magnetic field range will decrease the size of the error substantially. But it has to be taken into account, that the g-factors will change for large magnetic field. In addition, the hyperfine splitting of the $2S_{1/2}$ state corresponds to the difference of the $\alpha 1 \rightarrow \beta 4$ and the $\alpha 2 \rightarrow \beta 3$ transition energies or the sum of the transitions energies $\alpha 1 \rightarrow \alpha 2$ and $\beta 3 \rightarrow \beta 4$ independent of the magnetic field strength. Therefore, it is possible to average the values, measured at different fields to obtain an error of the hyperfine splitting of less than 1 kHz. The error is dominated by the Heisenberg uncertainty relation $\Delta\nu \times \Delta t \sim 1$, which will broaden the half with of the resonance. This problem can be solved by exiting the slow hydrogen beam of an atomic beam source (ABS) by electron bombardment before the hyperfine states are separated with the spinfilter.

In a proof-of-principle measurement [6] $E1$ transitions into the single Zeeman states of the $2P_{1/2}$ state were induced with a Lecher TEM (transverse electromagnetic) transmission line. Because of the short lifetime (10^{-9}s) of the $2P_{1/2}$ state the atoms will decay immediately into the ground state and the produced Lyman-α photons are detected with a photomultiplier as a function of the radio frequency at a stable power level (see Fig. 2).

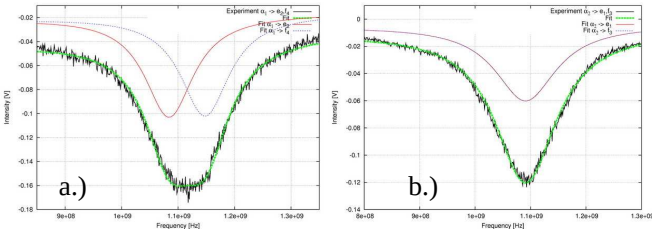

Fig. 2: The observed transitions $\alpha 1 \rightarrow f4$ and $\alpha 1 \rightarrow e2$ (a.) or $\alpha 2 \rightarrow f3$ and $\alpha 2 \rightarrow e1$ (b.) at a small vertical magnetic field ($B \sim 0.5$ G) in the transition region.

From the observed transitions at small magnetic fields the hyperfine splitting of the $2P_{1/2}$ state can be directly determined to 59.98 (2.03) MHz, which fits to the best known value of 59.22 (14) MHz [3]. A much better precision of $\Delta f_{hfs} < 10$ kHz can be obtained, because similar to the M1 transitions the combination of the transition $[(\alpha 1 \rightarrow f4) - (\alpha 2 \rightarrow f3) - (\alpha 1 \rightarrow e1) + (\alpha 2 \rightarrow e2)]$ corresponds to the hyperfine splitting f_{hfs} independent of the magnetic field at the interaction region. Another outcome of these measurements is a value of 1057.34 (1.11) MHz for the classical Lamb shift. This agrees with other measurements [2], but the error is at least two orders larger.

With this setup an error of $\Delta f = 100$ kHz for a single measurement is expected. This means, that the relative error of the g-factor for 100 measurements between 0 and 100 G will be around 10^{-5} and can be decreased further by increasing the magnetic field range. There exists a huge dipole magnet with 1.5 T magnetic field strength in the COSY test hall which may lead to a relative error of $\sim 10^{-8}$ for the g-factor of the $2P_{1/2}$ states. In addition, $E1$ transitions into the single Zeeman states of the $2P_{3/2}$ state can be induced with a modified TEM waveguide for radio frequencies around 10 GHz. The same method is applicable for deuterium, too. In this case, three Zeeman states ($\alpha 1$, $\alpha 2$ and $\alpha 3$) are selected by the spinfilter. In general this method may be useful for antihydrogen, because during the recombination of the antiproton and the positron $\sim$ 30% of the antihy-

drogen will populate the metastable $2S_{1/2}$ state.

Supported by JCHP - FFE

References:

[1] N. Kolachevsky et al.; Phys.Rev.Lett. **92** 033003 (2004).
[2] C. Schwob et al.; Phys.Rev.Lett. **82** 4960 (1999).
[3] S.R. Lundeen et al., Phys.Rev.Lett. **34** 377 (1975).
[4] W.E. Lamb and R.C. Retherford, Phys.Rev. **81** 222 (1951).
[5] R. Engels et al., Rev.Sci.Instr. **74**, 11 4607 (2003).
[6] M. Westig, diploma thesis, IKP (2008).

[a] Forschungszentrum Jülich, IKP, Jülich, Germany
[b] Universität zu Köln, IKP, Köln, Germany
[c] PNPI Gatchina, Gatchina, Russia

Preparations for studies of laser accellerated protons

N.Raab, M.Büscher, P.Gibbon[a], R.Jung[b], H.Ohm, M.Seltmann, O.Willi[b], Q.Zhang

Charged particles, like electrons, protons and ions, can be accelerated by focusing a high intensity laser pulse on a suitable target. Protons with energies of up to five MeV from a foil and electrons with energies of up to 200 MeV from a gas target have already been detected with the 100-TW laser system PULSAR at Düsseldorf University. Typically, the particle beams are polyenergetic with an exponentially dropping energy spectrum (although at the gas target quasi- monoenergetic electron beams have been observed, too). Optimisation of the laser-beam quality and targets is in progress, so that even higher proton energies can be expected.
In order to better understand the acceleration mechanisms, particle-in-cell (PIC) simulations have been performed with the BOPS program (Boosted Oblique Particle Simulation). It is a one and three halves (1 spatial, 3 velocity coordinates: 1D3V) PIC simulation code, written by Paul Gibbon and Tony Bell and described in Ref. [1]. Proton spectra for different laser intensities and incident angles, as well as foil thicknesses were obtained from the simulations. Although the absolute values of the simulated and measured proton energies are known to differ very much, systematic dependencies can be qualitatively studied. Recent simulation studies [2] have found a maximum in the proton energy for an incident angle of 30°. For this angle a series of simulations was carried out with different laser intensities. Also for the intensity of the Düsseldorfer Laser in the focus point of $5 \cdot 10^{20}\,\mathrm{W/cm^2}$, the maximum energy was calculated for different incident angles. The pulse length of 30 fs and the laser wave length of 800 nm match the experimental conditions. In Fig. 1 the result of the simulations is presented. Unsurprisingly, the maximum proton energy increases with laser intensity. At 30° a step in the distribution can be seen, but contrary to Ref. [2] the maximum energy appears to rise even further.

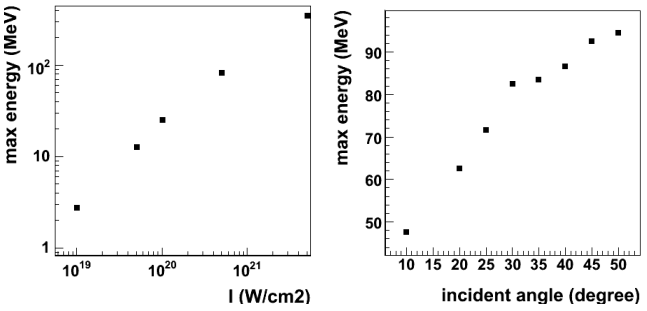

(a) (b)

Fig. 1: Maximum proton energy depending on (a): intensity in the laser focus at 30° incident angle, (b): the incident angle of the laser beam at constant intensity.

The laser plasma interaction produces short bunches with very high particle numbers, leading to difficulties for the detection. Currently, for the detection of protons and ions, film detectors and solid-state nuclear track detectors are used. Unfortunately with these methods no on-line analysis is possible, and also particle identification is difficult. To have results immidiately at hand after each laser shot, an ionisation detector and a dipol magnet for spectroscopy are being built at the IKP. They are intended to be set up at the foil target chamber, although an ionisation detector has also been tested detecting electrons from the gas target. That detector is described in this year's annual report by M.Büscher et al.
The spectrometer magnet was designed to be very compact. Estimations with GEANT4 have shown that multiple scattering in air would lead to high uncertanties of the energy measurement of the protons, making it necessary to place the spectrometer magnet within vacuum. Permanent magnets were used to provide high magnetic field intensity despite the small size of the dipol magnet. The ionisation detector, which cannot be operated in vacuum will be located behind a thin foil window.
The dipol magnet is H-shaped dipol with a gap height of 2 cm and a length of 30.6 cm. It consists of an overall of 24 neodym magnets that are placed in the return yokes. In order to obtain highest the possible field strength, the Pandira software package was used to calculate the optimum shape of the return yokes, which can be seen in Fig. 2(a).

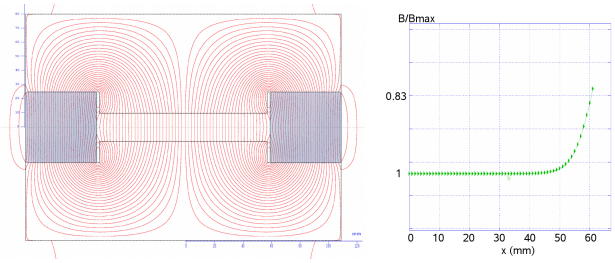

(a) (b)

Fig. 2: (a): cross section of the dipol magnet (blue: permanent magnets) with lines of magnetic flux as calculated with pandira (b): vertical component of the magnetic field.

The magnetic field strength in the gap is 0.55 ± 0.05 T in the homogeneous area of the gap. This variation of field strength along the symmetry axis can be explained by differences between the single permanent magnets which have been arranged such that these effects partially compensate. Due to stray fields in front of and behind the magnet the effective length of the magnet is 34.8 cm.

References:

[1] P. Gibbon, A. Andreev, E. Lefebvre, G. Bonnaud, H. Ruhl, J. Delettrez, and A. R. Bell. Calibration of one-dimensional boosted kinetic codes for modeling high-intensity laser–solid interactions. *Physics of Plasmas*, 6(3):947–953, 1999.

[2] T. Morita, T. Zh Esirkepov, S. V. Bulanov, J. Koga, and M. Yamagiwa. Tunable high-energy ion source via oblique laser pulse incidence on a double-layer target. *Physical Review Letters*, 100:145001, 2008.

[a]JSC, Forschungszentrum Jülich
[b]ILPP, Heinrich-Heine Universität Düsseldorf

A new tracking device for the investigation of laser-induced particle acceleration

M. Büscher[1], I. Császár[1,2], M. Md. Hossain[1,3], R. Jung[4], P. Kulessa[1,5], H. Ohm[1], G. Oswald[1,2], N. Raab[1,6], V. Serdyuk[1,7], O. Willi[4], Q. Zhang[1,8]

The interaction of terawatt laser pulses with suitable gas or foil targets can yield bunches with up to approx. 10^12 particles (e.g. protons) in the MeV region. For studies of these processes a position sensitive detector has been developed which is capable of detecting single charged particles as well as extremely intense bunches, see Fig. 1.

Single tracks are identified with a multiwire anode plane consisting of 9 parallel field wires (125 µm Cu/Be) with a spacing of 10 mm between which anode signal wires (20 µm W/Au) are centered. The anode-wire plane faces cathode planes (12 µm Mylar with double-sided Al layers) at distances of 5 mm at each side. For the detection of intense bunches the chamber is equipped with a planar position-sensitive ionization chamber stage. The active area of the 9x7 cm^2 anode plane consists of 32 rectangular pads on a printed circuit board.

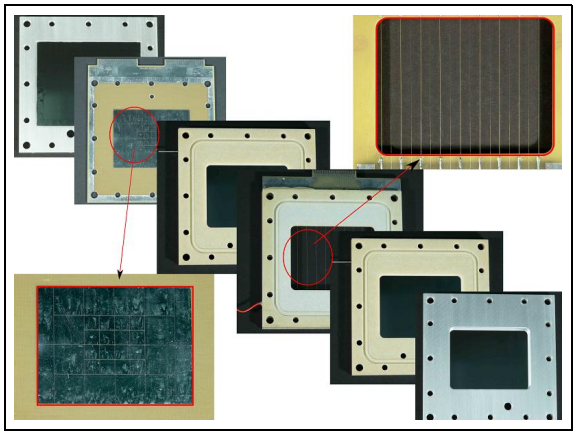

Fig.1: Exploded view of the chamber with the main components. Anode planes are additionally enlarged.

In view of the strong electromagnetic pulse expected to arise during interaction of the laser beam with the target the chamber has thoroughly been shielded with copper. No evidence has been found so far for any disturbing effect of the EMP. Fast current amplifiers with a gain of 100 were directly attached to the chamber und connected via 25 m twisted pair cable to the counting room. Signals are presently recorded with a 100 MHz 4-channel digital oscilloscope. A Camac-based DAQ system is under preparation. The chamber has been successfully tested using various standard gas mixtures like Ar/CO2, Ar/Ethane and Ar/Methane. With radioactive sources the detection efficiency for single particles was found to be close to 100 %. During the initial measurements at the laser target for practical reasons premixed gas with 90% Ar and 10% CH4 was used.

First data with a laser-induced plasma as a particle source were recorded at the Institute for Laser and Plasma Physics of the University of Düsseldorf. The detector was placed approx. 1 m behind the target. On the anode wires (blue and purple), see Fig. 2, signals with amplitudes of 1.2 V indicate that there is strong saturation of the chamber and the amplifiers. This is the reason why the pulse width strongly exeeds the value of about 100 ns expected from the maximum drift time of electrons in the active detector volume. The signal seen on a pad of the ionization chamber anode (green) is weak; its shape indicates cross-talk between the proportional and ionization chamber stages. In a modified version of the chamber this effect will be reduced by inserting an additional shielding plane between the two stages.

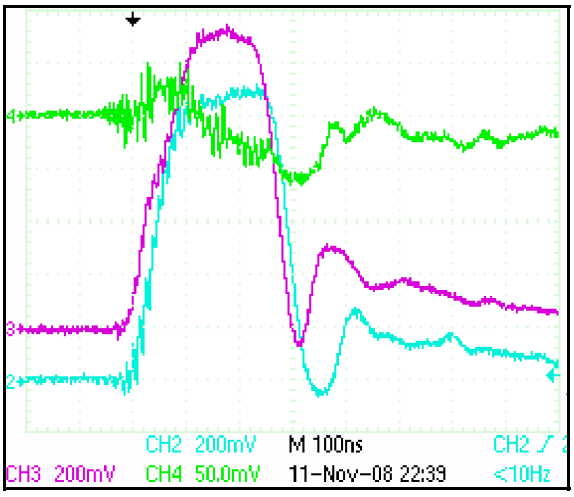

Fig. 2: Chamber signals measured near the laser target. Blue and purple: signals from anode wires, green: pad of the ionization chamber

[1] IKP, FZ-Jülich
[2] Hochschule Merseburg
[3] FH Aachen
[4] Universität Düsseldorf
[5] IFJ Pan, Krakow, Poland
[6] Universität Köln
[7] JINR Dubna
[8] RWTH Aachen

Supported by the FFE program of FZ-Juelich

2 COSY Operation and Developments

HESR stochastic momentum cooling is envisaged in the whole kinetic energy range covering *0.8 GeV* up to *14 GeV*. Filter momentum cooling will be applied above *3 GeV* and provides antiproton beams with nearly the requested momentum resolution in the High Resolution (HR) Mode [1]. Due to mixing from pickup to kicker limitations of the Filter method stochastic momentum cooling will be extended down to *0.8 GeV* by using the Time of flight (TOF) cooling method [2]. Filter cooling model predictions have been successfully tested with a COSY beam [1]. The model was enlarged now to include also TOF cooling. In this method COSY's notch filter is replaced by a *90 degree* broadband phase shifter so that mixing from pickup to kicker can be used to discriminate between particles of different momentum deviations. The model predictions show that the method can be tested in COSY with the present location of pickup and kicker devices.

The simulation was done for a *3.2 GeV/c* beam with $N = 1 \cdot 10^{10}$ protons and a hydrogen target of thickness $N_T = 2 \cdot 10^{15}\, atoms/cm^2$. The complete *(1 - 3) GHz* system has been applied for TOF cooling with an optimal additional delay $\Delta T_D = -244\, ps$ in the cooling path and a gain of *81 dB*. The frequency slip factor of COSY's lattice is $\eta = -0.12$. Figure 1 shows the time development of beam distributions during cooling and the action of the internal target. It is clearly visible that the strong mean energy loss induced by the target can not be compensated with cooling alone.

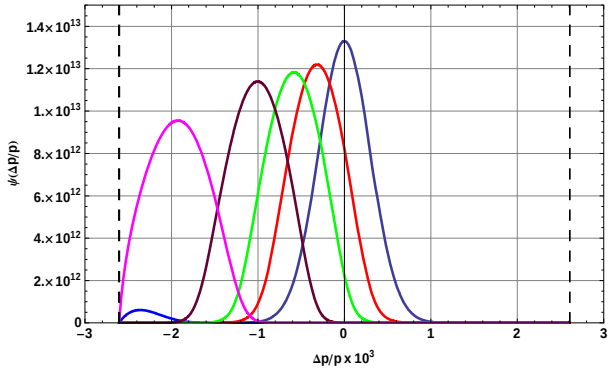

Fig. 1: Beam distributions during cooling and the action of an internal target at *t = 0* (black), *50 s* (red), *100 s* (green), *200 s* (brown), *600 s* (magenta), *2000 s* (blue). The initial relative momentum spread is $\delta_{rms} = 3 \cdot 10^{-4}$. Particles losses occur when the distribution reaches the acceptance limit $\delta_{rms} = \pm 2.6 \cdot 10^{-3}$ (dashed lines).

Severe beam losses start at about 400 s as shown in figure 2. If cooling is switched of particle losses already start at *200 s* and the beam is completely lost already after *500 s*. As has been demonstrated recently at COSY the beam center can be efficiently stabilized in a barrier bucket [3]. In this case the remaining heating of the momentum spread due to the internal target can be compensated with TOF cooling as is visible in figure 3. No particle losses occur.

For optimal cooling the open loop system transfer function S_{21} of the TOF cooling system including the beam response was optimized at each harmonic in the cooling bandwidth by an appropriate delay and gain setting (Figure 4).

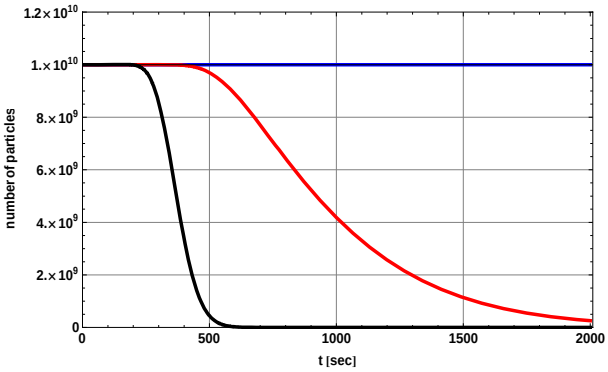

Fig. 2: Particle number versus time. Beam losses start after *200 s* (black cure) if the target is ON and cooling is switched OFF. Losses still occur with cooling ON (red curve). Losses are avoided if the mean energy loss is, additionally to cooling, compensated (blue curve).

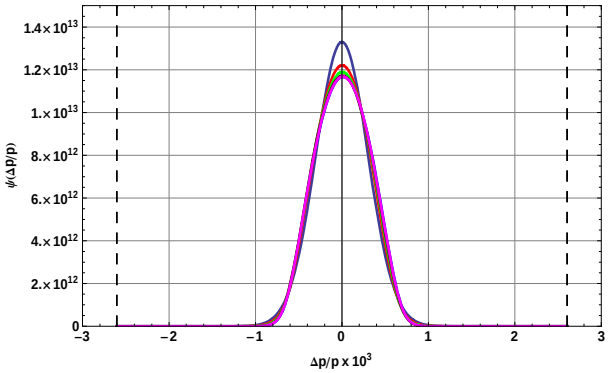

Fig. 3: Beam distributions during cooling and the action of an internal target. TOF cooling can keep the momentum resolution constant if the mean energy loss is compensated by a barrier bucket cavity.

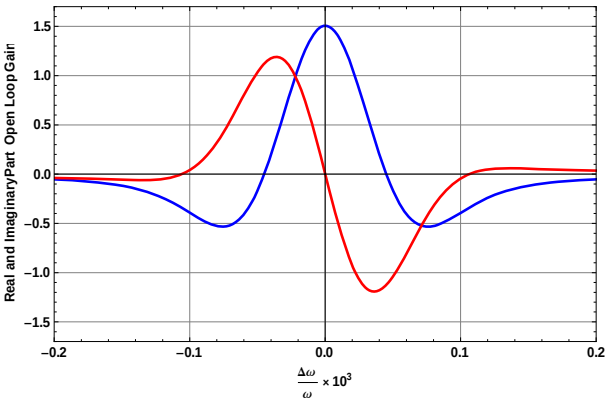

Fig. 4: Real (blue) and imaginary (red) part of S_{21} including the beam response at harmonic *1000* with an optimal delay and gain setting for the TOF cooling system. At the center of the harmonic the imaginary part shows the required change in sign for cooling.

References:

[1] H. Stockhorst et al., EPAC 2008, Genova

[2] W. Kells, "Filterless Fast Momentum Cooling", Proc. of the 11th Int. Conf. on High-Energy Accelerators, Geneva, Switzerland, July 7-11, 1980, p. 777

[3] R. Stassen et al., this annual report

Hardware and Software Changes of the COSY Vacuum Control

F. Jordan[1], W.Schmitz[1], B. Dahmen[2], H. Zens[2,] N Bongers[2]

The COSY vacuum control has been changed and extended permanently in the last years due to the requirements of the experiments ANKE and WASA. Operating the system with minor failure was still possible despite the increased specifications and regardless the fact that the programmable logic controllers reached slowly their limit. The main control COVAM2 (S5) was replaced for this reason with COVAM3 (S7). Single functions were intended to be transferred from the subordinated control COVAK2 (S5) to COVAM3 (S7). The S5-control was fully loaded because of the WASA installation. The computing power finally reached the borderline in its performance. The situation got worse because of the ANKE reorganization.

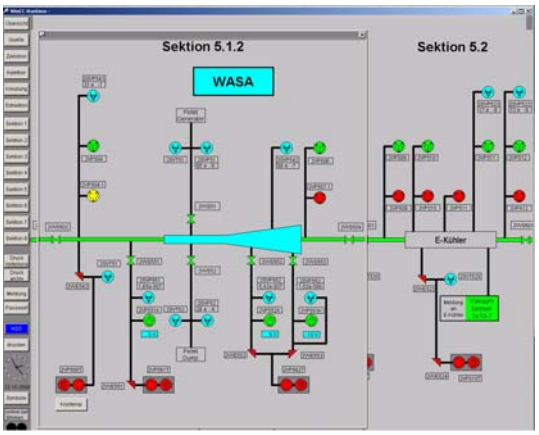

Fig. 1: WASA operation

The complete exchange of the S5 control against a S7 control offered the advantage of an extended functionality, higher computing power, bigger I/O address space, secure exchange parts and current development environment (SIMATIC-Manager, Step7 Version 5.3).

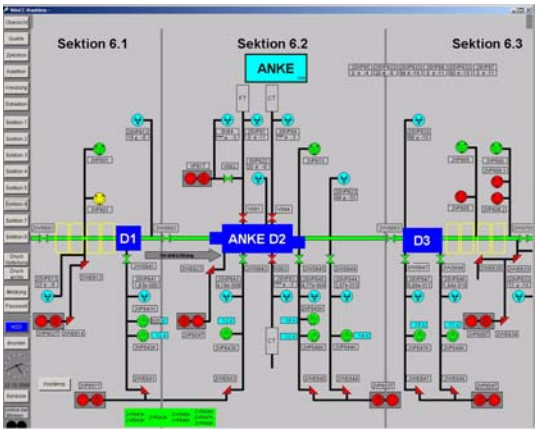

Fig. 2: ANKE operation

The modification of the PLC and the changes in the software structure were carried out step by step during several maintenance times so that the current operation was not interrupted.
As the first step the functionality of the old PLC was taken over by the new one. Because of the special variety of the ANKE experiment this control range had to be removed completely out of the old COVAK2 control.
The functionality could be covered easily by the new COVAM3. In addition larger changes of the wiring were necessary in the I/O range. The same method could successfully be accomplished at the WASA experiment with similar effort. The removal of the software components of the COVAK2 control led to essential shorter cycle times and much more reliable operating of the relieved control.

During the phase of rearrangement the visual display system based on SIEMENS/WinCC was adapted to the new configuration. These changes additionally enhanced the convenience.

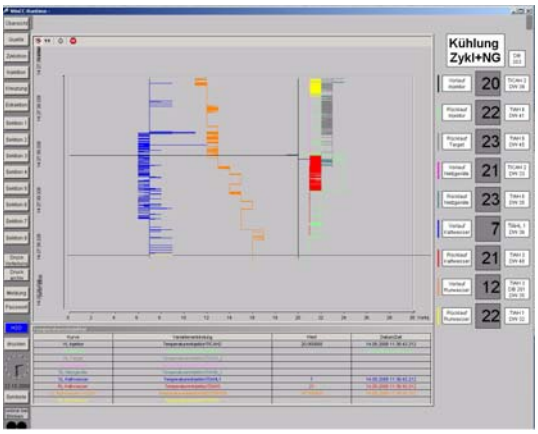

Fig. 3: Logbook water temperature

The COSY water cooling monitoring is integrated in the vacuum control. Some temperatures were not only presented but also archived. The data achievement of the temperature archive was extended to the duration of two months. The number of the recording points was doubled.

[1] Zentralabteilung Technologie
[2] Institut für Kernphysik

Improvements of the COSY RF-System

R. Stassen, M. Böhnke, F.J. Etzkorn

The COSY broadband RF-system is running now since 2000 [1] without any longer faults. It is one of the most reliable sub-systems in COSY. Nevertheless, the known problems with the magnetic septum last year caused a greater failure in the RF-system. Till this time the RF-power amplifier was connected to the same cooling water system as the magnetic septum. During the repair of the septum, the cooling water was switched on and off and caused always software resets by the SPS of the power amplifier. The consequence was a damage of one air blower.

Meanwhile the cooling water circuits were separated. Additionally a new SPS program was written which allows dedicated fault reports and more operation modes. The main focus was a reliable control of the whole power amplifier during startup and after fault detection. Error reasons are now stored and visible in clear text. The heating system has now a 2-stage mode to preserve the tubes and each component can be controlled individually for maintenance. The monitoring of anode voltage and current are included.

A gain decrease of one tube has been found. Meanwhile most of the available tubes reached the nominal lifetime (table 1). Thus two new tubes were ordered.

Table 1: available tubes TH120 at COSY

Tube	Operation / h	Remarks
S3	18000	Active in new cavity
10201	65000	Active in new cavity
P7	61700	Old amplifier for HESR tests
Q3	64200	Old amplifier for HESR tests
S2	21300	available
10202	40000	Limited available
U01	25500	
S1	14300	Short-circuited when cold
10401	1300	Def heating
10501	37800	Low standby current, sort out
T2	36700	Low standby current, sort out
W3		heater defect

Barrier- Bucket operation

The barrier-bucket operation has become a routinely used tool in COSY [2], although the installation of the HESR Barrier Bucket prototype cavity at COSY was nominally for HESR-relevant tests only. Detailed results are described in one highlight article of this annual report. A new central clock is installed which allows a synchronization of the COSY RF and the arbitrary-function generator used to feed the barrier bucket cavity. The signal synthesis to generate a periodic single sine signal at the acceleration gap is now implemented in a MATLAB routine.

A simple filter is used to test the capability of the signal synthesis under MATLAB. Figure 1 shows the starting single sine signal from the arbitrary-waveform generator and the corresponding response after the filter. 10 harmonics are used in the first version to generate the single-sine signal which has a 5 time shorter period than the revolution time (corresponding to the fundamental frequency at COSY).

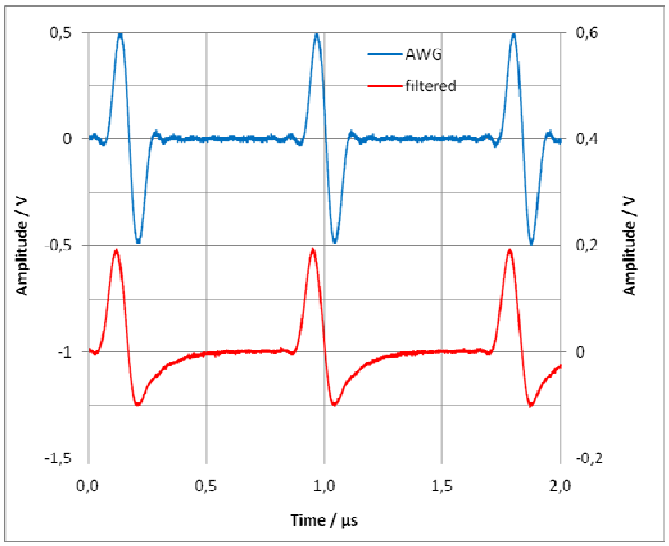

Fig. 1: periodic single-sine function from the start file of the arbitrary waveform generator (AWG) (blue) and the corresponding result after a test filter (red).

The MATLAB programm measured automatically the filtered signal from the scope, determins amplitude and phase of the 10 harmonics, calculates a new signal and sends the modified signal to the arbitrary waveform generator.

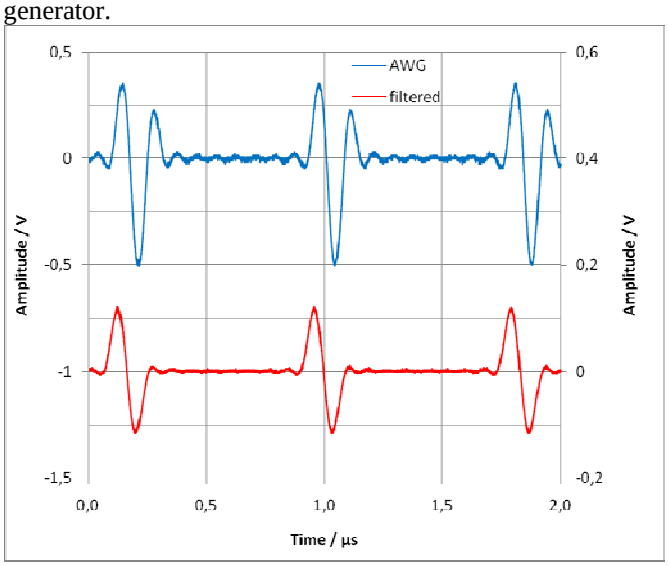

Fig. 2: Signals using Fourier synthesis. Red: approximation of the desired single-sine signal after filter; blue: arbitrary waveform generator signal generated by signal synthesis.

One iterations step is already sufficient to get a good approximation of the desired single-sine function (Fig. 2).

References:

[1] A. Schnase et al., Experience with a VitroPerm cavity in COSY, IKP Annual Report 2000

[2] R. Stassen, The HESR RF-system and tests in COSY, EPAC2008, Genoa, Italy

Upgrades and Maintenance of COSY Power Converters

K. Kruck, M. Retzlaff, R. Hecker, J. Schmitz, W. Classen. A. Richert, D. Ruhrig

Because of damages in the power supplies of the COSY-Vacuum pumps the quality of our 400V grid for the COSY building 7.3 was examined. To ensure a quality of the grid within its specifications a filter was installed to reduce the total harmonic distortion. A second filter for a compensation of the complex power was also set up at the machine transformer. The measurements and installation works have been done by a specialized external company.

New power converters were installed for the 26 IBL - steerer magnets. The old power converters manufactured by the company Waldorf contained special electronic parts which are no longer available since the company was closed several years ago. The new power converters delivered from Danfysik are set up in five racks, four racks with six power amplifiers and one with two amplifiers. Each rack has its own Profibus - interface for a connection to the control system.
The new Danfysik - system is fully compatible to the existing quadrupole magnet power converters of the ion source beamline and thus optimizes the storage of spare parts. For tests and repair one rack with six power amplifiers is available.

Four new power converters for the ring quadrupole magnets were ordered from the company Bruker. These power converters, which have a total output power of 280V and 600A, are built up with four IGBT H - Bridges in parallel. Each has to deliver 150A. A testing facility for the IGBT amplifiers has been developed and built up by ourselves. This testing equipment can simulate a fully bipolar operation at high performance resistors up to 4kW.

The original DCCT for the main electron cooler power converter of the company Földi delivered incorrect current values from time to time. It was impossible to repair this failure. Therefore a new DCCT from Danfysik had to be installed. The integration of the new DCCT also required changing the parameters (new resistors calculated) of the analogue current regulation module.

The ten years old field correction power converters for the electron cooler field correction became sensitive for failures and were not easy to repair. Moreover, some spare parts became rare or even no longer available. New switching power converters SM70-AR-24 from Delta Elektronika now replace the old versions. Each power converter has its own Ethernet interface to establish a connection to the control system.

Prototyping and Characterizing the Jülich Superconducting Triple Spoke Resonator within the HIPPI Project

W. Behr[1], H. Glückler[1], W. Günther, R. Maier, M. Pap[1], H. Singer, H. Soltner[1], R. Stassen, R. Tölle, E. Zaplatin

Europe is paving its way towards next generation secondary particle experiments e.g. with neutrino beams. In the beginning of the accelerator chain for producing these particles powerful pulsed proton injectors are needed. The sub-project HIPPI (High Intensity Pulsed Proton Injector) of the FP6 project CARE (Coordinated Accelerator Research in Europe) evaluates different approaches for such injectors. We proposed to use superconducting triple spoke resonators as a core element of a dedicated pulsed LINAC. During the HIPPI project the resonator was developed, manufactured and tested in Jülich for $\beta = 0.48$.

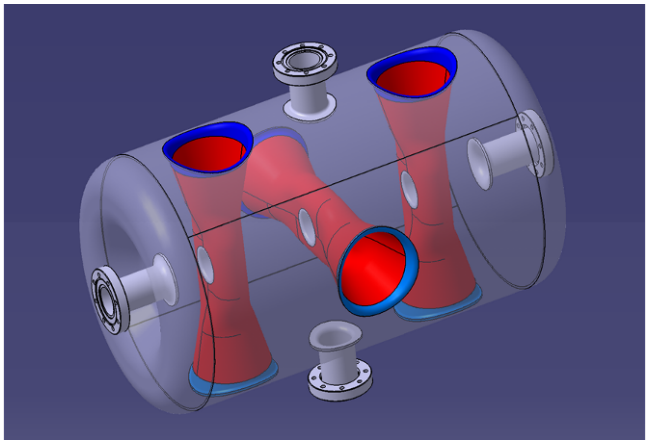

Fig. 1: Jülich HIPPI triple-spoke resonator. Beam ports (left and right) and ports for coupler and vacuum (top and bottom) are shown. In this picture the stiffening structure is omitted.

A very important parameter for pulsed operation of superconducting cavities is the Lorentz force detuning. It depends mainly on the stiffness of the cavity, which in turn can be influenced by using a clever geometry and a sufficient wall thickness. However, during operation with particle beams power is deposited on the inner surfaces of the cavity and has to be quickly distributed to the surrounding liquid helium. This requirement limits the acceptable wall thickness. A nominal wall thickness of 4 mm was adopted. The design is summarized in [1].

Manufacturing experience gained before with the 760 MHz ESS triple spoke resonator gave valuable hints how to efficiently build the 352 MHz HIPPI resonator. However, all electron beam welding parameters had to be developed from scratch as handling a sheet thickness of 4 mm niobium in superconducting cavity production was a pioneering job. RRR measurements revealed that the RRR value of the seam exceeded the RRR value of the bulk material.

Cleaning the inner surfaces of the cavity was achieved in close collaboration with our colleagues in Saclay (BCP) and Orsay (HPR) who supported us with equipment, know-how, and great personal commitment [2].

The frequency sensitivity was measured as -31.86 Hz/mbar (calculated value -21.43 Hz/mbar). The Lorentz force coefficient K_L was measured as -5.5 Hz/(MV/m)^2 (calculated value -4.1 Hz/(MV/m)^2). This value usually is strongly dependent on the mounting situation of the cavity inside the cryostat. For this specific cavity there is only little dependence on the mounting situation. Values for the two extreme cases (beam ports free / beam ports fixed) are between 3 and 5 Hz/(MV/m)^2. For more details see [3].

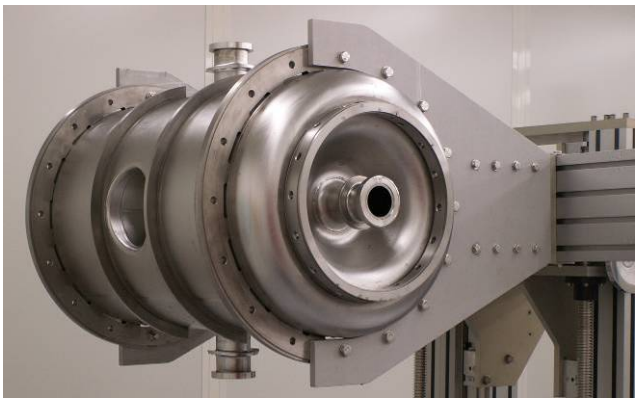

Fig. 2: Jülich HIPPI triple-spoke resonator mounted on the manipulator in the clean room at IPN, Orsay. Main stiffening rings are attached.

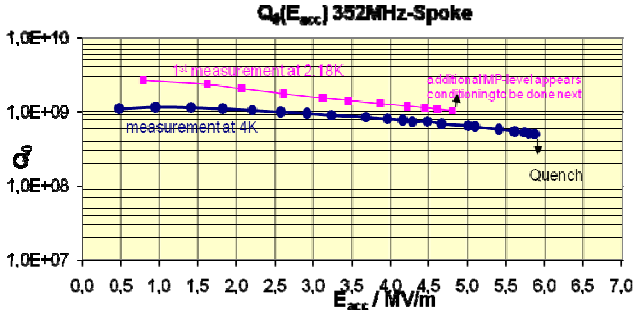

Fig. 3: $Q_0(E_{acc})$ diagram for the Jülich HIPPI triple spoke resonator. The dark blue line was measured at 4 K. Nearly 6 MV/m could be reached before quench. Data at 2K (pink line) terminate at about 5 MV/m where additional multi-pacting levels occurred.

The final report describing the different HIPPI approaches to pulsed injectors is expected to be available in Feb. 2009. Further performance checks are now beyond the scope of the HIPPI project. Now the resonator is in use at IPN Orsay to further examine its properties and push its performance.

References:

[1] CARE-Note-2006-001-HIPPI: Design of a Triple-Spoke Cavity for 352 MHz and β=0.48. E. Zaplatin, R. Maier, M. Pap, R. Toelle. http://www-dapnia.cea.fr/Phocea/file.php?class=std&&file=Doc/Care/note-2006-001-HIPPI.pdf

[2] CARE-Report-08-015-HIPPI: Construction Status of Juelich Triple Spoke Resonator, H. Glückler, W. Günther, M. Pap, R. Tölle, E. Zaplatin, G. Olry, G. Michel, S. Bousson, P. Szott, F. Eozenou, Y. Gasser. http://irfu.cea.fr/Phocea/file.php?class=std&&file=Doc/Care/care-report-08-015.pdf

[3] Talk at HIPPI08: E. Zaplatin, fzj hippi tsr. http://indico.cern.ch/getFile.py/access?contribId=18&sessionId=11&resId=0&materialId=slides&confId=39839

[1] Forschungszentrum Jülich, Zentralabteilung Technologie

Activities at the Injector Cyclotron of COSY/ Jülich

R. Brings, R. Gebel, O. Felden, A. Kieven, N. Rotert

Injector operation

In 2008 the injector cyclotron did provide beams for 7303 hours for the accelerator facility COSY. In December 2008 the injector passed 122474 hours of operation since it started delivering beams as COSY injector in 1989. The time distribution over the years is shown in fig. 1.

The operation of the cyclotron was interrupted for around 156 hours in 2008 due to several failures. The distribution of the failures exceeding 2 hours is depicted in fig. 2. The most common reasons for unavailability of the injector for times were the rf system and power failures. Intermediate unavailability, exceeding the start-up time of the main rf system, had been its originate in the rf system with varying reasons. Vacuum leaks at one beam probe and the septum needed additional attention. The operation of the ion sources showed no major failures in 2008.

Besides serving COSY as injector the cyclotron was successful in providing 7 irradiations with protons at the internal target station for the Institute for Nuclear Chemistry (INB-4). For the Frauenhofer Gesellschaft 6 irradiations were served. For a first test organic liquid crystals had been irradiated at the external target station with 1 µA protons for a collaboration from the FU Berlin and the TU Darmstadt. A new installation of an irradiation chamber from the INB-4, an adopted copy of a target station from the former INB-4 cyclotron, is foreseen to provide isotope production to the limits of available beams at the injector cyclotron. The new target is shown in fig. 3.

In addition two different set-ups of polarimeter components taken from the former COSY ring polarimeter have been prepared and calibrated.

Replacement of cyclotron components

The cyclotron is in use since the mid 60s of the last century. Most of the systems were refurbished between 1980 and 1989. In 2008 several amplifiers and gears of the central tuning elements have been replaced. Refurbished cryopumps have been qualified and have been prepared to replace old systems in order to match them to the updated control system. Sparking was the reason to exchange the electrostatic septum. By optimizing the replacement procedure only one shift has been lost for COSY operation. Identical spare septa, stored under vacuum conditions, are essential for high availability and are now available.

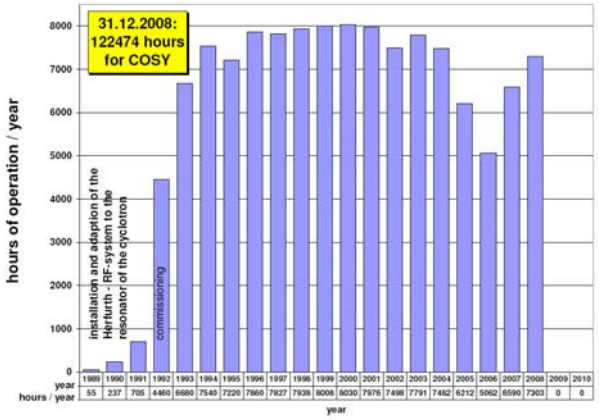

Fig. 1: Operation of the Cyclotron as the injector for COSY. At the end of 2008 the total operating time of the cyclotron rf for COSY reached 122474 hours.

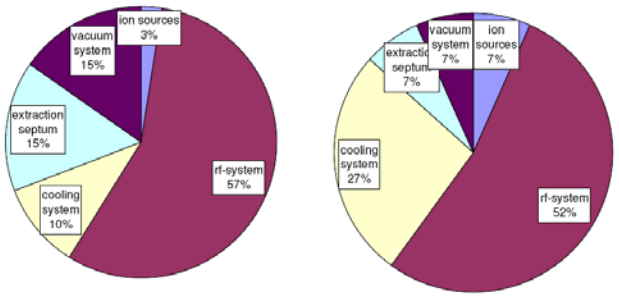

Fig. 2: The failure distribution of 15 events in 2007. The duration of all events summed up to about 156 hours.

Optimization of operations

After installation of an improved diagnostics in the power distribution of the research centre the technical services reported peak power consumption exceeding the short time limits for the transformer stations. In cooperation with the power supply group the source of that behavior was finally found after an extended search procedure. After increasing the limits defective transmission filters and feed-throughs were located and exchanged. No failures since replacement of these parts have been observed. The number of trips during operation and crosstalk to other subsystems of the injector has been greatly reduced.

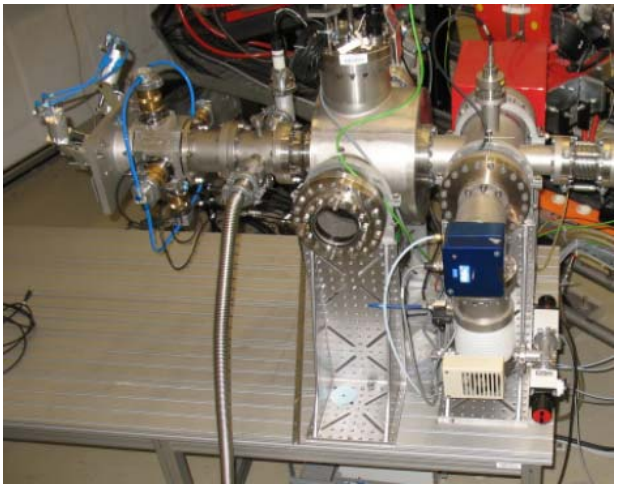

Fig. 3: The new irradiation target station from INB-4.

H.Borsch, O.Felden, J.Göbbels

In 2008 about 150 Persons (with only small fluctuations) of the IKP have been under radiation protection survey. Each of these persons is equipped with an official film badge (MPA-Gleitschattenfilmdosimeter [1]) and a Pencil-dosimeter. Around 110 of these and about 10 external experimentalists from universities (having their own Film-badges), who have access to the inner hall during operation of COSY have to wear an additional dosimeter, sensitive only to neutrons (MPA-Kernspurätzdosimeter [1]). During the last years a small number of neutron badges always showed doses above the detection limit up to 1.5 mSv. In spite of looking at the other personal dosimeters (film badge and pencil-dosimeter), these measures from the MPA (Material-Prüfungsamt) which is responsible for the analysis of the badges, could not be reconstructed. [2,3,4]

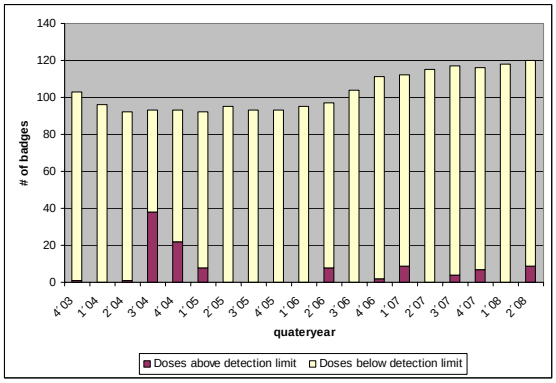

Fig. 1: Number of neutron badges showing doses above and below the detection limit

Beside this “passive” survey with film-badges there is an active neutron radiation survey system installed at COSY.
In order to allow access to the inner area of the COSY accelerator during its operation the local dose in the inner hall is permanently monitored for each individual of the group of persons having the right to access this area. The maximum accumulated dose must not exceed 400 µSv per week during the presence of those persons in the inner part of the COSY hall. This dose is being measured with eight neutron monitors installed at the access doors to the accelerator ring and one neutron monitor installed at the roof shielding of the COSY ring. Figure 2 gives an overview of the position of the different neutron-monitors in the inner hall. The first neutron monitor (NM1) is located at the access door under the staircase that leads to the inner hall, NM2 at the experiment WASA, NM3 at the electron-cooler, NM4 at the experiment ANKE, NM5 at the beam extraction, NM6 at the beam injection and HF Cavity, NM7 and NM8 located around EDDA.
Even looking at the working modes of COSY and the values from the 48 neutron monitors installed around COSY and inside the inner hall or the measures taken for everybody having access to the inner hall these neutron-measurements could not be reconstructed. Due to the fact that only a small number of this type of neutron badges is used the MPA decided in close connection to the IKP as well as to the FZJ central radiation protection service to change to CR-39-neutron badges [1,5] from the PSI, Switzerland which are in use at CERN, PSI e.g. as well as at DESY.

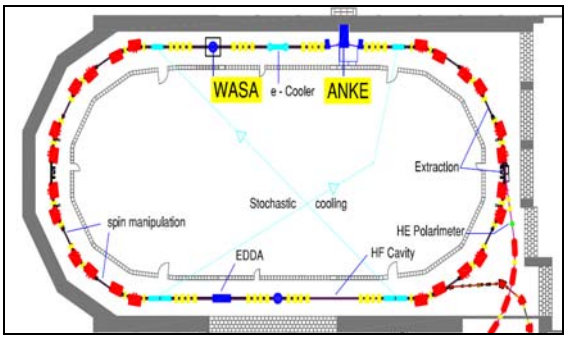

Fig. 2: COSY and experimental Setups

Before entering the inner hall of COSY the experimentalists are asked to inform themselves about the actual dose-levels inside the hall to avoid dangers due to radioactivity.
Therefore the Personal Safety System (PSA) gives in one significant picture information about the actual doses from each neutron-monitor as well as the maximum dose rate measured during the last hour. This information is available in the COSY Control room as well as at the entrance to the hall.

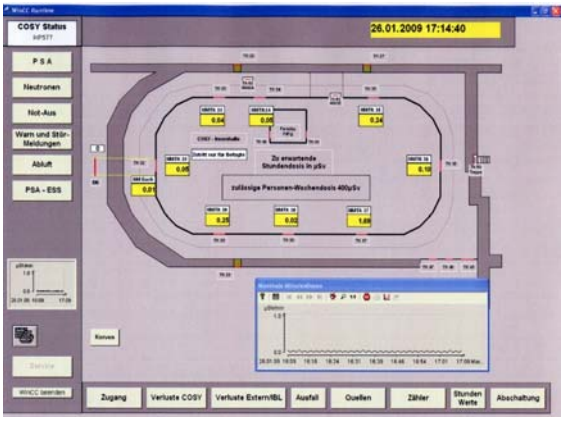

Fig. 3: Radiation protection survey of the inner hall of COSY

Another change in terms of radiation survey will be obtained in the next years because of new measures asked for by the radiation protection law [6]. The actual used pencil-dosimeters don’t cover these measures and therefore need to be replaced.

Fig. 4: Dosimeter Reading System test bench

From point of view of the central radiation protection service the favorite type will be an electronic device RADOS RAD62SE with directly showing doses as well as dose rates and giving alerts.
To get experience on the handling as well as on the functionality we installed a test bench with an electronic reading system and a database. Because of uncertainties if these electronic devices will do work proper in pulsed radiation fields as can be find at accelerators some more investigations covering this questionnaires are still ongoing.

References:

[1] www.mpa-nrw.de
[2] Radiation Protection, IKP Annual report 2003
[3] Radiation protection, IKP Annual report 2004
[4] Radiation Protection, IKP Annual report 2005
[5] Progress Report of the CR-39 Neutron Personal Monitoring Service at PSI, Rad.Prot.Dosimetry (2006), 1
[6] Strahlenschutzverordnung vom 20.07.2001

3 Theoretical Physics

3.1 Hadron Physics

Infrared regularization with vector mesons and baryons

P. C. Bruns (Bonn) and Ulf-G. Meißner (Bonn & FZJ)

We extend the method of infrared regularization to spin-1 fields coupled to baryons. As an application, we discuss the axial form factor of the nucleon [1].

References:

[1] P. C. Bruns and U.-G. Meißner, Eur. Phys. J. C **58** (2008) 407 [arXiv:0808.3174 [hep-ph]].

Electromagnetic corrections in $\eta \to 3\pi$ decays

C. Ditsche (Bonn), B. Kubis (Bonn) and Ulf-G. Meißner (Bonn & FZJ)

We re-evaluate the electromagnetic corrections to $\eta \to 3\pi$ decays at next-to-leading order in the chiral expansion [1], arguing that effects of order $e^2(m_u - m_d)$ disregarded so far are not negligible compared to other contributions of order e^2 times a light quark mass. Despite the appearance of the Coulomb pole in $\eta \to \pi^+\pi^-\pi^0$ and cusps in $\eta \to 3\pi^0$, the overall corrections remain small.

References:

[1] C. Ditsche, B. Kubis and U.-G. Meißner, Eur. Phys. J. C (2009) in print, [arXiv:0812.0344 [hep-ph]].

Resonance properties from the finite-volume energy spectrum

V. Bernard (Strasbourg), M. Lage (Bonn), Ulf-G. Meißner (Bonn & FZJ) and A. Rusetsky (Bonn)

A new method based on the concept of probability distribution is proposed to analyze the finite volume energy spectrum in lattice QCD [1]. Using synthetic lattice data, we demonstrate that for the channel with quantum numbers of the Δ-resonance a clear resonance structure emerges in such an analysis. Consequently, measuring the volume-dependence of the energy levels in lattice QCD will allow to determine the mass and the width of the Δ with reasonable accuracy.

References:

[1] V. Bernard, M. Lage, U.-G. Meißner and A. Rusetsky, JHEP **0808** (2008) 024 [arXiv:0806.4495 [hep-lat]].

The Δ-resonance in a finite volume

V. Bernard (Strasbourg), M. Lage (Bonn), Ulf-G. Meißner (Bonn & FZJ) and A. Rusetsky (Bonn)

We study the extraction of Δ-resonance parameters from lattice data for small quark masses, corresponding to the case of an unstable Δ. To this end, we calculate the spectrum of the correlator of two Δ-fields in a finite Euclidian box up-to-and-including $O(\epsilon^3)$ in the small scale expansion using infrared regularization. On the basis of our numerical study, we argue that the extraction of the parameters of the Δ-resonance (in particular, of the mass and the pion-nucleon-delta coupling constant) from the measured volume dependence of the lowest energy levels should be feasible [1, 2].

References:

[1] V. Bernard, M. Lage, A. Rusetsky and U.-G. Meißner, Eur. Phys. J. A **35** (2008) 281.
[2] V. Bernard, U.-G. Meißner and A. Rusetsky, Nucl. Phys. B **788** (2008) 1 [arXiv:hep-lat/0702012].

Near threshold $p\bar{p}$ enhancement in the $J/\psi \to \omega p\bar{p}$ decay

J. Haidenbauer, U.-G. Meißner, A. Sibirtsev (Bonn)

The near-threshold behavior of the $p\bar{p}$ invariant mass spectrum from the $J/\psi \to \omega p\bar{p}$ decay reported recently by the BES Collaboration is analyzed. Our study demonstrates that there is indeed a clear enhancement in the $p\bar{p}$ invariant mass spectrum near threshold as compared to the phase-space behavior. Moreover, this enhancement is nicely reproduced by the final state interaction in the relevant $(^{11}S_0)$ $p\bar{p}$ partial wave as given by the Jülich nucleon–antinucleon model. Therefore, contrary to the statement by the BES Collaboration, their new data on $J/\psi \to \omega p\bar{p}$ decay in fact strongly support the FSI interpretation of the $p\bar{p}$ enhancement, seen also in other decay reactions. The results are published in Ref. [1].

References:

[1] J. Haidenbauer, U.-G. Meißner and A. Sibirtsev, Phys. Lett. B **666**, 352 (2008) [arXiv:0804.1469 [hep-ph]].

Charmed meson rescattering in the reaction $\bar{p}d \to \bar{D}DN$

J. Haidenbauer, G. Krein (São Paulo), U.-G. Meißner, A. Sibirtsev (Bonn)

We examine the possibility to extract information about the DN and $\bar{D}N$ interactions from the $\bar{p}d \to D^0 D^- p$ reaction. We utilize the notion that the open-charm mesons are first produced in the annihilation of the antiproton on one nucleon in the deuteron and subsequently rescatter on the other (the spectator) nucleon. The latter process is then exploited for investigating the DN and $\bar{D}N$ interactions. We study different methods for isolating the contributions from the $D^0 p$ and $D^- p$ rescattering terms. The results are published in Ref. [1].

References:

[1] J. Haidenbauer, G. Krein, U.-G. Meißner and A. Sibirtsev, Eur. Phys. J. A **37**, 55 (2008) [arXiv:0803.3752 [hep-ph]].

Pion-nucleon charge-exchange amplitudes above 2 GeV

F. Huang, A. Sibirtsev (Bonn), S. Krewald, C. Hanhart, J. Haidenbauer, U.-G. Meißner

The amplitudes for the pion-nucleon charge exchange reaction of the Karlsruhe-Helsinki and the George-Washington-University partial wave analyses are compared with those of a Regge-cut model with the aim to explore the possibility to provide high energy constraints for theoretical baryon resonance analyses in the energy region above 2 GeV. The results are available as e-Print [1].

References:

[1] F. Huang, A. Sibirtsev, S. Krewald, C. Hanhart, J. Haidenbauer, U.-G. Meißner, arXiv:0810.2680 [hep-ph].

Backward pion photoproduction

A. Sibirtsev (Bonn), J. Haidenbauer, F. Huang, S. Krewald, U.-G. Meißner

We performed a systematic analysis of backward pion photoproduction for the reactions $\gamma p \to \pi^0 p$ and $\gamma p \to \pi^+ n$. Regge phenomenology is applied at invariant collision energies above 3 GeV in order to fix the reaction amplitude. A comparision with older data on π^0- and π^+ photoproduction at ϑ=180° indicates that the high-energy limit as given by the Regge calculation could be reached possibly at energies of around $\sqrt{s} \simeq 3$ GeV. In the energy region of $\sqrt{s} \leq 2.5$ GeV, covered by the new measurements of $\gamma p \to \pi^0 p$ differential cross sections at large angles at ELSA, JLab, and LEPS, we see no clear signal for a convergence towards the Regge results. The baryon trajectories obtained in our analysis are in good agreement with those given by the spectrum of excited baryons.

Comment on "Once more about the $K\bar{K}$ molecule approach to the light scalars"

Yu. S. Kalashnikova (ITEP), A. E. Kudryavtsev (ITEP), A. V. Nefediev (ITEP), J. Haidenbauer, C. Hanhart

In this work we comment on the criticism raised recently by Achasov and Kiselev [Phys. Rev. D 76, 077501 (2007)] on our work on the radiative decays $\phi \to \gamma a_0/f_0$ [Eur. Phys. J. A 24, 437 (2005)]. Specifically, we demonstrate that their criticism relies on results that violate gauge–invariance and is therefore invalid. The results are are published in Ref. [1].

References:

[1] Yu. S. Kalashnikova, A. E. Kudryavtsev, A. V. Nefediev, J. Haidenbauer and C. Hanhart, Phys. Rev. D **78**, 058501 (2008) [arXiv:0711.2902 [hep-ph]].

Simultaneous photoproduction of π^0 and η mesons on the proton.

J. Ajaka, M. Döring et al. [GRAAL]

The analysis of the $\gamma p \to \eta\pi^0 p$ reaction has been performed [1] using data from GRAAL experiment. The total and differential cross sections and the beam asymmetry have been obtained from threshold up to 1.5 GeV of beam energy. The two resonances $S_{11}(1535)$ and $\Delta(1700)$ could be excited in this reaction in the intermediate states. The results are used to test predictions based on the assumption that both resonances are dynamically generated from the meson-baryon interaction provided by chiral Lagrangians.

References:

[1] J. Ajaka *et al.*, Phys. Rev. Lett. **100**, 052003 (2008).

The role of the $N^*(1535)$ resonance and the $\pi^- p \to KY$ amplitudes in the OZI forbidden $\pi N \to \phi N$ reaction [1]

M. Döring, E. Oset (Valencia) and B.S. Zou (Peking)

We study the $\pi N \to \phi N$ reaction close to the ϕN threshold within the chiral unitary approach, by combining the $\pi^- p \to K^+\Sigma^-$, $\pi^- p \to K^0\Sigma^0$ and $\pi^- p \to K^0\Lambda$ amplitudes with the coupling of the ϕ to the K components of the final states of these reactions via quantum loops. We obtain a good agreement with experiment when the dominant $\pi^- p \to K^0\Lambda$ amplitude is constrained with its experimental cross section. We also evaluate the coupling of the $N^*(1535)$ to ϕN and find a moderate coupling as a consequence of partial cancellation of the large KY components of the $N^*(1535)$. We also show that the $N^*(1535)$ pole approximation is too small to reproduce the measured cross section for the $\pi^- N \to \phi N$ reaction.

References:

[1] M. Döring, E. Oset and B. S. Zou, Phys. Rev. C **78**, 025207 (2008) [arXiv:0805.1799 [nucl-th]].

Transition form factors of the $N^*(1535)$ as a dynamically generated resonance [1]

D. Jido (Kyoto), M. Döring, E. Oset (Valencia)

We discuss how electromagnetic properties provide useful tests of the nature of resonances, and we study these properties for the $N^*(1535)$ which appears dynamically generated from the strong interaction of mesons and baryons. Within this coupled channel chiral unitary approach, we evaluate the $A_{1/2}$ and $S_{1/2}$ helicity amplitudes as a function of Q^2 for the electromagnetic $N^*(1535) \to \gamma^* N$ transition. Within the same formalism we evaluate the cross section for the reactions $\gamma N \to \eta N$. We find a fair agreement for the absolute values of the transition amplitudes, as well as for the Q^2 dependence of the amplitudes, within theoretical and experimental uncertainties discussed in the paper. The ratios obtained between the $S_{1/2}$ and $A_{1/2}$ for the neutron or proton states of the $N^*(1535)$ are in qualitative agreement with experiment and there is agreement on the signs. The same occurs for the ratio of cross sections for the η photoproduction on neutron and proton targets in the vicinity of the $N^*(1535)$ energy. The global results support the idea of this resonance as being dynamically generated, hence, largely built up from meson baryon components. However, the details of the model indicate that an admixture with a genuine quark state is also demanded that could help obtain a better agreement with experimental data.

References:

[1] D. Jido, M. Döring and E. Oset, Phys. Rev. C **77**, 065207 (2008) [arXiv:0712.0038 [nucl-th]].

Analyzing the Effects of Neutron Polarizabilities in Elastic Compton Scattering off ^3He

D. Shukla (Ohio U.), A. Nogga (Jülich, Forschungszentrum), D.R. Phillips (Ohio U.)

Motivated by the fact that a polarized ^3He nucleus behaves as an 'effective' neutron target, we examine manifestations of neutron electromagnetic polarizabilities in elastic Compton scattering from the Helium-3 nucleus. We calculate both unpolarized and double-polarization observables using chiral perturbation theory to next-to-leading order ($\mathcal{O}(e^2Q)$) at energies, $\omega \propto m_\pi$, where m_π is the pion mass. Our results show that the unpolarized differential cross section can be used to measure neutron electric and magnetic polarizabilities, while two double-polarization observables are sensitive to different linear combinations of the four neutron spin polarizabilities. The results are published in [1].

References:

[1] D. Shukla, A. Nogga and D. R. Phillips, arXiv:0812.0138 [nucl-th].

Hadronic-loop induced mass shifts in scalar heavy–light mesons

F.-K. Guo, S. Krewald, Ulf-G. Meißner (Bonn & FZJ)

We calculate the mass shifts of heavy-light scalar mesons due to hadronic loops under the assumption that these vanish for the groundstate heavy-light mesons. The results show that the masses calculated in quark models can be reduced significantly. We stress that the mass alone is not a signal for a molecular interpretation. Both the resulting mass and the width suggest the observed D_0^* state could be a dressed $c\bar{q}$ state. We give further predictions for the bottom scalar mesons which can be used to test the dressing mechanism. The results are published in Ref. [1].

References:

[1] F. K. Guo, S. Krewald and U. G. Meißner, Phys. Lett. B **665**, 157 (2008) [arXiv:0712.2953 [hep-ph]].

Evidence that the $Y(4660)$ is an $f_0(980)\psi'$ bound state

F.-K. Guo, C. Hanhart, Ulf-G. Meißner (Bonn & FZJ)

We demonstrate that the experimental information currently available for the $Y(4660)$ is consistent with its being an $f_0(980)\psi'$ molecule. Possible experimental tests of our hypothesis are presented. The results are published in Ref. [1].

References:

[1] F. K. Guo, C. Hanhart and U. G. Meißner, Phys. Lett. B **665**, 26 (2008) [arXiv:0803.1392 [hep-ph]].

Subleading contributions to the width of the $D_{s0}^*(2317)$

F.-K. Guo, C. Hanhart, S. Krewald, Ulf-G. Meißner (Bonn & FZJ)

We construct the effective chiral Lagrangian involving the D–mesons and Goldstone bosons at next-to-leading order taking into account strong as well as electromagnetic interactions. This allows us to disentangle — to leading order in isospin violation — the electromagnetic and the strong contribution to the D–meson mass differences. In addition, we also apply the interaction to the decay $D_{s0}^*(2317) \to D_s\pi^0$ under the assumption that the $D_{s0}^*(2317)$ is a hadronic molecule. We find (180 ± 110) keV for the decay width $\Gamma(D_{s0}^*(2317) \to D_s\pi^0)$ — consistent with currently existing experimental constraints as well as previous theoretical investigations. The result provides further evidence that this decay width can serve as a criterion for testing the nature of the $D_{s0}^*(2317)$. The results are published in Ref. [1].

References:

[1] F. K. Guo, C. Hanhart, S. Krewald and U. G. Meißner, Phys. Lett. B **666**, 251 (2008) [arXiv:0806.3374 [hep-ph]].

Mass splittings within heavy baryon isospin multiplets in chiral perturbation theory

F.-K. Guo, C. Hanhart, Ulf-G. Meißner (Bonn & FZJ)

We calculate the mass splittings within the heavy baryon isospin multiplets $\Sigma_{c(b)}$ and $\Xi'_{c(b)}$ in chiral perturbation theory to leading one–loop order. The pattern of the mass splittings in the Σ_c iso-triplet, which is different from that of any other known isospin multiplet, can be explained. We predict $m_{\Xi_c'^+} - m_{\Xi_c'^0} = -0.2 \pm 0.6$ MeV, $m_{\Xi_b'^0} - m_{\Xi_b'^-} = -4.0 \pm 1.9$ MeV and the mass of the Σ_b^0 to be 5810.3 ± 1.9 MeV. The results are published in Ref. [1].

References:

[1] F. K. Guo, C. Hanhart and U. G. Meißner, JHEP **0809**, 136 (2008) [arXiv:0809.2359 [hep-ph]].

Quark mass dependence of the pion vector form factor

F.-K. Guo, C. Hanhart, F. J. Llanes-Estrada (Madrid U.), Ulf-G. Meißner (Bonn & FZJ)

We examine the quark mass dependence of the pion vector form factor, particularly the curvature (mean quartic radius). We focus our study on the consequences of assuming that the coupling constant of the ρ to pions $g_{\rho\pi\pi}$ is largely independent of the quark mass while the quark mass dependence of the ρ–mass is given by recent lattice data. By employing the Omnès representation we can provide a very clean estimate for a certain combination of the curvature and the square radius, whose quark mass dependence could be determined from lattice computations. This study provides an independent access to the quark mass dependence of the $\rho\pi\pi$ coupling and in this way a non-trivial check of the systematics of chiral extrapolations. We also provide an improved value for the curvature for physical values for the quark masses, namely $\langle r^4\rangle = 0.73 \pm 0.09$ fm^4 or equivalently $c_V = 4.00 \pm 0.50$ GeV^{-4}. The results are published in Ref. [1].

References:

[1] F. K. Guo, C. Hanhart, F. J. Llanes-Estrada and U. G. Meißner, arXiv:0812.3270 [hep-ph].

Quark mass dependence of ρ and σ
from dispersion relations and Chiral Perturbation Theory [1]

C. Hanhart, J. R. Peláez (Madrid), G.Rios (Madrid)

We use the one–loop Chiral Perturbation Theory ππ–scattering amplitude and dispersion theory in the form of the inverse amplitude method, to study the quark mass dependence of the two lightest resonances of the strong interactions, the $f_0(600)$ (σ) and the ρ–meson. As main results we find that the ρππ coupling constant is almost quark mass independent and that the ρ–mass shows a smooth quark mass dependence while that of the σ shows a strong non–analyticity. These findings are important for studies of the meson spectrum on the lattice.

References:

[1] C. Hanhart, J. R. Pelaez and G. Rios, Phys. Rev. Lett. **100** (2008) 152001 [arXiv:0801.2871 [hep-ph]].

3.2 Nuclear Physics

The role of the nucleon recoil for low-energy antikaon-deuteron scattering

V. Baru, E. Epelbaum and A. Rusetsky

The effect of the nucleon recoil for antikaon-deuteron scattering is studied in the framework of effective field theory. In particular, we performed a calculation of the nucleon recoil effect for the double scattering process. It is shown that the leading correction to the static term that emerges at order $\xi^{1/2}$, where $\xi = m_K/M_N$, vanishes due to a complete cancellation of individually large terms. The resulting recoil effect for the double scattering process is found to be of order of 10-15% compared to the static term. The results will be published in [1].

References:

[1] V. Baru, E. Epelbaum and A.Rusetsky, In the Proceedings of International Conference on Exotic Atoms (EXA 2008), Vienna, Austria, 15-18 Sep 2008, will be piblished in Hyperfine Interactions.

Isospin-breaking two-nucleon force with explicit Delta-excitations

E. Epelbaum (FZJ & Bonn), H. Krebs (Bonn) and Ulf-G. Meißner (Bonn & FZJ)

We study the leading isospin-breaking contributions to the two-nucleon two-pion exchange potential due to explicit Delta degrees of freedom in chiral effective field theory [1]. In particular, we find important contributions due to the delta mass splittings to the charge symmetry breaking potential that act opposite to the effects induced by the nucleon mass splitting.

References:

[1] E. Epelbaum, H. Krebs and U.-G. Meißner, Phys. Rev. C **77** (2008) 034006 arXiv:0801.1299 [nucl-th].

Renormalization of chiral two-pion exchange NN interactions: Momentum vs. coordinate space

D.R. Entem (Salamanca U.), E. Ruiz Arriola (Granada U.), M. Pavón Valderrama (Jülich, Forschungszentrum), R. Machleidt (Idaho U.)

The renormalization of the chiral np interaction in the $^1S_0$ channel to N3LO in Weinberg counting for the long distance potential with one single momentum and energy independent counterterm is carried out. This renormalization scheme yields finite and unique results and is free of short distance off-shell ambiguities. We observe good convergence in the entire elastic range below pion production threshold and find that there are some small physical effects missing in the purely pionic chiral NN potential with or without inclusion of explicit Delta degrees of freedom. We also study the renormalizability of the standard Weinberg counting at NLO and N2LO when a momentum dependent polynomial counterterm is included. Our numerical results suggest that the inclusion of this counterterm does not yield a convergent amplitude (at NLO and N2LO). The results are published in [1].

References:

[1] D. R. Entem, E. Ruiz Arriola, M. Pavón Valderrama and R. Machleidt, Phys. Rev. C **77** (2008) 044006 [arXiv:0709.2770 [nucl-th]].

Deuteron form factors in effective field theory: Regulator independent results and the role of two pion exchange

M. Pavón Valderrama, A. Nogga (Jülich, Forschungszentrum), E. Ruiz Arriola (Granada U.),
D.R. Phillips (Ohio U.)

We evaluate the deuteron charge, quadrupole, and magnetic form factors using wave functions obtained from chiral effective theory (χET) when the potential includes one-pion exchange, chiral two-pion exchange, and genuine contact interactions. We study the manner in which the results for form factors behave as the regulator is removed from the χET calculation, and compare co-ordinate- and momentum-space approaches. We show that, for both the LO and NNLO chiral potential, results obtained by imposing boundary conditions in co-ordinate space at $r = 0$ are equivalent to the $\Lambda \to \infty$ limit of momentum-space calculations. The regulator-independent predictions for deuteron form factors that result from taking the $\Lambda \to \infty$ limit using the LO χET potential are in reasonable agreement with data up to momentum transfers of order 600 MeV, provided that phenomenological information for nucleon structure is employed. In this range the use of the NNLO χET potential results in only small changes to the LO predictions, and it improves the description of the zero of the charge form factor. The results are published in [1].

References:

[1] M. Pavón Valderrama, A. Nogga, E. Ruiz Arriola and D. R. Phillips, Eur. Phys. J. A **36** (2008) 315 [arXiv:0711.4785 [nucl-th]].

Role of the delta isobar in pion-deuteron scattering at threshold within chiral effective field theory

V. Baru (ITEP), J. Haidenbauer, C. Hanhart, A. Kudryavtsev (ITEP), V. Lensky, Ulf-G. Meißner (Bonn & FZJ)

We investigate the role of the delta isobar in the reaction $\pi d \to \pi d$ at threshold in chiral effective field theory. We discuss the corresponding power counting and argue that this calculation completes the evaluation of diagrams up to the order $\chi^{3/2}$, where $\chi = m_\pi/M_N$. The net effect of all delta contributions at this order to the πd scattering length is $\delta a^{\Delta}_{\pi d} = (2.4 \pm 0.4) \times 10^{-3}\ m_\pi^{-1}$. The results are published in Ref. [1].

References:

[1] V. Baru, J. Haidenbauer, C. Hanhart, A. Kudryavtsev, V. Lensky and U.-G. Meißner, Phys. Lett. B **659**, 184 (2008) [arXiv:0706.4023 [nucl-th]].

He-3 spin-dependent cross sections and sum rules

K. Slifer, M. Amarian, L. Auerbach, T. Averett, J. Berthot, P. Bertin, B. Bertozzi, T. Black, E. Brash, D. Brown, E. Burtin, J. Calarco, G. Cates, Z. Chai, J.-P. Chen, Seonho Choi, E. Chudakov, C. Ciofi degli Atti, E. Cisbani, C.W. de Jager, A. Deur, R. DiSalvo, S. Dieterich, P. Djawotho, M. Finn, K. Fissum, H. Fonvieille, S. Frullani, H. Gao, J. Gao, F. Garibaldi, A. Gasparian, S. Gilad, R. Gilman, A. Glamazdin, C. Glashausser, W. Glöckle, J. Golak, E. Goldberg, J. Gomez, V. Gorbenko, J.-O. Hansen, B. Hersman, R. Holmes, G.M. Huber, E. Hughes, B. Humensky, S. Incerti, M. Iodice, S. Jensen, X. Jiang, C. Jones, G. Jones, M. Jones, C. Jutier, H. Kamada, A. Ketikyan, I. Kominis, W. Korsch, K. Kramer, K. Kumar, G. Kumbartzki, M. Kuss, E. Lakuriqi, G. Laveissiere, J. Lerose, M. Liang, N. Liyanage, G. Lolos, S. Malov, J. Marroncle, K. McCormick, R. D. McKeown, Z.-E. Meziani, R. Michaels, J. Mitchell, A. Nogga, E. Pace, Z. Papandreou, T. Pavlin, G.G. Petratos, D. Pripstein, D. Prout, R. Ransome, Y. Roblin, D. Rowntree, M. Rvachev, F. Sabatie, A. Saha, G. Salme, S. Scopetta, R. Skibinski, P. Souder, T. Saito, S. Strauch, R. Suleiman, K. Takahashi, S. Teijiro, L. Todor, H. Tsubota, H. Ueno, G. Urciuoli, R. Van der Meer, P. Vernin, H. Voskanian, H. Witala, B. Wojtsekhowski, F. Xiong, W. Xu, J.-C. Yang, B. Zhang, P. Zolnierczuk

We present a measurement of the spin-dependent cross sections for the ${}^3\vec{H}e(\vec{e},e')X$ reaction in the quasielastic and resonance regions at four-momentum transfer $0.1 < Q^2 < 0.9 GeV^2$. The spin-structure functions have been extracted and used to evaluate the nuclear Burkhardt–Cottingham and extended GDH sum rules for the first time. Impulse approximation and exact three-body Faddeev calculations are also compared to the data in the quasielastic region. The results are published in [1].

References:

[1] K. Slifer *et al.* [E94010 Collaboration], Phys. Rev. Lett. **101**, 022303 (2008) [arXiv:0803.2267 [nucl-ex]].

Studies of the three-nucleon system dynamics: Cross sections of the deuteron-proton breakup at 130 MeV

S. Kistryn, E. Stephan, N. Kalantar-Nayestanaki, A. Biegun, K. Bodek, I. Ciepal, A. Deltuva, E. Epelbaum, A.C. Fonseca, W. Glöckle, J. Golak, H. Kamada, M. Kis, B. Klos, A. Kozela , A. Nogga, M. Mahjour-Shafiei, A. Micherdzinska, P.U. Sauer, R. Skibinski, R. Sworst, H. Witala, J. Zejma, W. Zipper

The three-nucleon system is the simplest non-trivial testing ground in which the quality of modern nucleon-nucleon interaction models, as well as additional dynamical ingredients referred to as three-nucleon forces, can be probed quantitatively by means of a rigorous technique of solving the Faddeev equations. A large set of high precision, exclusive cross-section data for the H-1((d) over right arrow, pp)n breakup reaction at 130 MeV was obtained at KVI, Groningen. It allowed to establish for the first time a clear evidence of the three-nucleon force contributions to the cross sections of the breakup process and to confirm recent predictions of sizable influences of the Coulomb force in this reaction. The results are published in [1].

References:

[1] S. Kistryn et al., Few Body Syst. **44**, 11 (2008).

Subleading contributions to the chiral three-nucleon force: Long-range terms

V. Bernard (Strasbourg), E. Epelbaum (FZJ & Bonn), H. Krebs (Bonn) and Ulf-G. Meißner (Bonn & Jülich)

We derive the long-range contributions to the tree-nucleon force at next-to-next-to-next-to-leading order in the chiral expansion. We give both momentum and coordinate space representations [1].

References:

[1] V. Bernard, E. Epelbaum, H. Krebs and U.-G. Meißner, Phys. Rev. C **77** (2008) 064004 [arXiv:0712.1967 [nucl-th]].

Partial wave decomposition of 2pi-1pi exchange three-nucleon force in chiral effective field theory

H. Kamada (Kyushu Inst. Tech.), E. Epelbaum, Ulf-G. Meißner (Jülich, Forschungszentrum & Bonn U., HISKP),
A. Nogga (Jülich, Forschungszentrum), H. Witala, J. Golak, R. Skibinski (Jagiellonian U.),
W. Glöckle (Ruhr U., Bochum)

The 3-nucleon force at N3LO in the chiral perturbation effective theory is briefly reviewed. The two-pion-one-pion-exchange 3-nucleon force are decomposed in partial waves. The results are published in [1].

References:

[1] H. Kamada *et al.*, AIP Conf. Proc. **1011**, 59 (2008).

Forward $\bar{p}d$ elastic scattering and total spin-dependent $\bar{p}d$ cross sections at intermediate energies

J. Haidenbauer and Yu. N. Uzikov (Dubna)

Spin-dependent total $\bar{p}d$ cross sections are considered using optical theorem. For this aim a full spin-dependence of the forward $\bar{p}d$-elastic scattering amplitude is derived in model independent way. A single scattering approximation is used to relate this amplitude to elementary amplitudes of the $\bar{p}p$ and $\bar{p}n$ elastic scattering and the deuteron formfactor. A formalism allowing to take into account for Coulomb-nuclear interference effects in polarized $\bar{p}d$ cross sections is developed. Numerical calculations for the polarized total crosss sections are performed at beam anergies 50-300 MeV using the Jülich model(s) for $\bar{N}N$ interaction. Double scattering effects are estimated within the Glauber model and found to be less 10%. It is shown that for the used $\bar{N}N$- models the total longitudinal or transversal $\bar{p}d$ cross section is larger in absolute value as compared to the $\bar{p}p$-scattering. The results are available as e-Print [1].

References:

[1] Yu.N. Uzikov and J. Haidenbauer, arXiv:0810.3997 [nucl-th].

Chiral effective field theory on the lattice at next-to-leading order

B. Borasoy (Bonn), E. Epelbaum (FZJ & Bonn), H. Krebs (Bonn), D. Lee (Raleigh) and
U.-G. Meißner (Bonn & FZJ)

We study nucleon-nucleon scattering on the lattice at next-to-leading order in chiral effective field theory [1]. We determine phase shifts and mixing angles from the properties of two-nucleon standing waves induced by a hard spherical wall in the center-of-mass frame. At fixed lattice spacing we test model independence of the low-energy effective theory by computing next-to-leading-order corrections for two different leading-order lattice actions. The first leading-order action includes instantaneous one-pion exchange and same-site contact interactions. The second leading-order action includes instantaneous one-pion exchange and Gaussian-smeared interactions. We find that in each case the results at next-to-leading order are accurate up to corrections expected at higher order.

References:

[1] B. Borasoy, E. Epelbaum, H. Krebs, D. Lee and U.-G. Meißner, Eur. Phys. J. A **35** (2008) 343 [arXiv:0712.2990 [nucl-th]].

Few-nucleon forces and systems in chiral effective field theory

E. Epelbaum (FZJ & Bonn)

Chiral effective field theory provides a systematic framework to study nuclear forces based on the approximate and spontaneously broken chiral symmetry of QCD. We sketch the basic concepts of this method, outline the structure of the resulting few-nucleon forces and discuss some recent applications in the few-nucleon sector. [1].

References:

[1] E. Epelbaum, Few-Body Systems **43** (2008) 57.

Light nuclei from chiral EFT interactions

P. Navratil, V.G. Gueorguiev (LLNL, Livermore), J.P. Vary (LLNL, Livermore & Iowa State U.),
W.E. Ormand (LLNL, Livermore), A. Nogga (Jülich, Forschungszentrum), S. Quaglioni (LLNL, Livermore)

Recent developments in nuclear theory allow us to make a connection between quantum chromodynamics (QCD) and low-energy nuclear physics. First, chiral effective field theory (chiEFT) provides a natural hierarchy to define two-nucleon (NN), three-nucleon (NNN), and even four-nucleon interactions. Second, ab initio methods have been developed capable to test these interactions for light nuclei. In this contribution, we discuss ab initio no-core shell model (NCSM) calculations for s-shell and p-shell nuclei with NN and NNN interactions derived within chiEFT. The results are published in [1].

References:

[1] P. Navratil, V. G. Gueorguiev, J. P. Vary, W. E. Ormand, A. Nogga and S. Quaglioni, Few Body Syst. **43**, 129 (2008) [arXiv:0712.1207 [nucl-th]].

Neutron-proton mass difference in finite nuclei and the Nolen-Schiffer anomaly

Ulf-G. Meißner, A.M. Rakhimov (Tashkent, Seoul), A. Wirzba, U.T. Yakhshiev (Tashkent & FZJ)

The neutron-proton mass difference in finite nuclei is studied in the framework of a medium-modified Skyrme model. The possible interplay between the effective nucleon mass in finite nuclei and the Nolen-Schiffer anomaly is discussed. In particular, we find that a correct description of the properties of mirror nuclei leads to a stringent restriction of possible modifications of the nucleon's effective mass in nuclei. More results can be found in Ref. [1].

References:

[1] U.-G. Meißner, A.M. Rakhimov, A. Wirzba, U.T. Yakhshiev, Eur. Phys. J. A **36**, 37-48 (2008) [arXiv:0802.1455].

A-dependence of ϕ-meson production in $p+A$ collisions

A. Sibirtsev (JLAB & Bonn), H. W.Hammer (Bonn) and U.-G. Meißner (Bonn & FZJ)

A systematic analysis of the A-dependence of ϕ-meson production in proton-nucleus collisions is presented [1]. We apply different formalisms for the evaluation of the ϕ-meson distortion in nuclei and discuss the theoretical uncertainties of the data analysis. The corresponding results are compared to theoretical predictions. We also discuss the interpretation of the extracted results with respect to different observables and provide the relation between frequently used definitions. The perspectives of future experiments are evaluated and estimates based on our systematical study are given.

References:

[1] A. Sibirtsev, H. W. Hammer and U.-G. Meißner, Eur. Phys. J. A **37** (2008) 287 [arXiv:0802.3373 [nucl-th]].

Selfconsistent calculations within the Green's function method including particle-phonon coupling and the single-particle continuum.

N.Lyutorovich (St. Petersburg State U.), J. Speth, A.Avdeenkov (Obninsk), F.Grümmer,
S. Kamerzhiev (Obninsk), S.Krewald, V.I.Tselyaev (St. Petersburg State U.)

The Green's function method in the quasiparticle time blocking approximation is applied to nuclear excitations in the Sn isotopes. The calculations are performed self-consistently using a Skyrme interaction. The method combines the conventional RPA with an exact single-particle continuum treatment and considers in a consistent way the particle-phonon coupling. We reproduce not only the experimental values of low- and high-lying collective states, but we also obtain fair agreement with the data of non-colective low-lying states that are strongly influcenced by the particle-phonon coupling.

References:

[1] N. Lyutorovich, J. Speth,, A. Avdeenkov, F. Grummer, S. Kamerdzhiev, S. Krewald, V. I. Tselyaev, Eur. Phys. J. A **37**, 381 (2008)

Dilute neutron matter on the lattice at next-to-leading order in chiral effective field theory

B. Borasoy (Bonn), E. Epelbaum (FZJ & Bonn), H. Krebs (Bonn), D. Lee (Raleigh) and
U.-G. Meißner (Bonn & FZJ)

We discuss lattice simulations of the ground state of dilute neutron matter at next-to-leading order in chiral effective field theory [1]. In a previous paper the coefficients of the next-to-leading-order lattice action were determined by matching nucleon-nucleon scattering data for momenta up to the pion mass. Here the same lattice action is used to simulate the ground state of up to 12 neutrons in a periodic cube using Monte Carlo. We explore the density range from 2% to 8% of normal nuclear density and analyze the ground state energy as an expansion about the unitarity limit with corrections due to finite scattering length, effective range, and P-wave interactions.

References:

[1] B. Borasoy, E. Epelbaum, H. Krebs, D. Lee and U.-G. Meißner, Eur. Phys. J. A **35** (2008) 357 [arXiv:0712.2993 [nucl-th]].

Coherent photon-photon interactions in very peripheral relativistic heavy-ion collisions [1]

G. Baur

Heavy ions at high velocities provide very strong electromagnetic fields for a very short time. The main characteristics of ultraperipheral relativistic heavy ion collisions are reviewed, characteristic parameters are identified. The main interest in ultraperipheral heavy ion collisions at relativistic ion colliders like the LHC is the interactions of very high energy (equivalent) photons with the countermoving (equivalent) photons and hadrons (protons/ions). The physics of these interactions is quite different from and complementary to the physics of the strong fields achieved with current and future lasers.

References:

[1] G.Baur Eur. Phys. J.D, accepted for publication arXiv:0810.1400

Exchange of high and low energy photons in ultraperipheral relativistic heavy-ion collisions [1]

G. Baur

Ultraperipheral collisions at collider energies are a useful tool to study photon-hadron (proton/nucleus) and photon-photon interactions in a hitherto unexplored energy regime. Theoretical tools to study these processes are briefly described. Some current results and problems are discussed

References:

[1] G.Baur Nuclear Physics B (Proc. Suppl.) 179-180 (2008) 129 arXiv:0806.4305

Coulomb dissociation, a tool for nuclear astrophysics [1]

G. Baur, S. Typel*

A short status report on Coulomb dissociation, an indirect method for nuclear astrophysics is given. An analytically solvable approach to study electromagnetic excitation in ^{11}Be, the archetype of a halo nucleus, is proposed.

References:

[1] G.Baur and S. Typel, J.Phys. G (Proceedings of Nuclear Physics in Astrophysics III, 26-31 March 2007, Dresden, Germany) 35 (2008)014028, arXiv:0705.3307

* GSI, Darmstadt and Excellence Cluster Universe, München, Germany

Ultraperipheral Collisions at RHIC and LHC [1]

G. Baur

A brief introduction to the physics of ultraperipheral collisions at collider energies is given. Photon-hadron (proton/ nucleus) and photon-photon interactions can be studied in a hitherto unexplored energy regime.

References:

[1] G.Baur Nuclear Physics B (Proc. Suppl.) 184 (2008) 143 arXiv:0711.2882

Ionization of highly charged relativistic ions by neutral atoms [1]

G. Baur, I.L. Beigmann*, V. P. Shevelko*, I. Yu. Tolstikhina*, and Th. Stöhlker**

Ionization of highly charged relativistic ions by neutral atoms and ions is considered. Numerical results of recently developed computer codes based on the relativistic Born and the equivalent-photon approximations are presented. The ionization of the outer shells dominate. For the outer projectile electron shells, which give the main contribution to the process, the non-relativistic Schrödinger wave functions can be used. The formulae for the non-relativistic reduction of the Dirac matrix-elements are obtained for ionization of electrons with arbitrary quantum numbers n and ℓ.

References:

[1] G.Baur, I.L. Beigman, V.P. Shevelko, I.Yu. Tolstikhina, and Th. Stöhlker submitted to Phys. Rev. A arXiv:0811.1118

* P.N. Lebedev Physical Institute, Moscow, Russia
** GSI, Darmstadt and Physikalisches Institut, Universität Heidelberg, Germany

Scaling laws and higher-order effects in Coulomb excitation of neutron halo nuclei [1]

S. Typel*, G. Baur

Essential properties of halo nuclei can be described in terms of a few low-energy constants. For neutron halo nuclei, analytical results can be found for wave functions and electromagnetic transition matrix-elements in simple but well-adapted models. These wave functions can be used to study nuclear reactions; an especially simple and instructive example is Coulomb excitation. A systematic expansion in terms of small parameters can be given. We present scaling laws for excitation amplitudes and cross sections. The results can be used to analyze experiments like ^{11}Be Coulomb excitation. They also serve as benchmark tests for more involved reaction theories.

References:

[1] S. Typel, G.Baur Eur. Phys. J.A 38(2008) 355 arXiv:0808.3478

* GSI, Darmstadt and Excellence Cluster Universe, München, Germany

The Physics of Ultraperipheral Collisions at the LHC [1]

A. J. Baltz *, G. Baur, et al. (23 authors)

We discuss the physics of large impact parameter interactions at the LHC: ultraperipheral collisions (UPCs). The dominant processes in UPCs are photon-nucleon (nucleus) interactions. The current LHC detector configurations can explore small x hard phenomena with nuclei and nucleons at photon-nucleon center-of-mass energies above 1 TeV, extending the x range of HERA by a factor of ten. In particular, it will be possible to probe diffractive and inclusive parton densities in nuclei using several processes. The interaction of small dipoles with protons and nuclei can be investigated in elastic and quasi-elastic J/ψ and Υ production as well as in high t ρ^0 production accompanied by a rapidity gap. Several of these phenomena provide clean signatures of the onset of the new high gluon density QCD regime. The LHC is in the kinematic range where nonlinear effects are several times larger than at HERA. Two-photon processes in UPCs are also studied. In addition, while UPCs play a role in limiting the maximum beam luminosity, they can also be used a luminosity monitor by measuring mutual electromagnetic dissociation of the beam nuclei. We also review similar studies at HERA and RHIC as well as describe the potential use of the LHC detectors for UPC measurements.

References:

[1] A.J. Baltz et al. Physics Reports 458 (2008) 1 arXiv:0706.3356

* Physics Department, Brookhaven National Laboratory, Upton, NY, USA

The *s*-wave pion-nucleus optical potential [1]

M. Döring, E. Oset (Valencia)

We calculate the *s*-wave part of the pion-nucleus optical potential using a unitarized chiral approach that has been previously used to simultaneously describe pionic hydrogen and deuterium data as well as low energy πN scattering in the vacuum. This energy dependent model allows for additional isoscalar parts in the potential from multiple rescattering. We consider Pauli blocking and pion polarization in an asymmetric nuclear matter environment. Also, higher order corrections of the πN amplitude are included. The model can accommodate the repulsion required by phenomenological fits, though the theoretical uncertainties are bigger than previously thought. At the same time, we also find an enhancement of the isovector part compatible with empirical determinations.

References:

[1] M. Döring and E. Oset, Phys. Rev. C **77**, 024602 (2008) [arXiv:0705.3027 [nucl-th]].

3.3 Others

$B \to \gamma\gamma$ in an ACD model

I.I. Bigi (Notre Dame), G.G. Devidze (Tbilisi), A.G. Liparteliani (Tbilisi) and U.-G. Meißner (Bonn & FZJ)

We present a full calculation of the amplitudes for $B_{d[s]} \to \gamma\gamma$ in a simple ACD model that extends an incomplete one in a previous paper [1]. We find cancellations between the contributions from different KK towers and a small decrease relative to the SM predictions. It is conjectured that radiative QCD corrections might actually lead to an enhancement in the branching ratios and CP asymmetries, but no more than modest ones.

References:

[1] I. I. Bigi, G. G. Devidze, A. G. Liparteliani and U.-G. Meißner, Phys. Rev. D **78** (2008) 097501 [arXiv:0806.1541 [hep-ph]].

Spin filtering of stored (anti)protons:
from FILTEX to COSY to AD to FAIRThe role of the nucleon recoil for low-energy antikaon-deuteron scattering

N. Nikolaev and F. Pavlov

We discuss the theory of spin filtering of stored (anti)protons by multiple passage through the polarized internal target (PIT). Implications for the antiproton polarization buildup in the proposed PAX experiment at FAIR GSI are discussed. The results have been published in [1].

References:

[1] N. Nikolaev and F. Pavlov, POLARIZED ANTIPROTON BEAMS - HOW?: An International Workshop; Cockcroft Institute, Warrington, Cheshire, UK. AIP Conf. Proc. **1008** (2008) 34.

The Casimir effect as a scattering problem

A. Wirzba

The Casimir-force calculations for a finite number of non-overlapping obstacles can be mapped onto quantum-mechanical billiard-type problems which are characterized by the scattering of a fictitious point particle off the very same obstacles. With the help of a modified Krein trace formula the genuine/finite part of the Casimir energy is determined as the energy-weighted integral over the log-determinant of the multi-scattering matrix of the analog billiard problem. The formalism is self-regulating and inherently shows that the Casimir energy is governed by the infrared end of the multi-scattering phase shifts or the spectrum of the fluctuating field. The calculation is exact and in principle applicable for any separation(s) between the obstacles. In practice, it is more suited for large- to medium-range separations. We report especially about the Casimir energy of a fluctuating massless scalar field between two spheres or a sphere and a plate under Dirichlet and Neumann boundary conditions. But the formalism can easily be extended to any number of spheres and/or planes in three or arbitrary dimensions, with a variety of boundary conditions or non-overlapping potentials/non-ideal reflectors. More results can be found in Ref. [1].

References:

[1] A. Wirzba, J. Phys. A: Math. Theor. **41** (2008) 164003 (13pp).

4 Preparations for FAIR

Closed Orbit Correction and Non-linear Beam Dynamics for the Normal-conducting HESR

D. Welsch, A. Lehrach, B. Lorentz, R. Maier, D. Prasuhn, R. Tölle

The High Energy Storage Ring (HESR) [1] will be part of the future Facility for Antiproton and Ion Research (FAIR) [2] located at GSI in Darmstadt, Germany. The HESR will be operated with antiprotons in the momentum range from 1.5 to 15 GeV/c, which makes a long beam lifetime and a minimum of particle losses crucial. This and the demanding requirements of the PANDA experiment [3] lead to the necessity of a good orbit correction and an effective multipole compensation.

Closed orbit correction

Displacements of magnets are the most serious cause for distortions of the closed orbit. Alignment and measurement errors of beam position monitors also contribute to orbit distortions. Both types of errors have been included in the simulations. The goal of the here proposed closed orbit correction scheme is to reduce closed orbit deviations to below 5 mm while not exceeding 1 mrad of correction strength.

Closed Orbit Correction Scheme

The closed orbit correction scheme employed for this calculation consists of 64 beam position monitors and 36 closed orbit correction dipoles. There are 26 beam position monitors used per arc of which 12 are positioned at a large beta function in X and 14 at a large beta function in Y. This amount of beam position monitors just reflects the amount of chromatic sextupoles (see below) and is sufficient for the closed orbit correction. The amount of closed orbit correction dipoles is six per transverse direction and per arc.

There are six beam position monitors and also six closed orbit correction dipoles used per straight. Whereas in the arcs the orbit correction dipoles are planned to be unidirectional (because of beta functions), in the straights combined ones can be used for both transverse directions. Beam position monitors will be designed to measure always in X and Y.

Verification

In order to verify the closed orbit correction scheme, Monte-Carlo methods and the Orbit Response Matrix technique have been utilised [4]. We applied more than 1000 different sets of displacement and measurement errors. For all defined optical settings, we could demonstrate the effectiveness of the developed closed orbit correction scheme.

Orbit bump for H^0 detector

An orbit bump has been designed to include an H^0 detector into the HESR. This detector will be part of the electron cooler. The orbit bump will be set up symmetrically utilizing three steerers with maximum deflection strengths of 2 mrad in both transverse planes. The needed strengths are below the available 2 mrad allowing possible improvements [5].

Non-linear beam dynamics

By now, mainly sextupoles and higher order field errors are used to simulate non-linear beam dynamics.

Sextupoles

Since the natural chromaticity ranges down to -17, there is no possibility to avoid its correction. Despite correcting chromaticity, sextupoles drive different resonances and will affect the stability of the circulating antiproton beam. The here proposed chromaticity correction scheme utilises sextupoles in the arcs split into four families (two horiz. and two vert.). This is caused by the variation of the horizontal dispersion function in the different optical settings and a minimization of non-linear effects acting on the beam. Due to space restrictions in the arcs, sextupoles have a design length of 0.3 m. If we restrict the maximum normalised strength to $0.85 m^{-3}$, the proposed correction scheme contains 24 horizontal and 28 vertical sextupoles distributed evenly between both arcs.

Higher order multipoles

Besides sextupoles, higher order multipoles from field errors of dipoles and quadrupoles contribute to non-linear beam dynamics. Utilising the sympletic tracking code SIMBAD [6], simulations show that the effect of the field errors is stronger than the one of the sextupoles. This can be demonstrated by tune scans (see Fig. 1). Only two of all 15 visible resonances are upright sextupole resonances and are driven not only by the sextupole magnets but also by sextupole field components of dipoles and quadrupoles.

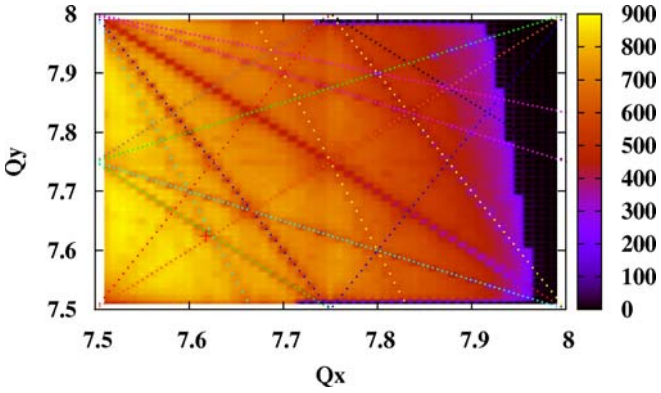

Fig. 1: Tune scan. Red cross denotes chosen standard tune at (7.617, 7.624). Dotted coloured lines represent all visible resonances. The strongest resonance is the octupole sum resonance 2Qx+2Qy=31.

References:

[1] Baseline Technical Report Vol. 2, http://www.gsi.de/fair/reports/btr.html
[2] Conceptional Design Report, http://www.gsi.de/GSI-Future/cdr/
[3] The PANDA experiment, http://www-panda.gsi.de/
[4] D.M. Welsch, Auslegung eines Orbitkorrektursystems für den Hochenergie Speicherring HESR im Projekt FAIR, Diploma thesis, Jül-4241, Forschungszentrum Jülich, Germany, 2007
[5] D.M. Welsch, Orbit bump for an H^0 detector internal report (to be published)
[6] SIMBAD tracking code, http://www.bnl.gov/csc/projects/High_Energy/SIMBAD/

Cycle Averaged Luminosities for both HESR User Modes

K. Bongardt, F. Hinterberger, A. Lehrach, R. Maier, D. Prasuhn, R. Tölle

General formulae are presented for cycle averaged HESR luminosities, where pbars are accumulated over long time in the RESR, injected as a 150 m long bunch at 3.8 GeV/c. Equilibrium leads to simplified results for both commissioning and final phase. For 15 GeV/c, cycle averaged particle numbers are shown for 4 different cases, from refill procedure without loss to no refill at all. Results are shown for pbar production rate of 10^7/s.

General formulae for cycle averaged luminosity $\overline{L}$

For particle injection into HESR, cycle averaged luminosity and beam life time values are given [1, 2] by

$\overline{L} = \beta f_0 n_t \; N_i \tau (1 - e^{-t_{\exp}/\tau}) / (t_{\exp} + t_{prep}) = \beta L_0 \overline{N}$.

βf_0 is the velocity dependent revolution frequency, n_t is the average target density, N_i is the initial particle number, $\tau(\beta)$ is the velocity dependent 1/e beam life time, t_{exp} is the experiment time (beam on target), t_{prep} is needed for beam preparation. Cycle averaged particle number is given by $\overline{N} = N_i \tau (1 - e^{-t_{\exp}/\tau}) / (t_{\exp} + t_{prep})$. After end of experimental phase the final particle number is $N_f = N_i e^{-t_{\exp}/\tau}$.

Described is the general case, no equilibrium, as initial particle number N_i is not connected to number of refilled particles N_r and can change from cycle to cycle.

Equilibrium case without using remaining particles

If no remaining particles N_f are used, initial particle number N_i is identical to the number of new injected particles $N_r = \dot{N}_{prod} \times t_{cyc}$ leading to: $\overline{N} = \tau \dot{N}_{prod} (1 - e^{-t_{\exp}/\tau})$.

A pbar production rate $\dot{N}_{prod}$ of 10^7/s is planned for the commissioning phase.

Pellet target with effective density of $n_t = 4\times10^{15}$ cm^{-2} for the 574 m HESR ring leads to $L_0 = 20.8\times10^{20} cm^{-2} s^{-1}$.

Table 1 shows resulting averaged luminosities for the HR mode with $N_i = 10^{10}$, identical cycle by cycle. During time $t_{cyc} = t_{\exp} + t_{prep}$ new particles are collected from RESR. Loss rate $\dot{N}_{loss} = N_i / \tau$ is not identical with production rate $\dot{N}_{prod}$, as particle number is decreasing during experiment.

Tab. 1: Particle numbers and averaged luminosities.

HR mode: $N_i = 10^{10}$, t_{cyc} = 1000s		
	1.5 GeV/c	9 GeV/c
1/e beam lifetime / s	~1540	~6000
Loss rate /s^{-1}	6.5x10^6	1.7 x10^6
Experiment time / s	950	900
cycle time / s	1000	1000
Particles from RESR	10^{10}	10^{10}
Initial particle number N_i	10^{10}	10^{10}
cycle **avg.** number $\overline{N}$	7.1×10^9	9×10^9
Final particle number N_f	5.4×10^9	8.5×10^9
avg. luminosity /10^{31} cm^{-2}s^{-1}	1.3	1.9

Table 2 shows resulting averaged luminosities for the HL mode with $N_i < 7.2\times10^{10}$. Even if all remaining particles are lost, average luminosities are about 2/3 of the optimum, if experimental time is longer than life time, see Fig 1.

Tab. 2: Particle numbers and averaged luminosities

HL mode: $N_i < 7.2\times10^{10}$, t_{cyc} < 7200 s			
	1.5 GeV/c	9 GeV/c	15 GeV/c
1/e beam lifetime / s	~1540	~6000	~7100
Experiment time / s	1450	6000	7100
cycle time / s	1500	6100	7200
Particles from RESR	1.5×10^{10}	6.1×10^{10}	7.2×10^{10}
Initial number N_i	1.5×10^{10}	6.1×10^{10}	7.2×10^{10}
avg. number $\overline{N}$	9.5×10^9	3.8×10^{10}	4.5×10^{10}
Final number N_f	5.7×10^9	2.2×10^{10}	2.6×10^{10}
avg. lumi /10^{31} cm^{-2}s^{-1}	1.7	8	9.5

Equilibrium case by partly using remaining particles

If remaining particles are partly re-used with survival factors x ≤ 1 (change momentum to injection level) and y ≤ 1 (formation of new bunch), the average particle number is $\overline{N} = y\tau \dot{N}_{prod} (1 - e^{-t_{\exp}/\tau}) / (1 - xy \times e^{-t_{\exp}/\tau})$. For no loss during acceleration and deceleration processes, the mean particle number $\overline{N} = \tau \dot{N}_{prod}$ is independent of details of the HESR cycle (Fig. 1) but depending on initial particle number N_i.

Fig. 1 shows $\overline{N}$ at 15 GeV/c for 4 different cases, $N_r < 10^{11}$, from refill without loss (x=y=1) to no refill (x=0, y=1) at all. Intermediate cases are: x=y=0.9 for 20% and x=0.75, y=0.85 for 40% loss. Without loss and t_{prep} = 300 s N_i is less than 1.8×10^{11} and shows a minimum of 9.4×10^{10} at t_{exp} = 2×10^3 s. For t_{exp} less than 10^4 s even 40% loss during refill procedure improves the average luminosity compared to the commissioning phase, see Tab 2.

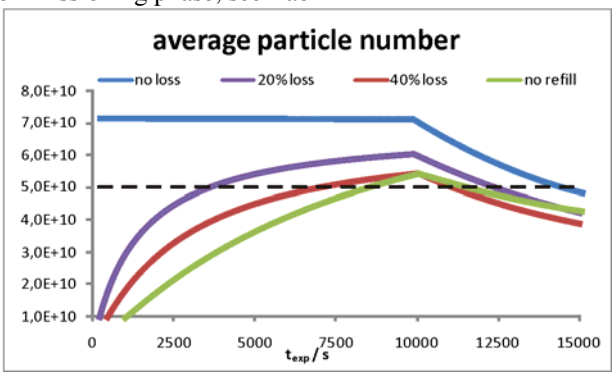

Fig. 1: Average particle number for 4 cases, $N_r < 10^{11}$: dashed line indicates 2/3 of optimum value.

Complicated refill procedure [3] starts with 150 m long RESR bunch and particle number N_i. Bunch rotation by dual harmonic RF system [4] reduces momentum spread of nearly DC beam before experiment starts.

After end of experiment phase DC beam is cooled to reduce momentum spread for transfer to 3.8 GeV/c injection momentum, survival factor x. Re-used bunch is compressed to 150 m, before adding new RESR bunch with reduced intensity. Cooling of created DC beam reduces momentum spread for the newly formed bunch, survival factor y, changed to experiment energy, again with number N_i.

References:

[1] F. Hinterberger, Jülich Report Jül-4206, 2006
[2] A. Lehrach et al, Proc. Stori 08, 2008
[3] R. Stassen et al, Proc. EPAC 08, p. 321
[4] S. An et al, Chinese Physics C, 2008,32(1) p. 60
http://hepnp.ihep.ac.cn/qikan/epaper/zhaiyao.asp?bsid=7496

The HESR Accelerating Cavity

R. Stassen, M. Böhnke, F.J. Etzkorn, H. Stockhorst, IKP, S. Papureanu, IFIN-HH, Romania, A. Schnase, JAEA, Japan

The HESR accelerating cavity will not only be used for beam acceleration, but also for deceleration and for bunch rotation. Additionally a barrier bucket (BB) with h=1..5 will be formed by this cavity to combine the decelerated bunch with a new injected RESR bunch in the high luminosity mode (HL).
The accelerating cavity of the HESR [1] will be operated as dual harmonic cavity with voltages up to 5kV [2]. The basic parameters of this cavity are summarized in table 2. A prototype was designed and built based on the broadband COSY cavity [3]. The HESR cavity consists of two tanks with a total length of about 80 cm including the acceleration gap. The outer diameter is slightly less than 60 cm. Each tank is loaded with 6 cores of FineMet 3M® [4].

Tab. 1: basic cavity parameters

HESR rev.frequencies	440 kHz – 520 kHz
Frequency-range	1..10 harmonics (0.4 - 5 MHz)
Gap voltage	100 < 5000V peak
No of gaps	1
No of tanks	2
Mode of operation	cw
Cooling	Water-cooled
Material	FineMet 3M

The impedances of all FineMet cores have been measured individually. This allowed a grouping into the two cavity tanks, showing similar impedances both for the real and the imaginary part (Fig. 1).

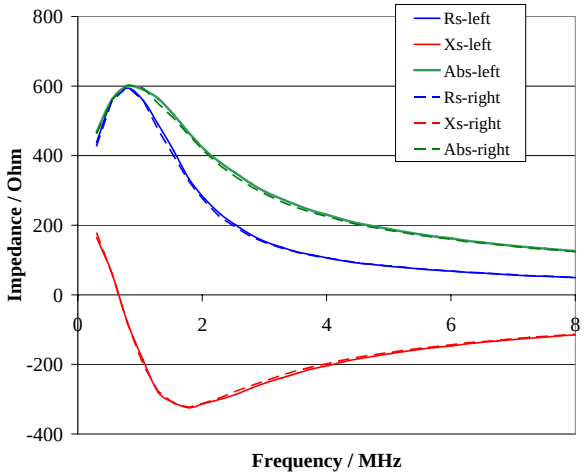

Fig. 1: Impedances of both cavity-tanks after arranging the FineMet cores and assembling the cavity with a dummy gap.

The cavity was installed on top of the former COSY tube amplifier. This amplifier was reactivated after an unused period of about 6 years. Most of the electrical plugs and cooling water hoses were replaced. The anode high voltage power supply as well as all other subsystems were checked before the tubes were heated for the first time after this long period of shutdown. A water leakage caused corrosion at one tube socket. The whole tube with socket was dismantled to clean the corroded places. After some modification concerning the coupling this amplifier is now suitable to fulfil all HESR relevant RF-requirements and can be used to test the prototype of the HESR cavity.

First RF-measurements have been carried out, reaching a gap-voltage of 4kV peak-peak at each cavity tank at 1MHz over several hours of operation.
Further tests including the dual harmonic and barrier bucket operation in the required frequency range will be done next.

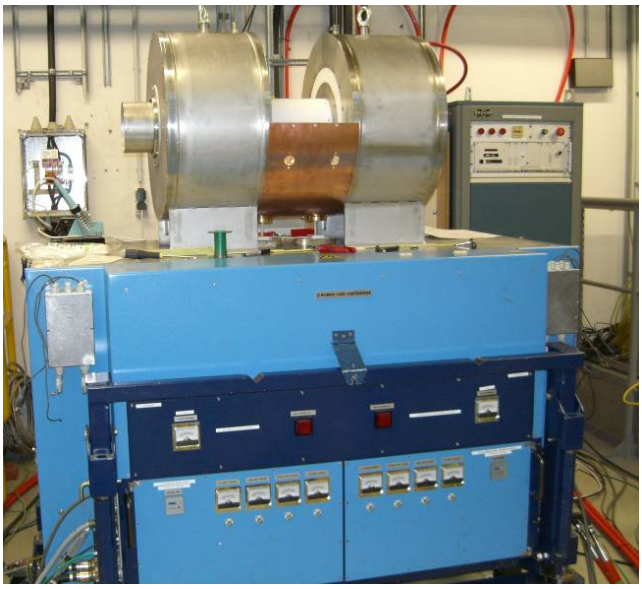

Fig. 2: Prototype of HESR accelerating cavity installed on top of the former COSY tube amplifier.

References:

[1] HESR, Baseline Technical Report http://www-win.gsi.de/FAIR-EOI/PDF/TDR_PDF/TDR_HESR-TRV3.1.2.pdf, March 2008
[2] S. An, K. Bongardt, J. Tang, R. Maier, Injection, Refill and Acceleration in the HESR Synchrotron, Annual Report 2005 IKP, Jülich.
[3] A. Schnase, et al., Experience with a Broadband Cavity at COSY, EPAC2000, Vienna
[4] Hitachi Metals, Ltd., http://www.hitachi-metals.co.jp/e/prod/prod02/prod02.html, Japan

Work supported by the European Community for Research Infrastructures under the FP6 "Structuring the European Research Area" program (DIRACSecondary-Beams, contract number 515873).

The pick-up unit (PU) of the stochastic-cooling system will now simultaneously take the longitudinal and both transversal beam signals. The first stage of the PU covers the frequency range of 2 to 4 GHz. The PU consists of two adjoining tanks of an active length of 0.8 m each and has a total length of about 3 m. The tanks are cryogenically cooled and are described in more details in the previous paper [1]. The corrector system will be separated in three tanks for the longitudinal and both transversal actions.
The nominal energy of the cooling system ranged from the injection energy (3 GeV) to the end energy (14.1 GeV) in the first HESR proposal. In this case most of the electrodes are combined inside the vacuum tank. Only a small number of vacuum feed-throughs and programmable delay lines are needed. The system modifications for an enhancement of the energy range down to 0.8 GeV with an emphasized energy range at 4 to 6 GeV is described in the following.
The appending figure shows a schematic circuit diagram of the combined PU. The signal paths of the corrector tanks will be similar but passed in the opposite direction.

PU signal processing in the vacuum tanks
The following 5 layers are placed within the vacuum envelopes and are cryogenically cooled:

- Each tank contains 64 wall-current monitoring ring gaps. Each ring has a length of 12.5 mm in the beam direction. (These rings are suppressed in the enclosed figure.)
- Each ring gap is coupled out to eight 50-ohm ports at a regular octagon around the beam centre line.
- Four hierarchic layers of two-step Wilkinson couplers accumulate the signal power of the longitudinal rows of 50-ohm ports. 16 such ports each are connected to one combining board.
- Up to here, the delay lines compensating for the beam drift times have fixed lengths. Only the 4th combining layer contributes a moderate part to the energy dependence of the signal path at beam energies below 1.2 GeV.

The transmission lines and the Wilkinson assemblies are constructed as microstrip elements at the combining boards. The corresponding conductor pattern has been milled out of doubly copper-clad TMM6 boards (traded by Rogers Corporation).

- Each tank contains 8 longitudinal rows of 4 combining boards each.
- A 5th Wilkinson layer at separate small microstrip boards adds the combined signals of the pairs of two adjacent (by 22.5 deg rotated) longitudinal rows of 16 50-ohm ports. Each tank contains 4 longitudinal rows of 4 such small boards each.
- Balancing resistors are applied at all Wilkinson couplers. These resistors are necessary at the first combining layer to broadband the PU system and at the subsequent layers to reduce the noise power of the previous layers. The resistors are cooled via the microstrip boards to limit the thermal noise.

RF components outside the tanks
The combined power of the pairs of 16 are coaxially fed through the vacuum envelope and put in 32 low-noise octave-band pre-amplifiers. These amplifiers will gain around 10 dB and will work in the air at ambient temperature.

- The pre-amplified signals will be combined in further 3 layers. Hereby, switchable delay lines are required to compensate for the energy-dependent beam drift time. The last Wilkinson layer adds the power of both adjoining tanks.
- The delay lines will be switched in steps of 10 mm of electrical length at the first layer (PV1) and 20 mm at the further layers (PV2, PV4).

A deviation of 10 mm from the ideal length leads to a phase difference between the Wilkinson inputs that causes at 4 GHz an additional attenuation of nearly 0.8 dB. This is in the order of the attenuation of two electronic RF switches along a switched path. We have chosen the electrical lengths of the switchable path to be binary multiples of 20 mm at the PV2 and PV4 units.
The switching elements essentially contribute to the frequency dependence of the combining network. The global compensation is facilitated by placing identical numbers of RF switches at all 32 pre-amplified signal paths. I.e. the same number of switchable stages is used at all Wilkinson input branches of PV1, PV2, and PV4. So, two switchable stages (10 and 20 mm) are also applied at the first combining layer of the pre-amplified signals (PV1elements) although one switchable stage of 20 mm would be sufficient for a maximum attenuation of 0.8 dB at 4 GHz caused by the phase difference between the arms of the combiners.

- The RF network will be concluded by two broadband hybrides forming the longitudinal signals at the sum outputs and the transversal signals at the difference outputs.

The enclosed figure shows the states of the switches at the lowest beam energy.

Beam-energy dependence of the combined beam power
Each Wilkinson layer ameliorates the signal-to-noise ratio (SNR) by nearly 3 dB at the centre frequency because the parasitic noise sources (resistors and pre-amplifiers) at the inputs of the combining elements are independent.
In the given energy range of 0.8 to 15 GeV, the beam-energy dependence of the SNR is mainly affected by the 4th layer within the tanks combining the power of the longitudinal rows of ports of 8 PU rings. In contrast, the programmable delay lines in the PV units will negligibly reduce the SNR of the pre-amplified signals. The former layer contains the largest fixed lengths of the delay lines compensating for the beam drift times. The largest phase differences are calculated at the Wilkinson inputs and therefore the largest spurious attenuation occurs at the frontiers of the energy range. Favoring the higher energies for the stochastic cooling requires to set the centre energy to 2.5 GeV at that 4th layer in contrast to 1.55 GeV at the first layers; the centre energy of the beam drift time between 0.8 and 15 GeV resides in nearly 1.4 GeV. The first 3 layers spuriously attenuate by less than 0.3 dB within 0.8 and 15 GeV whereas the total attenuation of the 4 layers amount to

- 2.1 dB at 800 MeV, 0.94 dB at 1 GeV, 0.5 dB at 1.2 GeV with
- a flat minimum of 0.03 dB near 2 GeV and

- a small rise to 0.26 dB at 15 GeV.

These values are computed at 4 GHz; half the values are found at 2.8 GHz and reduce to a fourth at 2 GHz.
The SNR will only be lowered by more than 0.5 dB at energies below 1.2 GeV and low beam intensities. In contrast, the combining networks outside the tanks don not commensurably deteriorate the SNR but generate a ripple (max. 2dB) of the amplitude versus the beam energy.

References:

[1] R. Stassen, P. Brittner, R. Greven, H. Singer, H. Stockhorst, L. Thorndahl, Recent Developments for the HESR Stochastic Cooling System, this annual report.

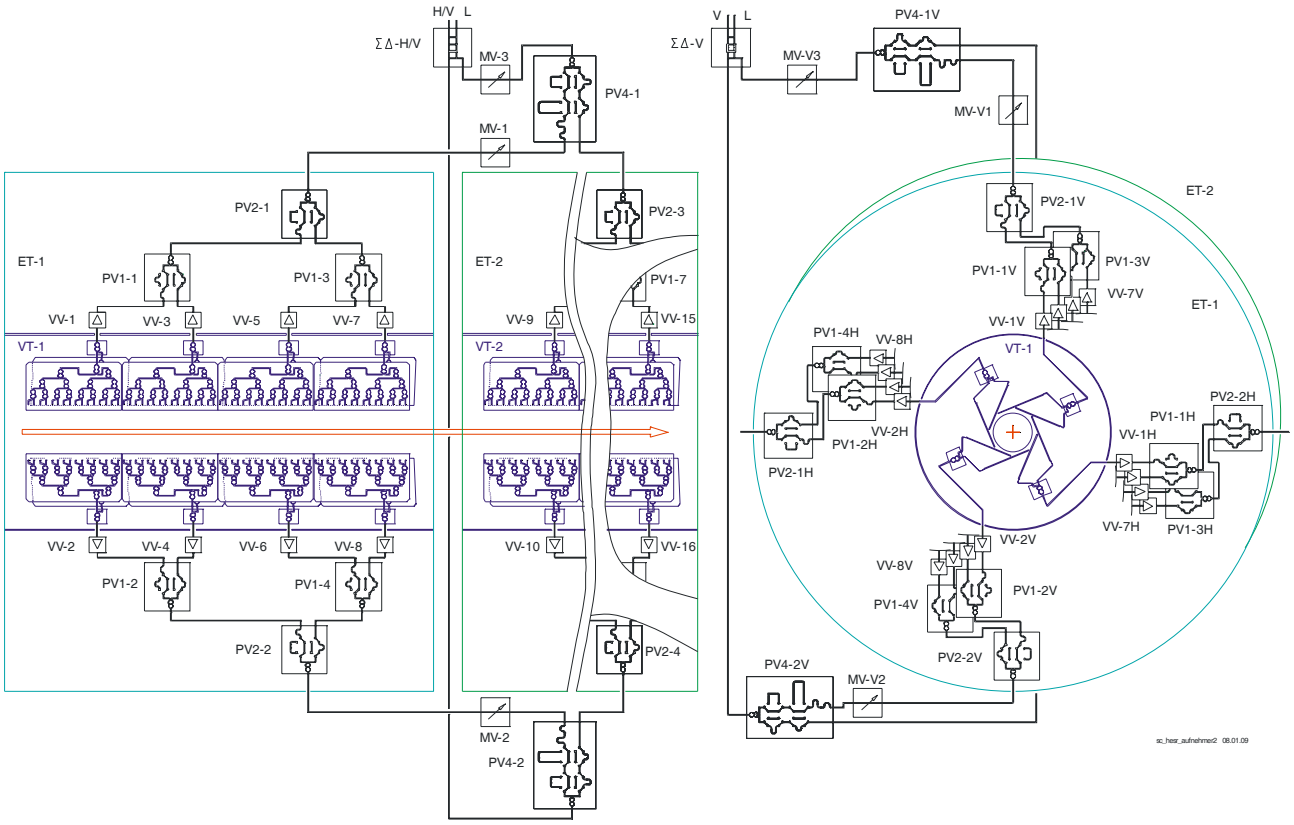

Fig 1: Combined longitudinal and transversal pick-up for the stochastic-cooling system of the HESR at 2 to 4 GHz. Length of double tank 3 m, active length 1.6 m. ===> beam direction,

H/V L :	longitudinal & horizontal or vertical outputs,	H L:	longitudinal & horizontal outputs
V L:	longitudinal & vertical outputs,	VT:	vacuum tank
ET:	electrical system per tank,	VV:	low-noise preamplifier

MV: mechanically adjustable delay line ca. 0...10 mm
PV1: combiner & programmable delay line 0, 10, 20, 30 mm
PV2: combiner & programmable delay line 0, 20, 40, 60 mm
PV4: combiner & programmable delay line 0, 20, 40,...300 mm

Recent Developments for the HESR Stochastic Cooling System

R. Stassen, P. Brittner, R. Greven, H. Singer, H. Stockhorst, L. Thorndahl

The High-Energy Storage Ring (HESR) of the future International Facility for Antiproton and Ion Research (FAIR) [1] at the GSI in Darmstadt will be built as an antiproton cooler ring in the momentum range from 1.5 to 15 GeV/c. Numerical simulations have shown the great benefit of the stochastic cooling system to achieve the requested beam spot and the high momentum resolution at the internal target [2].

Cooling structures

Two different cooling structures have been analysed to build a stochastic cooling system without movable electrode bar [3]. An octagonal arrangement of these structures increases the sensitivity which reaches values comparable to the complicate movable λ/4 electrodes [4]. In collaboration with the central workshop of the FZJ a cooling test tank has been built and equipped with both structures to measure the sensitivity with real beam in COSY. The modular design of the tank allows even the installation of additional structures like planar structures [5]. Two cold heads are installed at this tank to cool down the structures to approximately 20-30K. The whole inner part including the structures can be moved in vertical and horizontal direction to centre the structures according to the beam. The signals of each electrode row are fed through the vacuum system. Thus any combination of signal combining can be tested.

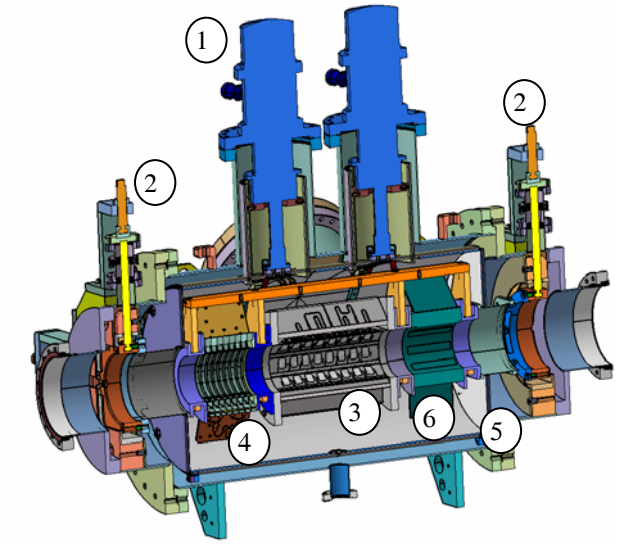

Fig. 1: Cooling structures test-tank: (1) cold heads, (2) x-y support, (3) printed loops, (4) ring slot coupler, (5) thermal shield, (6) contingency space, tank length: 1.15m flange to flange.

The λ/4 structures have already been modified. A new support structure closes the gaps between the electrode boards (fig. 2) and integrates high power water cooled resistors for kicker operation. Through-holes are no longer needed.

Right from the beginning, the design of the slot ring couplers [6] was influenced by the possibility to install different long stacks into the test tank. The numbers of rings could easily be increased. We used 8 rings for the first test, thus a direct comparison between printed loops and slot ring couplers is possible and the dimensions of the developed Wilkinson combiner board do not interfere with the tank size.

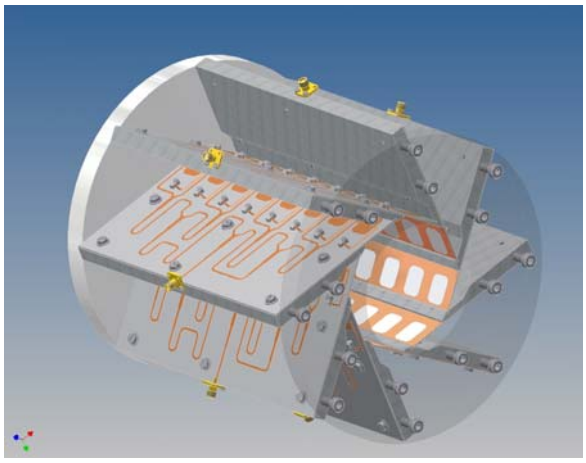

Fig. 2: Modified support with high-power resistors to operate the structure as pickup and as kicker.

Coaxial measurements

The 33 mm inner conductor of a 31/8" RF transmission line has been used to measure the longitudinal sensitivity of both structures in advance at the RF-laboratory. Together with 90 mm inner diameter of the structures a 60 Ohm coaxial system is formed. Both ends of this system are completed by commercial 31/8" to N-norm transitions. A TEM measurement was performed by feeding one transition and terminating the other one. 60 Ohms are close enough to the 50 Ohm of the network-analyzer impedance that reflections will not influence the TEM field very much. The slot coupler is not as wide-banded as the printed loops however it shows a much higher longitudinal coupling impedance than the printed loops, although the length in beam direction is only halved. The measurements are comparable to the simulations [7] taking into account the small losses of the combiner boards.

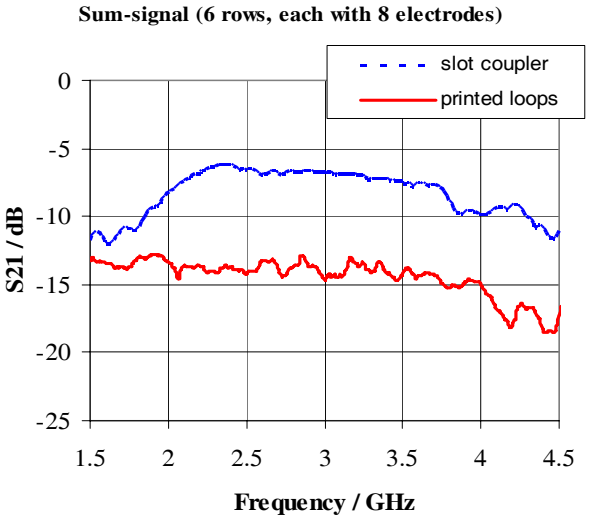

Fig. 3: Transmission from a 60 Ohm coaxial line simulating the beam to the output of the combined electrodes.

Measurements using the COSY beam

Immediately after installing the test-tank into the COSY-ring during the Christmas-shutdown 2007 first measurements of the longitudinal and transverse Schottky-spectra were carried out.

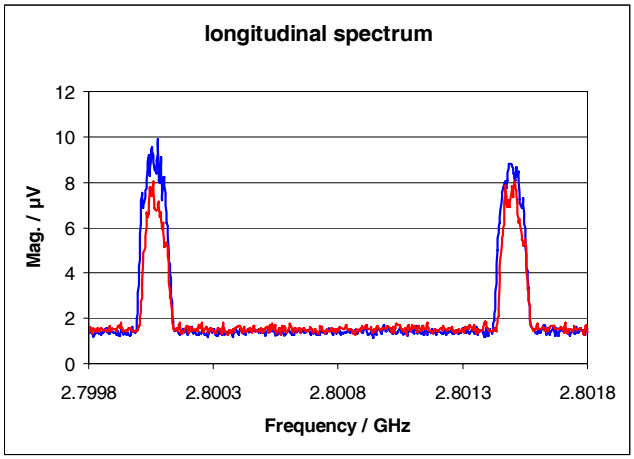

Fig. 4: Red: longitudinal signal of 6 rows λ/4 structure, blue: longitudinal signal of 4 electrode-rows slot coupler

Fig. 4 shows the 1958th and 1959th harmonic of a COSY run with $5 \cdot 10^{10}$ stored protons at a momentum of 1.69 GeV/c. Even with the reduced numbers of combined electrode-rows (4 instead of 6) the longitudinal Schottky signal of the slot coupler are slightly higher. This demonstrates the higher longitudinal coupling impedance together with the fact that the slot structures take only halve of the length of the λ/4 structures.

Betatron sidebands (fig. 5) are already visible although the beta-functions at the installation point of the test tank are relative small and the structure length amounts only 12 cm.

This offers the possibility to use the slot coupler not only for longitudinal cooling but also for transverse cooling. The arrangements of the electrodes allow even the simultaneous cooling of both transverse directions and of course with the sum-signal longitudinal cooling. The temperature inside the test tank was only 100 K. Thus a better signal to noise ratio is expected when the cooling problem of the tank is solved. The design value of the end temperature is about 20-30K.

The high longitudinal coupling of the slot coupler can be even seen by the strong longitudinal fractions in the transverse spectrum when the beam is not centred in the structure (fig. 5: red curve).

The temperature of the structures inside the test tank was only 100 K. In 2008 some mechanical modifications were done to enhance the thermal connections from the cold-heads to the inner structures. The numbers of slot coupler rings was increased to 16 and two neighbouring electrode rows are now combined inside the tank. These combiners are constructed as thermal trap for an additional decrease of heat flow towards the inner structures. The final temperature is now in the order of 50 K. The envisaged temperature of about 20 K seems feasible taking into account the short length of the test-tank and the heat flow by the semi-rigid lines of the λ/4 structures which do not have an additional thermal trap.

During the last beam times in 2008 additional RF-tests were carried out to analyse the transverse sensitivity of the slot couplers which cannot easily be simulated even with 3-d codes. A beam momentum of 2.2 GeV/c was chosen to reduce the value of the frequency slip factor.

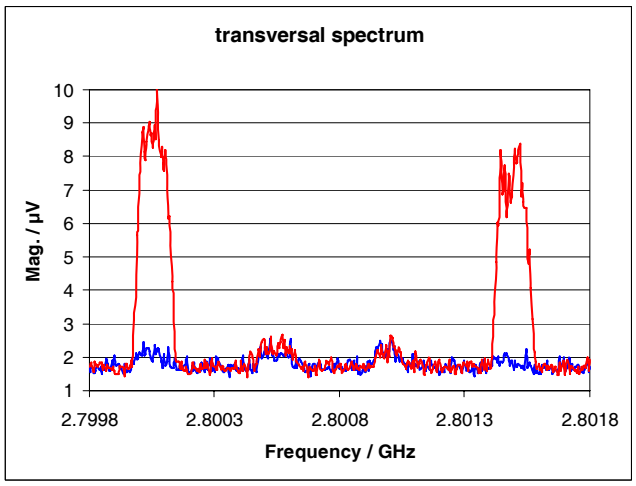

Fig. 5: Transverse spectra of slot coupler in horizontal direction, blue: centred beam, red: ~ 15 mm horizontal offset of beam.

The betatron sidebands of both directions were clearly visible although the beta-functions at the location of the test tank are always small. Different tunes (horizontal: 3.53, vertical: 3.64) were chosen to check whether there will be a coupling within the slot-coupler or not.

A strong longitudinal component can be measured in both directions when the beam is not exactly centred in the test tank (figure 6 and figure 7). Vertical and horizontal steerers were used to centre the beam in the test tank and thus to minimize the longitudinal component. The horizontal eccentricity did not visibly influence the vertical signal and vice versa. The different tune setting allowed a direct control of the coupling. Within the measurement accuracy of the combination of 16 rings no coupling was observed. Compared to the λ/4 structures the slot ring coupler showed the same or even better transverse sensitivity. Thus the same pickup structure can be used to measure the horizontal, vertical and longitudinal cooling direction simultaneously.

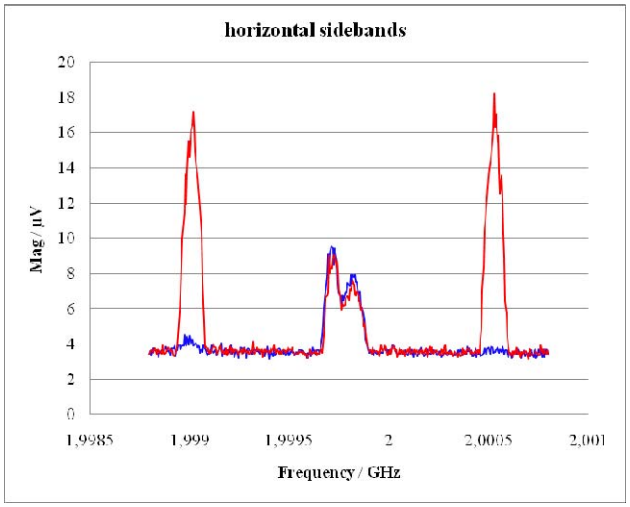

Fig. 6: Transverse spectra of slot coupler in horizontal direction, blue: centred beam, red: horizontal offset.

This is not possible with the λ/4 structures without minor changes in the arrangement and a decrease in sensitivity.

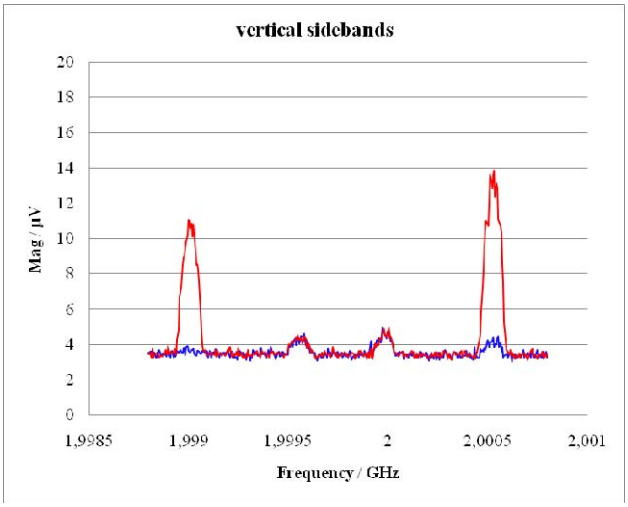

Fig. 7: Transverse spectra of slot coupler in vertical direction, blue: centred beam, red: vertical offset.

Figure 8 shows again the longitudinal comparison of both structures at about 3.1 GHz. In this case the length of both structures in the beam direction is the same. The longitudinal spectra of the λ/4 structure would be a little bit higher by using a 3:1 combiner instead of the available 4:1, but taking into account the number of combined rows (6 rows λ/4, 4 rows slot-coupler) the relation would be nearly the same. Thus, as expected from the simulations, the slot coupler shows in the longitudinal direction a much better performance and is in the transverse plane comparable to the λ/4 structure. This encourages us to use only the slot coupler for all three cooling planes.

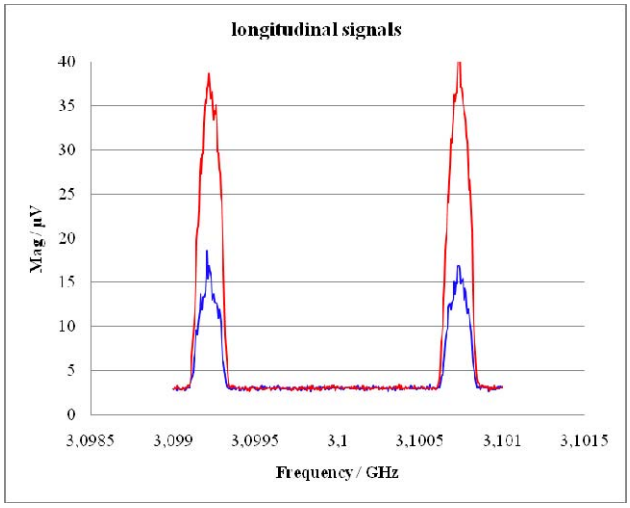

Fig. 8: Longitudinal spectra of slot coupler (red) and λ/4 structure (blue), same length in beam direction.

References:

[1] W.F. Henning, An International Accelerator Facility for Research with Ions and Antiprotons, proceedings of EPAC04, Lucerne, Switzerland

[2] H. Stockhorst, R. Stassen, R. Maier, D. Prasuhn, T. Katayama and L. Thorndahl, Stochastic Cooling Developments for the HESR at FAIR, EPAC2008, Genoa, Italy

[3] R. Stassen, Pickup structures for HESR stochastic cooling system, EPAC2006, Edinburgh, UK

[4] B. Autin, G. Carron, F. Caspers, S. Milner, L. Thorndahl, S. van der Meer, ACOL stochastic cooling systems, proceedings of PAC87, Washington, USA, 1987

[5] C. Peschke, F. Nolden, M. Balk, Planar pick-up electrodes for stochastic cooling, Nuclear Inst. & Methods, A 532, p. 459-464, 2004

[6] R. Stassen, P. Brittner, R. Greven, H. Heimbach, H. Singer, G. Schug, L. Thorndahl, Ring-Slot coupler for the HESR stochastic cooling system, IKP annual report 2006

[7] L. Thorndahl, Fixed 90mm Full-Aperture Structures with TM10-Mode propagation for Stochastic Cooling in HESR, 2006

A. Gillitzer and J. Ritman

The first Physics Performance Report for the PANDA experiment was completed [1]. This report of about 200 pages contains a general introduction discussing the major open questions in quantum chromodynamics, a technical part in which HESR, PANDA detector, and simulation and analysis software are described, and the main part addressing the full physics program of the PANDA experiment. For almost each of the physics topics at least one important benchmark reaction was selected for detailed simulation studies in order to assess the expected sensitivity of PANDA to the corresponding physics observables. For each of the selected reactions the expected most important background channels were also analyzed. The signal reconstruction efficiency and the signal-to-background ratio, in many cases due to the lack of data based on assumed cross sections, were determined. The following physics topics are discussed: charmonium, exotic excitations, heavy-light systems, strange and charmed baryons, non-perturbative QCD dynamics (i.e. reaction dynamics in strangeness and charm production), hadrons in the nuclear medium, hypernuclear physics, structure of the nucleon using electromagnetic processes, and electroweak physics.

Our group contributed the physics content of the sections on heavy-light systems, strange and charmed baryons, and on hadrons in medium as well as the coordination of the corresponding simulation studies.

Heavy-light systems

In analogy to the hydrogen atom in atomic physics, D mesons have two constituents with a large mass ratio. Their excitation spectrum combines aspects of heavy-quark symmetry with the pattern of spontaneous chiral symmetry breaking which is relevant in the light quark sector. The recently discovered narrow states $D_{s0}(2317)$ and $D_{s1}(2460)$ are particularly interesting since they don't fit well into the quark model systematics, and thus challenge the understanding of their nature, e.g. as meson-meson molecules or as tetraquarks. In order to further constrain the different theoretical approaches to describe the two D_s states it is essential to measure their width, for which so far only upper experimental limits have been given. Due to the small $\bar{p}$ momentum spread $\Delta p/p$ of about 10^{-5} at the HESR, the width of the D_s particles can be determined from a measurement of the excitation function in close vicinity of the threshold. The achievable accuracy in this approach is estimated to be of the order of 100 keV, whereas the invariant mass resolution obtained in the reconstruction from the final state particles is typically of the order of 10 MeV.

The simulation studies focused on the reconstruction of the $D_{s0}(2317)$ and the determination of its width in the reaction $\bar{p}p \to D_s^{\pm} D_{s0}(2317)^{\mp}$. Two possible approaches have been discussed:

(*i*) the exclusive reconstruction of the final state with $D_s^{\pm} \to \phi\pi^{\pm}$, $\phi \to K^+K^-$ and $D_{s0}(2317)^{\mp} \to D_s^{\mp}\pi^0$, $D_s^{\mp} \to \phi\pi^{\pm}$, $\phi \to K^+K^-$.

(*ii*) the inclusive reconstruction of the $D_{s0}(2317)$ by missing mass determination with $D_s^{\pm} \to \phi\pi^{\pm}$, $\phi \to K^+K^-$ and $D_{s0}(2317)^{\mp} \to$ anything.

At the present stage only the inclusive approach has been studied since in the exclusive reconstruction based on a single decay branch the small total branching ratio would result in unacceptably low signal rates. As background various specific channels with $D_s^{\pm}D_s^{\mp}$ in the final state as well as an event sample generated with the Dual Parton Model [2] event generator DPM [3] were considered. Based on an assumed cross section of 50 nb for the signal and for $D_s^{\pm}D_s^{\mp}$ background channels signal-to-background ratios of about 2 or 1/40, respectively, were obtained excluding or including the generic DPM background. This indicates that in further studies additional selection criteria based on the $D_{s0}(2317)$ decay have to be applied to achieve the required signal identification. The scan of the excitation function close to the threshold was also simulated for a specific set of parameters, and it was shown that the method allows to deduce the width of the $D_{s0}(2317)$ state in agreement with the assumed input value $\Gamma = 1$ MeV/c^2 (see Fig. 1).

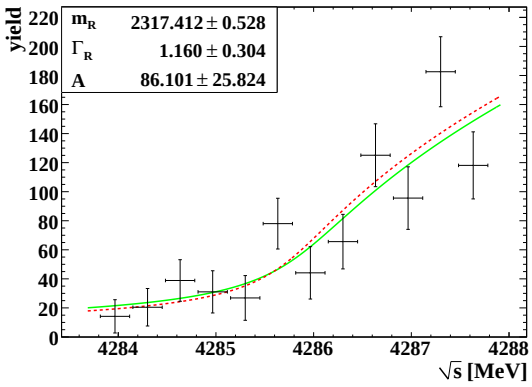

Fig. 1: Fit of the excitation function obtained from the reconstructed signal events, shown by the full green line. The red dotted line shows the excitation function corresponding to the generated events [4].

Strange and charmed baryons

Antiproton-proton collisions are well-suited to investigate the excitation spectrum of (multi-)strange and charmed baryons. In particular, we see a large discovery potential in the very little known spectrum of the double-strange Ξ resonances since the $\bar{p}p \to \bar{\Xi}\Xi$ cross section of about $2\,\mu$b is comfortably large. Studies of $\bar{p}p$ collisions with PANDA are expected to also contribute important information on the spectra of Λ, Σ, Ω, Λ_c, and Σ_c hyperons.

Simulation studies in this context focused on the reaction $\bar{p}p \to \bar{\Xi}^+\Xi^-\pi^0$ with $\Xi^- \to \Lambda\pi^-$, $\Lambda \to p\pi^-$ (+c.c.) which is relevant in the investigation of $\Xi^\star$ resonances coupling to $\Xi\pi$. At the present stage only phase space distributed $\bar{\Xi}^+\Xi^-\pi^0$ events have been generated and analyzed in order to investigate the PANDA acceptance across the full 3-body phase space as well as the achievable signal reconstruction efficiency and signal-to-background ratio. As background the channels $\bar{p}p \to \bar{\Lambda}\Lambda\pi^+\pi^-\pi^0$, $\bar{p}p \to \bar{\Sigma}(1385)^+\Sigma(1385)^-\pi^0$, $\bar{p}p \to \bar{p}p\pi^+\pi^-\pi^+\pi^-\pi^0$, and DPM events have been considered. The result of the simulation study is very promising. For a minimum required distance of the Λ decay vertex

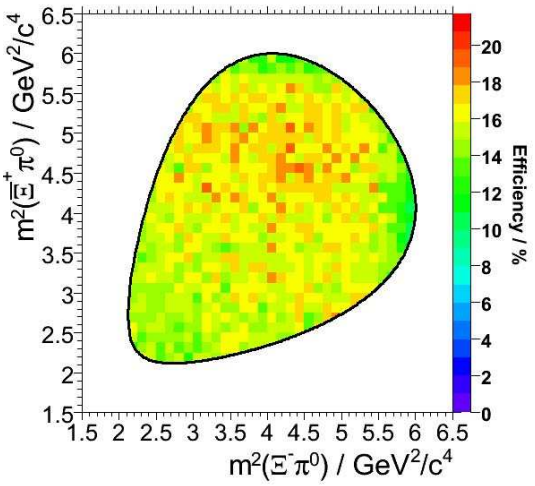

Fig. 2: Dalitz plot showing the reconstruction efficiency for the $\bar{p}p \to \bar{\Xi}^+\Xi^-\pi^0$ reaction [5].

from the primary interaction point between 2 cm and and 6 cm the signal reconstruction efficiency is between about 16% and 14%. It is found that the acceptance of PANDA covers the full $\bar{\Xi}^+\Xi^-\pi^0$ phase space showing only a smooth variation of the reconstruction efficiency (see Fig. 2). The obtained signal-to-background ratio is larger than 20 for all considered background channels.

Hadrons in the nuclear medium

Antiproton-nucleus collisions are well-suited to study a possible modification of the properties of the produced hadrons induced by the nuclear environment. As compared e.g. to proton induced reactions, antiproton induced annihilation processes due to the energy release of twice the proton mass allow to produce hadrons at lower momenta, being thus more sensitive to nuclear potentials. So far experiments addressing the issue of nuclear medium modifications have concentrated on hadrons in the light quark sector. With PANDA this type of studies may be extended to hadrons with charm quarks. However, due to their large mass, complicated reaction mechanisms involving more than a single target nucleon have to be employed in order to implant charmed hadrons in the nucleus at low momenta. In-medium mass shifts of charmed hadrons will therefore be addressed at a later stage of PANDA operation.

In contrast, the measurement of nuclear absorption effects on charmonium states in antiproton-nucleus collisions, in particular of J/ψ or ψ' is conceptually simple. In the considered energy range J/ψ and ψ' absorption is directly related to the dissociation cross section of these states with nucleons. This cross section, particularly its energy dependence, has a large uncertainty, but its knowledge is required in order to interpret the J/ψ and ψ' suppression observed in relativistic nucleus nucleus collisions as a signature for quark gluon plasma formation. With PANDA the J/ψ dissociation cross section can be determined at a well-defined J/ψ momentum in a model-independent way. The J/ψ momentum is given by its resonant formation of the incident antiproton with a nucleon approximately at rest in the target nucleus. In order to avoid assumptions on the Fermi momentum distribution, the $\bar{p}$ beam momentum is scanned across the value corresponding to the maximum J/ψ yield. The dissociation cross section is deduced from the target size dependence of the integrated J/ψ yield using Glauber analysis.

As benchmark channel the reaction 4.05 GeV/c $\bar{p}+{}^{40}$Ca $\to J/\psi + X$ with $J/\psi \to e^+e^-$ has been simulated. As generic background a sample of events generated with the Monte Carlo event generator UrQMD [6, 7] was analyzed for e^+e^- candidates at $M_{ee} \approx M_{J/\psi}$ in the final state. In addition the specific background channel $\bar{p}p \to \pi^+\pi^-$ with a target proton momentum distribution corresponding to the nuclear Fermi momentum has been analyzed for fake e^+e^- candidates.

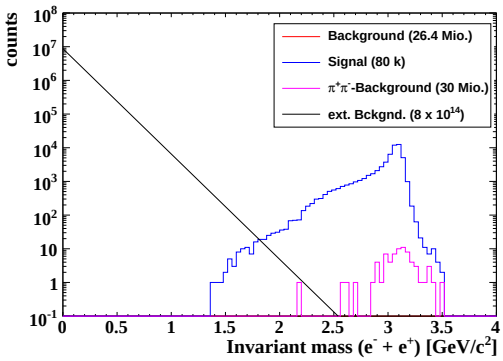

Fig. 3: Invariant mass distribution of e^+e^- pair candidates for signal (blue), UrQMD background (red: no event), and $\pi^+\pi^-$ background (magenta) events. The estimated distribution for a UrQMD background sample scaled up to 10^{10} times the number of signal events is shown by the black line [8].

Since the total antiproton nucleus cross section is of the order of 1 b and thus 9-10 orders of magnitude larger than the signal cross section, a fully realistic simulation study would require to generate and analyze 10^{10} background events for each signal event. This is obviously not possible. The non-observation of any e^+e^- pair candidate with approximate J/ψ mass in the UrQMD background sample thus corresponds to a lower limit in the achievable signal-to-background ratio S/B. With $\sigma_{total} = 0.5$ b and $\sigma_{J/\psi} = 0.3$ nb $S/B > 1.2 \cdot 10^{-2}$ is obtained. Assuming that the shape of the e^+e^- candidate mass distribution remains unchanged after applying kinematical selection criteria appropriate for $J/\psi \to e^+e^-$ signal events (which in fact removes all background e^+e^- candidate events), and scaling the distribution resulting for a single e^+e^- pair candidate to 10^{10} times the number of $8 \cdot 10^4$ signal events, still no background e^+e^- candidate in the J/ψ mass region would be seen (see Fig. 3). For the background reaction $\bar{p}+{}^{40}\text{Ca} \to \pi^+\pi^- + X$ the achievable signal-to-background ratio is estimated to be about 4.

References:

[1] see http://www-panda.gsi.de.
[2] A. Capella *et al.*, Phys. Rept. 236 (1994) 225.
[3] V.V. Uzhisky and A.S. Galoyan, hep/ph-0212369.
[4] K. Goetzen, priv. comm. (2008).
[5] J. Zhong, priv. comm. (2008).
[6] M. Bleicher *et al.*, J. Phys. G25 (1999) 1859
[7] S.A. Bass *et al.*, Prog. Par. Nucl. Phys. 41 (1998) 225.
[8] P. Bühler, priv. comm. (2008).

Missing mass reconstruction of $D_s^*(2317)^\mp$ in the $p\bar{p} \to D_s^\pm D_s^*(2317)^\mp$ reaction

V. Jha, A. Gillitzer and J. Ritman for the PANDA collaboration

Several open charm meson states such as $D_s^*(2317)$ and $D_s(2460)$, have been discovered in recent years which are surprisingly light. The intrinsic width of these states are small enough so that only the upper limits have been measured ($\Gamma \leq 4.6$ MeV and $\Gamma \leq 5.5$ MeV for the $D_s^*(2317)$ and $D_s(2460)$, respectively). Precise measurement of their mass and width is essential to understand the true nature of these states. The PANDA experiment at FAIR will provide a suitable environment to measure the width of these states with much higher precision because of the high quality phase space cooled antiproton beam. We perform a study of $D_s^*(2317)$ signal in the $p\bar{p} \to D_s^\pm D_s^*(2317)^\mp$ reaction with other possible background channels. In earlier experiments the $D_s^*(2317)^+$ has been observed in the $D_s^*(2317)^+ \to D_s^+\pi^0$ decay mode. However, due to the low formation cross section of $D_s^*(2317)^\mp$ in the $p\bar{p} \to D_s^\pm D_s^*(2317)^\mp$ reaction, full reconstruction of the event with sufficient statistics is not experimentally feasible in a resonable time. Instead, by reconstructing the recoil particle D_s, and tagging only some of the decay products of the $D_s^*(2317)$, it is hoped that a sufficiently precise measurement of the width can be performed.

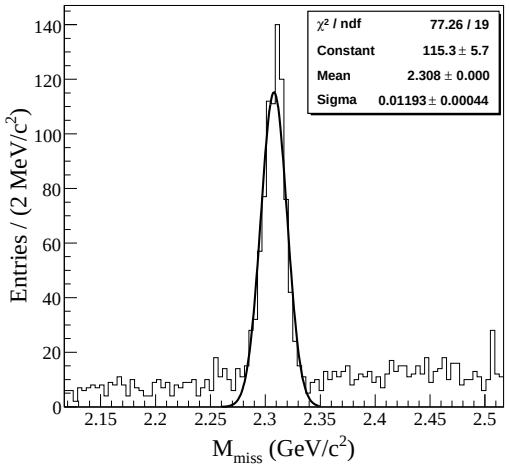

Fig. 1: Missing mass for the $D_s^*(2317)$ obtained from the reconstructed $D_s^\pm$ candidates in the $p\bar{p} \to D_s^\pm D_s^*(2317)^\mp$ reaction.

Simulations have been performed within the Pandaroot framework, to reconstruct the events of the reaction $p\bar{p} \to D_s^\pm D_s^*(2317)^\mp$ at a centre of mass energy of 4.291 GeV, which is ≈ 5 MeV above the threshold energy. The primary $D_s^\pm$ has been reconstructed in the $D_s^\pm \to \phi\pi^\pm$, $\phi \to K^+K^-$ decay modes. For this purpose, the selected pairs of ϕ and $\pi^\pm$ candidates are combined to form the $D_s^\pm$ candidates. Further, the reconstructed mass of the ϕ and D_s mass are required to be within 10 MeV and 30 MeV/c^2 of their nominal values. The missing mass corresponding to reconstructed $D_s^\pm$ candidates is obtained using its four momentum vectors together with the initial energy of $p\bar{p}$ system. The missing mass spectra obtained from the simulation is shown in Fig. 1. As expected, it peaks around the mass of $D_s^*(2317)$.

To estimate the residual background level in the signal region, various decay channels with simliar kinematics to that of the signal channel, have been investigated. We considered those background channels, which involve apart from a the primary $D_s^\pm$ particle, one non-resonant D_s or D_s^* particle and also one or two pions or gammas. The primary $D_s^\pm$ meson was reconstructed from the decays to the same final states like those in the signal events. Assuming similar cross sections for all the background channels, contribution due to $p\bar{p} \to D_s^\pm D_s^\mp \pi^+\pi^-$, $p\bar{p} \to D_s^\pm D_s^\mp 2\pi^0$ and $p\bar{p} \to D_s^\pm D_s^{*\mp}\pi^0$ channels are found to be the maximum.

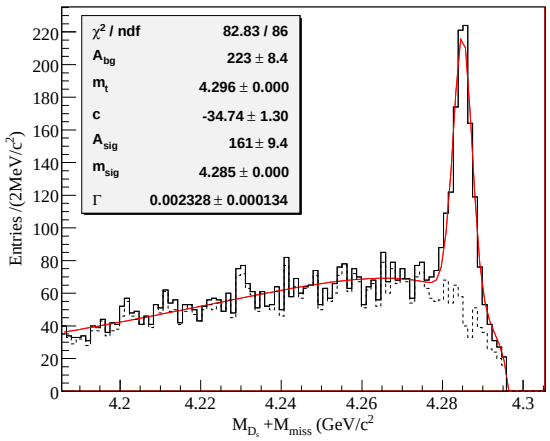

Fig. 2: The sum of missing mass for the $D_s^*(2317)$ M_{miss} and mass of $D_s^\pm$ M_{D_s} candidates for the background (dashed histograms) and signal plus background (solid histograms). The fit is performed by a combination of Argus function (for the background) and a gaussian (for the signal).

Both the missing mass and the invariant mass for the reconstructed D_s particle have relatively poor energy resolution (≈ 12 MeV), but these quantities are highly correlated. This feature can be exploited to use a different observable M_{sum} which represents the sum of missing mass (M_{miss}) and mass of reconstructed D_s (M_{D_s}) candidates . This quantity, which is plotted in Fig. 2., shows a smaller width (≈ 2.3 MeV) for the signal peak as compared to the width of the peak from the missing mass distribution (≈ 12 MeV). In contrast to the signal events, the background events are not correlated, so they are distributed over the mass range. Therefore, a good discrimination between the signal and the background can be achieved from the summed mass (M_{sum}) distribution.

The real signal to background ratio however, is expected to be decided by the generic hadronic background, which has not been considered in the present studies. The reconstruction procedure for the signal and background channels described above can be used to determine the line shape of the excitation function in the vicinity of threshold. The widths of narrow resonance state can be then extracted from the measurement of energy dependant cross section at few energy points near threshold. Simulation studies in this direction are in progress.

The Central Straw Tube Tracker for the PANDA Experiment

P. Wintz, V. Kozlov, S. Orfanitski, J. Ritman and A. Sokolov

The new technique of pressurized, self-supporting, straw double-layers developed for the COSY-TOF tracker [1] has also been adopted for the PANDA Straw Tube Tracker (STT) for its unique feature of highest mechanical stability at lowest weight. The STT as the PANDA [2] central tracking detector consists of a set of two semi barrels with an inner radius of 150 mm, outer radius of 420 mm and length of 1500 mm along the beam axis, mounted around the intersection point of horizontal beam pipe and vertical target pipe. The cylindrical detector volume is filled by close-packed, planar double-layers of 4200 straw tubes arranged in a hexagon shape (see Fig. 1). The outer gap between hexagonal and circular circumference is filled by single layers.

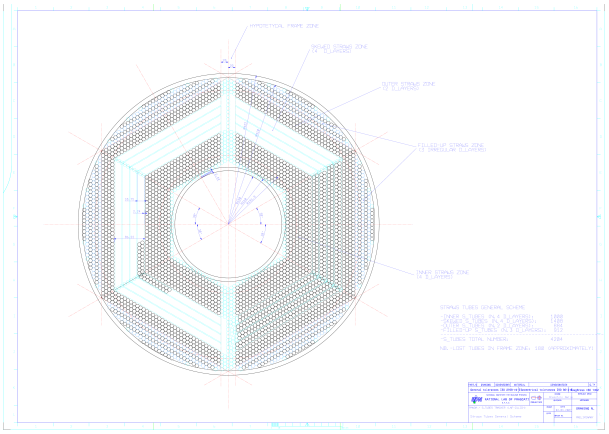

Fig. 1: Cross-section layout of the PANDA Straw Tube Tracker. Some double-layers of the skewed geometry were left out for better view. The CAD file was created by Dario Orecchini (INFN Frascati).

The straws are made of two layers of aluminised mylar film strips, wrapped around a mandrel and glued together to tubes of 10 mm inner diameter and 1500 mm length. The glued film has a wall thickness of 27 μm. Extensive tests of several film types with different wrapping technique and thickness have been performed at IKP. The chosen film tubes are the thinnest used for straw detectors, but still show sufficient mechanical stability for the assembly to self-supporting double-layers.

The STT reconstructs particle tracks in three dimensions by two blocks of axially oriented layers and a block of skewed double-layers (skew angle $\pm 3^o$). The proposed weight of tubes and mechanical frame structure for a semi barrel is below 25 kg. The expected spatial resolution confirmed by test measurements for the COSY-TOF straws [3] is about 150 μm ($\sigma_{r\phi}$) and 2.9 mm (σ_z). Together with the low detector radiation length of X/X_0=1.2% a momentum resolution from simulation of about 1% (σ_{p_t}/p_t) is reached.

The PANDA-STT development will benefit from the experience and results gained during the construction and operation of the COSY-TOF straw tracker which was installed and commissioned in 2008 [4]. In particular, calibration and tracking methods developed for COSY-TOF can be an input for the PANDA-STT since the geometry of the straw tubes and planar double-layers is the same for both detectors.

The end plug design developed for the COSY-TOF straw tracker has been slightly improved for the PANDA straws (see Fig. 2). A new precision snap ring made of POM (polyacetal) thermoplastic is used for better position fixing of the end plug. All designs were developed at IKP. The end plugs from ABS thermoplastic are made by extrusion moulding.

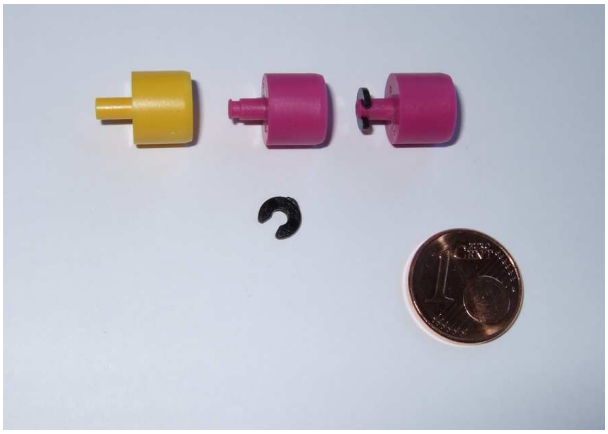

Fig. 2: Old (yellow) and new (purple) end plugs with an additional snap ring (black) for improved fixing of the plug. All designs were developed at IKP.

In April 2008 a technical workshop at IKP was organized to introduce collaboration groups from INFN Frascati (Italy), INFN Ferrara (Italy) and Krakow University (Poland) to the straw assembly technique developed at IKP. About 500 straws were assembled and glued to double-layers at IKP and then sent to Frascati to setup a prototype close to the PANDA-STT straw geometry.

A prototype built at IKP was sent to the Cracow group to develop and test electronic readout options. In the meantime the PANDA collaboration decided to switch for the PANDA forward trackers from Multi-Wire-Proportional-Chambers (MWPC) to straw tube layers based on the design and technique developed at IKP. Using a proton test beam at COSY it was demonstrated that the straws could cope much better with the high particle rates expected at PANDA than a MWPC test detector [5].

References:

[1] P.Wintz, AIP Conf. Proc. 698:789-792, 2004.
[2] M. Kotulla et al., PANDA Technical Progress Report, http://www-panda.gsi.de/archive/public/panda_tpr.pdf, 2005.
[3] P. Wintz et al., Resolution and Efficiency of the Straw Tracker for COSY-TOF, IKP Annual Report 2004.
[4] Commissioning of the COSY-TOF Straw Tracker, IKP Annual Report 2008, p10.
[5] P. Wintz et al., Aging Tests of Straw Tubes for the PANDA-Experiment, IKP Annual Report 2007.

M. C. Mertens, J. Ritman and T. Stockmanns

During the research and design phase of the PANDA MVD, a powerful test system is needed for the tests of frontend electronics. Thus, we developed a modularly designed digital readout system based on a reconfigurable digital readout board featuring a powerful Xilinx Virtex 4 FPGA.

A standard PC which is equipped with a SIS 1100 optical gigabit link is used to connect to the digital readout board and provides enough computing power for data control and acquisition.

The currently connected device under test is an Atlas frontend type FE-I3 which is used for the silicon pixel detectors of the Atlas experiment at CERN. This chip already features integrated analog-to-digital-converters via time-over-threshold determination and a purely digital external interface eliminating the need for external analog circuitry.

The corresponding support board which carries the FE-I3 features a 3.3V LVDS interface and thus can be directly connected to the LVDS I/O panel of the digital readout board, using only a very simple interconnect adapter to match the connectors.

In order to verify the basic functionality of the frontend chip, an automated register test can be executed with the digital readout system. Throughout this test routine, known data is written to each of the frontend chip's global configuration registers as well as each of the individual configuration registers of the pixel cells. The same data is then read back from the registers on the frontend chip and compared with the known values.

The next step is to determine the analog performance of the pixel cells found on the FE-I3. For this purpose a threshold scan is used.

Each pixel converts an analog input signal into digital data by measuring the time in clock units the signal is larger than a reference signal (threshold). This information is proportional to the amplitude of the analog signal (time over threshold, TOT).

The response of a pixel to charge deposition can be characterized in terms of its threshold and its noise. If there was no noise at all, the pixel response would be a step function with no pixel response at all below threshold, and full response above threshold. However, in a real system which is subject to noise, the step function is smeared to an error function.

A threshold scan is executed by injecting a known charge repeatedly into the pixel.

For this purpose, each pixel features a set of injection capacitors which transform an external voltage step into a charge which is fed into the preamplifier circuit of the pixel cell.

The percentage of how often a hit is actually detected is recorded as a function of injected charge (Fig. 1). From these data, the pixel's threshold and noise can be extracted.

In Fig. 2, the threshold distribution of all the pixels on a frontend chip is shown. The variation of the threshold results from the individual thresholds not being tuned but instead all being set to the same nominal value. In practice, the data gained from this test is used to tune the individual thresholds in such a way, that the observed pixel response to charge injection would be the same, or at least as similar as possible, for all pixels.

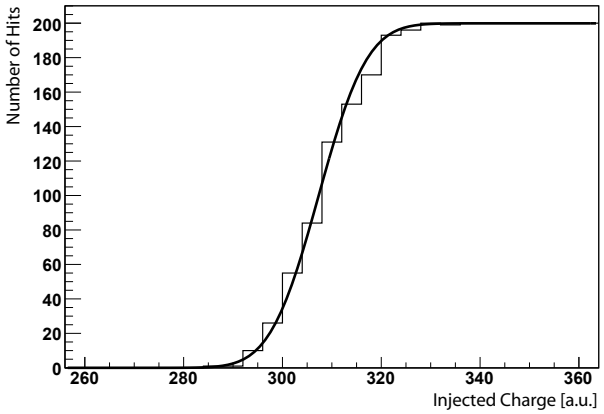

Fig. 1: Threshold scan results of a single pixel on an Atlas FE-I3. The response (total count of reported hits) of a single pixel to a threshold scan with 200 iterations per injected charge is shown. An error function has been fitted to the data. Image taken from [1].

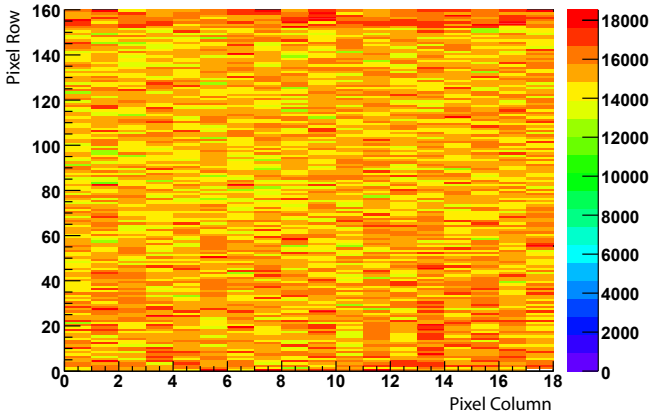

Fig. 2: Threshold scan results of all FE-I3 pixels arranged in 18 columns and 160 rows. The threshold distribution of the individual pixels for an uncalibrated frontend chip are plotted in arbitrary units. Image taken from [1].

Another important property is the dependence of the measured TOT value on the injected charge. Although this dependency is not exactly linear,a linear function describes the data sufficiently well. In Fig. 3 the response of a single pixel as a function of the injected charge is shown.

The slope of the TOT data as a function of the injected charge characterizes the pixel's gain. Fig. 4 shows the distribution of the gain of all pixels on a frontend chip.

With these measurements the basic functionality of the FE-I3 is verified. Further tests need to be done in order to assess the performance of the chip.

The next application is the connection of the ToPiX frontend chip prototype to the digital readout system. This frontend chip is specifically designed for use in the PANDA MVD and is currently under development at INFN Torino. Both its

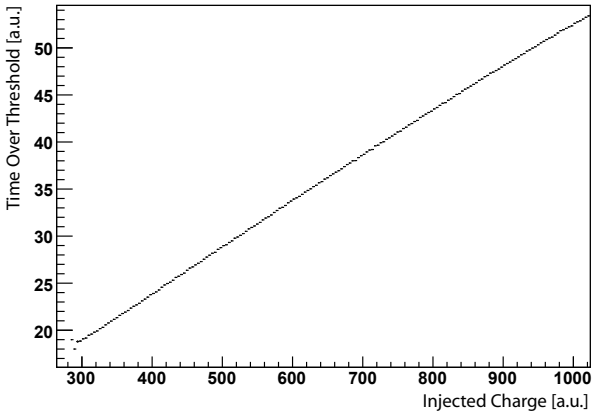

Fig. 3: Result of the time over threshold measurement (arbitrary units) as a function of the injected charge (arbitrary units) for a single pixel. A linear function has been fitted to the data.

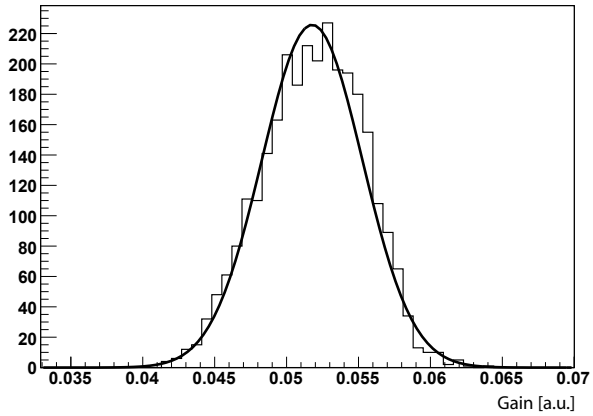

Fig. 4: Gain distribution of all FE-I3 pixels. The distribution of the slope of the TOT measurement as a function of injected charge (arbitrary units, see Fig. 3) is shown. A Gaussian bell curve has been fitted to the data.

communication protocol and electrical specifications are different from those of the Atlas FE-I3. Thus, a new adapter board which features a logic level conversion circuit was designed to connect the ToPiX frontend to the digital readout board. Currently, the adapter board itself is undergoing performance tests and has proven to yield clean signals at frequencies up to 100 MHz.

References:

[1] M. C. Mertens, F. Hügging, J. Ritman, and T. Stockmanns. A versatile digital readout system for the PANDA MVD. In *IEEE Conference Record NSS-MIC-RTSD*, pages 3430–3433, 2008.

Radiation damage studies for the $\overline{\text{P}}$ANDA Micro Vertex Detector

T. Stockmanns*, M.C. Mertens, J. Ritman and Y. Shaposhnik

One major component of the approved **F**acility for **A**ntiproton and **I**on **R**esearch (FAIR) at the GSI in Darmstadt is the **H**igh **E**nergy **S**torage **R**ing (HESR) with the "Anti**P**roton **AN**nihilations at **DA**rmstadt" - experiment ($\overline{\text{P}}$ANDA). The HESR will provide an intense, phase space cooled antiproton beam of unsurpassed quality. A momentum range up to 15 GeV/c together with an average interaction rate of 10 MHz will allow the detailed study of a wide variety of topics, such as the structure of hadrons in the charmonium mass range, the spectroscopy of double hyper nuclei and electromagnetic processes.
An ongoing activity of the IKP for the $\overline{\text{P}}$ANDA detector is focused on the design of the Micro Vertex Detector (MVD). The MVD plays a key role in the PANDA experiment to identify open charm and strangeness by detecting secondary decays of particles displaced from the primary interaction point. These decay lengths range from several 100 μm for charmed mesons and baryons up to several cm for strange hadrons.

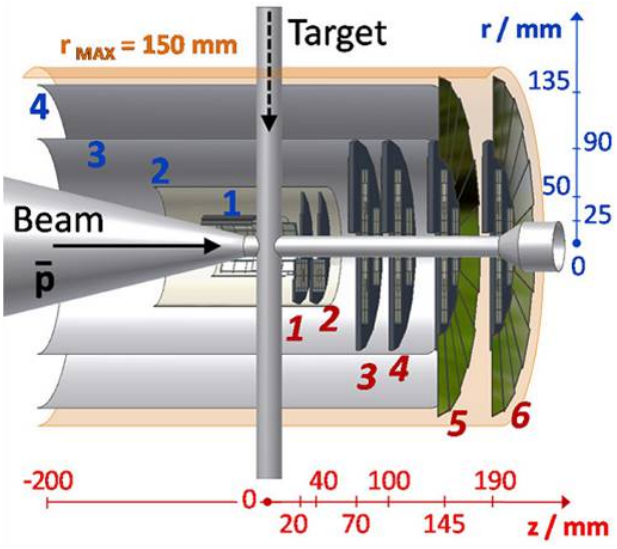

Fig. 1: CAD model of the Micro-Vertex-Detector(MVD).

The MVD is only separated from the interaction region by the beam-target pipe (Fig. 1). The MVD consists of two barrel layers of pixel detectors and two layers of double sided strip detectors. In the forward direction it has six additional disks made out of pixel and strip detectors. A couple of design decisions of the MVD strongly depend on the expected radiation dose, such as the materials which can be used to build the detector or the operation temperature. A previous estimate of the radiation dose was based on two different event generators simulating the basic processes in a collision of an antiproton-beam with a hydrogen target and heavier nuclear targets.
Significant progress has now been achieved to optimize the event generators to include more physical processes on one hand side and in the design of the MVD on the other hand side. Therefore, the radiation damage studies were reiterated. For the simulation different settings were used: $\bar{p}p$ Geant-3 at 5 GeV/c, $\bar{p}p$ Geant-4 at 5 GeV/c, $\bar{p}p$ Geant-3 at 15 GeV/c, $\bar{p}Au$ Geant-4 at 4.05 GeV/c

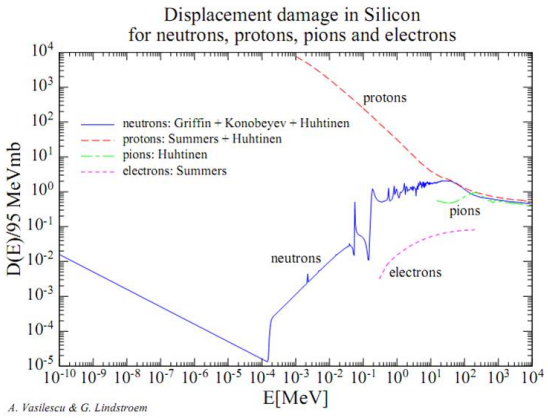

Fig. 2: Displacement damage for different particle types and energies.

The outcome of the Monte-Carlo simulation is the information which detector element was hit where, by how many particles, their type and energy. The damage these particles generate in the detector strongly depends on the type and the kinetic energy of these particles. To get comparable results one normalizes the damage of a single particle to the damage a neutron with a kinetic energy of 1 MeV would do via a hardness factor which is shown for the most important particle types in Fig. 2.
Normalized to the area and multiplied with the expected operation time of $\overline{\text{P}}$ANDA one gets the total expected 1MeV neutron equivalent particle flux which should not be higher than $5 \cdot 10^{14}$ $[n_{eq}/cm^2]$. For the operation time it is assumed that $\overline{\text{P}}$ANDA will operate with $2 \cdot 10^7$ antiproton collisions per second with the hydrogen target and approximately 1/10 of it with a nuclear target. In addition a duty cycle of 50 % per year is assumed.
Table 1 shows the maximum flux in the barrel part and the forward disk part for the different target materials, beam momenta and particle propagators. The maxima in the flux are always at the detector layers which are closest to the interaction point, as expected. The maximum flux is in the barrel part and it is two to eight times higher then in the forward part and reaches a maximum of $4.5 \cdot 10^{13}$ $[n_{eq}/cm^2]$ for $\bar{p}Au$ collisions, which is close to the critical boundary of $1 \cdot 10^{14}$ $[n_{eq}/cm^2]$. For antiproton-proton collisions the flux is approximately two times lower than for the antiproton-gold reactions.

Simulation results

inter.	sim.	beam mom. [GeV/c]	max. disk $[n_{eq}/cm^2]$	max. barrel $[n_{eq}/cm^2]$
$\bar{p}p$	G3	5 GeV/c	$5 \cdot 10^{12}$	$2 \cdot 10^{13}$
$\bar{p}p$	G4	5 GeV/c	$5 \cdot 10^{12}$	$2 \cdot 10^{13}$
$\bar{p}p$	G3	15 GeV/c	$7 \cdot 10^{12}$	$1.6 \cdot 10^{13}$
$\bar{p}Au$	G4	4.05 GeV/c	$6 \cdot 10^{12}$	$4.5 \cdot 10^{13}$

Table 1: Expected maximum neutron equivalent flux for one year of $\overline{\text{P}}$ANDA operation

Digitization for the Silicon Strip Detector of the Luminosity Monitor for the PANDA Experiment.

T. Randriamalala, J. Ritman and T. Stockmanns

The elastic $\overline{p}p$ scattering process will be taken as the reference channel for the luminosity monitoring of the PANDA experiment. A silicon strip telescope located between $z \simeq +10\ m$ and $+12\ m$ downstream from the interaction point is conceived. This will allow the Coulomb interaction part of the process in which antiprotons are scattered to polar angles below $\sim 8\ mrad$ to be measured.

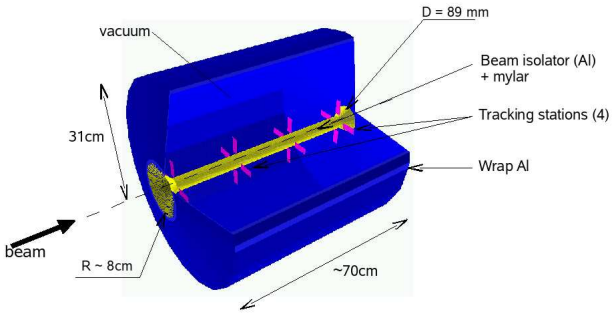

FIG. 1: Schematic overview of the luminosity monitor.

It consists of four tracking stations placed one after the other along z-axis direction, each consists of four double-sided sensors (2 cm x 5 cm x 30 μm with 50 μm pitch) arranged radially from the beam axis. The distance between two consecutive planes is 20 cm.

Performance studies of this luminosity monitor are performed within the pandaroot framework. Tracks are selected where the outgoing antiproton hits all the four stations. Since the tracks are nearly normal to the surface of the sensors, most of the charge deposited in one sensor is collected by no more than two strips.

The digitization considers the charge per hit to be shared among the strips fired depending on the path length they contain, then diffused over the sensor by a Gaussian distribution with 8 μm width. This last is considered as the drift of the electrons and holes process model to each strip. As a result, if the charge expands to more than one strip, the ratio of the charges $Q_r/(Q_r + Q_l)$ (the index r stands for right and the index l for left of a cluster) becomes non-linear and has a "S" curve (see FIG.2b). The total charge deposited follows a Landau distribution with an average of 80 keV for sensor thickness of 300 μm (see FIG.2a).

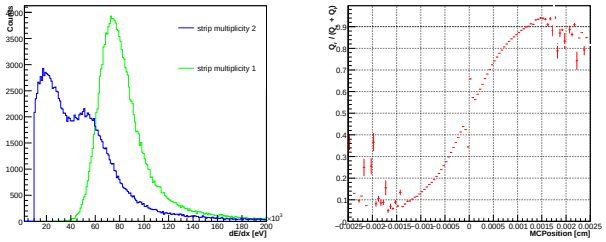

(a) (b)

FIG. 2: (a) Charge deposited in the sensor for strip multiplicity one (green) and more the one(blue), including noise of 5 keV and setting a threshold of 10 keV. (b) Charge ratio $Q_r/(Q_r + Q_l)$ between left and right in a cluster. The value 0 in the x-axis corresponds to the between two strips.

For the clusters with strip multiplicity one, the reconstructed position is the center of the strip fired. When charge is shared among several strips, the reconstructed position is obtained by fitting the curve in FIG 2b. The position resolution is determined to be 10 μm for strip multiplicity one and 2 μm for strip multiplicity two or more.

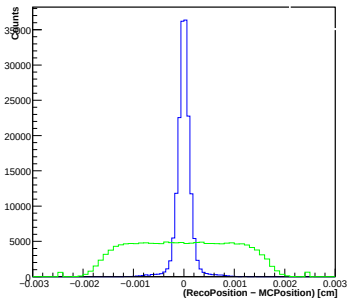

FIG. 3: Difference between the reconstructed position and MC truth position, green corresponds to strip multiplicity one and blue to strip multiplicity larger than one.

Conceptual design of the luminosity monitor for PANDA was established by exploiting the elastic $\overline{p}p$ scattering. A simulation program is ongoing in order to optimize the detector layout.

Latest developments for the Moscow-Jülich pellet target*

A.Boukharov[a], M.Büscher[b], V.Chernetsky[c], P.Fedorets[b,c], A.Gerasimov[c], A.Semenov[a]

During 2008 main efforts of the pellet-target group aimed at two important issues: improvement of the target-operation times by decreasing residual impurities and stabilisation of the thermodynamic parameters in the cryostat.

Even small amounts of residual impurities dissolved in the main target gas (hydrogen, nitrogen, argon etc.) lead to the formation of crystals in the gas flux during cooling. These crystals follow the liquid stream into the nozzle and may block it. This effect is illustrated in Fig. 1 when hydrogen with 7.0 purity is used. The stable straight jet (Fig. 1a) after some time starts to curve (b) and later disappears completely (c).

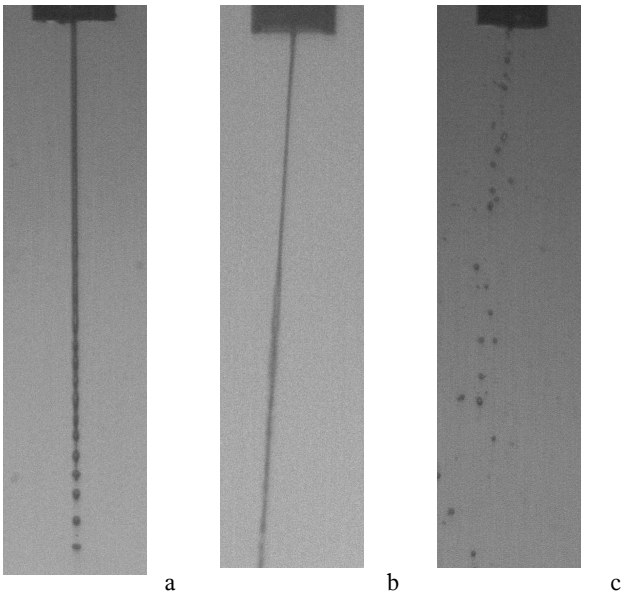

Fig. 1: Nozzle blocking caused by sedimentation of impurities in the target-gas flux(hydrogen 7.0).

In order to determine the kind and amount of impurities, several measurements with hydrogen 7.0 have been carried out. The hydrogen is cooled, liquefied and a stable jet is produced at the nozzle outlet. In the moment of nozzle blocking the main hydrogen flow is switched off and the cryostat is warmed up to room temperature. As the temperature rises inside the cryostat, the impurities start to evaporate and the pressure above the nozzle increases. This leads to rapid pressure rises when the evaporation temperature of a certain substance is reached. The impurities can thus be detected with a pressure gauge as a function of the nozzle temperature. As an example, Fig. 2 shows the results of such measurements after two different target operation times.

Main conclusion is that the purity of the target gas crucially determines the target operation time. Lowest possible levels of gas impurities must be aimed at. As the next step the necessary gas purity level for long target operation are being defined, and the construction of an additional gas cleaning system has already begun.

In a second set of experiments we have investigated the temperature stability of the helium vapors that are used to liquefy the the target gases in the condensor. Figure 3 shows the measured vapor temperature in dependence of the liquid helium cooling-bath level inside the cryostat. It can be seen that for stabilization of the vapor temperature — and finally of the sizes of the droplets and pellets — it is necessary to maintain a constant liquid helium level. In the future a dedicated system, comprising a helium siphon and an automatic helium valve, will provide the required constant helium level.

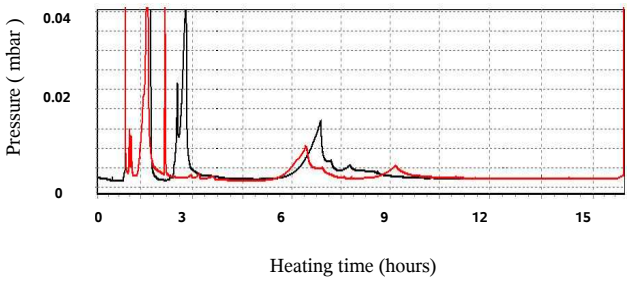

Fig. 2: Measured pressure over the nozzle as a function of the heating time after 2 (red) and 4 (black) hours of target operation.

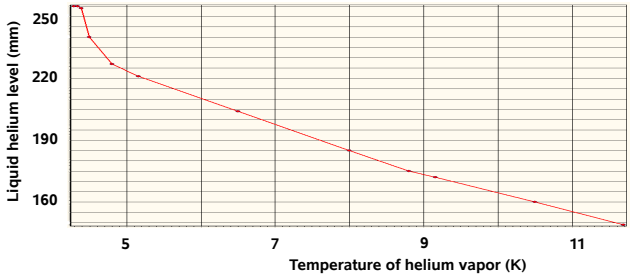

Fig. 3: Influence of the liquid helium level on the helium vapor temperature.

Further tests during the year 2008 have been devoted to the development of stable regimes for hydrogen (nitrogen) droplet production at high jet velocities. For these studies a new droplet generator with maximum frequency of 120 kHz has been used. Stable jet disintegration has been observed at a frequency of around 100 kHz (90 kHz) for hydrogen (nitrogen) at jet diameters of around 17 μm. Solid granules passing through the sluice have been observed in parallel.

[a]MPEI, Moscow, Russia
[b]IKP & JCHP, Forschungszentrum Jülich
[c]ITEP, Moscow, Russia
*Supported by grants INTAS 06-1000012-8787, DFG 436 RUS 113/948/0-1, DFG 436 RUS 113/975/0-1, COSY-FFE-095, EU-FP6, RFFI 07-08-00747, RFFI 08-08-91950-NNIO.

5 Technical Developments

Electronics Laboratory

C.Berchem, N.Dolfus, W.Ernst, H.Metz-Nellen, M.Nau, R.Nellen, J.Sarkadi, H.Schiffer, T.Sefzick

The activities of the IKP Electronics Laboratory can be assigned to mainly the following three topics:

Electronics and Data Acquisition for experiments

Installation of servers for storage and analysis of data taken by the TOF experiment was supported. This included an extension of the internal computer network, required for control and read-out of the newly installed STRAW chambers, which was coordinated by us in collaboration with the ZEL. The S7 based vacuum control system was modified and extended. High density vacuum tight signal feedthrough boards made of specially blackened PCB material were developed, designed and produced for the STRAW detector.

For the spectator detector at ANKE 72 power supplies, needed for the preamplifiers, were reworked. The Labview based control program needed to test the silicon microstrip detectors was improved. Production of ADCs was supervised. Development and production of test units for the wire chambers was supported as well. Printed circuit boards for the Gas Electron Multiplier (GEM) detector were designed. Design und production of frames for large wire chambers was done.

The atomic beam source (ABS) setup for the polarized internal target (PIT) was checked under beam time conditions at the ANKE experiment, desired modifications were done, the process visualisation was improved. Axis speed measurements at the X-Y table of the positioning system were carried out.

For the beam quality test purposes at the PAX experiment the air-cooled dissociator has been replaced with a liquid cooled microwave one. New devices (Lauda flow-in, flow-out and bath temperatures, cooling liquid flow measurements) were implemented into the interlock system. Due to the change of the dissociator, modifications of the interlock system were necessary. The cabling of the complete Breit-Rabi polarimeter and the target chamber systems was finished. These components were integrated into the control interlock system of the ABS setup, the PLC program code was adapted. Process visualisation using WinCC was prepared. First measurements were supported. The patch fields needed for electrical supply of the PAX experiment together with the needed cables were produced.

Additional splitter boxes for the WASA experiment were produced. Voltage distributor PCBs for preamplifiers and discriminators at the FPC detector were designed and produced. A prototype for a new photomultiplier base for the central detector was developed. Used photomultipliers and bases were tested for usability. The electronic lab assisted in purchasing needed materials. Installation of servers for storage and analysis of data taken by the experiment was supported. This included an extension of the internal network infrastructure.

Protoypes of bus interfaces for the Topix based readout system at the PANDA experiment were developed.

For the ATRAP-II experiment pre-amplifiers were repaired and 16-fold photomultipliers were tested. The electronic lab assisted in maintenance and repair of the power supplies for the superconducting Penning trap coils.

Printed curcuit boards as detectors for laser experiments at the university of Düsseldorf were designed.

COSY diagnostics

A finepitch printed circuit board was developed for the FROST64 readout of a beam induced flourescence monitor together with test boards for selection of appropriate photomultipliers.

Maintenance was provided for the multi-wire chambers for beam diagnostics in the extraction beamlines und for the viewer cameras. This also included repair of broken components, e.g. power supplies.

Computer network

After planning and measurements the installation of wireless LAN access points in the institute and cyclotron buildings has been completed. At several location the fiber based network was extended. Frequent support was granted to ensure continuous operation of the existing networks.

Miscellaneous

Like every year substantial support was given with regard to short term maintenance and repair or replacement of electronics. In some cases the urgent demand didn't allow a time consuming outside repair procedure, in other cases the manufacturer doesn't even exists anymore, but the electronics can not be replaced easily, or the manufacturer was unable to perform the repair.

Prototypes and small series of cables or electronics, for which an outside production would not have been reasonable, were delegated to infrastructure facilities or done here, mainly by trainees and student auxiliary workers.

The standard data acquisition systems at several COSY experiments were taken care of to assure stable operation during several beamtimes.

Regarding S5 and S7 systems continuous support was given to the experiments TOF and WASA, the radiation safety division, and to the cyclotron group.

Part time supervision of BSc and MSc students of the FH Aachen was provided in the field of process automation.

Maintenance of the IKP webpages is ongoing, future modifications of the pages await further specifications from the public relations office.

Administrative activities for the safety inside the institute were carried out.

A versatile setup for studies of tracking and particle identification with drift chambers and GEM amplification stages

V. Serdyuk[1,2], W. Erven [5], P. Kulessa[4,1], J.Majewski[3], H. Ohm[1], K. Pysz[4,1], P.Wuestner [5], S. Dymov[2,6], D. Tsirkov [1,2]

Gaseous tracking detectors play a key role in existing and planned hadron and particle physics experiments. A universal device has been set up for optimizing the tracking performance of existing (ANKE at COSY, WASA at COSY) and for developing new concepts (PANDA@FAIR). In previous reports [1], [2], [4] a detector containing a Gas Electron Multiplier [3] was inserted in a drift chamber (GEM DC) for tracking and charged particle identification (PID) by multiple ionization measurements was (fig.1). Here we present new results on the development of this device and measurements performed with the use of Fast QDC - a flash ADC with a sampling frequency of 160 MHz (WASA at COSY experiment).

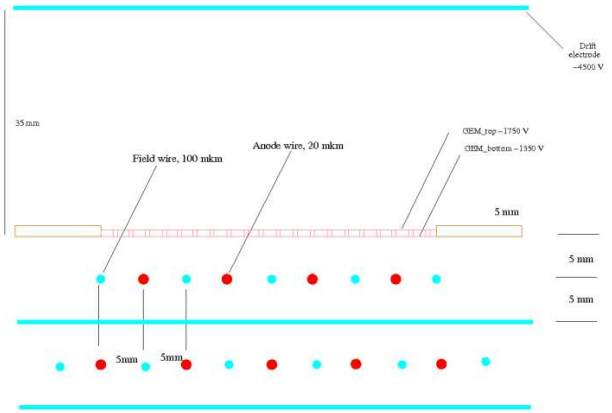

Fig. 1: The geometry of the GEM DC chamber

For the flexibility of investigations three independent high voltages are applied to GEM DC: a drift potential, a top GEM potential, and a common potential on the bottom GEM electrode and cathode. The last potential defines the gas amplification in a drift chamber on the wires, while the first and second provide the drift electric field and the amplification inside the GEM foil. The main functions of the introduced GEM stage is to improve the single electron sensitivity and to provide more performance flexibility. The overall charge amplifications of the detector can be shared between the preamplification in the GEM itself and the amplification on the anode wires. Since the majority of ionization clusters are single electrons this additional amplification in GEM can be critical to improve the efficiency of cluster registration. Keeping a relatively small GEM amplification [5] provides an efficient suppression of the positive ion backflow into the drift volume - one of the major problem in Time Projection Chambers (TPC) especially for high rate applications. The GEM foil forms a sharp transition region between low drift field in a drift volume and relatively high field in the volume of the drift chamber providing a time expansion of the distances between ionization clusters. With appropriate settings of the electrode potentials an adjustment of the drift velocity, electron diffusion, overall charge amplification and transfer can be investigated and optimized. A signal induced on the bottom GEM electrode can be also used for trigger purposes.

In addition a module of a 6 plane drift chamber and a module of a 2 layer straw tube detector (ANKE at COSY) are placed on the top and bottom around the GEM DC together with two scintillation counters for cosmic ray triggering and external tracking.

In the GEM DC signals from anode wires were registered using a fast transresistance current amplifier with a gain of 10 $mV/\mu A$ and a risetime of about 8 ns. The bipolar signals are then transfered into unipolar ones by a booster amplifier [6] and through coaxial cables are sent to the FQDC [7] where the digitization is done. The FQDC has a FPGA programmed algorithm which identifies the number of pulses in the readout window (up to 40 pulses in a window of 6.4 μs maximal width) and analyzes the time position, amplitude and charge of each pulse.

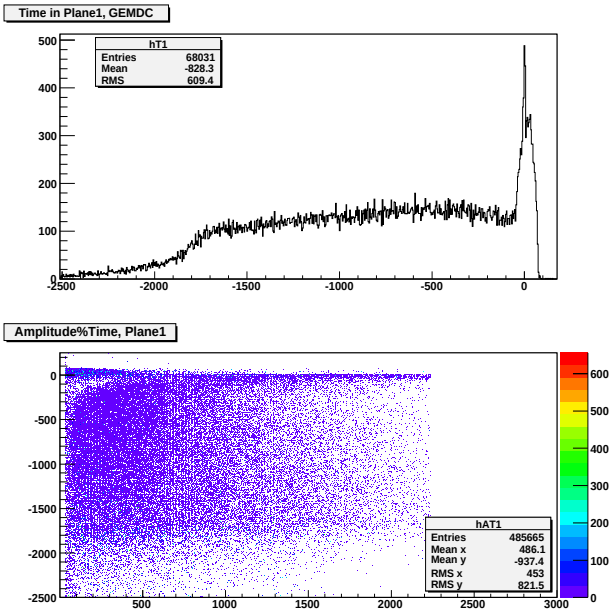

Fig. 2: Time spectrum (top), Amplitude time - correlation (bottom), high voltage on GEM 400V, drift field $E_{dr} = 42.9\,V/cm$

Cosmic ray data were obtained with the following high voltage settings: cathode and GEM_{bottom} - 1.4 kV, GEM_{top} - 1.8 kV, drift - 1.95 kV. This corresponds to a GEM voltage of 400 V, and $E_{dr} = 42.9\,V/cm$.

The relatively low drift field assures for this gas mixture ($80\%Ar + 20\%C_2H_6$), higher cluster registration efficiency due to low drift velocity and therefore bigger time intervals between ionization clusters.

The time spectra and correlations amplitude-time, amplitude - number of pulses and time - number of pulses (fig.2, fig.3) are presented for one selected central channel. The wide region spreading practically from T=0 till the maximum negative limit corresponds to the maximum drift time which depends on the drift velocity and therefore on the drift field. This is a basic working domain for the registration of the ionization clusters produced in the drift volume.

Several identical GEM DC modules consecutively rotated by 90 degrees (X-Y-X-Y) for better pattern recognition can be exploited for particle ionization measurements and tracking together and complementary with an external tracking device

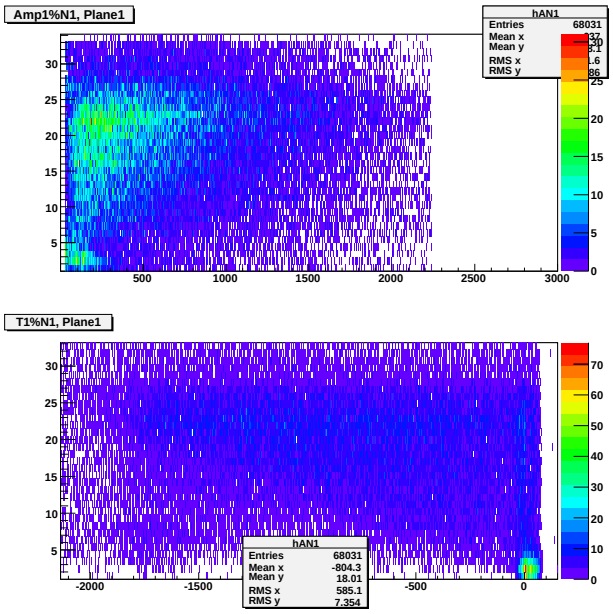

Fig. 3: Correlations amplitude- number of pulses (top), time - number of pulses (bottom), high voltage on GEM 400V, $E_{dr} = 42.9\,V/cm$ drift field

or without it. Each module represents in some sense a small one projectional TPC. One additional DC plane will provide a coordinate point in order to fix together with GEM DC itself the track crossing point in the GEM DC anode plane. Combining the information from other modules this permits the spacial track angle determination. Track fitting with hits from ionization clusters will be performed. Some preliminary calibration procedures would be necessary in accelarator beam test runs to obtain precise correction for the time - coordinate relation. During this calibration the drift times will be associated with the cluster z-coordinate (along the beam direction) for tracks with different angles. At the same time a flash ADC will provide in addition to time positions the amplitude, the charge and the number of clusters. Two methods can be applied simultaneously and independently [8], [9] to measure the particle ionization loss (dE/dx). The truncated mean method provides the dE/dx estimator by excluding the measurements (i.e. clusters) with highest energy depositions (from 40% to 60% of the highest amplitudes) and calculats the mean value of the remaining samples. Thus the contribution of the long Landau distribution tail is reduced and the PID resolution is improved.

In the second method the number of clusters per particle track is taken as an estimator of the specific ionizations. Since the number of primary ionization clusters follows the Poisson distribution which is narrower than the Landau distribution one can expect a comparable or better dE/dx resolution. Using this method in principle gives an opportinity of a simplified digital readout version for the detector with no flash ADC and only an amplifier-discriminator and a simple logic which can be also used for fast second level triggering.

A proposed version of the detector is simple and cheap in comparision with a classical TPC. A small drift volume is supposed to be used in four modules of detectors: 10 - 15 cm (typically 1 m and more in a TPC). This provides a significant reduction of the detector size and improves the rate capabilities with respect to standard TPCs in high intensity applications. The detector contains a very moderate number of channels since it uses the readout from the anode wires in a drift chamber (pitch 1 cm). Measurements were performed using current amplifiers and fast flash ADC (WASA FQDC) with cosmic rays and radioactive β-source ^{90}Sr. The gas mixtures $80\%Ar + 20\%C_2H_6$ and $90\%Ar + 5\%CO_2 + 5\%CF_4$ were investigated in more detail and low values of the drift field $\approx 40 - 60 V/cm$ were found optimal for the efficient cluster registration.

References:

[1] V.Serdyuk, WASA at COSY 1st collaboration meeting, 2005, Julich

[2] V.Serdyuk, "Tracking detectors at ANKE and WASA", 2nd COSY-FFE Workshop, Bad Honnef, Germany, 2007

[3] http://gdd.web.cern.ch/GDD

[4] V.Serdyuk et al., 2006 Annual Report, FZJ, Julich, p.150

[5] F.Sauli, L.Ropelewski and P. Everaerts , CERN-PH-EP/2005-056, "Ion feedback suppression in Time Projection Chamber."

[6] J. Majewski et al., "Development of universal set of test electronic for tracking detectors at WASA and ANKE", 2007 Annual Report, FZJ, Julich, p.141

[7] W. Erven et al.,"DAQ QDC", Berichte zum Datenerfassunssystem für physikalische Experimente, ZTL, FZJ, Julich, 2006

[8] W.B. Atwood et al., "Performance of ALEPH Time Projection Chamber", Nucl. Instr. and Meth. A306 (1991) 446

[9] B. Dolgoshein, "Complementary particle ID:transition radiation and dE/dx relativistic rise", Nucl. Instr. and Meth. A433 (1999) 533

[1] Institut für Kernphysik, Forschungszentrum Jülich, Germany

[2] Joint Institute for Nuclear Research, Dubna, Russia

[3] Institute of Physics, Jagellonian University, Cracow, Poland

[4] Institute of Nuclear Physics, Polish Academy of Science, Cracow, Poland

[5] Zentrallabor für Elektronik, Forschungszentrum Jülich, Germany

[6] Physikalisches Institut II, Universität Erlangen-Nürnberg, Germany

Particle identification with a Straw Tracker by means of dE/dx measurement - feasibility studies

K. Pysz[1,2], P. Kulessa[1,2], J. Majewski[1], H. Ohm[1], V. Serdyuk[1,3]

Two candidates for the central tracker of the PANDA@FAIR experiment, a set of straw tubes and a GEM-TPC are under discussion. While the GEM-TPC is designed to deliver tracking and energy-loss information, from straw detector usually only timing information is taken which is converted into precise position information. The final goal of the work presented here is to investigate possibilities to measure the energy-loss also with straw tubes in order to identify particles.

First test of the dE/dx capability were undertaken using a set of straws of the type which is used in the MDC-tracker of WASA@COSY. The length of the tubes is 42 cm and the diameter 4, 6 and 8 mm. The anode wires have 20 μm diameter. A dE-E scintillator telescope serves as time reference in measurement with ^{90}Sr source. Both the scintillator telescope and the ^{90}Sr source have collimators with ϕ = 1 mm which permits precise scanning of the straw tube. For this purpose the scintillator telescope and the source are mounted and aligned on a linear drive. Signals from the straws were feed into a fast transresistance amplifier [1] (risetime = 8 ns) and subsequently analyzed with 100 MHz bandwidth oscilloscope.

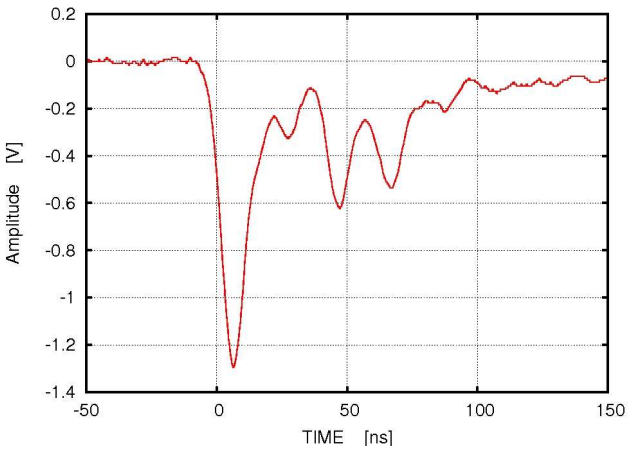

Fig. 1: An example of the signal obtained for β-particle penetrating the 8 mm straw tube at the central position. The multi-peak structure of the signal reflects the ionization cluster formation on the ionization track inside the straw.

Fig. 1 shows an example of the signal shape obtained for β-particle penetrating the 8 mm diameter straw tube at the central position, i.e. the path length is about 8 mm. The tube is filled with Ar-ethane (80/20) mixture at atmospheric pressure. The multi-peak structure of the signal reflects the ionization cluster formation on the ionization track inside the straw. In fact - due to limited bandwidth of amplifier - it is only an envelope of the more fine cluster structure of the ionization process along the path of particle.

From the data the energy-loss spectra and the number of ionization clusters (actually number of resolved groups of clusters) are deduced for two different source/scintillator positions. Fig. 2 in the left side column presents the measured energy-loss distributions calculated as a sum of amplitudes of resolved groups of clusters. Upper one is obtained for the

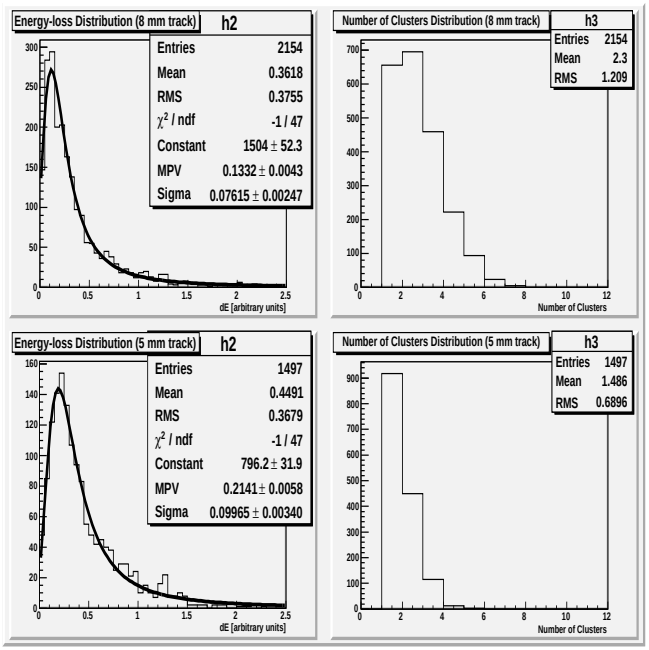

Fig. 2: Left column: energy-losses distributions for the 8 mm ionization path (top) and for 5 mm ionization path (bottom). Right column: a respective distributions of number of clusters.

longest ionization path, i.e. the β-particles traversed the straw in vicinity of the anode wire, whereas the lower distribution is found for track shifted from the center of the tube by 3 mm (it means that the track length was about 5 mm long). The left panels of the figure shows the respective distributions of the cluster numbers.

As expected - for the shorter tracks the less clusters contribute to the signals and the broadening of the Landau distribution with a shift of the mean value to the higher energies is visible. A lower value of clusters visible for shorter track results not only from the shorter ionization distance, but also from the geometry - the clusters are collected on the wire from more narrower angle then it is for central particles trajectories, and the readout 'see' them as a grouped into bigger sets.

The measurements will be continued with the improved data-taking system for various gas-mixtures, pressures, and field conditions. Systematic investigations of the various options of the signal pre-shaping, influence of the coupling parameters, cables length, threshold level are foreseen.

References:

[1] IKP-COSY Annual Report 2007, page 141

[1] FZ-IKP Jülich
[2] IFJ PAN Kraków
[3] JINR Dubna

A Councils

A.1 Hadron Physics Program Advisory Council

Prof. R. Beck	Universität Bonn	
Prof. J.-P. Blaizot	CEA Saclay, FR	
Prof. D.F. Geesaman	Argonne National Laboratory, U.S.A.	
Dr. P. Gianotti	Laboratori Nazionali di Frascati, I	
Prof. M. Harakeh	KVI Groningen, NL	
Prof. E. Jaeschke	Humboldt Universität Berlin	
Prof. K. Königsmann	Albert-Ludwigs-Universität Freiburg	
Prof. R. Kulessa	Jagellonian University Cracow, PL	
Prof. St. Paul	TU München	Chairperson
Prof. K. Peters	GSI Darmstadt	
Prof. U. Wiedner	Universität Bochum	
Prof. U.-J. Wiese	Universität Bern	

A.2 COSY Program Advisory Committee

Prof. M. Anselmino	L'Universita di Torino, IT	
Prof. D. Barber	DESY, DE	
Prof. J. Bijnens	Lund University, SE	
Prof. N. Herrmann	Universität Heidelberg, DE	
Prof. B. Kämpfer	FZ Dresden-Rossendorf, DE	
Prof. H. Löhner	KVI Groningen, NL	
Prof. A. Magiera	Jagellonian University Cracow, PL	
Prof. W. Meyer	Ruhr-Universität Bochum, DE	
Prof. W.T.H. van Oers	University of Manitoba, CA	Chairperson
Prof. A.K. Opper	George Washington University, USA	
Prof. E. Oset	Universitat de Valencia, ES	
Prof. U. Thoma	Universität Bonn, DE	

B Publications, Patents

1. Experiment

1. Abd El-Bary, S.; COSY-TOF, Collaboration
Two-pion production in proton-proton collisions with a polarized beam
European Physical Journal A **37** (2008) 267.

2. Abdel-Bary, M.; COSY-TOF, Collaboration
Analyzing power *Ay* for ω meson production in proton-proton collisions
Physics Letters B **662** (2008) 14.

3. Abdel-Bary, M.; COSY-TOF, Collaboration
Single pion production in *np* collisions for excess energies up to 90 MeV
European Physical Journal A **36** (2008) 7.

4. Bargholtz, Chr.; CELSIUS-WASA, Collab.
The WASA detector facility at CELSIUS
Nuclear Instruments and Methods in Physics Research Section A **594** (2008) 339.

5. Berlowski, M.; Bargholtz, Chr.; Bashkanov, D.; Bogolawsky, D.; Bondar, A.; Calén, H.; Cappellaro, F.; Clement, H.; Demirörs, L.; Ekström, C.; Fransson, K.; Geren, L.; Gustafsson, L.; Höistad, B.; Ivanov, G.; Jacewicz, M.; Jiganov, E.; Johansson, T.; Keleta, S.; Koch, I.; Kullander, S.; Kupsc, A.; Kuzmin, A.; Kuznetsov, A.; Laukhin, I.V.; Lindberg, K.; Marciniewski, P.; Meier, R.; Morosov, B.; Oelert, W.; Pauly, C.; Pettersson, H.; Petukhov, Y.; Povtorejko, A.; Ruber, R.J.M.Y.; Schönning, K.; Scobel, W.; Shafigullin, R.; Shwartz, B.; Skorodko, T.; Sopov, V.; Stepaniak, J.; Tegner, P.-E.; Thörngren Engblom, P.; Tikhomirov, V.; Turowiecki, A.; Wagner, G.J.; Wolke, M.; Yamamoto, A.; Zabierowski, J.; Zartova, I.; Złomanczuk, J.
Measurement of η meson decays into lepton-antilepton pairs
Physical Review D **77** (2008) 032004.

6. Boukharov, A.V.; Büscher, M.; Gerasimov, A.S.; Chernetsky, V. D.; Fedorets, P.V.; Maryshev, I.N.; Semenov, A.A.; Ginevskii, A.F.
Dynamics of Cryogenic Jets: Non-Rayleigh Breakup and Onset of Nonaxisymmetric Motions
Physical Review Letters **100** (2008) 174505.

7. Budzanowski, A.; Fidelus, M.; Filges, D.; Goldenbaum, F.; Hodde, H.; Jarczyk, L.; Kamys, B.; Kistryn, M.; Kistryn, St.; Kliczewski, St.; Kowalczyk, A.; Kozik, E.; Kulessa, P.; Machner, H.; Magiera, A.; Piskor-Ignatowicz, B.; Pysz, K.; Rudy, Z.; Siudak, R.; Wojciechowski, M.
Competition of coalescence and "fireball" processes in nonequilibrium emission of light charged particles from *p*+Au collisions
Physical Review C **78** (2008) 024603.

8. Covita, D.S.; Ay, M.; Schlesser, S.; Gotta, D.; Simons, L. M.; Le Bigot, E.-O.; dos Santos, J.M.F.
Accurate miscut angle determination for spherically bent Bragg crystals
Review of Scientific Instruments **79** (2008), 033102

9. Dzyuba, A.; Büscher, M.; Hanhart, C.; Kleber, V.; Koptev, V.; Ströher, H.; Wilkin, C.
Interpretation of $K\bar{K}$ pair production in *pp* collisions
European Physical Journal A **38** (2008) 1.

10. Dzyuba, A.; Büscher,M.; Hartmann,M.; Keshelashvili,I.; Koptev,V.; Maeda,Y.; Sibirtsev,A.; Ströher,H.; Wiklin,C.
Coupled-channel effects in the $pp \to ppK^+K^-$ reaction
Physics Letters B **668** (2008) 315.

11. Gabrielse, G.; Larochelle, P.; Le Sage, D.; Levitt, B.; Kolthammer, W. S.; McConnell, R.; Richerme, P.; Wrubel, J.; Speck, A.; George, M.C.; Grzonka, D.; Oelert, W.; Sefzick, T.; Zhang, Z.; Carew, A.; Comeau, D.; Hessels, E.A.; Storry, C. H.; Weel, M.; Walz, J.
First Antihydrogen Production within a Penning-Ioffe Trap
Physical Review Letters **100** (2008) 113001.

12. Gotta, D.; Rashid, K.; Fricke, B.; Indelicato, P.; Simons, L. M.
X-ray transitions from antiprotonic noble gases
European Physical Journal D **47** (2008), 11

13. Jayanti, R.; Machner, H.; Buhr, G.; Nolte, M.; Palarczyk, M.
Correlations of projectile like fragments in heavy ion reactions at Fermi energy
European Physical Journal A **38** (2008) 35.

14. Kleines, H.; Zwoll, K.; Wüstner, P.; Erven, W.; Kämmerling, P.; Kemmerling, G.; Loevenich, H.; Ackens, A.; Wolke, M.; Hejny, V.; Ohm, H.; Sefzick, T.; Nellen, R.; Marciniewski, P.; Fransson, K.; Gustafsson, L.; Kupsc, A.; Calén, H.
Performance Issues of the New DAQ System for WASA at COSY
IEEE Transactions on Nuclear Science **55** (2008) 261.

15. Komarov, V.; Azaryan, T.; Chiladze, D.; Dymov, S.; Hartmann, M.; Kacharava, A.; Keshelashvili, I.; Khoukaz, A.; Kulikov, A.; Kurbatov, V.; Macharashvili, G.; Merzliakov, S.; Mikirtytchiants, S.; Papenbrock, M.; Nekipelov, M.; Rathmann, F.; Serdyuk, V.; Ströher, H.; Tsirkov, D.; Uzikov, Yu.; Wiklin, C.
Observation of inverse diproton photodisintegration at intermediate energies
Physical Review Letters **101** (2008) 102501.

16. Kurbatov, V.; Büscher, M.; Dymov, S.; Gusev, D.; Hartmann, M.; Kacharava, A.; Khoukaz, A.; Komarov, V.; Kulikov, A.; Macharashvili, G.; Mersmann, T.; Merzliakov, S.; Mikirtytchiants, S.; Prasuhn, D.; Rathmann, F.; Schleichert, R.; Ströher, H.; Tsirkov, D.; Uzikov, Yu.; Wilkin, C.; Yaschenko, S.
Energy depence of forward $^1S_0$ diproton production in the $pp \to pp\pi^0$ reaction
Physics Letters B **661** (2008) 22.

17. Maeda, Y.; Hartmann, M.; Keshelashvili, I.; Barsov, S.; Büscher, M.; Drochner, M.; Dzyuba, A.; Hejny, V.; Kacharava, A.; Kleber, V.; Koch, H.R.; Koptev, V.; Kulessa, P.; Lorentz, B.; Mersmann, T.; Mikirtytchiants, S.; Mussgiller, A.; Nekipelov, M.; Ohm, H.; Prasuhn, D.; Schleichert, R.; Stein, H.J.; Ströher, H.; Valdau, Yu.; Wilkin, C.; Wüstner, P.
Kaon pair production in proton-proton collisions
Physical Review C **77** (2008) 015204.

18. Maeda, Y.; Segawa, M.; Ishida, T.; Kacharava, A.; Nomachi, M.; Shimbara, Y.; Sugaya, Y.; Tamura, K.; Yagita, T.; Yasuda, K.; Yoshida, H.P.; Wilkin, C.
Differential cross section and analyzing power of the $pp \to pp\pi^0$ reaction at a beam energy of 390 MeV
Physical Review C **77** (2008) 044004.

19. Murata, I.; Filges, D.; Goldenbaum, F.
A new approach to estimate importance for weight window in forward Monte-Carlo calculations
Nuclear Science and Engineering **159** (2008) 273.

20. Nünighoff, K.; Pohl, C.; Koulikov, S.; Cantargi, F.; Conrad, H.; Filges, D.; Glückler, H.; Goldenbaum, F.; Granada, F.; Hansen, G.; Matzerath, T.; Paul, N.; Petriw, S.; Schaal, H.; Soltner, H.; Stelzer, H.; Ninaus, W.; Wohlmuther, M.
Neutron experiments with cryogenic methane hydrate and mesitylene moderators
European Physical Journal A **38** (2008) 115.

21. Siudak, R.; Budzanowski, A.; Chatterjee, A.; Clemens, H.; Dorochkevitsch, E.; Ernst, J.; Hawranek, P.; Hinterberger, F.; Jahn, R.; Jarczyk, L.; Joosten, R.; Kilian, K.; Kirillov, Di.; Kliczewski, S.; Kolev, D.; Kravcikova, M.; Machner, H.; Magiera, A.; Martinska, G.; Massmann, F.; Munkel, J.; Piskunov, N.; Protic, D.; Ritman, J.; von Rossen, P.; Roy, B.; Sitnik, I.; Slepnev, I.; Smyrski, J.; Tsenov, R.; Ulbrich, K.; Urban, J.; Vankova, G.; Wagner, G. J.; Ziegler, R.
A threshold Cherenkov detector for K^+/π^+ separation using silica aerogel
Nuclear Instruments and Methods in Physics Research Section A **596** (2008) 311.

22. Skorodko, T.; Bashkanov, M.; Bogoslawsky, D.; Calén, H.; Cappellaro, F.; Clement, H.; Demirörs, L.; Doroshkevich, E.; Duniec, D.; Ekström, C.; Fransson, K.; Gustafsson, L.; Höistad, B.; Ivanov, G.; Jacewicz, M.; Jiganov, E.; Johansson, T.; Khakimova, O.; Kaskulov, M.; Keleta, S.; Koch, I.; Kren, F.; Kullander, S.; Kupsc, A.; Kuznetsov, A.; Marciniewski, P.; Meier, R.; Morosov, B.; Pauly, C.; Petterson, H.; Petukhov, Y.; Povtorejko, A.; Schönning, K.; Scobel, W.; Shwartz, B.; Sopov, V.; Stepaniak, J.; Thörngren Engblom, P.; Tikhomirov, V.; Wagner, G.J.; Wolke, M.; Yamamoto, A.; Zabierowski, J.; Złomanczuk, J.
Excitation of the Roper resonance in single- and double-pion production in nucleon-nucleon collisions
European Physical Journal A **35** (2008) 317.

23. Stein, H.J.; Hartmann, M.; Keshelashvili, I.; Maeda, Y. ; Wilkin, C.; Dymov, S.; Kacharava, A.; Khoukaz, A.; Lorentz, B.; Maier, R.; Mersmann, T.; Mikirtychiants, S.; Prasuhn, D.; Stassen, R.; Stockhorst, H.; Ströher, H.; Valdau, Yu.; Wüstner, P.
Determination of target thickness and luminosity from beam energy losses
Physical Review ST-AB **11** (2008) 052801.

24. Zychor, I.; Büscher, M.; Hartmann, M.; Kacharava, A.; Keshelashvili, I.; Khoukaz, A.; Kleber, V.; Koptev, V.; Maeda, Y.; Mersmann, T.; Mikirtychiants, S.; Schleichert, R.; Ströher, H.; Valdau, Yu.; Wilkin, C.
Lineshape of the $\Lambda(1405)$ hyperon measured through its $\Sigma^+\pi^0$ decay
Physics Letters B **660** (2008) 167.

2. Theory

25. Baltz, A. J.; Baur, G.; d'Enterria, D.; Frankfurt, L.; Gelis, F.; Guzey, V.; Hencken, K.; Kharlov, Yu.; Klasen, M.; Klein, S. R.; Nikulin, V.; Nystrand, J.; Pshenichnov, I. A.; Sadovsky, S.; Scapparone, E.; Seger, J.; Strikman, M.; Tverskoy, M.; Vogt, R.; White, S. N.; Wiedemann, U. A.; Yepes, P.; Zhalov, M.
The Physics of Ultraperipheral Collisions at the LHC
Physics Reports **458** (2008) 1.

26. Baru, V.; Haidenbauer, J.; Hanhart, C.; Kudryavtsev, A. E.; Lensky, V.; Meißner, U.-G.
Role of the $\Delta(1232)$ in pion-deuteron scattering at threshold within chiral effective field theory
Physics Letters B **659** (2008) 184.

27. Baur, G.; Typel, S.
Coulomb dissociation, a tool for nuclear astrophysics
Journal of Physics G **35** (2008) 014028.

28. Belushkin, M. A.; Hammer, H. W.; Meißner, U.-G.
Model-independent extraction of two-photon effects in elastic electron-proton scattering
Physics Letters B **658** (2008) 138.

29. Bernard, V.; Epelbaum, E.; Krebs, H.; Meißner, U.-G.
Subleading contributions to the chiral three-nucleon force I: long-range terms
Physical Review C **77** (2008) 064004.

30. Bernard, V.; Lage, M.; Meißner, U.-G.; Rusetsky, A.
Analysis of the Δ-resonance in a finite volume
European Physical Journal A **35** (2008) 281.

31. Bernard, V.; Lage, M.; Meißner, U.-G.; Rusetsky, A.
Resonance properties from the finite-volume energy spectrum
Journal of High Energy Physics **08** (2008) 024.

32. Bernard, V.; Meißner, U.-G.; Rusetsky, A.
The Δ-resonance in a finite volume
Nuclear Physics B **788** (2008) 1.

33. Bigi, I.I.; Devidze, G.G.; Liparteliani, A.G; Meißner, U.-G.
$B \to \gamma\gamma$ in an Appelquist-Cheng-Dobrescu model
Physical Review D **78** (2008) 097501.

34. Borasoy, B.; Bruns, P. C.; Meißner, U.-G.; Nißler, R.
A gauge invariant chiral unitary framework for kaon photo- and electroproduction on the proton
European Physical Journal A **34** (2008) 161.

35. Borasoy, B.; Epelbaum, E.; Krebs, H.; Lee, D.; Meißner, U.-G.
Chiral effective field theory on the lattice at next-to-leading order
European Physical Journal A **35** (2008) 343.

36. Borasoy, B.; Epelbaum, E.; Krebs, H.; Lee, D.; Meißner, U.-G.
Dilute neutron matter on the lattice at next-to-leading order in chiral effective field theory
European Physical Journal A **35** (2008) 357.

37. Bruns, P.C.; Meißner, U.-G.
Infrared regularization with vector mesons and baryons
European Physical Journal C **58** (2008) 407.

38. Capstick, S.; Svarc, A.; Tiator, L.; Gegelia, J.; Giannini, M.M.; Santopinto, E.; Hanhart, C.; Scherer, S.; Lee, T.-S.H.; Sato, T.; Suzuki, N.
The physical meaning of scattering matrix singularities in coupled-channel formalisms
European Physical Journal A **35** (2008) 253.

39. Döring, M.; Ajaka, J.; Assafiri, Y.; Bartalini, O.; Bellini, V.; Bouchigny, S.; Castoldi, M.; D'Angelo, A.; Didelez, J. P.; Di Salvo, R.; Fantini, A.; Fichen, L.; Gervino, G.; Ghio, F.; Girolami, B.; Giusa, A.; Guidal, M.; Hourany, E.; Kunne, R.; Lapik, A.; Sandri, P. L.; Moricciani, D.; Muskarenkov, A.; Nedorezov, V.; Oset, E.; Randieri, C.; Rudnev, N.; Russo, G.; Schaerf, C.; Sperduto, M.; Sutera, M.; Turinge, A.
Simultaneous Photoproduction of η and π^0 Mesons on the Proton
Physical Review Letters **100** (2008) 05200.

40. Döring, M.; Oset, E.
s wave pion nucleus optical potential
Physical Review C **77** (2008) 024602.

41. Döring, M.; Oset, E.; Jido, D.
Transition form factors of the $N(1535)$ as a dynamically generated resonance
Physical Review C **77** (2008) 065207.

42. Döring, M.; Oset, E.; Zou, B. S.
Role of the N(1535) resonance and the $\pi^- p \to KY$ amplitudes in the OZI forbidden $\pi N \to \phi N$ reaction
Physical Review C **78** (2008) 025207.

43. Entem, D.R.; Ruiz Arriola, E.; Pavon Valderrama, M.; Machleidt, R.
Renormalization of chiral two-pion exchange NN interactions. Momentum vs. coordinate space
Physical Review C **77** (2008) 044006.

44. Epelbaum, E.
Chiral dynamics of few-nucleon systems
Nuclear Physics A **805** (2008) 439.

45. Epelbaum, E.
Few-nucleon forces and systems in chiral effective field theory
Few-Body Systems **43** (2008) 57.

46. Epelbaum, E.
Isospin-breaking nuclear forces with Δ degrees of freedom
Few-Body Systems **44** (2008) 129.

47. Epelbaum, E.; Krebs, H.; Meißner, U.-G.
Δ-excitations and the three-nucleon force
Nuclear Physics A **806** (2008) 65.

48. Epelbaum, E.; Krebs, H.; Meißner, U.-G.
Isospin-breaking two-nucleon force with explicit Δ-excitations
Physical Review C **77** (2008) 034006.

49. Guo, F.-K.; Hanhart, Chr.; Krewald, S.; Meißner, U.-G.
Subleading contributions to the width of the $D^*_{s0}(2317)$
Physics Letters B **666** (2008) 251.

50. Guo, F.-K.; Hanhart, Chr.; Meißner, U.-G.
Evidence that the $Y(4660)$ is a $f_0(980)\Psi'$ bound state
Physics Letters B **665** (2008) 26.

51. Guo, F.-K.; Krewald, S.; Meißner, U.-G.
Hadronic-loop induced mass shifts in scalar heavy-light mesons
Physics Letters B **665** (2008) 157.

52. Guo, F.-K.; Hanhart, Chr.; Meißner, U.-G.
Mass splittings within heavy baryon isospin multiplets in chiral perturbation theory
Journal of High Energy Physics **09** (2008) 136.

53. Haidenbauer, J.
Meson production in nucleon-nucleon collisions
Few-Body Systems **43** (2008) 83.

54. Haidenbauer, J.; Krein, G.; Meißner, U.-G.; Sibirtsev, A.
Charmed meson rescattering in the reaction $\bar{p}d \to D\bar{D}N$
European Physical Journal A **37** (2008) 55.

55. Haidenbauer, J.; Meißner, U.-G.; Sibirtsev, A.
Near threshold $p\bar{p}$ enhancement in the $J/\Psi \to \omega p\bar{p}$ decay
Physics Letters B **666** (2008) 352.

56. Hanhart, C.
How and when can one identify hadronic molecules in the baryon spectrum
European Physical Journal A **35** (2008) 271.

57. Hanhart, Chr.; Pelaez, J. R.; Rios, G.
Quark mass dependence of the rho and sigma from dispersion relations and Chiral Perturbation Theory
Physical Review Letters **100** (2008) 152001.

58. Kalashnikova, Yu. S.; Kudryavtsev, A. E.; Nefediev, A. V.; Haidenbauer, J.; Hanhart, C.
Comment on 'Once more about the $K\bar{K}$ molecule approach to the light scalars'
Physical Review D **78** (2008) 058501.

59. Kistryn, St.; Stephan, E.; Kalantar-Nayestanaki, N.; Biegun, A.; Bodek, K.; Ciepal, I.; Deltuva, A.; Epelbaum, E.; Fonseca, A. C.; Glöckle, W.; Golak, J.; Kamada, H.; Kis, M.; Klos, B.; Kozela, A.; Nogga, A.; Mahjour-Shafiei, M.; Micherdzinska, A.; Sauer, P. U.; Skibinski, R.; Sworst, Z.; Witala, H.; Zejma, J.; Zipper, W.
Studies of the three-nucleon system dynamics: Cross sections of the deuteron-proton breakup at 130 MeV
Few-Body Systems **44** (2008) 11.

60. Lyutorovich, N.; Speth, J.; Avdeenkov, A.; Grümmer, F.; Kamerdzhiev, S.; Krewald, S.; Tselyaev, V.I.
Self-consistent calculations within the Green's function method including particle-phonon coupling and the single-particle continuum
European Physical Journal A **37** (2008) 381.

61. Meißner, U.-G.; Rakhimov, A. M.; Wirzba, A.; Yakhshiev, U. T.
Neutron-proton mass difference in finite nuclei and the Nolen-Schiffer anomaly
European Physical Journal A **36** (2008) 37.

62. Navratil, P.; Gueorguiev, V.G.; Vary, J.P.; Ormand, W.E.; Nogga, A.; Quaglioni, S.
Light nuclei from chiral EFT interactions
Few-Body Systems **43** (2008) 129.

63. Nogga, A.
Approaching light nuclei and hypernuclei based on chiral interactions
Few-Body Systems **43** (2008) 137.

64. Pavon Valderrama, M.; Nogga, A.; Ruiz Arriola, E.; Phillips, D. R.
Deuteron form factors in chiral effective theory: Regulator-independent results and the role of two-pion exchange
European Physical Journal A **36** (2008) 315.

65. Polinder, H.
Strange two-baryon interactions using chiral effective field theory
Few-Body Systems **44** (2008) 113.

66. Sibirtsev, A.; Hammer, H.-W.; Meißner, U.-G.
A-dependence of ϕ-meson production in $p+A$ collisions
European Physical Journal A **37** (2008) 287.

67. Slifer, K.; Amarian, M.; Auerbach, L.; Averett, T.; Berthot, J.; Bertin, P.; Bertozzi, B.; Black, T.; Brash, E.; Brown, D.; Burtin, E.; Calarco, J.; Cates, G.; Chai, Z.; Chen, J.-P.; Choi, S.; Chudakov, E.; Ciofi degli Atti, C.; Cisbani, E.; de Jager, C.W.; Deur, A.; DiSalvo, R.; Dieterich, S.; Djawotho, P.; Finn, M.; Fissum, K.; Fonvieille, H.; Frullani, S.; Gao, H.; Gao, J.; Garibaldi, F.; Gasparian, A.; Gilad, S.; Gilman, R.; Glamazdin, A.; Glashausser, C.; Glöckle, W.; Golak, J.; Goldberg, E.; Gomez, J.; Gorbenko, V.; Hansen, J.-O.; Hersman, B.; Holmes, R.; Huber, G.M.; Hughes, E.; Humensky, B.; Incerti, S.; Iodice, M.; Jensen, S.; Jiang, X.; Jones, C.; Jones, G.; Jones, M.; Jutier, C.; Kamada, H.; Ketikyan, A.; Kominis, I.; Korsch, W.; Kramer, K.; Kumar, K.; Kumbartzki, G.; Kuss, M.; Lakuriqi, E.; Laveissiere, G.; Lerose, J.; Liang, M.; Liyanage, N.; Lolos, G.; Malov, S.; Marroncle, J.; McCormick, K.; McKeown, R.D.; Meziani, Z.-E.; Michaels, R.; Mitchell, J.; Nogga, A.; Pace, E.; Papandreou, Z.; Pavlin, T.; Petratos, G.G.; Pripstein, D.; Prout, D.; Ransome, R.; Roblin, Y.; Rowntree, D.; Rvachev, M.; Sabatie, F.; Saha, A.; Salme, G.; Scopetta, S.; Skibinski, R.; Souder, P.; Saito, T.; Strauch, S.; Suleiman, R.; Takahashi, K.; Teijiro, S.; Todor, L.; Tsubota, H.; Ueno, H.; Urciuoli, G.; Van der Meer, R.; Vernin, P.; Voskanian, H.; Witala, H.; Wojtsekhowski, B.; Xiong, F.; Xu, W.; Yang, J.-C.; Zhang, B.; Zolnierczuk, P.
^{3}He spin-dependent cross sections and sum rules
Physical Review Letters **101** (2008) 022303.

68. Sworst, R.; Kistryn, St.; Stephan, E.; Biegun, A.; Bodek, K.; Ciepal, I.; Epelbaum, E.; Glöckle, W.; Golak, J.; Kalantar-Nayestanaki, N.; Kamada, H.; Klos, B.; Kozela, A.; Nogga, A.; Skibinski, R.; Witala, H.; Zejma, J.; Zipper, W.
Influence of three-nucleon force effects on polarization observables of the ^{1}H($\vec{d}$,$\vec{pp}$)n breakup reaction at 130 MeV
Acta Physica Polonica B **39** (2008) 401.

69. Typel, S.; Baur, G.
Scaling laws and higher-order effects in Coulomb excitation of neutron halo nuclei
European Physical Journal A **38** (2008) 355.

70. Wirzba, A.
The Casimir effect as a scattering problem
Journal of Physics A **41** (2008) 164003.

3. Accelerator (including conference proceedings)

71. An, S.Z.; Bongardt, K.; Maier, R.; Tang, J.; Zhang, T.J.
Collective effects for long bunches in dual harmonic RF Systems
Chinese Journal of Physics **32** (2008) 139.

72. An, S.Z.; Bongardt, K.; Maier, R.; Tang, J.; Zhang, T.J.
Emittance-dominated long bunches in dual harmonic RF System
Chinese Journal of Physics **32** (2008) 60.

73. Bongardt, K.
ESS Plans and Synergy with CERN
Beam07 Proceedings (CERN Yellow Report 2008-005), p. 152

74. Dietrich, J.; Böhme, C.; Kamerdzhiev, V.
Beam Profile Measurements Based on Beam Interaction with Residual Gas
Proceedings of the 8th International Topical Meeting on Nuclear Applications and Utilization of Accelerators (ACCAPP'07), p. 138

75. Dietrich, J.; Bryzgunov, M.I.; Goncharov, A.D. ; Parkhomchuk, V.V.; Reva, V.B.; Skorobogatov, D.N.
Prototype of the High Voltage Section for the 2 MeV Electron Cooler at COSY
Proceedings of the EPAC 2008, Genoa, Italy, June 23–27, 2008.

76. Dietrich, J.; Weis, T.; Boehme, C.; Botha, A.; Conradie, J.; Crombie, M.A.; Du Toit, H.; Fourie, D.T.; Mostert, H.; Rohwer, P.; van Schalkwyk, P.
Non-destructive Beam Position and Profile Measurements Using Light Emitted by Residual Gas in a Cyclotron Beam Line
Proceedings of the EPAC 2008, Genoa, Italy, June 23-27, 2008

77. Garishvili, A.; Lorentz, B.; Nass, A.; Lehrach, A.; Lenisa, P.; Maier, R.; Martin, S.; Rathmann, F.; Statera, M.; Steffens, E.; Ströher, H.
Storage Ring Section for a Polarized Gas Target with High Angular Acceptance
Proceedings of PSTP2007, AIP Conference Proceedings **980**, p. 176

78. Garishvili, A.; Nass, A.; Steffens, E.; Lehrach, A.; Lorentz, B.; Maier, R.; Rathmann, F.; Schleichert, R.; Ströher, H.; Lenisa, P.; Statera, M.; Martin, S.
Lattice Studies for Spinfiltering Experiments at COSY and AD
Proceedings of the EPAC 2008, Genoa, Italy, June 23–27, 2008.

79. Gebel, R.; Brings, R.; Felden, O.; Maier, R.
Operation of the Injector Cyclotron JULIC for the Cooler Synchrotron COSY/Jülich
Proceedings of Cyclotrons 2007

80. Gebel, R.; Felden, O.; Maier, R.
Polarized H^- and D^- Beams at COSY/Jülich
Proceedings of PSTP2007, AIP Conference Proceedings **980**, p. 231

81. Lorentz, B.; Lehrach, A.; Maier, R.; Prasuhn, D.; Stockhorst, H.; Tölle, R.
HESR Linear Lattice Design
Proceedings of the EPAC 2008, Genoa, Italy, June 23–27, 2008.

82. Luccio, A.U.; Lehrach, A.
Simulation of Spin Resonances of Polarized Deuterons in COSY
Proceedings of the EPAC 2008, Genoa, Italy, June 23–27, 2008.

83. Morozov, V.S.; Chao, A.W.; Krisch, A.D.; Leonova, M.A.; Raymond, R.S.; Sivers, D.W.; Wong, V.K.; Garishvili, A.; Gebel, R.; Lehrach, A.; Lorentz, B.; Maier, R.; Prasuhn, D.; Stockhorst, H.; Welsch, D.M.; Hinterberger, F.; Ulbrich, K.; Schnase, A.; Stephenson, E.J.; Brantjes, N.P.M.; Onderwater, C.J.G.; da Silva, M.
Experimental verification of striking predicted oscillations near a spin resonance
Physical Review Letters **100** (2008) 054801.

84. Senichev, Yu.
The advanced HESR lattice for improved stochastic cooling
Proceedings of the Workshop on Beam Cooling and Related Topics (COOL07), p. 102

85. Senichev, Yu.
The lattice with imaginary gamma-transition for the CERN Proton Synchrotron PS2
Proceedings of CARE-HHH-APD Workshop "Beam-07"

86. Senichev, Yu., Chechenin, A.
Theory of "Resonant" Lattices for Synchrotrons with Negative Momentum Compaction Factor
Journal of Experimental and Theoretical Physics **105** (2008) 1127.

87. Senichev, Yu., Chechenin, A.
Construction of "resonant" magneto-optical lattices with controlled momentum compaction factor
Journal of Experimental and Theoretical Physics **105** (2008) 1141.

88. Smirnov, A. V.; Meshkov, I. N.; Sidorin, A. O.; Dietrich, J.; Noda, A.; Shirai, T.; Souda, H.; Tongu, H.; Noda, K.
Necessary Condition for Beam Ordering
Proceedings of the Workshop on Beam Cooling and Related Topics (COOL07), p. 87

89. Stassen, R.; Bongardt, K.; Etzkorn, F.J.; Stockhorst, H.; Papureanu, S.; Schnase, A.
The HESR RF-System and tests in COSY
Proceedings of the EPAC 2008, Genoa, Italy, June 23–27, 2008.

90. Stockhorst, H.; Stassen, R.; Prasuhn, D.; Maier, R.; Katayama, T.; Thorndahl, L.
Stochastic cooling developments for the HESR at FAIR
Proceedings of the EPAC 2008, Genoa, Italy, June 23–27, 2008.

91. Welsch, D.M.; Lehrach, A.; Lorentz, B.; Maier, R.; Prasuhn, D.; Tölle, R.
Closed Orbit Correction and Multipole Compensation Schemes for Normal-conducting HESR
Proceedings of the EPAC 2008, Genoa, Italy, June 23–27, 2008.

4. Patents

1. I. Mohos, J. Dietrich
   German patent 10 2004 028 441
   Verfahren und Vorrichtung zur Ermittlung der Spitzenwerte von periodisch auftretenden Nutzsignalen

C Talks and Colloquia

1. Baur, G.
   Pair production and ionization in relativistic ion-ion collisions
   WE-Heraeus-Seminar — Highly Charged Ions and Antiprotons
   Bad Honnef, Germany: 04.04.2008 – 12.04.2008

2. Baur, G.
   Exchange of high and low energy photons in ultraperipheral relativistic heavy ion collisions
   Workshop on High Energy Photon Collisions at the LHC
   Geneva, Switzerland: 22.04.2008 – 25.04.2008

3. Baur, G.
   Coherent photon-photon interactions in very peripheral relativistic heavy ion collisions
   Workshop and School on Fundamental Physics with Ultra-high Field
   Frauenwoerth: 29.09.2008 – 02.10.2008

4. Büscher, M.
   The Light Scalar Mesons $a_0/f_0(980)$ at COSY-Jülich
   Workshop on Scalar Mesons and Related Topics (Scadron 70)
   Lisboa, Portugal: 11.02.2008 – 16.02.2008

5. Büscher, M.
   Target TDR for PANDA: The Moscow-Jülich Pellet Target
   Plenary talk at the PANDA collaboration meeting
   Darmstadt, Germany: 11.12.2008

6. Czerwinski, E.
   Study of the Properties of the η' Meson at COSY-11
   CANU 2008 and JCHP-FFE Workshop
   Bad Honnef, Germany: 15.12.2008 – 16.12.2008

7. Dietrich, J.
   Beam Profile Measurements Based on Beam Interaction with Residual Gas
   Goethe-Universität Frankfurt am Main, Winterseminar Beschleunigerphysik
   Riezlern, Germany: 03.03.2008

8. Dietrich, J.
   Status 2 MeV Electron Cooler
   22nd HESR-Consortium
   Jülich, Germany: 11.03.2008

9. Dietrich, J.
   2 MeV Elektronenkühler für COSY-Jülich
   Johannes-Gutenberg-Universität Mainz
   Mainz, Germany: 23.10.2008

10. Dietrich, J.
    COSY — Status and Future
    University of Witwatersrand and iThemba LABS Gauteng
    Johannesburg, South Africa: 10.11.2008

11. Dietrich, J.
    COSY — Status and Future
    iThemba LABS
    Faure, South Africa: 20.11.2008

12. Dymov, S.
    Hadron Physics with Diproton Final States at ANKE-COSY
    MESON 2008
    Cracow, Poland: 06.06.2008 – 10.06.2008

13. Dymov, S.
Hadron Interactions with Diproton Final States at ANKE-COSY
STORI08
Lanzhou, China: 14.09.2008 – 18.09.2008

14. Dzhygadlo, R.
Hyperon-Rekonstruktion im COSY-TOF Straw Tube Tracker
CANU 2008 and JCHP-FFE Workshop
Bad Honnef, Germany: 15.12.2008 – 16.12.2008

15. Engels, R.
Precision Spectroscopy of Metastable Hydrogen or Antihydrogen with a Lamb-Shift Polarimeter
LEAP 2008
Vienna, Austria: 16.09.2008 – 19.09.2008

16. Engels, R.
How we recently switched on the magnet
WASA-at-COSY Collaboration Meeting
Jülich, Germany: 22.09.2008 – 23.09.2008

17. Engels, R.
First experiments with the Polarized Internal Target at ANKE/COSY
SPIN2008
Charlottesville, Va., U.S.A.: 06.10.2008 – 11.10.2008

18. Engels, R.
Precision Spectroscopy of Metastable Hydrogen with a Lamb-Shift Polarimeter
SPIN2008
Charlottesville, Va., U.S.A.: 06.10.2008 – 11.10.2008

19. Engels, R.
The Lamb-Shift Polarimeter: How it works and what it can be used for
Technische Universität München, Physik Department E18
München, Germany: 20.10.2008

20. Engels, R.
Precision Spectroscopy of Hydrogen: History and Future Experiments
Universität Basel
Basel, Switzerland: 05.12.2008

21. Epelbaum, E.
Few nucleons in chiral effective field theory
Universität Basel, Seminar
Basel, Schweiz: 13.03.2008

22. Epelbaum, E.
Effective field theory for few-nucleon systems
Donnersberg Workshop 2008 (A1 Collaboration)
Dannenfels, Germany: 31.03.2008 – 03.04.2008

23. Epelbaum, E.
Chiral dynamics of few-nucleon systems
Universität Bonn, Physikalisches Kolloquium
Bonn: 09.05.2008

24. Epelbaum, E.
Chiral dynamics of few-nucleon systems: Recent developments
VIQCD Meeting
Ferrara, Italy: 01.06.2008

25. Epelbaum, E.
Chiral EFT for few-nucleon systems
INT Workshop on Soft Photons and Light Nuclei
Seattle, Wash., U.S.A.: 16.06.2008 – 20.06.2008

26. Epelbaum, E.
Chiral effective field theory: the status
X Workshop on Electron-Nucleus Scattering
Elba, Italy: 23.06.2008 – 27.06.2008

27. Epelbaum, E.
Subleading contributions to the chiral three-nucleon force
410. WE-Heraeus-Seminar
Bad Honnef, Germany: 28.07.2008 – 30.07.2008

28. Epelbaum, E.
Chiral dynamics of few-nucleon systems: recent developments
Conference on Quark Confinement and the Hadron Spectrum
Mainz, Germany: 01.09.2008 – 06.09.2008

29. Epelbaum, E.
Effective theory with singular long-range interactions
ECT* Workshop on Bound States and Resonances in Effective Field Theories
Trento, Italy: 29.09.2008 – 03.10.2008

30. Epelbaum, E.
Chiral dynamics in nuclei
International Conference on Particles and Nuclei (PANIC08)
Eilat, Israel: 09.11.2008 – 14.11.2008

31. Epelbaum, E.
Nuclear lattice simulations based on chiral effective field theory
Universität Gießen, Graduiertenkolleg-Kolloquium
Gießen: 20.11.2008

32. Fedorets, P.
Pellet target (current status)
XXIV PANDA Collaboration Meeting
Darmstadt, Germany: 03.03.2008 – 07.03.2008

33. Fedorets, P.
Production of hydrogen, nitrogen and argon pellets with the Moscow-Jülich pellet target
STORI08
Lanzhou, China: 13.09.2008 – 19.09.2008

34. Fedorets, P.
Analysis of the reaction $pd \to {}^3\mathrm{He}(\pi^0\pi^0)/(\pi^0\eta) \to 3\mathrm{He}\,4\gamma$
WASA@COSY Collaboration Meeting
Jülich, Germany: 25.09.2008

35. Fedorets, P.
Scalar Mesons at WASA status and perspectives
WASA@COSY Collaboration Meeting
Jülich, Germany: 23.09.2008

36. Fedorets, P.
Status of high energy pd and dd data analysis
WASA-at-COSY Collaboration Meeting
Jülich, Germany: 27.03.2008

37. Fedorets, P.
Status of $pd \to {}^3\mathrm{He}\,X$ at $p = 2.935$ GeV/c ($T = 2.143$ GeV) from November 2007
WASA-at-COSY Workshop on Analysis of η and η' Decays
Uppsala, Sweden: 29.02.2008 – 02.03.2008

38. Gebel, R.
Status Report of the Injector Cyclotron JULIC at COSY/Jülich
European Cyclotron Progress Meeting
Berlin, Germany: 15.10.2008 – 18.10.2008

39. Gillitzer, A.
Charm in nuclei
LEAP 2008
Vienna, Austria: 16.09.2008 – 19.09.2008

40. Goldenbaum, F.
Experimental data on evaporation and pre-equilibrium emission in GeV p-induced spallation reactions
Advanced Workshop on Model Codes for Spallation Reactions
Trieste, Italy: 04.02.2008 – 08.02.2008

41. Gotta, D.
Conclusions for Recent Pionic-Atom Experiments
International Workshop on Cold Antimatter Plasmas and Application to Fundamental Physics (pbar08)
Okinawa, Japan: 20.02.2008 – 22.02.2008

42. Gotta, D.
X-ray Spectroscopy of Light Hadronic Atoms
International Conference on Exotic Atoms (EXA08)
Vienna, Austria: 15.09.2008 – 19.09.2008

43. Grigoryev, K.
The Polarized Internal Gas Target of ANKE at COSY
STORI08
Lanzhou, China: 14.09.2008 – 18.09.2008

44. Grzonka, D.
Study of the spin triplet proton-lambda interaction using the COSY-11 detector
Symposium on Meson Physics
Cracow, Poland: 01.10.2008 – 04.10.2008

45. Guo, F.-K.
Two topics on new charm mesons
VIQCD Meeting
Ferrara, Italy: 01.06.2008

46. Haidenbauer, J.
Hyperon-Nucleon Interaction: From meson exchange to effective field theory
Universität Gießen, Kolloquium
Gießen, Germany: 08.05.2008

47. Haidenbauer, J.
Investigating the D meson interaction in antiproton-deuteron collisions
Hadrons at Fair, FIAS
Frankfurt/Main, Germany: 25.06.2008 – 27.06.2008

48. Haidenbauer, J.
$\bar{p}p$ and $\bar{p}d$ interactions at medium energies
409. WE-Heraeus-Seminar — Polarized Antiprotons
Bad Honnef, Germany: 23.06.2008 – 25.06.2008

49. Haidenbauer, J.
Strangeness $S = -2$ Baryon-Baryon Interaction in Chiral Effective Field Theory
XVIIIth International Conference on Particles and Nuclei (PANIC08)
Eilat, Israel: 09.11.2008 – 14.11.2008

50. Haidenbauer, J.
The Interaction of D-Mesons with Nucleons
XVIIIth International Conference on Particles and Nuclei (PANIC08)
Eilat, Israel: 09.11.2008 – 14.11.2008

51. Hanhart, C.
A method to identify hadronic molecules and its application to X(3872) and X(3875)
GSI Darmstadt, Seminar
Darmstadt, Germany: 30.01.2008

52. Hanhart, C.
How to find molecules in the meson and baryon spectrum
International Workshop on Bound States and Resonances in Effective Field Theory
Trento, Italy: 29.09.2008 – 03.10.2008

53. Hanhart, C.
How to identify hadronic molecules in the spectrum: method and applications
Universität Bonn, Seminar
Bonn, Germany: 10.04.2008

54. Hanhart, C.
How to identify hadronic molecules in the spectrum: method and applications
University of Uppsala, Seminar
Uppsala, Sweden: 23.05.2008

55. Hanhart, C.
How to identify hadronic molecules in the spectrum: method and applications
Institute of High Energy Physics (IHEP), Seminar
Beijing, China: 19.09.2008

56. Hanhart, C.
Meson production from hadronic probes
STORI08
Lanzhou, China: 14.09.2008 – 18.09.2008

57. Hartmann, M.
Hyperon Physics at COSY
Frühjahrstagung der Deutschen Physikalischen Gesellschaft
Darmstadt, Germany: 14.03.2008

58. Hartmann, M.
Some Experimental Techniques at Storage Rings
STORI08
Lanzhou, China: 14.09.2008 – 18.09.2008

59. Hejny, V.
Charge symmetry breaking in $dd \to {}^4\mathrm{He}\,\pi^0$
WASA-at-COSY Collaboration Meeting
Jülich, Germany: 27.03.2008 – 28.03.2008

60. Hejny, V.
Passive base test on the calorimeter
WASA-at-COSY Analysis Meeting
Jülich, Germany: 26.03.2008 – 27.03.2008

61. Janusz, M.
Feasibility of $\eta \to \pi^+\pi^- e^+ e^-$
WASA-at-COSY Workshop on Analysis of η and η' Decays
Uppsala, Sweden: 29.02.2008 – 02.03.2008

62. Janusz, M.
Status Report from CDC group
WASA-at-COSY Workshop on Analysis of η and η' Decays
Uppsala, Sweden: 29.02.2008 – 02.03.2008

63. Janusz, M.
PID (electron-pion) in CD (purity and efficiency)
WASA-at-COSY Workshop on Analysis of η and η' Decays
Uppsala, Sweden: 29.02.2008 – 02.03.2008

64. Janusz, M.
Status of analysis of April 2007 data
WASA-at-COSY Analysis Meeting
Jülich, Germany: 09.06.2008 – 10.06.2008

65. Janusz, M.
Study of the $\eta \to \pi^+\pi^-e^+e^-$ decays with WASA-at-COSY
Symposium on Meson Physics
Cracow, Poland: 01.10.2008 – 04.10.2008

66. Janusz, M.
Charged Decays of η with WASA-at-COSY
CANU 2008 and JCHP-FFE Workshop
Bad Honnef, Germany: 15.12.2008 – 16.12.2008

67. Jany, B.R.
Feasibility of $\eta' \to \pi^+\pi^-\eta$
WASA-at-COSY Workshop on Analysis of η and η' Decays
Uppsala, Sweden: 29.02.2008 – 02.03.2008

68. Jany, B.R.
Bayesian Likelihood based FD Kinetic Energy reconstruction
WASA-at-COSY Workshop on Analysis of η and η' Decays
Uppsala, Sweden: 29.02.2008 – 02.03.2008

69. Jany, B.R.
FD Kinetic Energy Reconstruction
WASA-at-COSY Collaboration Meeting
Jülich, Germany: 27.03.2008 – 28.03.2008

70. Jany, B.R.
Trigger conditions for η' run
WASA-at-COSY Analysis Meeting
Jülich, Germany: 26.03.2008 – 27.03.2008

71. Jany, B.R.
In search of an η' signal: Status of April 08 data
WASA-at-COSY Collaboration Meeting
Jülich, Germany: 22.09.2008 – 23.09.2008

72. Jany, B.R.
In search of η' – Analysis of η' feasibility run
WASA-at-COSY Analysis Meeting
Jülich, Germany: 09.06.2008 – 10.06.2008

73. Kacharava, A.
Physics Program at COSY-Jülich with Polarized Hadronic Probes
SPIN2008
Charlottesville, Va., U.S.A.: 06.10.2008 – 11.10.2008

74. Khoukaz, A.
Hadron Physics at COSY
MESON 2008
Cracow, Poland: 06.06.2008 – 10.06.2008

75. Khoukaz, A.
Hadron Physics at COSY
STORI08
Lanzhou, China: 14.09.2008 – 18.09.2008

76. Kowalczyk, A.
Pion production in proton induced spallation reactions in the energy range of few GeV order
MESON 2008
Cracow, Poland: 06.06.2008 – 10.06.2008

77. Kowalzcyk, A.
Strangeness Production with WASA-at-COSY
CANU 2008 and JCHP-FFE Workshop
Bad Honnef, Germany: 15.12.2008 – 16.12.2008

78. Krewald, S.
Determination of Resonance Poles in Pion Nucleon Scattering
Workshop on Pion-Nucleon Partial Wave Analysis
Washington, DC, U.S.A.: 17.03.2008 – 20.03.2008

79. Krzemien, W.
Search for the ^{3}He-η bound state at COSY-11
MESON 2008
Cracow, Poland: 06.06.2008 – 10.06.2008

80. Lehrach, A.
Anwendung von Petawatt-Lasern
Universität Bonn: Habilitationskolloquium
Bonn, Germany: 27.05.2008

81. Lehrach, A.
Siberian Snakes for Spin-Filter Experiments
409. WE-Heraeus-Seminar — Polarized Antiprotons
Bad Honnef, Germany: 23.06.2008 – 25.06.2008

82. Lehrach, A.
The High Energy Storage Ring (HESR) for FAIR
STORI08
Lanzhou, China: 14.09.2008 – 18.09.2008

83. Lehrach, A.
Antimaterie — die gespiegelte Welt
Universität Bonn: Antrittsvorlesung
Bonn, Germany: 03.12.2008

84. Leonova, M.A.
SPIN@COSY: Spin-Manipulating Polarized Deuterons and Protons
SPIN2008
Charlottesville, Va., U.S.A.: 06.10.2008 – 11.10.2008

85. Lorentz, B.
Machine Aspects of Spin Filtering Experiments
RuPAC 08
Zvenigorod, Russia: 28.09.2008 – 03.10.2008

86. Luccio, A.U.
Simulation of deuteron polarization at COSY
SPIN2008
Charlottesville, Va., U.S.A.: 06.10.2008 – 11.10.2008

87. Machner, H.
New developments in NN and NY Interactions
Bhabha Atomic Research Centre, seminar
Mumbai, India: 14.02.2008

88. Machner, H.
Recent developments in NN and NY Interactions — News from an old field
IV DAE-BRNS: Workshop on Hadron Physics
Aligarh, India : 18.02.2008 – 23.02.2008

89. Machner, H.
Correleations of projectile-like fragments in heavy-ion reactions at fermi energy
International School of Nuclear Physics
Erice, Italy: 16.09.2008 – 24.09.2008

90. Machner, H.
Recent developments in NN and NY Interactions — News from an old field
XIX International Baldin Seminar on High Energy Physics Problems
Dubna, Russia: 29.09.2008 – 04.10.2008

91. Meißner, U.-G.
    An introduction to chiral perturbation theory
    XXI Heidelberg Physics Graduate Days of the Graduate School of Fundamental Physics
    Heidelberg, Germany: 29.09.2008 – 02.10.2008

92. Meißner, U.-G.
    Gauge invariance and chiral coupled-channel dynamics
    Workshop on Quark Hadron Dynamics
    Almunecar, Spain: 25.09.2008 – 28.09.2008

93. Meißner, U.-G.
    Nuclear lattice Simulations
    410. WE-Heraeus Seminar
    Bad Honnef, Germany: 28.07.2008 – 30.07.2008

94. Meißner, U.-G.
    Nuclear physics from simulations
    CEA-FZJ Workshop on High Performance Computing
    Jülich, Germany: 21.01.2008 – 22.01.2008

95. Meißner, U.-G.
    Nucleon form factors from dispersion theory
    ECT* Workshop on Hadron Electromagnetic Form Factors
    Trento, Italy: 12.05.2008 – 23.05.2008

96. Meißner, U.-G.
    Theory of nuclear forces
    The 7th CNS-EFES Summer School
    Riken, Tokyo: 26.08.2008 – 01.09.2008

97. Meißner, U.-G.
    Topics in baryon chiral perturbation theory
    International Conference on Quark Confinement and the Hadron Spectrum (Confinement08), plenary talk
    Mainz, Germany: 01.09.2008 – 06.09.2008

98. Mertens, M.
    Frei konfigurierbares digitales Auslesesystem für den PANDA MVD
    Frühjahrstagung der Deutschen Physikalischen Gesellschaft
    Darmstadt, Germany: 10.03.2008 – 14.03.2008

99. Mertens, M.
    A Versatile Digital Readout System for the PANDA MVD
    IEEE Nuclear Science Symposium
    Dresden, Germany: 19.10.2008 – 25.10.2008

100. Morozov, V.
     Experimental Verification of Predicted Oscillations near a Spin Resonance
     SPIN2008
     Charlottesville, Va., U.S.A.: 06.10.2008 – 11.10.2008

101. Nass, A.
     Spin Filtering Studies at COSY and AD
     SPIN2008
     Charlottesville, Va., U.S.A.: 06.10.2008 – 11.10.2008

102. Nass, A.
     Studies on Beam Formation in an Atomic Beam Source
     SPIN2008
     Charlottesville, Va., U.S.A.: 06.10.2008 – 11.10.2008

103. Nogga, A.
     Using light nuclei to probe chiral nuclear interactions
     International Workshop XXXVI on Gross Properties of Nuclei and Nuclear Excitations
     Hirschegg, Austria: 13.01.2008 – 19.01.2008

104. Nogga, A.
Few-body systems with chiral interactions
Workshop of the SFB 634
Bad Godesberg: 22.10.2008 – 24.10.2008

105. Oelert, W.
Auf dem Weg zu Antiwasserstoff in Ruhe
Frühjahrstagung der Deutschen Physikalischen Gesellschaft
Darmstadt, Germany: 10.03.2008 – 14.03.2008

106. Oelert, W.
Das Spiegelbild der Antimaterie
Ansbach Gymnasium, Schülerseminar
Jülich, Germany: 12.03.2008

107. Oelert, W.
Antimaterie, das Gegenüber der Materie
Haus Overbach, Seminar
Jülich, Germany: 25.03.2008

108. Oelert, W.
On the way to physics with anti-hydrogen
409. WE-Heraeus — Polarized Antiprotons
Bad Honnef, Germany: 23.06.2008 – 25.06.2008

109. Oelert, W.
Introduction to the COSY accelerator at Jülich/Germany and examples of typical experiments
York University, Physics Department, Colloquium
Toronto, Canada: 09.12.2008

110. Oellers, D.
Measurement of the Depolarizing *pe* Spin Flip Cross Section using co-moving electrons
Frühjahrstagung der Deutschen Physikalischen Gesellschaft
Darmstadt, Germany: 14.03.2008

111. Oellers, D.
Polarized Antiprotons
Physikzentrum Bad Honnef
Bad Honnef, Germany: 23.06.2008

112. Pauly, Chr.
News from WASA
Crystal Ball Collaboration Meeting
Mainz, Germany: 21.09.2008

113. Pauly, Chr.
Search for Symmetry Breaking Patterns with WASA-at-COSY
International Conference on Particles and Nuclei (PANIC08)
Eilat, Israel: 09.11.2008 – 14.11.2008

114. Pavon-Valderrama, M.
Deuteron Form Factors in Effective Field Theory
Workshop on Soft Photons and Light Nuclei
Seattle, U.S.A.: 16.06.2008 – 20.06.2008

115. Pavon-Valderrama, M.
Deuteron Form Factors in Effective Field Theory
410. WE Heraeus-Seminar
Bad Honnef: 28.07.2008 – 30.07.2008

116. Pavon-Valderrama, M.
Renormalization, Modified Effective Range Expansion and Deuteron Form Factors
Bound States and Resonances in EFT
Trento, Italy: 29.09.2008 – 03.10.2008

117. Podkopal, P.
Report on analysis of break-up reaction $dd \rightarrow \pi AN$ measured with WASA-at-COSY
Frühjahrstagung der Deutschen Physikalischen Gesellschaft
Darmstadt, Germany: 10.03.2008 – 14.03.2008

118. Podkopal, P.
Normalization with elastic and quasi-elastic channels for dd experiments
WASA-at-COSY Analysis Meeting
Jülich, Germany: 26.03.2008 – 27.03.2008

119. Podkopal, P.
Performance of PSC during Apr08 beam time
WASA-at-COSY Analysis Meeting
Jülich, Germany: 09.06.2008 – 10.06.2008

120. Przerwa, J.
Isospin dependence of the η' meson production in nucleon-nucleon collisions
MESON 2008
Cracow, Poland: 06.06.2008 – 10.06.2008

121. Rathmann, F.
Towards Polarized Antiprotons
LEAP 2008
Vienna, Austria: 16.09.2008 – 19.09.2008

122. Raymond, R.
Experimental Test of New Technique to Overcome Spin-Depolarizing Resonances
SPIN2008
Charlottesville, Va., U.S.A.: 06.10.2008 – 11.10.2008

123. Redmer, C.F.
Status and Future Plans for WASA-at-COSY
CANU 2008 and JCHP-FFE Workshop
Bad Honnef, Germany: 15.12.2008 – 16.12.2008

124. Ritman, J.
Charm Physics in PANDA: which components could be enhanced for optimal physics output
Interaction Meeting for Planning Indian Participation in PANDA at FAIR: DAE-BRNS Theme Meeting
Mumbai, India: 15.04.2008

125. Ritman, J.
WASA-at-COSY: PANDA's Little Brother is up and Running
B.A.R.C, Kolloquium
Mumbai, India: 17.04.2008

126. Ritman, J.
WASA-at-COSY & PANDA: 4π Detectors for Fixed Target Experiments on Hadron Structure and Dynamics
STORI08
Lanzhou, China: 17.09.2008

127. Ritman, J.
Hadron physics at COSY: a step towards PANDA@FAIR
IHEP, Kolloquium
Beijing, China: 23.09.2008

128. Ritman, J.
Wir sind Sternenstaub: Nukleosynthese nach dem Urknall
Saturday Morning Physics
Bochum, Germany: 15.11.2008

129. Ritman, J.
Hadron Physics at COSY: a Step Towards PANDA@FAIR
Cairo Cyclotron Project, Cairo, Kolloquium
Cairo, Egypt: 19.11.2008

130. Ritman, J.
Untersuchungen der starken QCD mit Antiprotonen
Komitee für Hadronen- und Kernphysik (KHuK), Jahrestagung
Bad Honnef, Germany: 17.12.2008

131. Röder, M.
Commissioning of the Straw Tube Tracker for the COSY-TOF experiment
CANU 2008 and JCHP-FFE Workshop
Bad Honnef, Germany: 15.12.2008 – 16.12.2008

132. Salmin, R.
Omega Meson Production with WASA-at-COSY
CANU 2008 and JCHP-FFE Workshop
Bad Honnef, Germany 15.12.2008 – 16.12.2008

133. Schadmand, S.
Hadron Physics with WASA-at-COSY
Workshop on Hadron Dynamics
Almunecar, Spain: 25.09.2008 – 28.09.2008

134. Schadmand, S.
Hadrons in Nuclei with Elementary Probes
Justus-Liebig-Universität Gießen, Seminar
Gießen, Germany: 08.11.2008

135. Schröder, W.
Strangeness Production at COSY-TOF
MESON 2008
Cracow, Poland: 06.06.2008 – 10.06.2008

136. Schult, O.
Entfesselte Finanzmärkte – Physik trifft Kapital
Diskussionsveranstaltung
Vallendar: 01.07.2008

137. Senichev, Yu.
Magnetoopic Structures for Synchrotrons with Negative Momentum Compaction
RuPAC 2008
Zvenigorod, Russia: 28.09.2008 – 03.10.2008

138. Sibirtsev, A.
Charged Pion Photoproduction and High Mass Baryons
Duke University, Seminar
Durham, NC, U.S.A.: 14.02.2008

139. Sibirtsev, A.
Charged pion photoproduction at Jlab
Institute of High Energy Physics (IHEP), Seminar
Beijing, China: 26.09.2008

140. Sibirtsev, A.
Perspectives on Baryon spectroscopy at COSY
Institute of High Energy Physics (IHEP), Seminar
Beijing, China: 23.09.2008

141. Sibirtsev, A.
ϕ meson decay in pp collisions
MESON 2008
Cracow, Poland: 06.06.2008 – 10.06.2008

142. Sibirtsev, A.
ϕ meson production in pp interactions
Institute of High Energy Physics (IHEP), Seminar
Beijing, China: 24.09.2008

143. Sibirtsev, A.
Spectroscopy of Excited hyperons at PANDA
Institute of High Energy Physics (IHEP), Seminar
Beijing, China: 25.09.2008

144. Sibirtsev, A.
Strangeness production
STORI08
Lanzhou, China: 14.09.2008 – 18.09.2008

145. Smirnov, A.
Simulation of Pellet Target Experiments with BETACOOL Code
21st Russian Particle Accelerator Conference (RuPAC 2008)
Zvenigorod, Russia: 28.09.2008 – 03.10.2008

146. Sokolov, A.
The lightweight straw tube trackers for the COSY-TOF and PANDA experiments
Frühjahrstagung der Deutschen Physikalischen Gesellschaft
Darmstadt, Germany: 10.03.2008 – 14.03.2008

147. Stockhorst, H.
Stochastische Kühlung von Antiprotonen im HESR der FAIR-Anlage
Universität Frankfurt
Frankfurt, Germany: 30.05.2008

148. Stockmanns, T.
The readout concept of the PANDA Micro-Vertex-Detector
Frühjahrstagung der Deutschen Physikalischen Gesellschaft
Darmstadt, Germany: 10.03.2008 – 14.03.2008

149. Strauch, Th.
Pionic Deuterium
Frühjahrstagung der Deutschen Physikalischen Gesellschaft
Darmstadt, Germany: 14.03.2008

150. Strauch, Th.
Pionic Deuterium
International Conference on Exotic Atoms (EXA08)
Vienna, Austria: 15.09.2008 – 19.09.2008

151. Ströher, H.
Towards Polarized Antiprotons
BARC
Mumbai, India: 15.02.2008

152. Ströher, H.
Hadron Physics with Hadronic Probes: Present and Future
Fourth DAE-BRNS Workshop on Hadron Physics
Aligarh, India: 18.02.2008 – 23.02.2008

153. Ströher, H.
Antiproton Polarization Studies for FAIR (How to polarize antiprotons and what to use them for?)
Transversity'08
Ferrara, Italy: 28.05.2008 – 31.05.2008

154. Ströher, H.
Towards Polarized Antiprotons
VI-QCD Seminar
Ferrara, Italy: 01.06.2008

155. Ströher, H.
Towards Polarized Antiprotons
MESON 08
Cracow, Poland: 06.06.2008 – 10.06.2008

156. Ströher, H.
Polarized Antiprotons (Summary-1)
409. WE-Heraeus-Seminar — Polarized Antiprotons
Bad Honnef, Germany: 23.06.2008 – 25.06.2008

157. Ströher, H.
Antiproton Polarization Studies for FAIR
Stockholm University, Department of Physics
Stockholm, Sweden: 12.06.2008

158. Ströher, H.
Double Pion Production in the $dd \rightarrow \alpha\pi\pi$ Reaction
Thesis opponent, Dissertation of Samson Kelata
Uppsala, Sweden: 13.06.2008

159. Ströher, H.
Summarizing Remarks
STORI08
Lanzhou, China: 14.09.2008 – 18.09.2008

160. Ströher, H.
Application to host SPIN2010: The Case for Jülich
SPIN2008
Charlottesville, Va., U.S.A.: 06.10.2008 – 11.10.2008

161. Ströher, H.
Spin Physics at COSY — Now and in Future
SPIN2008
Charlottesville, Va., U.S.A.: 06.10.2008 – 11.10.2008

162. Ströher, H.
Polarized Antiprotons
Dalpiaz-Symposium
Ferrara, Italy: 17.10.2008 – 18.10.2008

163. Tolba, T.
A Pellet Tracking System for WASA at COSY
Frühjahrstagung der Deutschen Physikalischen Gesellschaft
Darmstadt, Germany: 10.03.2008 – 14.03.2008

164. Urban, J.
The polarized $d + d \rightarrow \alpha + \eta$ reaction and search for η-nucleus bound states
MESON 2008
Cracow, Poland: 06.06.2008 – 10.06.2008

165. Vlasov, P.
$\eta \rightarrow 3\pi^0$ decay with WASA-at-COSY
Frühjahrstagung der Deutschen Physikalischen Gesellschaft
Darmstadt, Germany: 10.03.2008 – 14.03.2008

166. Weglorz, W.
WASA-at-COSY
Institute of Modern Physics, Seminar
Lanzhou, China: 21.06.2008

167. Weglorz, W.
Status of the CSB Program at WASA-at-COSY
CANU 2008 and JCHP-FFE Workshop
Bad Honnef, Germany: 15.12.2008 – 16.12.2008

168. Weidemann, Ch.
Chemical Shift of K transitions in Manganese
Frühjahrstagung der Deutschen Physikalischen Gesellschaft
Darmstadt, Germany: 14.03.2008

169. Wirzba, A.
The Casimir effect as a scattering problem
Universität Duisburg-Essen, Seminar
Duisburg, Germany: 28.05.2008

170. Wirzba, A.
Fermionic and Scalar Casimir Effect within the Scattering Approach
University of California, Kavli Institut for Theoretical Physics
Santa Barbara, CA, U.S.A.: 23.10.2008

171. Wirzba, A.
Fermionic Casimir Effect within the Scattering Approach
European Science Foundation 1st Network Meeting
Royaumont, France: 29.11.2008

172. Wolke, M.
Symmetries and Symmetry Breaking — First Experiments with WASA at COSY
Universität Mainz: Institutsseminar Kernphysik
Mainz, Germany: 14.01.2008

173. Wolke, M.
Fundamental Symmetries, Hadron Structure and Dynamics
Uppsala University: Department of Physics and Astronomy
Uppsala, Sweden: 28.08.2008

174. Yurev, L.
MDC calibration and e^+e^- reconstruction
WASA-at-COSY Workshop on Analysis of η and η' Decays
Uppsala, Sweden: 29.02.2008 – 02.03.2008

175. Yurev, L.
Feasibility of $\eta \to e^+e^-e^+e^-$
WASA-at-COSY Workshop on Analysis of η and η' Decays
Uppsala, Sweden: 29.02.2008 – 02.03.2008

176. Yurev, L.
MC studies on $\eta \to e^+e^-e^+e^-$ pair selection
WASA-at-COSY Analysis Meeting
Jülich, Germany: 26.03.2008 – 27.03.2008

177. Yurev, L.
Online Analysis and Trigger Preparation for the May08 η run
WASA-at-COSY Analysis Meeting
Jülich, Germany: 26.03.2008 – 27.03.2008

178. Yurev, L.
MDC layer efficiency studies
WASA-at-COSY Analysis Meeting
Jülich, Germany: 09.06.2008 – 10.06.2008

179. Yurev, L.
Status of $\eta \to e^+e^-e^+e^-$ from Apr07
WASA-at-COSY Analysis Meeting
Jülich, Germany: 09.06.2008 – 10.06.2008

180. Yurev, L.
MDC fit performance; Status of $\eta \to e^+e^-e^+e^-$ from Apr07
WASA-at-COSY Analysis Meeting
Jülich, Germany: 24.09.2008 – 25.09.2008

181. Zheng, C.
Analysis of matching trigger
WASA-at-COSY Analysis Meeting
Jülich, Germany: 26.03.2008 – 27.03.2008

182. Zheng, C.
Evaluation of the matching trigger in Apr08
WASA-at-COSY Analysis Meeting
Jülich, Germany: 09.06.2008 – 10.06.2008

183. Zheng, C.
Matching Trigger with High threshold for 'fHedwrH1'
WASA-at-COSY Analysis Meeting
Jülich, Germany: 24.09.2008 – 25.09.2008

184. Zychor, I.
Excited hyperons produced in pp collisions with ANKE at COSY
STORI08
Lanzhou, China: 14.09.2008 – 18.09.2008

D Diploma and Ph.D. Theses, Habilitation

1. Bachelor, Master, Diploma

1. S. Bertelli,
   Studio della reazione di deuteron breakup in esperimenti di spin-filtering per la polarizzazione di fasci di antiprotoni,
   University of Ferrara, Italy

2. H. Bongen,
   Entwicklung eines objektorientierten Biometriemoduls für das Teilchentransport-Monte-Carlo-Programm HERMES++,
   Fachhochschule Aachen.

3. I. Császár,
   Bau einer Ionisationskammer zur Untersuchung von laserbeschleunigten Ionen,
   Hochschule Merseburg (FH)

4. P. Goslawski,
   Hochpräzise Impulsbestimmung des COSY-Beschleunigerstrahls im Rahmen der Messung zur Bestimmung der η-Masse am Experimentaufbau ANKE,
   Universität Münster

5. Martin Hausner,
   On the charge dependence of ρ meson properties,
   Universität Bonn

6. S. Kölling,
   The two-pion exchange contribution to the nuclear current operator in chiral effective field theory,
   Universität Bonn

7. David Minossi,
   Modified effective range expansion for nucleon-nucleon scattering in chiral effective field theory,
   Universität Bonn

8. G. Oswald,
   Bau, Test und Inbetriebnahme einer Ionisations- und Proportionalkammer zum Nachweis laserbeschleunigter Ionen,
   Hochschule Merseburg (FH).

9. M. Silarski,
   Analysis of the differential cross sections for the reaction $pp \to ppK^+K^-$ in view of the K^+K^- interaction,
   Jagiellonian University Cracow, Poland

10. M. Westig,
    Preparation of a precision spectroscopy measurement of metastable Hydrogen and deuterium with a modified Lamb-shift polarimeter,
    Universität zu Köln

11. M. Zielinski,
    Feasibility study of the $\eta' \to \pi^+\pi^-\pi^0$ decay using WASA-at-COSY apparatus,
    Jagiellonian University Cracow, Poland

2. Ph.D.

12. A. Chechenin,
Non-linear high resolution beam dynamics in anti-proton storage ring,
St. Petersburg University, Russia

13. D. Chiladze,
Polarised Charge-Exchange Reaction $dp \to (pp)n$ Studies at the ANKE-COSY Spectrometer,
Tbilisi State University, Georgia

14. P. Klaja,
Correlation femtoscopy for studying η and η' mesons production collisions,
Jagiellonian University Cracow, Poland

15. M. A. Leonova,
Achieving high spin-flip efficiency with an rf magnet and discovery of spin-resonance strength formulae problem,
Michigan University, U.S.A.

16. M. Lesiak-Bzdak,
Production of the eta meson in the $d+d \to {}^4He+\eta$ reaction using the polarised deuteron beam,
Jagiellonian University Cracow, Poland

17. V. S. Morozov,
Using spin resonances to manipulate the polarization of spin-1/2 and spin-1 particle beams,
Michigan University, U.S.A.

18. J. Przerwa,
Isospin dependence of the η' meson production in nucleon-nucleon collisions,
Jagiellonian University Cracow, Poland

19. P. Vlasov,
Analysis of the $\eta \to 3\pi^0$ decay in the pp interaction,
Ruhr-Universität Bochum

20. X. Yuan,
Measurement of the $dd \to \alpha K^+K^-$ production cross section with the ANKE spectrometer at COSY-Jülich" ,
IMP Lanzhou, China

3. Habilitation

21. A. Lehrach,
Strahl- und Spindynamik von Hadronenstrahlen in Mittelenergie-Ringbeschleunigern,
Rheinische-Friedrich-Wilhelms-Universität Bonn
Schriften des Forschungszentrums Jülich; Reihe Schlüsseltechnologien / Key Technologies 08 II, 2008, ISBN 978-3-89336-548-7

E Awards & Offers for Professorships

I. Császár: *Best Bachelor Thesis 2008* Hochschule Merseburg

S. Krewald: *Outstanding Referee Award* by American Physical Society

H. Machner: *Merentibus Award* by Jagellionian University, Cracow (May 2008)

U.-G. Meißner: *Outstanding Referee Award* by American Physical Society

C. Hanhart: Received call as Associate Professor/Senior Lecturer at the Department of Physics and Astronomy, Uppsala University, Sweden

Yu. Senichev: Received Professorship with Specialization "Physcis of Charged-Particle Beams and Accelerator Physics" from Ministry of Education and Science, Russia

M. Wolke: Accepted position as Associate Professor/Senior Lecturer in Experimental Hadron Physics at the Department of Physics and Astronomy, Uppsala University, Sweden

F Funded Projects

Project	Responsible	Partner Institute	Funded by
Virtual Institute Spin and Strong QCD	U.-G. Meißner	GSI, Univ.'s Bern, Bonn, Ferrara, Cracow, Torino	HGF
Few Nucleon Systems in χEFT	E. Epelbaum	Univ. Bonn	HGF
CARE	R. Tölle		EU/FP6
TA-COSY	D. Grzonka		EU/FP6
Hadron Physics Theory Netzwerk	U.-G. Meißner	Network	EU/FP6
Pellet Target	M. Büscher	ITEP, MPEI Moscow (Russia)	EU/FP6
EURONS/EXL	D. Grzonka		EU/FP6
EUROTRANS/NUDATRA	F. Goldenbaum		EU/FP6
DIRAC Secondary Beams	R. Tölle		EU/FP6
DIRAC Phase 1	R. Tölle		EU/FP6
DIRAC Secondary Beams PANDA-2	J. Ritman		EU/FP6
DIRAC Secondary Beams PANDA-4	J. Ritman		EU/FP6
Advanced Residual Gas Profile Monitor	J. Dietrich	GSI	EU/FP6
Design Study for Pick-up Electronic Development	J. Dietrich	GSI	EU/FP6
Project FAIR	R. Toelle	GSI	EU/FP7
Scalar Mesons	M. Büscher	ITEP, INR Moscow (Russia)	DFG
Pellet Target	M. Büscher	ITEP, MPEI Moscow (Russia)	DFG
Laser applications of a pellet target	M. Büscher	ITEP, MPEI Moscow (Russia), Univ. Düsseldorf	DFG
K^- Production in Nuclei	M. Hartmann	ITEP Moscow (Russia)	DFG
Isospin Violation	M. Büscher	IMP Lanzhou (China)	DFG
Jets in Hard Processes	N.N. Nikolaev	Landau Inst., ITEP Moscow (Russia)	DFG
Properties of Unstable Nuclei	S. Krewald	Petersburg State Univ., IPPE Obninsk (Russia)	DFG
Pion Reactions on Few Nucleon Systems	C. Hanhart	ITEP Moscow (Russia)	DFG
ATRAP	W. Oelert	Univ. Mainz	DFG
Fundamental Research with Hadrons	W. Oelert	Jagiellonian Univ. Cracow (Poland)	DFG
Neutron Properties from light nuclei	E. Epelbaum	Univ.'s Bochum, Bonn, Gießen	SFB/TR 16
Broken Symmetries	H. Machner	Univ. Helsinki (Finland)	DAAD
PPP Kanada	D. Grzonka	York Univ., Toronto (Canada)	DAAD
PANDA luminosity monitor	J. Ritman	Madagascar	HGF-DAAD
Rare Decays of η and η' Mesons	S. Schadmand	Indian Inst. of Technology Bombay	DAAD/DST India
Polarization observables in $\bar{p}d$ elastic scattering	J. Haidenbauer	JINR Dubna (Russia)	Heisenberg-Landau Program
Eta-Meson Physics	H. Machner	BARC Mumbai (India)	Int. Büro BMBF
Target Development for nuclear physics experiments at COSY and AEA cyclotron	J. Ritman	AEA Cairo (Egypt)	Int. Büro BMBF
Medical Applications of Accelerators	J. Dietrich	iThemba LABS (South Africa)	Int. Büro BMBF
A Pellet Target for PANDA	M. Büscher	ITEP, MPEI Moscow (Russia) Uppsala Univ. (Sweden), GSI	INTAS
Advanced Beam Dynamic for Storage Rings	A. Lehrach	GSI, TEMF (Darmstadt) TSL Uppsala (Sweden) ITEP Moscow, JINR Dubna (Russia) Univ. Kiev (Ukraine)	INTAS
Projectile Electron Losses in the Collisions of Fast and Relativistic Low Charged Ions	G. Baur	GSI, Stockholm, Tashkent, Moscow, Arkhangelsk	GSI-INTAS
Polarized Target	F. Rathmann	PNPI Gatchina (Russia)	ISTC
Baryon Resonance Analysis	U.-G. Meißner	JLAB (U.S.A.)	JLAB
Development of a high energy electron cooler	J. Dietrich	TU Dortmund; BINP Novosibirsk, JINR Dubna (Russia)	HGF
Calculations of the Radiation Load to the PANDA MVD	J. Ritman	Israel	NRW-Israel

G COSY-FFE Projects

Project	Responsible	Institute
Frozen Spin Target	Prof. W. Meyer	Univ. Bochum
Entwicklung von Software zur Teilchenidentifikation und Erkennung von split-offs im el.-magn. Kalorimeter des WASA-Experiments	Prof. U. Wiedner	Univ. Bochum
Zusammenarbeit von HISKP-Bonn an internen Experimenten an COSY	Prof. J. Bisplinghoff	Univ. Bonn
Theorectical studies of strangeness and charm production at COSY and PANDA/FAIR	Prof. H.-W. Hammer	Univ. Bonn
Entwicklung eines Partialwellenprogrammes für die Analyse von Daten von WASA	Prof. E. Klempt	Univ. Bonn
Inelastic baryon resonances from lattice QCD	Prof. A. Rusetsky	Univ. Bonn
Zusammenarbeit an COSY H-Strahl Laserdiagnose	Prof. T. Weis	Univ. Dortmund
COSY-TOF detector	Prof. H. Freiesleben	TU Dresden
Bau von Detektoren für ANKE und K^--Nachweis	Prof. B. Kämpfer	FZ Dresden
Measurement of the degree of polarisation of laser accelerated protons	Prof. O. Willi	Univ. Düsseldorf
Bau eines Cherenkovdetektors für WASA at COSY	Prof. W. Eyrich	Univ. Erlangen-Nürnberg
Experimente mit COSY-TOF	Prof. W. Eyrich	Univ. Erlangen-Nürnberg
Polarization experiments with ANKE at COSY	Prof. E. Steffens	Univ. Erlangen-Nürnberg
FPGA-based trigger system for WASA	Prof. W. Kühn	Univ. Gießen
Schwellenexperimente an COSY-11 und ANKE	Dr. A. Khoukaz	Univ. Münster
Baryon resonance, g_A und die effektive Restrukturierung der chiralen Symmetrie	Prof. A. Schäfer	Univ. Regensburg
Installation und Inbetriebnahme des WASA-Detektors am COSY-Ring und Durchführung von Experimenten an WASA at COSY	Prof. H. Clement	Univ. Tübingen
Experimente an COSY-TOF	Prof. H. Clement	Univ. Tübingen

Project	Responsible	Institute
Lattice calculations of axial charges for baryons	Prof. C. Gattringer	Univ. Graz (Austria)
Polarized internal target for ANKE at COSY	Prof. M. Nioradze	Tbilisi State Univ. (Georgia)
Spin dependence in *pd* interactions	Prof. P. Dalpiaz	Univ. Ferrara (Italy)
Photonendetektor an ANKE	Prof. A. Magiera	Jagellionian Univ. Cracow (Poland)
Investigation of CP symmetry with WASA	Prof. P. Moskal	Jagellionian Univ. Cracow (Poland)
Strangeness production with WASA	Prof. B. Kamys	Jagellionian Univ. Cracow (Poland)
Study of the decay $\eta' \to \eta\pi\pi$ with WASA	Prof. Z. Rudy	Jagellionian Univ. Cracow (Poland)
WASA at COSY	Prof. M. Jezabek	INP Crakow (Poland)
Excited Hyperon Production at ANKE and WASA	Dr. G. Wrochna	IPJ Otwock-Swierk (Poland)
Study of the nature of the $\Lambda(1405)$ with WASA	Prof. W. Zipper	Univ. Silesia (Poland)
Neutron tagging and strangeness production at ANKE	Dr. V. Koptev	PNPI Gatchina (Russia)
Set-up and research with the spectator/vertex detection system at ANKE-COSY	Prof. V. Kulikov	JINR Dubna (Russia)
Reanalysis of the measurement of the η mass	Dr. D. Kirillov	JINR Dubna (Russia)
ω-meson production with WASA	Prof. E. Strokovsky	JINR Dubna (Russia)
Development of a frozen-pellet target	Dr. A. Gerasimov	ITEP Moscow (Russia)
ϕ-meson production in *pn* and *pA* reactions	Prof. V. Kiselev	ITEP Moscow (Russia)
Development, commissioning and operation of components for the COSY experiments WASA and ANKE and spin-filtering studies at COSY as preparation of the PAX experiment in the framework of the FAIR project at GSI	Dr. A. Vasilyev	PNPI Gatchina (Russia)
Development of online software tools for COSY-TOF	Prof. V.N. Afanasiev	MIEM Moscow (Russia)
Cooperation COSY-WASA for $pp \to pp\eta$ and $pp \to pp\eta\pi^0$	Prof. T. Johansson	Uppsala Univ. (Sweden)
Trigger based on digitized QDC information for WASA	Prof. B. Höistad	Uppsala Univ. (Sweden)
Search for mixing between light mesons	Prof. A. Rudchik	INR Kiev (Ukraine)
Physics of antihydrogen	Prof. E. Hessels	Univ. of York (Canada)
Unified analysis of meson production in hadronic reactions	Prof. K. Nakayama	Univ. of Georgia (U.S.A.)
SPIN@COSY: Spin-Manipulating Polarized Deuterons and Protons	Prof. A. Krisch	Univ. of Michigan (U.S.A.)

H Conferences (co-)organized by the IKP

H.1 Hadron Physics Summer School 2008

More than 80 graduate and advanced undergraduate students from 14 countries and 4 continents participated in the Hadron Physics Summer School HPSS2008 held at Physikzentrum Bad Honnef, Germany, August 11 – 15, 2008. Similar to the preceding COSY Summer School (CSS) 2002, 2004, and 2006, this school consisted of lectures and working groups on theoretical, experimental, and accelerator aspects. The focus was on current issues in hadron physics with emphasis on the latest programs at the accelerators COSY and ELSA (Bonn), also featuring future FAIR projects like HESR/PANDA and PAX. During the very successful school, the students were given a guided tour to COSY.

The HPSS2008 was jointly organized by scientists working at the IKP and by the DFG Transregio TR 16 (Subnuclear Structure of Matter) of the Universities Bonn, Bochum, and Giessen. In addition, the HPSS2008 was sponsored by DAAD (German Academic Exchange Service) and DPG (Deutsche Physikalische Gesellschaft), making the participation of young motivated students into this challenging enterprise possible.

It is intended to conduct the HPSS every second year. The series will be supplemented by lecture weeks in the alternate years, which will consist of invited lectures and student contributions. The lecture weeks are self-contained and will also be an excellent opportunity for graduate students and early post-graduates to deepen the knowledge gained at HPSS.

For more detailed information, see www.fz-juelich.de/ikp/hpss2008/.

Fig. 1: Participants of HPSS2008 in front of Physikzentrum Bad Honnef.

H.2 The 7th International Conference on Nuclear Physics at Storage Rings, STORI'08

STORI'08, the 7th International Conference on Nuclear Physics at Storage Rings, took place on September 14 – 18, 2008 in Lanzhou (China). It was organized by the Institute of Modern Physics (IMP) of the Chinese Academy of Sciences (CAS) with Guoqing Xiao (HIRFL, Heavy Ion Research Facility in Lanzhou) as Chairman. Approximately 90 scientists from all over the world attended the meeting (see enclosed photograph).
During STORI'08, a wealth of new scientific results from the operating hadron and electron rings as well as new plans were presented in 25 invited talks and 20 contributions — in particular first nuclear mass measurements from the newly commissioned pair of storage rings for ions at Lanzhou, CSRm and CSRe. The attendants not only discussed physics issues but also technological challenges around the rings, like electron and stochastic cooling and polarized beams (of antiprotons), the targets (liquid and cluster jets, pellets and polarized) and the internal and external detectors. A number of talks was devoted to the transition from existing detectors/rings to planned future facilities, *e.g.* from COSY/WASA to HESR/PANDA and from ESR to NESR (at FAIR). A visit to HIRFL-CSR was provided during the meeting, where the impressive progress in setting up and commissioning their storage rings could be observed.
The next STORI conference will be held in 2011 in Frascati (Italy). The chairman will be Stefano Bianco (LNF, INFN): by that time we should be able to witness the start of the construction of new facilities, in particular FAIR at Darmstadt (Germany).

Fig. 2: Some of the STORI'08 participants in front of the IMP main building

H.3 MESON 2008

The bi-annual conference MESON 2008 took place in the Jagiellonian University Kraków, Poland in the time 6 – 10 June. It was jointly organised by Forschungszentrum Jülich, Germany, INFN Frascati, Italy, Jagiellonian University, Kraków, Poland, and Inst. Nuclear Physics, PAN, Kraków, Poland. Again as since 1991 physicists from all over the world met to discuss meson physics. Since mesons and baryons are hadrons, they interact mainly

Fig. 3: Participants of the MESON 2008 in front of the Lecture Hall of the Jagiellonian University, Kraków, Poland.

via the strong interaction. Studies of the production, interactions with mesons and baryons as well as their decays shed light on their structure. Interest in bound states of mesons with nucleons and light nuclei has renewed interest by recent new findings. Probes to produce mesons are by now mainly baryons as well as electromagnetic probes. The detectors are now commensurate in complexity to the problems to be attacked. Just to name a few being represented at the present meeting: ANKE, BABAR, BES, CLAS, CLEO, Compass, COSY-GEM, COSY TOF, Crystal Ball, Crystal Barrel, HADES, SPRING8, WASA. The rich harvest of experimental results was accompanied by theory ranging from π-π interaction to medium modification of mesons in nuclei.
The conference saw presentations from delegates being quite senior and eminent scientists indeed. However, a great number of young researchers from both the experimental and theoretical fraternity complemented the programme. The conference benefitted from suggestions contributed by the international advisory committee. It was supported by

- Forschungszentrum Jülich, Germany
- INFN Frascati, Italy
- Jagiellonian University, Kraków, Poland
- Inst. Nuclear Physics, PAN, Kraków, Poland
- Jefferson Lab, Newport News, Virginia, USA
- Hadron Physics I3 project within FP6

The next conference will take place June 2010 again in Kraków.

H.4 409$^{\text{th}}$ WE-Heraeus-Seminar; Polarized Antiprotons

The suggestion of the PAX collaboration to utilize polarized antiprotons at the new FAIR facility at Darmstadt has been well received within the hadronic physics community. A polarized antiproton beam would allow unprecedented measurements of many fundamental physics observables. Among them, transversity; this describes the distribution of transversely polarized quarks in a transversely polarized nucleon. Polarized antiprotons would provide in particular a direct determination of transversity by measurement of a double-spin asymmetry in the production of Drell-Yan events. Other aspects address the determination of the phases of time-like electromagnetic form factors, and other scattering observables in hard proton antiproton reactions.
At present, the most promising method fort he production of a polarized antiproton beam is spin filtering, where one employs the spin-dependence of the strong interaction of an initially unpolarized antiproton beam impinging on a polarized hydrogen gas target. Although the proof of principle experiment (FILTEX) has already been successfully carried out in 1993 with a proton beam at the TSR in Heidelberg, the underlying mechanisms are not completely understood yet. In order to accomplish that, a series of judiciously chosen experiments using protons at COSY is necessary. During the past year, the effect of electrons on the polarization of a stored beam was studied. Since little is known about the spin-dependence of the antiproton-proton interaction, subsequently, experiments at the AD have to be carried out. The results of these investigation will provide a data basis which can be used to design an optimized, dedicated storage ring fort he proton of polarized antiprotons, a so-called Antiproton-Polarized Ring, which shall later be employed at the FAIR facility.
With this in mind, the goal of the 409$^{\text{th}}$ WE-Heraeus seminar, which took place during June 23–25, 2008, was to evaluate the physics potential polarized antiprotons would bear for hadron physics. In addition, the status of the experimental and theoretical efforts towards these goals has been emphasized during the meeting. The exciting search for the optimum approach brought together experts in the field with young student — in total 60 participants. This successful combination produced exciting debates.
The organizers and participant would like to thank the Wilhelm und Else Heraeus-foundation for their generous support. We also would like to thank in particular Dr. E. Dreisigacker and Frau H. Uebel of the Heraeus foundation, and the members of the Physikzentrum Bad Honnef for their assistance.

I Teaching Positions

Institute	Name	University
IKP-1	PD Dr. A. Gillitzer	Bonn
	PD Dr. F. Goldenbaum	Wuppertal
	Prof. Dr. H. Machner	Duisburg-Essen
	Prof. Dr. J. Ritman	Bochum
	PD Dr. S. Schadmand	Gießen
	Dr. T. Stockmanns	Bochum
IKP-2	PD Dr. M. Büscher	Köln
	PD Dr. D. Gotta	Köln
	PD Dr. F. Rathmann	Erlangen-Nürnberg
	Prof. Dr. H. Ströher	Köln
	Dr. M. Wolke	Bochum
IKP-3	Prof. Dr. G. Baur	Basel
	Prof. Dr. E. Epelbaum	Bonn
	Univ. Doz. Dr. J. Haidenbauer	Graz
	PD Dr. C. Hanhart	Bonn
	Prof. Dr. S. Krewald	Bonn
	Prof. Dr. U.-G. Meißner	Bonn
	Prof. Dr. N.N. Nikolaev	Moscow
	Dr. A. Nogga	Bonn
	PD Dr. A. Wirzba	Bonn
IKP-4	Prof. Dr. Dr. h.c. J. Dietrich	Dortmund
	PD Dr. A. Lehrach	Aachen, Bonn
	Prof. Dr. R. Maier	Bonn

J Beam Time at COSY

The scheduled beam time for COSY in the year 2008 was 7224 hours. With an down time of 375 hours the COSY complex features a reliability of 95%. Two main causes for downtime are the aged cyclotron and the magnetic septum of COSY needed for external experiments. The distribution of user hours is listed in Table 1 and depicted in Fig. 4.

Table 1: Overview over COSY user beam time in 2008.

Date	Experiment	Duration	Reaction, experiment #
19.01.08–27.01.08	WASA	1 week	$pn \to d\pi\pi$, 183
09.02.–24.02.	PAX	2 weeks	$\vec{p}$-depolarization, 181
08.03.–30.03.	ANKE	3 weeks	$\vec{d}p \to {}^3\mathrm{He}\,\eta$, 187
26.04.–04.05.	WASA	1 week	$pp \to pp\eta$, 182
05.05.–11.05.	WASA	1 week	$pp \to pp\eta'$, 184
17.05.–25.05.	SPIN@COSY	1 week	$\vec{d}$ beam, 180
31.05.–08.06.	WASA	1 week	$\vec{d}d \to {}^4\mathrm{He}\,\eta$, 186
09.06.–15.06.	dEDM	1 week	$\vec{d}$ beam, 176.1
21.06.–06.07.	WASA	2 weeks	$dd \to {}^4\mathrm{He}\,\pi^0$, 173.1
12.07.–27.07.	ANKE	2 weeks	$pn \to d\omega$, 175.1
02.08.–10.08.	TOF	1 week	commissioning, 179
30.08.–07.09.	PAX	1 week	accept.studies, 190
13.09.–21.09.	dEDM	1 week	$\vec{d}$ beam, 176.2
27.09.–26.10.	WASA	4 weeks	$pd \to {}^3\mathrm{He}\,\eta$, 188
01.11.–16.11.	WASA	2 weeks	$pp \to pp\eta$, 182
22.11.–30.11.	SPIN@COSY	1 week	$\vec{d}$ beam, 180.1
06.12.–21.12.	TOF	2 weeks	Hyperon prod., 141.4
Total '08		27 weeks	

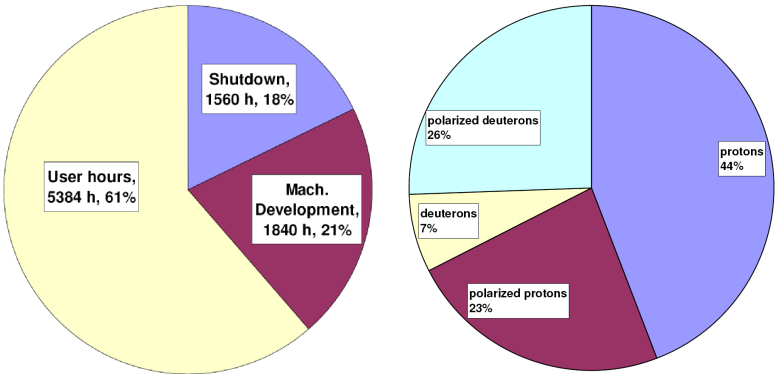

Fig. 4: COSY beam-time statistics. The scheduled beam time sums up to 7224 hours with a reliability of 95%.

K Personnel

K.1 Scientific Staff

Dr. V. Baru (IKP-3) (since 1 April, 2008)
Prof. Dr. G. Baur (IKP-3)
Dr. U. Bechstedt (IKP-4)
Dr. K. Bongardt (IKP-4)
H. Bongen (IKP-1) (until 21 Februar, 2008)
DI N. Bongers (IKP-4)
DI R. Brings (IKP-4)
PD Dr. M. Büscher (IKP-2)
DP A. Chechenin (IKP-4) (until 15 Februar, 2008)
DP E. Czerwinski (IKP-1)
Prof. Dr.Dr.h.c. J. Dietrich (IKP-4)
DI N. Dolfus (IKP-TA)
Dr. M. Döring (IKP-3)
Dr. R. Engels (IKP-2)
Prof. Dr. E. Epelbaum (IKP-3)
DI F.-J. Etzkorn (IKP-4)
Dr. P. Fedorets (IKP-2)
Dr. O. Felden (IKP-TA)
A. Filin (IKP-3) (since 16 October, 2008)
Dr. W. Gast (IKP-1)
Dr. R. Gebel (IKP-4)
Dr. M. George (IKP-1) (until 30 September, 2008)
PD Dr. A. Gillitzer (IKP-1)
PD Dr. F. Goldenbaum (IKP-1)
PD Dr. D. Gotta (IKP-2)
Dr. F. Grümmer (IKP-3)
Dr. D. Grzonka (IKP-1)
DI W. Günther (IKP-4)
Dr. F.-K. Guo (IKP-3)
Univ. Doz. Dr. J. Haidenbauer (IKP-3)
R. Halver (IKP-1)
PD Dr. C. Hanhart (IKP-3)
Dr. M. Hartmann (IKP-2)
M. Hausner (IKP-3) (until 31 July 2008)
Dr. V. Hejny (IKP-2)
DI K. Henn (IKP-4)
DP M. Hodana (IKP-1)
Dr. F. Hügging (IKP-1) (until 31 March 2008)
Dr. V. Kamerdjiev (IKP-4)
Dr. A. Kacharava (IKP-2)
S. Kazmierowski (IKP-3) (since 1 May, 2008)
D. Khaneft (IKP-2)
DP P. Klaja (IKP-1) (until 31 January 2008)
St. Kölling (IKP-3)
DP A. Kowalczyk (IKP-1) (until 14 May 2008)
Prof. Dr. S. Krewald (IKP-3)
DI K. Kruck (IKP-4)
DP W. Krzemien (IKP-1) (since 1 May, 2008)
PD Dr. A. Lehrach (IKP-4)
S. Liebig (IKP-3) (since 15 February, 2008)
Dr. B. Lorentz (IKP-4)
Prof. Dr. H. Machner (IKP-1)
Prof. Dr. R. Maier (IKP-4)
Prof. Dr. U.-G. Meißner (IKP-3)
DP M. Mertens (IKP-1)
DP S. Mikirtychiants (IKP-2)
D. Minossi (IKP-3)
DI I. Mohos (IKP-4) (until August 2008)
Dr. M. Nekipelov (IKP-2)
Prof. Dr. N.N. Nikolaev (IKP-3)
Dr. A. Nogga (IKP-3)
Prof. Dr. W. Oelert (IKP-1)
DP D. Oellers (IKP-2)
Dr. H. Ohm (IKP-2)
DI N. Paul (IKP-1)
Dr. C. Pauly (IKP-1)
Dr. M. Pavon-Valderrama (IKP-3)
Dr. D. Prasuhn (IKP-4)
J. Przerwa (IKP-1) (until 31 January, 2008)
Dr. A. Raccanelli (IKP-4)
PD Dr. F. Rathmann (IKP-2)
DP Ch.F. Redmer (IKP-1)
DP M. Retzlaff (IKP-4)
DI A. Richert (IKP-4)

Prof. Dr. J. Ritman (IKP-1)
Dr. E. Roderburg (IKP-1)
M. Röder (IKP-1) (since 1 April, 2008)
DI J. Sarkadi (IKP-TA)
DP P. Saviankou (IKP-3)
Dr. H. Schaal (IKP-1)
PD Dr. S. Schadmand (IKP-1)
Dr. R. Schleichert (IKP-2)
DI G. Schug (IKP-4)
Dr. Th. Sefzick (IKP-TA)
DI E. Senicheva (IKP-4) (until 31 March 2008)
Prof. Dr. Y. Senichev (IKP-4)
DI M. Simon (IKP-4)
Dr. A. Sokolov (IKP-1) (until 31 August 2008)
Dr. R. Stassen (IKP-4)
Dr. H. Stockhorst (IKP-4)
Dr. T. Stockmanns (IKP-1)
DP Th. Strauch (IKP-2)
Prof. Dr. H. Ströher (IKP-2)
T. Tolba (IKP-1)
Dr. R. Tölle (IKP-4)
DI T. Vashegyi (IKP-4)
Dr. N. Vasiukhin (IKP-4) (until 31 May 2008)
DP P. Vlasov (IKP-1)
P. Voigtländer (IKP-1) (since 1 May, 2008)
Chr. Weidemann (IKP-2)
DP D. Welsch (IKP-4)
Dr. P. Wintz (IKP-1)
PD Dr. A. Wirzba (IKP-3)
DI J.-D. Witt (IKP-4)
Dr. M. Wolke (IKP-2)
Dr. E. Zaplatin (IKP-4)
F. Zarife (IKP-4) (until 14 March 2008)
M. Zielinski (IKP-1) (since 9 July, 2008)

K.2 Technical and Administrative Staff

J. Ahlschläger (IKP-4)

J. Artz (IKP-TA) (since 15 July 2008)

C. Berchem (IKP-TA)

P. Birx (IKP-4) (until 31 January 2008)

M. Böhnke (IKP-4)

J. Borsch (IKP-TA)

P. Brittner (IKP-4)

J. But (IKP-TA)

W. Classen (IKP-4)

M. Comuth-Werner (IKP-TA)

B. Dahmen (IKP-4)

C. Deliege (IKP-4)

W. Derissen (IKP-TA)

G. D'Orsaneo (IKP-2)

R. Dosdall (IKP-1)

R. Enge (IKP-4)

P. Erben (IKP-2)

B. Erkes (IKP-4)

W. Ernst (IKP-TA) (until 31 May 2008)

K. Esser (IKP-TA)

H.-P. Faber (IKP-4) (until 30 November 2008)

H.-W. Firmenich (IKP-TA)

J. Göbbels (IKP-TA)

H. Hadamek (IKP-TA)

R. Hecker (IKP-4)

E. Heßler (IKP-TA)

M. Holona (IKP-TA)

H.-M. Jäger (IKP-1)

H. J. Jansen (IKP-TA) (until 31 December 2008)

A. Kieven (IKP-4)

Ch. Krahe (IKP-TA) (until 31 March 2008)

M. Kremer (IKP-TA)

G. Krol (IKP-4)

M. Küven (IKP-4)

K.-G. Langenberg (IKP-4)

H. Metz-Nellen (IKP-TA)

S. Müller (IKP-TA)

M. Nau (IKP-TA) (until 31 March 2008)

R. Nellen (IKP-TA)

St. Nießen (IKP-TA) (until 31 March 2008)

H. Pütz (IKP-4)

G. Roes (IKP-TA)

N. Rotert (IKP-4)

D. Ruhrig (IKP-4)

T. Sagefka (IKP-4)

F. Scheiba (IKP-4)

H. Schiffer (IKP-TA)

J. Schmitz (IKP-4)

F. Schultheiß (IKP-TA)

H. Singer (IKP-4)

D. Spölgen (IKP-2)

G. Sterzenbach (IKP-1)

J. Strehl (IKP-TA)

J. Uehlemann (IKP-1)

P. Wieder (IKP-2)

J. Wimmer (IKP-1) (until 31 December 2008)

H. Zens (IKP-4)

IKP-1 = Experimental Hadron Structure
IKP-2 = Experimental Hadron Dynamics
IKP-3 = Theoretical Nuclear Physics
IKP-4 = Large-Scale Nuclear Physics Equipment
IKP-TA = Technical Services and Administration

L List of Authors